List of Research Papers per Teachers in the journals notified on UGC website during the year 2016

Sl.NO	NAME OF THE FACULTY	TITLE OF PAPER	NAME OF JOURNAL	VOLUME	NAME OF THE DEPART MENT	PAGE NO
1	Dr.B.Kalaavathi	Agerl Based Enhanced Map Reduce Technique In Cloud Scheduling	SSRG International Journal of Computer Science and Engineering	Volume 3, Issue 10	CSE	3-8
2	Dr.B.Kalaavathi	Enhanced Scheduling Approach Using Heuristics Flow Equilibrium Based Load Balancing Algorithm In Cloud	International Journal of Control Theory and Applications	Volume 9, Issue 2	CSE	9-20
3	Dr.B.Kalaavathi	Attack Resistant Analysis Using Secure Singular Value Decomposition and Markov Random Field Based on Rotation Scaling Transformation Invariant Image Watermarking for deo Frames	Asian Journal of Information Technology	Volume 15, Issue 17	CSE	21-34
4	Mrs. P.Vijayalakshmi	A Misdirected Route Avoidance Using Topological Transform Adaptive Relational QOS Routing In Wireless Sensor Network	Asian Journal of Information Technology	Volume 15, Issue 17	CSE	35-43
5	Dr.K.Gowsic	Resource Optimized Spectral Route Selection Protocol for WMSN Surveillance Application	Asian Journal of Information Technology	Volume 15, Issue 19	CSE	44-47
6	Dr.R Jeyabharath	A High Step-Up Hybrid DC-DC Converter With Reduced Voltage Stress For Renewable Energy Applications	World Applied Sciences Journal	Volume 34, Issue 7	EEE	48-54
7	Dr.R Jeyabharath	Fuzzy Controlled Bridgeless CUK Converter Fed Switched Reluctance Motor	Asian Journal of Information Technology	Volume 15, Issue 22	EEE	55-62
8	Dr.R Jeyabharath	Evolutionary Computing Technique for Torque Ripple Minimization of 8/6 Switched Reluctance Motor	Advances in Natural and Applied Sciences	Volume 10, Issue 8	EEE	63-71
9	Dr.R Jeyabharath	Performance Analysis and Speed Regulation Estimation of SR Motor Using FT-ANN Controller With Steady State Stability and FFT Analysis	Middle-East Journal of Scientific Research	Volume 24, Issue 12	EEE	72-83

10	Dr.P.Veena	A High Step-Up Hybrid DC-DC Converter With Reduced Voltage Stress for Renewable Energy Applications	World Applied Sciences Journal	Volume 34, Issue 7	EEE	84-90
11	Dr.P.Veena	Fuzzy Controlled Bridgeless CUK Converter Fed Switched Reluctance Motor	Asian Journal of Information Technology	Volume 15, Issue 22	EEE	91-98
12	Dr.P.Veena	Evolutionary Computing Technique for Torque Ripple Minimization of 8/6 Switched Reluctance Motor	Advances in Natural and Applied Sciences	Volume 10, Issue 8	EEE	99-107
13	Mr.T Srihari	Evolutionary Computing Technique for Torque Ripple Minimization of 8/6 Switched Reluctance Motor	Advances in Natural and Applied Sciences	Volume 10, Issue 8	EEE	108-116
14	Mr.A.Murugesan	Performance Analysis and Speed Regulation Estimation of SR Motor Using FT-ANN Controller With Steady State Stability and FFT Analysis	Middle-East Journal of Scientific Research	Volume 24, Issue 12	EEE	117-128
15	Mr. R.Nandakumar	Analysis of Abnormalities in Common Carotid Artery Images Using Multiwavelets	ICTACT Journal on Image and Video Processing	Volume 07, Issue 02	ECE	129-134
16	Dr. N.Lalithamani	Analyzed on Domination and Diameter In Graphs	International Journal of Applied Research	Volume 11, Issue 01	Mathematics	135-139
17	Dr. N.Lalithamani	Edge Regular Property of Complement and Meu Complement of A Fuzzy Graph and Edge Adjacency Sequence In Fuzzy Graph	International Journal of Pure and Applied Mathematics	Volume 107, No 03	Mathematics	140-149

Agerl Based Enhanced Map Reduce Technique in Cloud Scheduling

S.Selvi[#1], Dr.B.Kalaavathi[#2]

[#1]Assitant Professor/CSE, Angel College of Engineering and Technology, (Affiliated to Anna University) ,Tirupur, Tamil Nadu, India

[#2]Professor/CSE, K.S.R. Institute for Engineering and Technology, Affiliated to Anna University), Tiruchengode, Tamil Nadu, India

ABSTRACT *- Today's real time big data applications mostly rely on map-reduce (M-R) framework of Hadoop File System (HDFS). Hadoop makes the complexity of such applications in a simpler manner. This paper works on two goals: maximizing resource utilization and reducing the overall job completion time. Based on the goals proposed, we have developed Agent Centric Enhanced Reinforcement Learning Algorithm (AGERL) .The algorithm concentrates in four dimensions: variable partitioning of tasks, calculation of progress ratio of processing tasks including delays, XMPP based multi attribute query posting and Hopkins statistics assessment based dynamic cluster restructuring . An Enhanced Reinforcement Learning Process with the above features is employed to achieve the proposed goal. Finally performance gain is theoretically proved.*

Keywords: *map reduce, Hopkins, multi attribute query, reinforcement learning*

1. INTRODUCTION:

The Map Reduce implementation in a Hadoop framework is an upcoming platform to handle larger applications involving parallel data processing. Research and scientific calculations for a single task can be carried out with substantial parallelism techniques. Improving job completion time and efficient utilization of resources are the main considerations in this framework. This can be achieved when allocation of map and reduce slots are scheduled optimally. The scheduling adopts two types of reinforcement methodologies, one is a discrete process and the other is a continuous process. A continuous reinforcement with a dynamic restructuring mechanism is applied in our work to reschedule the map & reduce tasks whenever there is a necessity occurs.

Identifying and improving the straggler tasks in a heterogeneous cluster[13] is one of the milestones in the process of optimization of scheduling. Our paper enhances the characteristics of RL process. The RL algorithm is composed of the following components: Agent, Environment, State Space and Reward. The characteristics of agent are improved in the existing MRRL scheduler [12] and it performs the following:

a) Variable partitioning of the incoming tasks
b) Computing Progress ratio of the tasks in execution
c) XMPP based multi attribute query model
d) Cluster restructuring based on Hopkins statistical calculation

The agent plays an important role in the identification of straggler tasks and who invokes the multi attribute query based technique to retrieve the requirement of resources needed to convert the straggler tasks into faster tasks.

The environment is the configuration settings of cloud based device. The state representation is the classification of straggler tasks and quicker tasks. The nodes also classified into slow nodes or non scalable nodes and faster nodes or scalable nodes. An objective of RL algorithm is taking actions based on the computation value of reward function. It is positive(>0) and negative(<0) rewards. If the straggler task is able to be executed in the scalable node, then it is a positive reward else it is a negative reward. The scalable nodes can posses more number of staggler tasks with positive reward and non scalable node possess more number of straggler tasks with negative reward.

PRINCIPAL
K. S. R. INSTITUTE FOR
ENGINEERING AND TECHNOLOGY,
K. S. R. KALVI NAGAR,
TIRUCHENGODE-637 215,
NAMAKKAL Dt, TAMIL NADU.

Previous works [11-13] has not involved the data transfer delays, bandwidth delays in calculating the status of tasks, but in our paper we have included the above delays also for calculation, so that the percentage of accuracy and efficiency can be still improved. Scaling of the resources is made dynamically as like earliest works, but multiattribute based query strategy is adopted in the agent phase of Reinforcement Learning (RL) process to identify the amount of resources left idle at the particular instant. Based on the progress ratio and query results, the agent checks the possibility of the conversion of straggler tasks (including the tolerable percentage of 30%) into quicker one. NOSql is employed for the query retrieval process for transparency.

Section 2 discusses the previous works, section 3 describes the proposed model, section 4 outlines the conclusion and future works.

2. PREVIOUS WORKS:

Implementation of Hadoop Map Reduce Framework is carried out in earlier works and each work was aimed to optimize the framework in various issues like data locality, resource utilization, makespan, performance enhancement,QoS,etc.

Lena et. al. in paper[1] proposed two Energy Aware Map Reduce Scheduling Algorithms EMRSA –I and II to minimize the consumption of energy during the execution of a application, thereby decreasing the overall completion time. Various scheduling algorithms have been studied and analyzed in paper[2]. Liya et. al. worked out the comparision of the mapreduce algorithms by exploring the merits and demerits. Zhuo Tang in paper[3] explored an idea of optimizing the scheduling in a heterogeneous cluster in two phases(job prioritizing phase and task assignment phase).The authors gave a new dimension of scheduling the jobs based on the category of I/O intensive and Compute intensive. Then the jobs are allotted to the machines based on data locality. The paper[4] focuses on a flexible scheduling scheme adopted for any variety of metrics such as deadline, makespan, SLA,etc. Also FLEX aimed to guarantee minimum number of slots to each job and make sure a degree of fairness among the jobs.

A novel scheduler named Resource Aware Adaptive Scheduler (RAS)[5] had been developed to improve the resource utilization and job performance, but RAS cannot resolve the network bottlenecks that occur due to inefficient placement of reduce tasks. Matei et al. in his paper[6] focused on multiuser workloads by adopting two simple techniques namely, delay scheduling and copy compute splitting. The authors applied the concept of statistical multiplexing and achieve high throughput and low response time.

A combination of K-means clustering and self adaptive map reduce had been employed to improve the performance of scheduling by doing less computation and providing higher accuracy[7]. But Thangaselvi et al. proposed her work by assigning only one task for each data node which failed to improve the overall throughput of multiple task.

An iterative computation was done by Ekanayake et al. in [8] and the authors proposed a programming model and architecture in a map reduce framework and showed the improvement in the execution time of incoming jobs. Based on input data, machine slots and complexity of reduce function, a cost function was proposed by Tian et al. in paper[9] and showed the minimization of cost within the job deadline and budget.

Paper[10] focused on demand resource provisioning by employing a two tiered allocation mechanism ie, locally and globally and a feedback mechanism was also employed to manage the on demand capacities to the concurrent applications.

Pastorelli et al. in his paper[11] evaluated job size online in a multi server system using aging technique and achieved fault tolerance, scale-out upgrades and attempt to eliminate the starvation issues both for smaller and larger jobs.

Reinforcement Learning technique [12] is adopted in a heterogeneous cluster to identify and reduce the straggler tasks .Nenavath et al. tried to improve the utilization of resources and minimizes the overall job completion time. But we have extended the RL by assessing using Hopkins statistics to guide in cluster restructuring.

Dynamic Proportional Share Model is designed using multiattribute range query technique in paper[13] and the query model is extended by adopting XMPP protocol in our paper.

PRINCIPAL,
K. S. R. INSTITUTE FOR
ENGINEERING AND TECHNOLOGY,
K. S. R. KALVI NAGAR,
TIRUCHENGODE-637 215,
NAMAKKAL Dt. TAMIL NADU.

3. THE PROPOSED AGERL ALGORITHM:

3.1. HOPKINS STATISTICS ASSESSMENT BASED CLUSTER RESTRUCTERING:

Map Reduce Framework works in a heterogeneous cluster and when the user submits the tasks, the task is partitioned into required number of map and reduces tasks in a non homogenous manner. The partition takes place based on the configuration of machines in the cluster, nature of tasks and data locality. For this, the clustering tendency is assessed based on Hopkins statistics methodology.

3.1.1. Procedure to perform Hopkins Statistics Assessment:

Step 1: Assume the set of points within a node $n_k = \{p_1,p_2,\ldots,p_n\}$

Step 2: For every point p_i in the node n_i and its nearest neighbouring point p_j , compute the Manhautten Distance between p_i and p_j and it is represented as

U_m = Manhautten Distance(p_i, p_j).

Manhautten Distance(p_i, p_j) = $|x1 - x2|+|y1-y2|$,

where (x1,y1) and (x2,y2) are the coordinates of p_i and p_j respectively.

Step 3: For every points p_i and p_j within the node n_k, compute the Manhautten Distance between p_i and p_j and it is represented as

V_m = Manhautten Distance(p_i,p_j).

Step 4: Compute Hopkins Statistics (H)

$$H = \frac{\sum U_m}{\sum U_m + \sum V_m}$$

Step 5: H value for every node is computed in the similar manner and if H(avg) > 0.5,then the cluster to be restructured would be a meaningful cluster.

3.2. PROGRESS RATIO CALCULATION:

Assume the task is splitted into m number of map tasks $M=\{M_1,M_2,\ldots,M_m\}$ and n number of Reduce tasks $R=\{R_1,R_2,\ldots,R_n\}$

The current status of the tasks in execution is calculated on a periodic basis and is given by

Progress Ratio of Task (M_i/R_i) =

$$\left(\frac{\text{Length of the task} - \text{Amount of Task Completed}}{\text{Length of the task}} \right) + (DT_i + BD_i) \times 100 \quad (1)$$

$$\text{Progress Ratio avg} = \frac{\sum_{i=1-m}(M_i) + \sum_{j=1-n}(R_i)}{(m+n)} \quad (2)$$

Nenavath et al. [12] set the tolerable limit to 20% and we have considered data transfer delay (DT_i) and bandwidth delay(BD_i) to improve the accuracy of scheduling.

3.3.XMPP BASED MULTI ATTRIBUTE QUERY MODEL:

It is the responsibility of the agent to identify suitable node for the processing of straggler tasks. The agent based on the progress ratio of each tasks posts query to the nodes in the cluster. Extensible Messaging and Presence Protocol (XMPP) based multiattribute query model is employed in our work.

XMPP protocol works as follows: A query message is send to the machine A. If the message is send to the right node, then the execution proceeds, otherwise A itself sends it to the next nearest optimal node. This continues until the right node is found.

The query is first posted to the nodes with data locality and based on the reply (if that node's resources are able to process the straggler task in a faster mode), restructuring of the cluster is predicted with Hopkins statistical assessment. If the assessment results above 0.5, then the prediction are preceded, otherwise the query is posted to nearest nodes and the same procedure is repeated till the prediction becomes correct. The query structure is evaluated in NoSQL. The query includes the attributes such as CPU, memory, Data Transfer and Bandwidth. These resources are included as a part of the query. The result of the query posted to a node gives the information whether that node can run the straggler task, otherwise restructuring is predicted with Hopkins. If not, the query is posted to the nearest neighbor nodes(secondary priority nodes). This process goes on until a suitable node is selected, if not that conversion of that particular straggler task into a quicker one has to be dropped. In this manner, we try to reduce the number of straggler tasks in the heterogeneous cluster.

3.4. PSEUDOCODE : PROPOSED AGERL ALGORITHM

Step 1: Get the task T as input from the user

Step 2: Job Tracker analyze the task for its

PRINCIPAL.
K. S. R. INSTITUTE FOR
ENGINEERING AND TECHNOLOGY,
K. S. R. KALVI NAGAR,
TIRUCHENGODE-637 215,
NAMAKKAL Dt, TAMIL NADU.

characteristics

Step 3: From the characteristics, Agent A performs variable partitioning of the tasks into m Map tasks and n Reduce tasks

Step 4: for each Mi/Ri tasks

compute the $PR(M_i/R_j)$ & PR_{avg} (as in Eqn 1 & 2)

Shoot a query to the higher priority nodes

Compute the reward.

if reward>0

possible to convert the straggler tasks into a quicker task

compute Hopkins statistics(H) and check

if (H)>0.5

restructure the cluster

Step 5: Compute performance gain.

4. CONCLUSION:

The paper proposed an Enhanced version of Reinforcement Learning Approach in the aim of optimizing the scheduling in Map Reduce Framework. The agent centric RL approach is extended in four dimensions: partitioning the task into map and reduce tasks based on the variable nature of nodes, minimizing the number of straggler tasks based on progress ratio and predicting to convert into a quicker one, XMPP based multi attribute query posting to identify the right node to process the straggler tasks, restructuring the cluster dynamically based on Hopkins statistical assessment. The agent in RL process plays an important role for minimizing the overall job completion time and effective resource utilization. We have tried to improve the accuracy of optimization by setting the tolerable limit to 30% and including the delays for progress ratio calculation. As a part of future work, other methodologies can be incorporated for variable partitioning and cluster restructuring to further improve the effectiveness in scheduling.

5. REFERENCES:

[1] Lena Mashayekhy, Mahyar Movahed Nejad, Daniel Grosu, Quan Zhang, Weisong Shi, "Energy-Aware Scheduling of MapReduce Jobs for Big Data Applications", IEEE Transactions on Parallel and Distributed Systems, vol. 25,September 2014.

[2] Liya Thomas, Syama R," Survey on MapReduce Scheduling Algorithms", International Journal of Computer Applications (0975 – 8887) Volume 95– No.23, June 2014.

[3] Zhuo Tang, Min Liu, Kenli Li, Keqin Li," An Optimized MapReduce Workflow Scheduling Algorithm for Heterogeneous Computing", The Journal of Supercomputing, Volume 72 Issue 6, June 2016,Pg no. 2059-2079.

[4] Joel Wolf, Deepak Rajan, Kirsten Hildrum, Rohit Khandekar, Vibhore Kumar, Sujay Parekh, Kun-Lung Wu and Andrey Balmin," FLEX: A Slot Allocation Scheduling Optimizer for MapReduce Workloads", ," in Proc. ACM/IFIP/USENIX 11th Int. Conf. Middleware, 2010, pp. 1–20.

[5] Jord`a Polo, Claris Castillo, David Carrera, Yolanda Becerra, Ian Whalley, Malgorzata Steinder2, Jordi Torres, and Eduard Ayguade," Resource-Aware Adaptive Scheduling for MapReduce Clusters", Proceedings of 12th International Middleware Conference, Lisbon, Portugal, pg no. 187-207 ,December 12-16, 2011.

[6] Matei Zaharia, Dhruba Borthakur, Joydeep Sen Sarma, Khaled Elmeleegy,Scott Shenker,Ion Stoica," Job Scheduling for Multi-User MapReduce Clusters", EECS Department University of California, Berkeley Technical Report No. UCB/EECS-2009-55,April 30,2009.

[7] R.Thangaselvi, S.Ananthbabu, R.Aruna," An Efficient Mapreduce Scheduling Algorithm in Hadoop", International Journal of Engineering Research & Science (IJOER), Vol-1, Issue-9, December, 2015.

[8] J. Ekanayake, H. Li, B. Zhang, T. Gunarathne, S.-H. Bae, J. Qiu, and G. Fox, "Twister: A runtime for iterative MapReduce," in Proc. 19th ACM Int. Symp. High Performance Distributed Computing, pg no.810–818,2010.

[9] A. Verma, L. Cherkasova, and R. H. Campbell, "ARIA: Automatic resource inference and allocation for MapReduce environments,"in Proc. 8th ACM Int. Conf. Autonomic Comput., 2011, pp. 235–244.

[10] Y. Song, Y. Sun, and W. Shi, "A two-tiered on-demand resource allocation mechanism for VM-based data centers," IEEE Trans. Services Comput., vol. 6, no. 1, pp. 116–129, Jan. 2013.

[11] M. Pastorelli, A. Barbuzzi, D. Carra, M. Dell'Amico, and P. Michiardi,"HFSP: Size-based scheduling for Hadoop," in Proc. IEEE Int. Conf. Big Data, 2013, pp. 51–59.

[12] Nenavath Srinivas Naik, Atul Negi, V. N. Sastry, "Performance Improvement of MapReduce Framework in Heterogeneous Context using Reinforcement Learning", 2nd International Symposium on Big Data and Cloud Computing,2015.

[13]Gayathri, Selvi and Kalavathi " An Efficient Performance and Monetary Cost Optimization on Resource Allocation in Cloud" International Journal of Innovative Science, Engineering & Technology, Vol. 2 Issue 5, May 2015.

PRINCIPAL.
K. S. R. INSTITUTE FOR ENGINEERING AND TECHNOLOGY,
K. S. R. KALVI NAGAR,
TIRUCHENGODE-637 215,
NAMAKKAL Dt. TAMIL NADU.

Authors Bibilography

S.Selvi is currently doing Ph. D. degree in the area of Cloud Computing in Anna University,Chennai and working as an Assistant Professor in the department of Computer Science and Engineering at Angel College of Engineering, Tirupur. She received her B.E. degree in 2002 and M.E. degree in 2009. Her area of interests includes Cloud Computing ,Compiler Design and Data Structures.

Dr. B. Kalaavathi received B.E. (Computer Science and Engineering) degree in 1993 from Bharathiyar University, M.Tech from Pondicherry University in 2000 and Ph.D from Periyar University in 2010. She is currently working as a Professor/Head in the Department of CSE in K.S.R. Institute for Engineering andTechnology,Tiruchengode. She has about 19 years of experience in teaching. She is a member of CSI & ISTE, INDIA. Her current areas of interest include Mobile Computing, Data Structures and Algorithms and Wireless Networks

PRINCIPAL.
K. S. R. INSTITUTE FOR
ENGINEERING AND TECHNOLOGY,
K. S. R. KALVI NAGAR,
TIRUCHENGODE-637 215,
NAMAKKAL Dt. TAMIL NADU.

APPENDIX DATA FLOW DIAGRAM OF AGERL ALGORITHM:

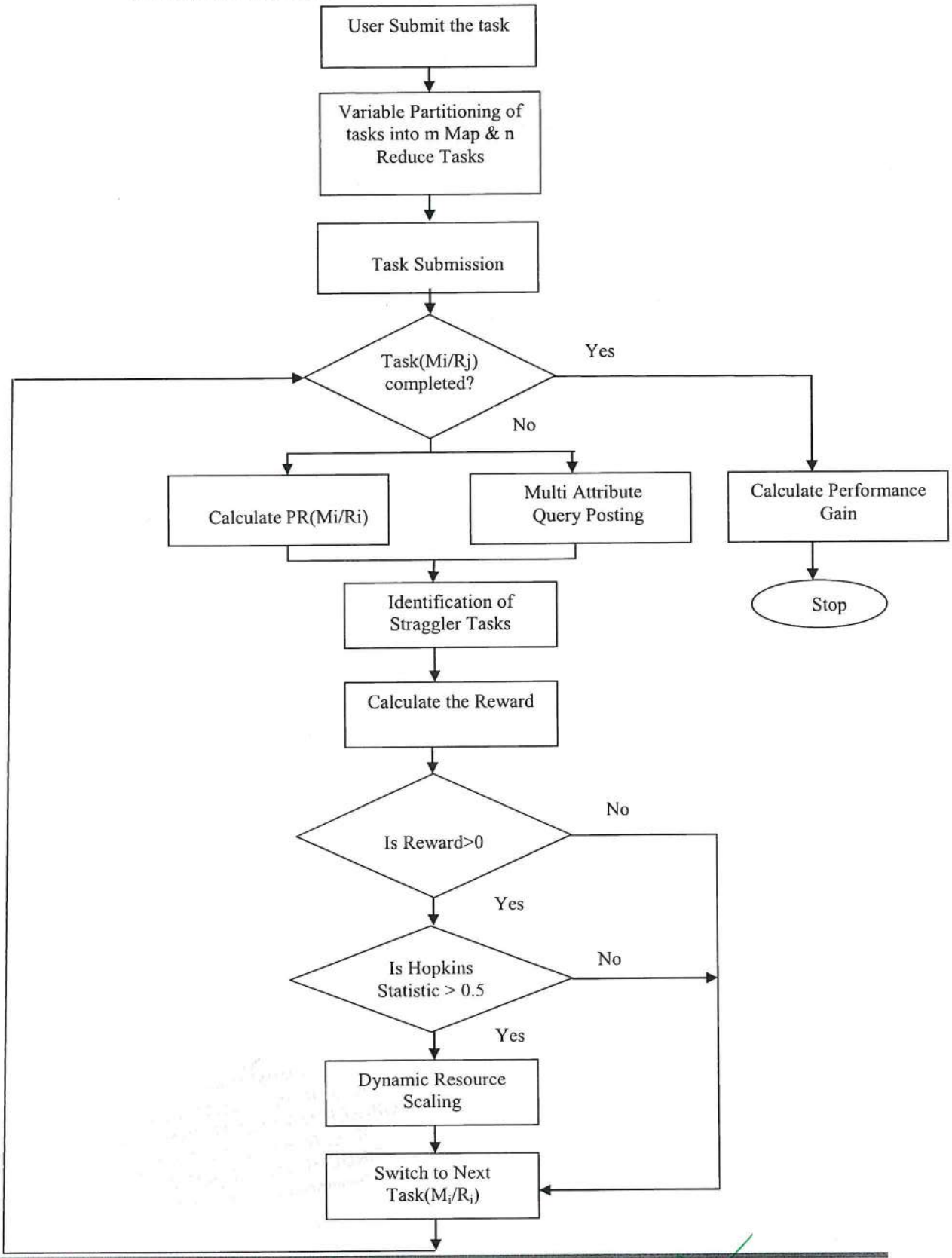

PRINCIPAL.
K. S. R. INSTITUTE FOR
ENGINEERING AND TECHNOLOGY.
K. S. R. KALVI NAGAR
TIRUCHENGODE-637 215,
NAMAKKAL DT, TAMIL NADU.

I J C T A, 9(2) 2016, pp. 1023-1034
© International Science Press

Enhanced Scheduling Approach Using Heuristics Flow Equilibrium Based Load Balancing Algorithm In Cloud

S. Selvi* and B. Kalaavathi**

ABSTRACT

Scheduling based on load balancing is a very big riddle in Cloud computing. Various techniques are available to optimize cloud scheduling so as to effectively utilize the cloud resources and thereby improving the response time of the users. Users on request for resources to execute their job, providers either allocate them a new Virtual Machine (VM) or an ideal existing Virtual Machine or schedule accordingly. Response time varies based on the distribution of load to the VMs. Though the load sharing is balanced statically, there may be unavoidable circumstances dynamically due to which load distribution becomes uneven. Many existing technologies are available to balance the load among the VMs, but still there are drawbacks and hence it is still in research. This paper proposes Heuristic Flow Equilibrium based Load Balancing (HFEL) algorithm to improve scheduling in the Cloud. HFEL algorithm would reduce the latency, reduce the response time and increase the throughput than compared to the existing systems

1. INTRODUCTION

Cloud is a massively using computing model in the internet world. Nowadays customers prefer cloud for doing their work, since it is a metered service. As the number of user requests increases, the challenges also gets increased which has to be solved by both the cloud providers and cloud users [1]. When the user submits the job to the providers, the provider analyzes the job, and checks the availability of resources. Then the provider assigns the tasks to the new virtual machines or to the existing one based on their load in a static manner [2].

Virtualization helps the providers to schedule the incoming tasks based on their needs. Each physical machine encompasses many virtual machines. Load balancing plays a significant role in the optimization of scheduling in Cloud. Scheduling gets optimized both in static and dynamic manner. Improved response time, increased resource utilization and achieving maximized QoS are the parameters to be concentrated in scheduling [3]. Though incoming loads are balanced among the virtual machines initially, there will be a high degree of unpredictability of resource utilization by the running tasks and there may be the over dump of new tasks to the overloaded machines which is a serious issue to be monitored and which may be the root cause for the deviation in the submission of results to the user, that leads to increase in the response time to the users than what he/she is expected. Balancing the loads helps in solving the above issue [4].

Load Balancing is achieved by migration of running tasks or infrastructure from heavy loaded machines to lightly loaded machines which will reduce the response time of the user. Migration is majorly classified into Process Migration and Live Migration [5]. Process Migration is further divided into Operating System migration, User level migration and Object based migration. Process Migration concentrates on the transferring of running tasks from higher tasks machine to a lower tasks machine, whereas Live Migration

* Assitant Professor/CSE, Angel College of Engineering and Technology, Tirupur, *E-mail: selviresearch@gmail.com*

** Professor & Head /CSE, K.S.R. Institute for Engineering and Technology, Tiruchengode.

PRINCIPAL,
K. S. R. INSTITUTE FOR
ENGINEERING AND TECHNOLOGY,
K. S. R. KALVI NAGAR,
TIRUCHENGODE - 637 215,
NAMAKKAL Dt, TAMIL NADU.

transfers the virtual infrastructure from one machine to another machine. Our work focuses on process migration. Heuristic Flow Equilibrium based Load Balancing algorithm is the proposed work of our paper to balance the load dynamically, thereby achieving the QoS of the user. HFEL uses indexing based mechanism to find out the heavy loaded and least loaded machines. Number of virtual machines included in the physical machine depends upon its level of configuration. Our paper considers on memory, bandwidth, speed, I/O access to determine the load of virtual machines.

2. RELATED WORK

Achievement of an efficient scheduling using load balancing is one of the approaches to provide an expected Qos for the users. Various researches have been undergone on load balancing among the virtual machines and it has to be done as a continuous process in order to reduce the response time of the users.XuChaoqun *et al.* [6] proposed a load balancing approach with key resource relevance(KRR) and they considered number of tasks, average waiting time and assignment of loads to the VMs as the primary factors for the optimization of scheduling in Cloud. The authors formerly divided the virtual resources in to groups by creating VMs and categorized on the basis of relevance between the user tasks and the priorities of the tasks are being calculated dynamically and then assigned to their appropriate VMs. The paper [7] sketched out Artificial Bee Colony(ABC) for balancing the load in Grid. The ABC algorithm tried to optimizes the algorithm based on the behavior of honey bee swarm. The makespan and deadlines are the constraints considered to achieve load balancing. Omer et. al. In his paper [8] took the challenge of running High Performance Computing (HPC) jobs in the virtual machines on the grid environment. The authors aimed at better provisioning of underlying resources and customization of execution environment at run time.

The paper [9] developed a deadline aware algorithm to reduce the job execution delays and thereby optimizing jobs dynamically to meet their job obligations. The algorithm encompasses training phase and steady phase in the scheduling model that not only maximizes the success rate of the jobs but also concentrating on the high utilization of virtual resources. The authors divided the user jobs based on unlimited deadlines and tight deadlines. Jobs with unlimited deadlines are those which are aimed to finish their jobs with no time constraints and not bothering about the virtualization overhead. Jobs with tight deadlines are those that are strictly adhered for the completion of their jobs with the prescribed deadline. The authors in [10] projects on two approaches for efficient resource management in a grid environment. First approach attempts on sub optimal scheduling based on prior information about local schedules and resource reservation status. Cyclic Scheduling Scheme was used for this approach. Backfilling approach was undertaken for the second approach to dynamically perform rescheduling with an aim to improve the overall resource utilization.Genetic algorithm based load balancing was undergone in Koushik et.al's paper[11] to make an optimal utilization of resources in a cloud environment. But the authors considered all the user's jobs were all of the same priority which would be impossible for all the cases ina real time environment. A survey paper of Karthik *et al.* [12] gave an overview on various background techniques of offloading computations in mobile systems.A monitoring tool [13] was proposed for KVM based virtual machines to identify bottlenecks among virtual machines and resource profiling with a motto of measuring the performance of KVM hosted web servers.

Grain size was the parameter considered to check the load balancing in the heterogeneous systems both in a static and dynamic environme nt. The authors in [14] presented a performance model to find out an optimal value of grain size and improve the performance in the context of sparse grid interpolation. A soft computing based load balancing was developed by the authors in [15] and they allocated the resources to the virtual machines based on the analysis of the properties of the tasks. Branko Radojevic [16] propose a decision making based load balancing approach for dividing the whole tasks into sub tasks using the session switching process. The session switching is done with the help of the round robin process. Ratan Mishra

PRINCIPAL,
K. S. R. INSTITUTE FOR
ENGINEERING AND TECHNOLOGY,
K. S. R. KALVI NAGAR,
TIRUCHENGODE - 637 215,
NAMAKKAL Dt, TAMIL NADU.

[17] uses the Ant Colony optimization technique for distributing the whole tasks into the different sub tasks which avoids the drawback of the heavy load in the network.

Martin Randles [18] uses the round robin techniques for dividing the process between processors. These divided processes are equal, but the job processing time is different from process to processors. This algorithm mostly used in the web servers and the services are distributed manually and equally. Yi Lua, [19] uses the power of medium approach for reducing the system overloads by applying the join idle queue process. Then the process manages the tasks and resources in the virtual machine.

3. DISCUSSION ABOUT DIFFERENT ALGORITHMS

In this section discusses the various discussions about the cloud load balancing algorithm like Join-idle Queue, Ant Colony Optimization algorithm and the decision making based queue process.

Join-Idle Queue based Load Balancing Algorithm

This algorithm uses the single shared queue and the jobs are waiting in the queue while one job completed in task it transfer into the next queue. If the server process one job then the other requested jobs need to wait in the idle queue. After completing the process of the particular job the next job is chosen according to the arrival time of the job. Then the arrival time is calculated as follows,

$$\frac{\lambda n}{m}.\rho.\frac{1}{r(1-\lambda)}=\frac{\lambda\rho}{(1-\lambda)} \tag{1}$$

Where λn is the job arrival rate in the queue.

$(1-\lambda)$ is the job proportional rate of the job in the queue.

Based on the job arrival rate it distributes to the different server for managing the load in the cloud environment.

Ant Colony Optimization based Load Balancing algorithm

Ant Colony Optimization is worked based on the behavior of the insects which have the limited amount of memory and large random components. The behavior of the insects used to estimate the shortest path while making the large trail in the optimization process. During the load balancing process, each task should be maintaining the probability table, source and destination point to manage the task while distribution. Initially the tasks are analyzed and the variables and the table has been initialized. Then the time of each task is calculated and the optimized solution has been determined using the minimum execution time of the task. The new task value is updated as follows,

$$X_{new} = \min \{f_{obj}(P_k)\}$$

Where k=1, 2, 3... K

After estimating the new task value the probability table value is updated simultaneously for assigning the tasks to each machine.

Round Robin Techniques based Load Balancing Algorithm

The next approach is Round Robin based load balancing technique which is applied in Honey Bee Foraging load balancing Algorithm. The algorithm uses the time for executing the particular task in which each task time is divided into the multiple slice based on the time scheduling process. The time is managed by using the bee optimization algorithm and the resources are allocated to the particular job. Based on the execution time the load is balanced in the distributed manner. These methods have some of the drawbacks like single

PRINCIPAL,
K. S. R. INSTITUTE FOR
ENGINEERING AND TECHNOLOGY,
K. S. R. KALVI NAGAR,
TIRUCHENGODE - 637 215,
NAMAKKAL DT, TAMIL NADU.

queue management system, time exists and so on. So the proposed system uses the Heuristic Flow Equilibrium based Load Balancing (HFEL) algorithm based approach for scheduling task in the cloud environment.

4. PROPOSED WORK

This section discusses the proposed scheduling algorithm based load balancing in the cloud environment. In cloud, load balancing placing an important role because several users request services simultaneously during that time collusion or some issues like response time increasing, the cost may be increased [20]. For this above issue scheduling based load balancing is used to distribute the resources with efficient manner. So, the proposed system uses the Heuristic Flow Equilibrium based Load Balancing (HFEL) approach for scheduling and distribute the work in the cloud environment. Then the proposed system architecture is shown in the figure 1.

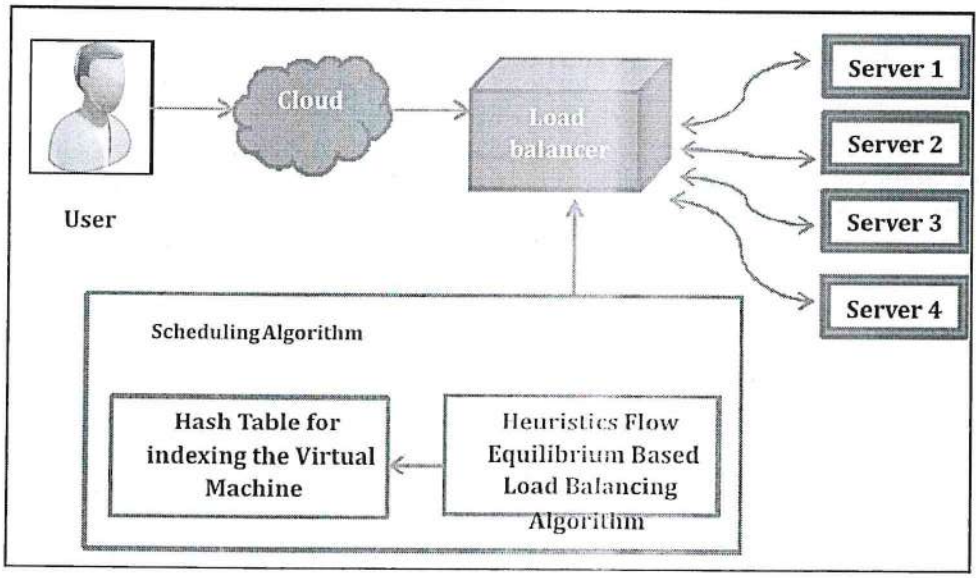

Figure 1: Proposed System Architecture

The above figure 1 explains that the working process of the proposed system. The cloud user request resources in the cloud environment. The related resources are fetched from the cloud service provider server and those services are balanced by the load balancer. The load balancer allocates, each process to the particular machine based on the scheduling algorithm. Then the step by step procedure of the Heuristics Flow Equilibrium Load Balancing algorithm is explained as follows.

Heuristics Flow Equilibrium Based Load Balancing Algorithm:

The proposed algorithm aims at optimizing the scheduling of incoming jobs by balancing the load among virtual machines throughout the execution of the tasks and thereby decreasing the response time of the users.

The algorithm uses the following heuristics:

- Number of virtual machines for each physical machine get varied based on its level of configuration.
- The incoming workflow is divided into sub tasks by considering the dependency relationship
- The sub tasks are then classified into simple, medium and complex based on their resource requirements
- Physical machines along with their virtual machines are identified for their lower, medium and higher configuration

PRINCIPAL,
K. S. R. INSTITUTE FOR
ENGINEERING AND TECHNOLOGY,
K. S. R. KA[illegible] NAGAR,
TIRUCH[illegible]DE - 637 215,
NAMAKKA[illegible] TAMIL NADU.

- Each virtual machine is assumed to have resources such as memory, bandwidth capacity, speed and I/O access.

Each physical machine maintains an index that contains name of the virtual machine, number of tasks allocated to it, execution status of the virtual machines, resource status, utilization status and so on. The index table gets updated whenever a virtual machine is removed from physical machine or a new virtual machine is added to the physical machine. The execution status of every task is also updated in the table.

The incoming workflow is divided into subtasks and a classifier is used to classify the tasks based on its interdependency, complexity of the tasks and resource requirements. The tasks are divided based on the execution time and the minimum execution time tasks are grouped.The classified tasks are made into groups based on its level of complexity, dependency, etc and their loads are calculated. Then they are scheduled accordingly to the virtual machines group. A load balancer is used to perform the following operations:

(i) Calculate the capacity of each virtual machine and determine the cumulative total capacity

(ii) Update the indexes of each virtual machine when a new task is being assigned or completed tasks is removed from the VM.

(iii)Determine whether there is an exceed in the load of VMs when compared to their tolerable capacity and also check whether there is a load imbalance between virtual machine groups. Then the working flow of the load balancing process is shown as follows,

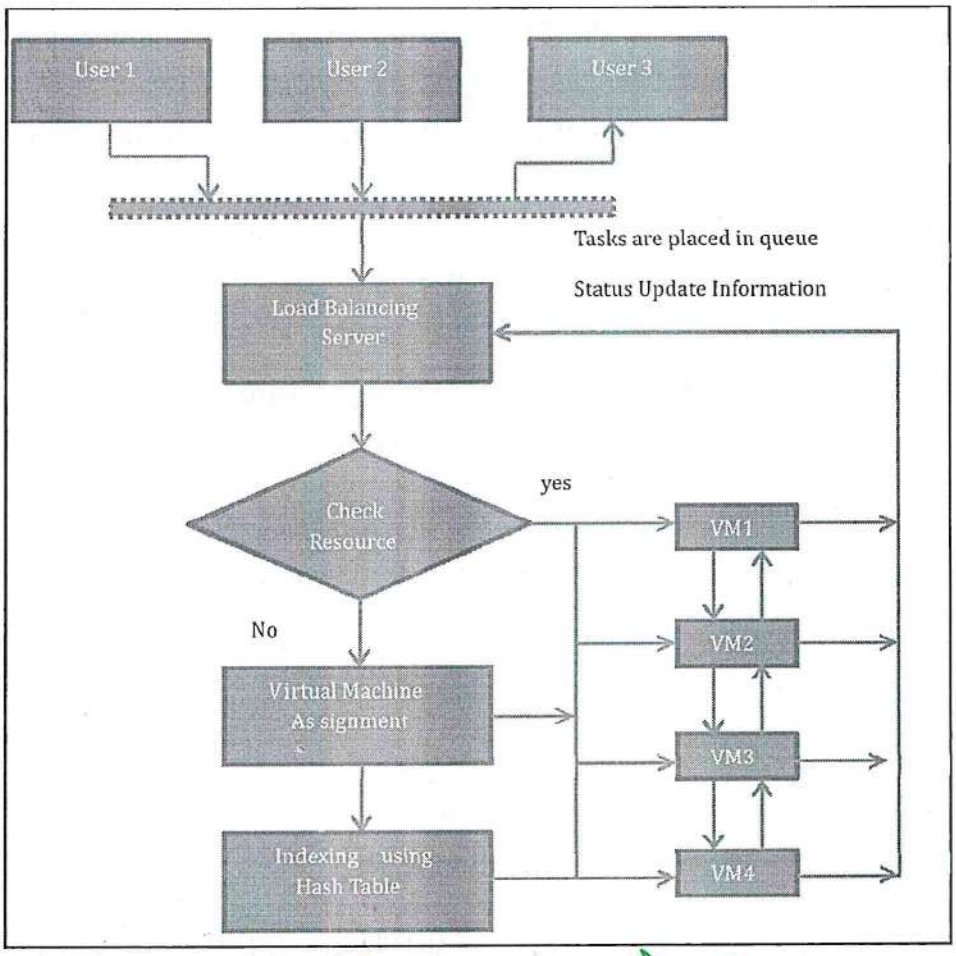

Figure 2: Load Balancing Workflow

PRINCIPAL,
K. S. R. INSTITUTE FOR
ENGINEERING AND TECHNOLOGY,
K. S. R. KALVI NAGAR,
TIRUCHENGODE - 637 215,
NAMAKKAL Dt, TAMIL NADU.

The figure 2 describes the flow of virtual machine assignment based on hash table indexing and load balancing.Here the user tasks are placed in the queue and assigned to the virtual machine by using the hash indexing table. During the assignment, the resources availability of the virtual machine should be estimated.Based on the resource particulars, virtual machine has been identified and the resources are assigned to that virtual machine for reducing the response time. Then the scheduling and load balancing process is explained by using the following algorithm.

Algorithm for Heuristics Flow Equilibrium Based Load Balancing Algorithm

Input: Set of Incoming tasks T{T_1, T_2, T_3,...T_n } and set of Physical Machines having VirtualMachineM as {$P_1(VM_1,VM_2,VM_3,...VM_n$} and $P_2(VM_{n+1},VM_{n+2},...VM_m)$}

Output: Every incoming task *i* optimally assigned to thevirtual machines there by balancing the load dynamically.

Procedure:

Step 1: Classify the incoming tasks into n subtasks

Step 2: Group the sub tasks based on its dependency and complexity

Step 3: For every group of tasks, calculate the load,

do

{

$L_{VMi} = \frac{N(T,t)}{VM_{bwj}(t)}$ (Load balancing of each virtual machine)

Then calculate the resource utilization of the virtual machine

$R(T_i) = ET_i * \left[\frac{(m*R_K)}{m}\right]$ (Resource Utilization of each virtual machine)

}

Step 4: Allocate the task to virtual machine according to minimum load balanced and minimum resource utilization VM.

Mathematical Model to Calculate The Load Value and Resource Utilization

Let us consider an ordered set of m virtual machines as VM=(VM_1,VM_2,VM_3,...VM_n} and a set of n incoming tasks as T={T_1, T_2, T_3,...T_n}. Let us take Gmax as the maximum throughput obtained during the execution of tasks and ET_{ij} be the Execution Time for task T_i and Virtual Machine VM_j.

Execution Time of all tasks in VM_j can be calculated by the formula,

$$ET_j = \Sigma_{i=1}^{n} ET_{ij} \text{ (j lies between 1 to m)} \quad (1)$$

Throughput can be calculated by the following formula,

$$Gmax = \{\max_{i=1} CT_i, \max_{j=1} \Sigma_{i=1} ET_{ij}\} \quad (2)$$

where the first component gives the completion time of task i,

the second component gives the execution time of VMj in task i.

In addition the capacity, load, resource utilization, execution time and variance of the virtual machine has been calculated for determining the virtual machine allocation process which calculated as follows,

PRINCIPAL,
K. S. R. INSTITUTE FOR
ENGINEERING AND TECHNOLOGY,
K. S. R. KALVI NAGAR,
TIRUCHENGODE - 63
NAMAKKAL Dt, TAMIL NA

Capacity of VM_j

$$C_j = P_{nj} * P_{mips_j} + VM_{bwj} * VM_{i/o} \tag{3}$$

Where,

P_{nj} – Number of Processors in VM_j

P_{mips_j} – Million Instructions per second of all processors in VM_j

VM_{bwj} – Communication Bandwidth ability of VM_j

$VM_{i/o}$ -I/O Contention of VM_j

Overall Capacity of all active VMs

$$C = \Sigma_{i=1} C_i \tag{4}$$

where,

C_i – is the value of active VM_i calculated in *Eq. 3*

Load Calculation on a single VM

Total Length of tasks assigned to VM is given by,

$$L_{VMi,t} = \frac{N(T,t)}{VM_{bwj}(t)} \tag{5}$$

$N(T, t)$ – Number of tasks active at time 't' on service queue of VM

$VM_{bwj}(t)$ - Communication bandwidth of VM_j at time 't'

Load Calculation of all active VMs

$$L = \Sigma_{i=1}^{m} L_{VMi} \tag{6}$$

Execution Time of a Single VM

Now the Execution Time of a Single VM can be calculated as,

$$ET_i = \frac{L_{VMi}}{C_i} \tag{7}$$

Execution Time of all active VMs

Therefore, the Execution Time of all active VMs can be calculated as,

$$ET = \frac{L}{C} \tag{8}$$

Variance Calculation of Load

$$\sigma = \sqrt{\frac{1}{m} * \Sigma_{i=1}^{m} (ET_i - ET)^2} \tag{9}$$

PRINCIPAL,
K. S. R. INSTITUTE FOR
ENGINEERING AND TECHNOLOGY,
K. S. R. KALVI NAGAR,
TIRUCHENGODE - 637 215,
NAMAKKAL Dt, TAMIL NADU.

$$Variance V = \left(\frac{1}{m} * (ET_i - ET)^2 \right) \tag{10}$$

Overall Resource Utilization

$$R(T_i) = ET_i * \left[\frac{(n * R_k)}{m} \right] \tag{11}$$

$R(T_i)$ – Resources utilized for Task T_i

n- Number of Virtual Machines

R_k – Number of units of resources available in VM

m - Units of Resources that each server has

ET_i -Execution Time of Task i

Thus the proposed Heuristics Flow Equilibrium Based Load Balancing Algorithm schedule the job to various users with minimum response time and minimum resource utilization. Then the overall load of the particular virtual machine also reduced because it divides the whole task into sub tasks which lead to increase in the throughput of the load balancer. The performance of the proposed system is evaluated by using the experimental result and discussion.

5. PERFORMANCE ANALYSIS

This section discusses about the performance analysis of the proposed Heuristics Flow Equilibrium Based Load Balancing Algorithm using the execution time of the virtual machine, response time, throughput metrics. The experiments are carried out in Java based implementation and the virtual machines are chosen according to the data centers. Then the RAM, hard disks are selected and the resources are provided based on the task execution time. The table 1 represent that the overall performance analysis of the proposed system with several existing methods [21] such as Central Load Balancing Decision Module (CLBDM), Ant Colony Optimization Based Load Balancing Algorithm (ACO), Honeybee Foraging load balancing Algorithm (Honey Bee Foraging) and Join Idle Queue Load Balancing Algorithm (JIQ).

Table 1
Representation of Performance of the Load Balancing Algorithm in Cloud

Performance Metrics	*CLBDM*	*ACO*	*Honeybee Foraging*	*JIQ*	*HFEL*
Throughput	High	Low	Low	Moderated	High
Speed	Moderated	Low	Moderated	Low	High
Complexity	Moderated	High	Moderated	High	Low
Fault Tolerance	Low	High	Moderated	Low	High
Response Time	High	Moderated	Low	Moderated	Low
Performance	Moderated	Low	Moderated	Low	High

The above table 1 clearly shows that the proposed system provides the optimized results when compared to the other load balancing algorithms. The response time of the proposed load balancing algorithm is listed in the table 2.

PRINCIPAL,
K. S. R. INSTITUTE FOR
ENGINEERING AND TECHNOLOGY,
K. S. R. KALVI NAGAR,
TIRUCHENGODE - 637 215,
NAMAKKAL Dt, TAMIL NADU.

Table 2
Response Time of the Different Load Balancing Techniques

Load Balancing Techniques	*Response Time (ms)*
CLBDM	5.36
ACO	4.16
Honey Bee	3.47
Foraging	2.01
JIQ	1.34
HFEL	0.33

The graph representation of the proposed system response time is shown in the figure 3.

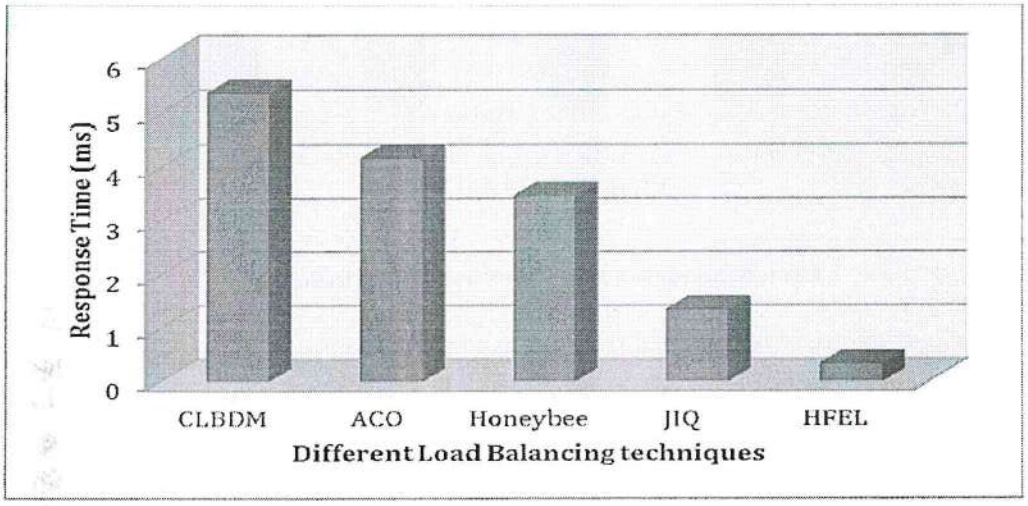

Figure 3: Response Time of the Different Load Balancing Techniques

The above figure 2 clearly shows that the proposed system consumes minimum time which means the algorithm produces the resources with minimum time when compared to other load balancing algorithm. Then the throughput of the proposed system is increased which is shown in the figure 4.

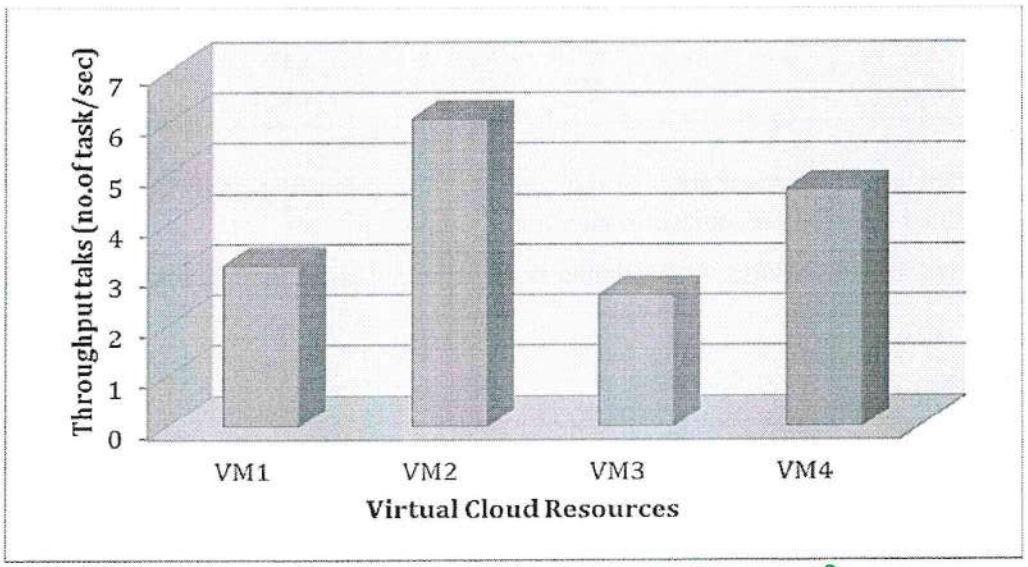

Figure 4: Throughput of the Virtual Cloud Resources

PRINCIPAL,
K. S. R. INSTITUTE FOR
ENGINEERING AND TECHNOLOGY,
K. S. R. KALVI NAGAR,
TIRUCHENGODE - 637 215,
NAMAKKAL Dt, TAMIL NADU.

Thus the figure 4 explains that the throughput of the different virtual resource on various tasks which produces the highest throughput when compared to the different virtual machines. Based on the resources the scheduling utilization is explained in the figure 5.

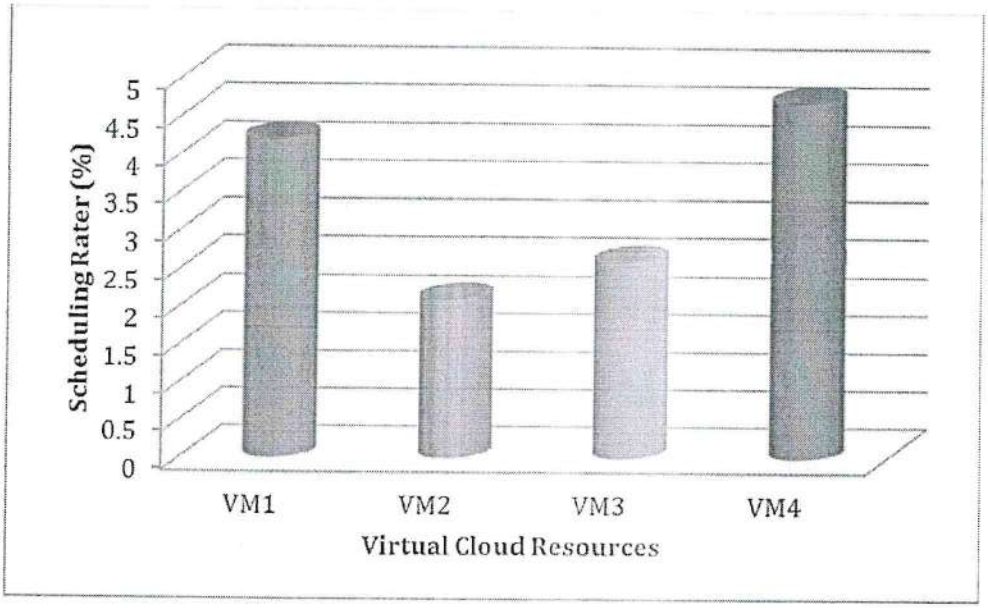

Figure 5: Scheduling Rate of the Virtual Cloud Resources

The figure 5 shows that the VM4 has high scheduling rate (97%) than compared to the other virtual machines which means that the tasks are effectively utilized by the VM4 for every resource. Based on the scheduling rate, response time, the task resource utilization rate is shown in following table 3.

Table 3
Resource Utilization Rate

Tasks	*Resource Utilization Rate*			
	VM1	*VM2*	*VM3*	*VM4*
T1	1.3	2.36	3.65	2.3
T2	2.6	1.35	4.39	3.14
T3	3.7	3.48	5.47	4.01
T4	4.01	3.47	4.36	5.46

Finally, the related graph representation of the resource utilization rate of different virtual machine using the proposed load balancing technique is shown in the figure 6

Thus the proposed system ensures the minimum response time based load balancing approach in the cloud environment.

6. CONCLUSION

Thus the paper discusses the proposed Heuristics Flow Equilibrium Based Load Balancing Algorithm for scheduling the various tasks to the different virtual machines in the cloud environment. The Heuristic method indexed each virtual machine based on the hash table which is used to schedule the process. During the scheduling process, each task is subdivided into different groups and the complexity, resource utilization of the virtual machine is estimated. Based on the complexity and resource utilization the task is allocated to

PRINCIPAL,
K. S. R. INSTITUTE FOR
ENGINEERING AND TECHNOLOGY,
K. S. R. KALVI NAGAR,
TIRUCHENGODE - 637 215,
NAMAKKAL Dt, TAMIL NADU.

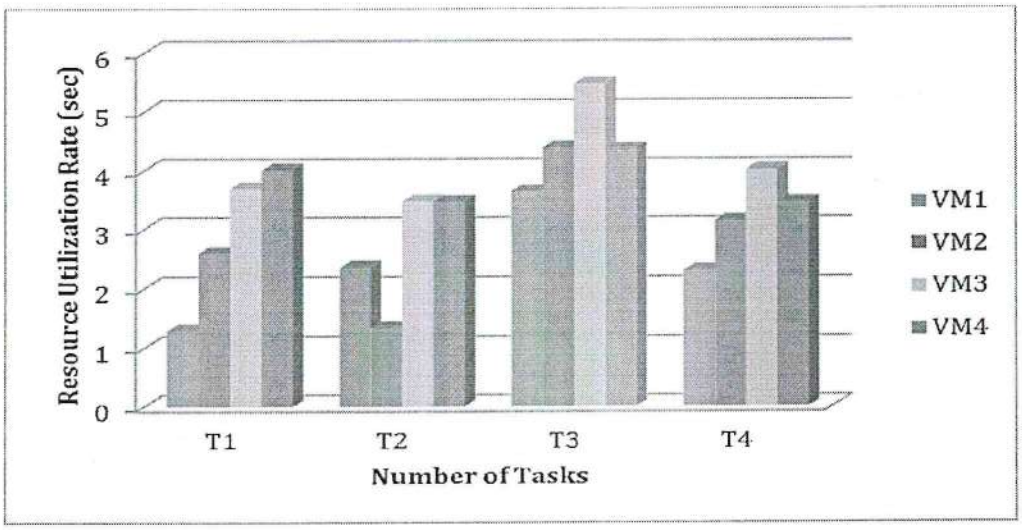

Figure 6: Resource Utilization Rate

the virtual machine with minimum response time. Thus the heuristic approach schedules the task and effectively utilizes the cloud resources and improves the response time of the users. Then the performance of the system is evaluated using the response time, average throughput and scheduling rate. Thus the proposed system consumes minimum response time 0.33 ms and the task scheduled rate is 97% when compared to the existing methods. This enhanced scheduled rate helps the tasks to utilize the virtual machines in an effective manner.

REFERENCES

[1] Mayanka Katyal, Atul Mishra, "A Comparative Study of Load Balancing Algorithms in Cloud Computing Environment", Article can be accessed online at *http://www.publishingindia.com.*

[2] Abhijit A. Rajguru, S.S. Apte, "A Comparative Performance Analysis of Load Balancing Algorithms in Distributed System using Qualitative Parameters", *International Journal of Recent Technology and Engineering (IJRTE)* ISSN: 2277-3878, Volume 1, Issue 3, August 2012.

[3] Zhang Bo, Gao Ji ; Ai Jieqing, "Cloud Loading Balance algorithm" *International Conference on Information Science and Engineering in IEEE* 2010.

[4] Domanal, Reddy, "Optimal load balancing in cloud computing by efficient utilization of virtual machines" *International Conference on Communication Systems and Networks in IEEE* 2014.

[5] Domanal, Reddy, "Load Balancing in Cloud Computing using Modified Throttled Algorithm" IEEE International Conference on Cloud Computing in Emerging Markets, 2013.

[6] XuCh aoqun, ZhuangYi and ZhuWei," A Load Balancing Algorithm with Key Resource Relevance for Virtual Cluster" (2013) ,Vol 6, No. 5 *International Journal of Grid and Distributed Computing,* pp 1-16.

[7] Preeti Gulia and Deepika Nee Miku," Analysis and Review of Load Balancing in Grid Computing using Artificial Bee Colony" (2013), *International Journal of Computer Applications* (0975 – 8887), Volume 71– No. 20,

[8] Omer Khalid, Ivo Maljevic, Richard Anthony," Dynamic Scheduling of Virtual Machines Running HPC Workloads in Scientific Grids"(2009), IEEE.

[9] Stelios Sotiriadis, Nik Bessis, Pawel Gepner, Nicolas Markatos "Analysis of requirements for virtual machine migration in dynamic clouds".

[10] Victor Toporkov, Anna Toporkova, Alexey Tselishchev, Dmitry Yemelyanov, and Petr Potekhin,"Preference-Based Fair Resource Sharing and Scheduling Optimization in Grid VOs",(2014),Elseveir, ICCS 2014. 14th International Conference on Computational Science, Volume 29, 2014, PP 831–843.

[11] Kousik Dasgupta, Brototi Mandal, Paramartha Dutta, Jyotsna Kumar Mondal,Santanu Dam, "A Genetic Algorithm (GA) based Load Balancing Strategy for Cloud Computing", Elseveir, International Conference on Computational Intelligence: Modeling Techniques and Applications,(CIMTA) (2013).

PRINCIPAL,
K. S. R. INSTITUTE FOR
ENGINEERING AND TECHNOLOGY,
K. S. R. KALVI NAGAR,
TIRUCHENGODE - 637 215,
NAMAKKAL DT. TAMIL NADU.

[12] Karthik Kumar, Jibang Liu, Yung-Hsiang Lu, Bharat Bhargava, "A Survey of Computation Offloading for Mobile Systems", © Springer Science+Business Media, LLC 2012, Mobile Netw Application, DOI 10.1007/s11036-012-0368-0.

[13] Ankit Anand, Mohit Dhingra, J. Lakshmi, S. K. Nandy ," Resource usage monitoring for KVM based virtual Machines".

[14] Alin Murara_su, Josef Weidendorfer, and Arndt Bode," Workload Balancing on Heterogeneous Systems: Case Study of Sparse Grid Interpolation".

[15] Brototi Mondal, Kousik Dasgupta, Paramartha Dutta, "Load Balancing in Cloud Computing using Stochastic Hill Climbing-A Soft Computing Approach", *Procedia Technology* 4 (2012) 783–789.

[16] Branko Radojevic, Mario Žagar, "Analysis of Issues with Load Balancing Algorithms in Hosted (Cloud) Environments", available at., *https://bib.irb.hr/datoteka/536452.MIPRO_-_LB_v3.pdf*

[17] Ratan Mishra and Anant Jaiswal, "Ant colony Optimization: A Solution of Load balancing in Cloud", *International Journal of Web & Semantic Technology* (IJWesT) Vol.3, No.2, April 2012.

[18] Martin Randles, Enas Odat, David Lamb, Osama Abu- Rahmeh and A. Taleb-Bendiab, "A Comparative Experiment in Distributed Load Balancing", 2009 Second International Conference on Developments in eSystems Engineering.

[19] Yi Lua, Qiaomin Xiea, Gabriel Kliotb, Alan Gellerb, "Join-Idle-Queue: A Novel Load Balancing Algorithm for Dynamically Scalable Web Services, *http://research.microsoft.com/pubs/153348/idleq.pdf.*

[20] Omer Khalid, Ivo Maljevic, Richard Anthony ,"Deadline Aware Virtual Machine Scheduler for Grid and Cloud Computing" IEEE 24th International Conference on Advanced Information Networking and Applications, 2010.

[21] Dharmesh Kashyap, Jaydeep Viradiya, "A Survey Of Various Load Balancing Algorithms In Cloud Computing", *International Journal of Scientific & Technology Research*, Volume 3, Issue 11, November 2014.

PRINCIPAL,
K. S. R. INSTITUTE FOR
ENGINEERING AND TECHNOLOGY,
K. S. R. KALVI NAGAR,
TIRUCHENGODE - 637 215,
NAMAKKAL DT, TAMIL NADU.

Asian Journal of Information Technology 15 (17): 3182-3195, 2016
ISSN: 1682-3915
© Medwell Journals, 2016

Attack Resistant Analysis Using Secure Singular Value Decomposition and Markov Random Field Based on Rotation Scaling Transformation Invariant Image Watermarking for Video Frames

[1]S. Poongodi and [2]B. Kalaavathi
[1]Department of ECE, K.S.R. College of Engineering
[2]Department of CSE, K.S.R Institute for Engineering and Technology,
Anna University, Chennai, Tamil Nadu, India

Abstract: This research proposes a novel video watermarking model for video frames based on Rotation Scaling Transformation (RST). Most of the available watermarking methods utilize image processing techniques to execute the watermarking task. This proposal adopts a K Dependency Bayesian (KDB) Model for the approximation of the frames according to probability values. In the study presented, video frames are segmented using the Markov Random Field (MRF) segmentation technique where KDB represents every part of the frame region. Singular Value Decomposition (SVD) is used for encryption of the selected feature points. The encrypted areas located at the feature points are utilized for watermark embedding and extraction. During the stage of embedding, the text files are converted into a matrix. Both the matrices are then merged using the sum of the matrices. The watermark embedding strength is adapted according to the noise visibility function and the analysis of the probability of error is performed mathematically. Simultaneously, the watermark embedding and extraction techniques are assessed based on a proven mathematical model. Experimental results prove that the proposed MRF-SVD video watermarking method performs better in terms of invisibility and robust behavior in comparison to the previous methodologies under potential attacks such as cropping, rotation, scaling, sharpening and Gaussian noise in case of videos.

Key words: Rotation Scaling Transformation (RST), K Dependency Bayesian (KDB) Model, Marko Random Field (MRF) segmentation technique, Singular Value Decomposition (SVD), watermark embedding and extraction techniques

INTRODUCTION

The fast growth of new information methodologies has enabled easy access to digital information. On the other hand, it has also worsened the issue of illegal copying and redistribution of digital media. The technique of digital watermarking was introduced when there were attempts made to resolve issues in relation to the intellectual property rights of media management. A digital image watermarking scheme must be effective enough to tackle a variety of potential attacks. Geometric distortions pose more difficulty in thwarting in comparison to other types of attacks. The technology of digital watermarking was put into application when trying to resolve the troubling issues associated with the management of intellectual property of digital products (Zheng *et al*., 2007).

A watermark is a digitized code which is implanted into the digital cover content i.e., text, audio or video sequence. Digital video is basically a collection of sequential still images. A watermark can be used to carry any kind of data but the amount of the data that it can carry is limited. The amount of information that can be embedded into the video is referred to as payload. The level of vulnerability of information increases in proportion with the amount of the information a watermark carries. Again, the amount of information that a watermark can carry is purely restrained by the size of a specific video sequence. Watermarking gives more preference to robustness rather than capacity. Hence, a watermark basically carries tens to thousands of concealed data in bits per video frame (Jayamalar and Radha, 2010).

Digital watermarking is found to be an efficient solution to the issues of multimedia video frames and data authentication. Myriad of geometric invariant algorithms have been put forward in the last few years (Zheng *et al*., 2007). Digital image watermarking technologies can be classified into three important categories: implanting the

Corresponding Author: S. Poongodi, Department of ECE, K.S.R. College of Engineering, Anna University, Chennai, Tamil Nadu, India

PRINCIPAL.
K. S. R. INSTITUTE FOR
ENGINEERING AND TECHNOLOGY,
K. S. R. KALVI NAGAR,
TIRUCHENGODE-637 215,
NAMAKKAL Dt, TAMIL NADU.

watermark in the geometric invariant domain (Zheng *et al*., 2007); implanting a template along with the watermark (Zheng *et al*., 2007) and implanting the watermark on the basis of feature selection techniques which in the recent times has shown good performance with respect to robustness (Seo and Yoo, 2006; Zheng *et al*., 2009).

A strategy for the detection of watermarks after geometric distortion is the identification of the distortions and the application of inverse transform before watermark extraction. This can be performed by embedding a template along with the watermark (Fouda, 2015) into the cover image. Researchers have proposed embedding of two watermarks, a template and a spread spectrum message which contains the information or payload. The template comprises no data by itself but is utilized for detection of the transformations made to the watermarked image. This type of template is suitable for all images. However, it has the limitation of being easy to remove as the template generally corresponds to peaks in a transform domain. This fact may increase conniving attempts to reveal the registration pattern and, after its discovery; the removal of registration pattern from the watermarked image could be done, thus posing a restriction on the reversible capability of any geometric distortions.

Nowadays, most of the watermarking schemes exhibit poor performance against geometrical attacks. The general geometrical attacks are rotation, flipping, translation, aspect ratio changes, resizing and cropping. Watermarking schemes apply several synchronization techniques for handling geometrical attacks. These approaches generally attempt to identify the geometrical distortions and reverse them before the watermark detector is made use of. The identification of the geometrical distortions is accomplished by the examination of a registration pattern embedded along with the watermark in the host image (Coria *et al*., 2007). However, the addition of the registration pattern to the data-carrying watermark decreases the fidelity of the watermarked image in addition to the scheme's capacity. Another drawback of this technique is that, generally all the watermarked images carry the same registration watermark. Hence, it is an easy task to detect the registration watermark through illegal attempts. Once the registration pattern is found, it could be removed from all the watermarked images, thus limiting the chances of the invertibility of any geometric distortions. In addition, these techniques increase the computational time considerably and in few cases their performance is poor. This issue is resolved by using the feature points based watermarking scheme which again performs the detection of the attacks against geometric properties.

Recently researches have put forward a digital video watermarking scheme (Yuan and Pun, 2013) which is efficient to geometric distortions, such as rotation, scaling and cropping. The embedding/extraction of the watermark is based on feature selection and local Zernike transform in/from each selected frame. The feature selection technique called Adaptive Harris Detector which follows the revised traditional Harris Corner Detector and the local Zernike moments-based technique is used for watermarking. In each selected frame, the selected circular patches are broken down into a collection of binary patches with Bit-Plane Decomposition method. It has been established that the selected feature points can subsist a wide range of attacks and can be used as reference points for both watermark embedding and extraction. Results obtained from experiments show that the performance of the watermarking technique is not up to the mark against sharpening and noise in the attack. It can also be inferred from these experiments that the removal of feature point's noise is not performed precisely, if the watermarked image undergoes distortions and geometrical transforms. Significant improvement cannot be obtained even with higher order moments calculation.

A new video watermarking technique was proposed on the basis of the rotation invariant feature and image normalization to resolve the problems quoted above. The K-Dependence Bayesian (KDB) image segmentation technique has been applied for segmentation of the video frames image into several homogeneous areas. One feature point is selected using Markov Random Field (MRF) for each region. These points are strong against rotation, scaling and cropping. Rotation of the area is done for every feature points disk, to align it with the feature point. Then image normalization is used to transform the disk region to its compact size which is scale invariant. After the rotation and scaling of video frame samples, the encryption of video frame content is done using Singular Value Decomposition (SVD). Using these techniques, the security of video content is assured, watermark embedding and extraction is done. In watermarking embedding stage the encryption of the snapshots and text file of the question paper to video frames is performed, then attack resistance is conducted for embedded watermarked video frame image. A mathematical model is very important for the analysis of the watermarking process. The estimation of KDB parameters is done using MRF. The adaptive adjustment of the quality of the embedded video watermarked image samples is done based on the characteristics of the embedding region, by using noises. The results are figured based on the PSNR and MSE.

PRINCIPAL.
K. S. R. INSTITUTE FOR
ENGINEERING AND TECHNOLOGY,
K. S. R. KALVI NAGAR,
TIRUCHENGODE-637 215,
NAMAKKAL Dt, TAMIL NADU.

Literature review: Mirza *et al.* (2007) have suggested a digital video watermarking approach based on Principal Component Analysis (PCA). An undetectable watermark is embedded into the three different RGB channels of the video frame using PCA transform in isolation. The chief advantage of this technique is that the same or multi-watermark can be implanted into the three color channels of the image for increasing the robustness of the watermark. The usage of PCA transform helps in the choice of the desirable substantial components into which to embed the watermark. The results from previous experiments demonstrate a high degree of reliability against the general video attacks, especially frame dropping, cropping and rescaling for a good quality perception.

Al-Taweel and Suma (2009) have introduced a new DWT-based video watermarking algorithm on the basis of a three level DWT making use of Haar filter which is again efficient against geometric distortions such as Downscaling, Cropping and Rotation. It is also very reliable against image processing attacks such as Low Pass Filtering (LPF), Median filtering and Weiner filtering. Moreover, the algorithm is strong against Noise attacks such as Gaussian noise, Salt and Pepper attacks. The embedded data rate is high and it is less prone to attacks. It has been observed from the experimental results that the embedded watermark is hard and not seen.

Mostafa *et al.* (2009) presented a new method for a binary logo watermark embedding into video frames. Discrete Wavelet transform is performed on every video frame. PCA is then applied to each block of the two bands (LL-HH). The watermark is embedded into the principal components of the LL blocks and HH blocks in many ways. The test results depict that there is no easily observable difference between the watermarked frames and the original frames and show the efficiency against a wide range of attacks such as MPEG coding, JPEG coding, Gaussian noise addition, histogram equalization, gamma correction, contrast adjustment, sharpen filter, cropping, resizing and rotation. Combination of the two transforms help in the improvement of the performance of the watermark algorithm.

Bhatnagar and Raman (2012) introduced a Wavelet Packet Ttransform (WPT)-based robust video watermarking algorithm. A visible comprehensive binary image is used as the watermark. In the first stage, frames in sequence are extracted from the video clip. The WPT algorithm is then employed on each frame and from each orientation, selection of one sub-band is done on the basis of block mean intensity value called robust sub-band. The embedding of Watermark is done in the robust sub-bands according to the relationship between wavelet packet coefficient and its 8-neighbour (D8) coefficients taking into consideration the robustness and invisibility. Experimental results prove the robustness and the better performance of the algorithm and in comparison with other available algorithms in the literature.

A real-time video watermarking technique (Wang *et al.*, 2011) against geometric distortions has been suggested for DCT-encoded compressed video data. The full DCT coefficients have been established to be unvarying to scaling and local geometric attacks. Hence, watermarks are embedded into Watermark Minimal Sequences (WMS) by the modulation of the low-frequency full DCT coefficients. To satisfy the needs of real-time performance, a fast inter transformation is applied for the construction of full DCT obtained directly from block DCTs. The changes of full DCT coefficients are applied to inverse transformation of the differences of block DCT coefficients that are added in subsequent steps to the original block DCTs for the generation of the WMS. The technique can withstand rotation attacks with the employment of a rotation compensation strategy.

An adaptive blind video watermarking technique (Park *et al.*, 2006) using video characteristics according to the Human Visual System (HVS) in three-dimensional discrete cosine transform (3D-DCT) domain has been proposed. The patterns of 3D-DCT cubes and the types of video segments are classified for the optimization of the weight factors for watermarking. Classification utilizes the texture and motion information of 3D-DCT cubes. An optimized watermark is embedded into the mid-range coefficients of 3D-DCT cubes with the help of trained optimal weight factors. The results obtained from experiments prove that the proposed method offers good performance in the presence of various potential attacks such as MPEG compression, frame dropping, frame insertion and frame swapping with respect to invisibility and robustness than the techniques in prevalence before.

A new robust video watermarking system on the basis of Hidden Markov Model (HMM) and Artificial Neural Network (ANN) (Elbasi, 2007) has been developed. The suggested watermarking approach splits the video sequences into Group of Pictures (GOP) with HMM. Parts of the binary watermark have been embedded into each GOP with a chosen transformation domain watermarking algorithm. ANN constructs the optimal transformation algorithm for each corresponding GOP. The embedding procedure is the standard additive algorithm in low and high frequencies in varied transformation domains.

MATERIALS AND METHODS

Proposed video file is secured using SVD with markov random field watermarking scheme and attack resistant analysis: This research work introduces a new attack tolerant analysis schema for video watermarking image. Initially the video file is given as input for the original

PRINCIPAL,
K. S. R. INSTITUTE FOR
ENGINEERING AND TECHNOLOGY,
K. S. R. KALVI NAGAR,
TIRUCHENGODE-637 215,
NAMAKKAL Dt. TAMIL NADU.

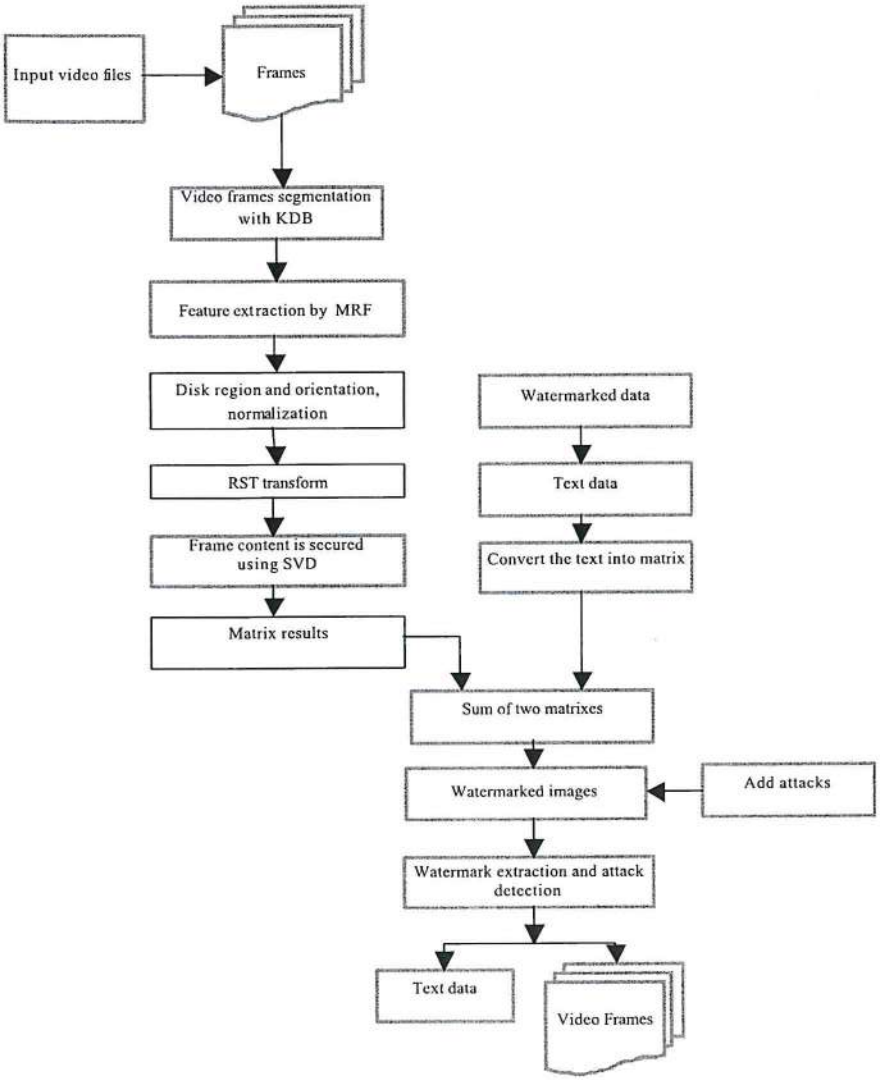

Fig. 1: Architecture of the proposed system

image. The conversion of video files into frames takes place next. Random selection of any one frame in the video file is done, then the frame is segmented into a number of homogeneous parts and the feature points are selected. The frames in the video files are segmented on the basis of K-Dependence Bayesian (KDB). The circular areas for watermark embedding or extraction are then determined. The rotation, scaling and translation invariant areas can be used for watermark embedding and extraction on the basis of the image normalization and orientation assignment. The segmented image is simulated as Markov Random Field of mathematical analysis for various features of the watermarking processes such as embedding strength adjustment. Encryption is done to provide more security to video frames. Encryption is done using the Singular Value Decomposition (SVD). The encrypted output is given as input to the watermarking process. There are four important parameters which are generally utilized for the determination of the quality of the watermarking scheme. They are robustness, imperceptibility, payload and security. Robustness is defined as the measure of resistance of watermark, against attempts to image modification and manipulation like filtering, rotation, scaling, resizing, cropping, etc. Methods such as filtering, rotation, scaling, sharpening, cropping are used to perform attack detection for watermarked video and text data. Question papers with text files (Snapshot of the question paper) are considered as watermarked images. The proposed architecture is illustrated in Fig. 1.

PRINCIPAL,
K. S. R. INSTITUTE FOR
ENGINEERING AND TECHNOLOGY,
K. S. R. KALVI NAGAR,
TIRUCHENGODE-637 215,
NAMAKKAL Dt, TAMIL NADU.

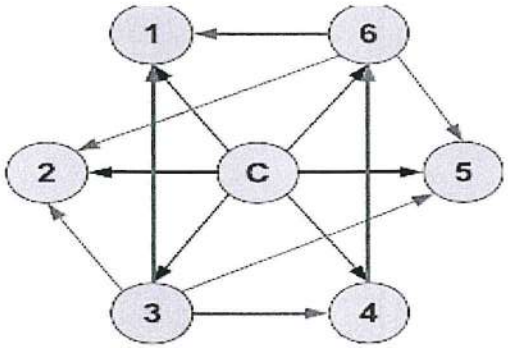

(d) kDB, $k = 2$

Fig. 2: The K-Dependence Bayesian (KDB) classifier

A simplified mathematical representation of video frames suggested has been suggested in (Rubio and Gamez, 2011). Cox's method uses spread spectrum communication techniques to embed the watermark in the image as shown in the following equation:

$$Y = VF + \times W \tag{1}$$

Where the original frame of the video is estimated as a communication channel. The watermark W is considered as a signal to be transmitted in the channel. The embedding strength, gives the amplification or reduction of the power of the signal. In this technique, the video frame is simulated using Markov Random Field (MRF). The video frame is segmented into much similar regions using K-Dependence Bayesian (KDB) image segmentation (Fig. 2). Each area is simulated using MRF. The pixels in each area have alike statistical features. Several issues like false positive probability and watermark embedding strength can be deduced mathematically with this model, rather than proving experimentally.

K-Dependence Bayesian (KDB) for frames segmentation: Segmentation is the procedure of division of the video frame VF samples into video frame areas and the representation is given as VFOR. In recent times, several research works have been conducted with the use of Bayesian network for classification jobs. Hence, it is used for image segmentation for videos or images. The visible video frame results are represented as VFOR and the segmentation is given by VF, for each subregion VF, of the segmentation. Since it computes approximate posterior probability value (c*) for each video frame region, it is applied to images video frame predictor observed values. The likelihood is then given by:

$$p(VF_s \mid VFOR_s) = p(VF_s \mid VFOR_s)p(VF_s) / p(VFOR_s) \tag{2}$$

$$VFOR^* = \arg\max_{vfor} P(VFOR = vfor \mid VF_S = vf_1,\ldots,vf_n,\theta)$$
$$= \arg\max_{vfor} \rho(VF_i = vf_1,,, VF_n = vf_n,\omega \mid VFOR = vfor) = vfor$$

Noting that $p(vs_i)$ does not depend on the labeling vfor, we have,

$$\rho(vf_1,\ldots.Vf_n \mid vfor) = \prod_{i\in s} \rho(vf_i,\theta \mid vfor) \tag{3}$$

Where $\rho(vf_i,\theta \mid vfor)$ denotes the θ degree of sparsity with maximum likelihood of video frame predictor observed values vfor, for known video frames sub regions, vf ,it captures information about. In the usual Bayesian learning technique, the probability values are computed on the basis of conditional independence function between video frame predictor observed values ($VFOR_1,\ldots VFOR_n$) and their values are obtained from the Cartesian product. It becomes a presumption as time passes by. Data with k-Dependence Bayesian (kDB) classifier (Rubio and Gamez, 2011) is additionally considered for solving the assumption problem in Bayesian learning techniques. It is an extension f basic Naive Bayes classifier with number of parents for each set of video frame predictor observed values. Navie Bayesian classifier is also defined as Markov Blanket (MB) for videos or images. Each and every Markov Blanket (MB) of class variables indicates the exact video frame predictor observed values for each video frame and their sub areas:

$$P(VFOR \mid VR_1,\ldots,VR_n,\theta) = P(VFOR \mid MB(VFOR)) \tag{4}$$

The most important property of this K-Dependence Bayesian (KDB) is that MB, a video frame sub region of is conditionally independent of all video frames.

Markov Random Field (MRF) for salient feature detection: In this research, the MRF method uses the Difference of Gaussian (DoG) to perform the approximation. The result of the KDM segmentation information is used to locate of the geometrical-transform-invariant feature points which will be utilized as the reference for watermark embedding and detection. In this research work, the videos frame VF is a manifestation of the underlying video frames. Thus, the MRF salient feature extraction comprises of the hidden results from KDB segmentation and the observable noisy free video frames as VF. The goal of MRF is the discovery of salient features of video frames v for which increases the posterior probability, that is given by:

PRINCIPAL.
K. S. R. INSTITUTE FOR
ENGINEERING AND TECHNOLOGY,
K. S. R. KALVI NAGAR,
TIRUCHENGODE-637 215,
NAMAKKAL Dt. TAMIL NADU.

$$MRF_{R^{NS}} = \arg\max_{VFOR} P(VF|VFOR)P(VFOR) \quad (5)$$

P(VFOR) follows a Gibbs distribution:

$$P(VFOR)_{R^{NS}} = \frac{1}{z}\exp\exp(-U(VFOR)) = \frac{1}{z}\exp\exp(-\sum_{Cec} V_c(VFOR_c)) \quad (6)$$

where, U(VFOR) is called an energy function, $z = \Sigma_{VFOR}$ exp(-U(VFOR)) is the normalizing constant and V_c represents the clique potential for selected video frame . The feature points with strong edge responses will be eliminated due to their sensitivity to noise. Suppose that the original frame of the video is denoted as f(VF,VFOR) and the MRF blurred frame filtered by gaussian mr(VF,VFOR) filter defined in Eq. 5 is:

$$mr_1(VF,VFOR) = MRF_{R^{NS}} MRF_{R^{NS}} \times f(VF,VFOR) \quad (7)$$

$$mr_2(VF,VFOR) = MRF_{kR^{NS}} MRF_{kR^{NS}} \times f(VF,VFOR) \quad (8)$$

mr_1(VF,VFOR) and mr_2(VF,VFOR) are basically different from each other in scale by a constant factor K. Then, the DOG filtered video frame can be measured as follows :

$$\begin{aligned} DOG &= mr_2(VF,VFOR) - mr_1(VF,VFOR) \\ &= MRF_{KR^{NS}} * f(VF,VFOR) - MRF_{R^{NS}} * f(VF,VFOR) \end{aligned} \quad (9)$$

With the result of frame segmentation, one feature point is selected for each segmented area and the circular region centered at the selected feature point with radius will be utilized for the watermark embedding and detection. In each segmented region, the selection of the feature point with the most number of pixels in its circular region which fits into the same distribution is done. Once the selection of reference feature points are done, the rotation and scaling invariant properties are assigned to the circular regions centered at the selected feature points.

Orientation assignment and circular region alignment: The orientation assignment (Lowe, 2004) is useful for making the circular regions rotation invariant. To do so, a window centered at the selected feature points is fixed. The gradients of all frames in the pixels in these windows are calculated using the first order derivative. The histogram of the gradient is then computed and the peak of the histogram is assigned as the orientation of the feature point. Hence, the orientation would not be disturbed by noise, small local distortion or some displacement of the feature point position. The gradient of pixel (VF_0,$VFOR_0$) in the video frame of V is computed as follows:

$$\nabla V(VF_0,VFOR_0) = \left[\frac{\partial V}{\partial VF}, \frac{\partial V}{\partial VFOR}\right]_{(VF_0,VFOR_0)} \quad (10)$$

The magnitude of this gradient is given by:

$$\sqrt{\left(\frac{(\partial V)}{(\partial VF)}\right)^2 + \left(\frac{(\partial V)}{(\partial VFOR)}\right)^2} \quad (11)$$

and it orientation is given by $\tan^{-1}((\partial V)(\partial VFOR)/\partial VF)$. The frame content from the probability distribution function results with RST orientation estimation content is made secure using the singular value decomposition. The suggested techniques can encrypt a frame based on SVD and it can be applied for both grayscale and colored frames, for color image same technique applied for each color band.

Step 1: The first step in this study is the creation of the needed keys for scrambling the frame feature point data which suggest three real keys which are created on the basis of the following relations which are decided by experiments:

$$\begin{aligned} &[7 < Key_1 < 10] \\ &[0.9 < Key_2 < 3 \text{and} \text{int}(Key_2 * |100) \neq 150] \\ &[0 < Key_3 < 3] \end{aligned} \quad (12)$$

Step 2: The frame values are scrambled using the according to the following relations:

$$FFP_1 = Key_1 \times Max(AFFP_1) - FFP \quad (13)$$

$$FFP_2 = Key_1 \times Max(FFP_1) - FFP_1 \quad (14)$$

Employ a scrambling process to the frames feature points (matrices) (FFP_1,FFP_2) for the conversion of their values to extremist values; the output of this step is two matrices ($FFPE_1$,$FFPE_2$) with extremist elements, one for the positives elements while the other is for the negative elements:

$$FFPE_1 = FFP_1 - FFP_2 \quad (15)$$

$$FFPE_2 = Key_2 \times FFPE_1 + FFP_2 \quad (16)$$

PRINCIPAL,
K. S. R. INSTITUTE FOR
ENGINEERING AND TECHNOLOGY,
K. S. R. KALVI NAGAR,
TIRUCHENGODE-637 215,
NAMAKKAL Dt, TAMIL NADU.

Step 3: Apply SVD for both matrices resulting from the previous step ($FFPE_1$ and $FFPE_2$). Three matrices are obtained for each matrix from SVD:

$$[UFFPE_1, SFFPE_1, VFFPE_1] = SVD(FFPE_1) \quad (17)$$

$$[UFFPE_2, SFFPE_2, VFFPE_2] = SVD(FFPE_2) \quad \textbf{(18)}$$

Step 4: Rebuild new matrix from the results of SVD process in step 3, this can be done by interchanging the singular values (SFFPE) of $FFPE_1$ with singular values of $FFPE_2$:

$$CFFP_1 = UFFPE_1 \times SFFPE_2 \times VFFPE_1^T \quad (19)$$

$$CFFP_2 = UFFPE_2 \times SFFPE_1 \times VFFPE_2^T \quad (20)$$

Step 5: For more complexes, the same steps above can be repeated for the creation of new matrices. Scrambling the elements in matrices ($CFFP_1$, $CFFP_2$) to get new matrices ($DFFP_1$, $DFFP_2$):

$$DFFP_1 = CFFP_1 - CFFP_2 \quad (21)$$

$$DFFP_2 = Key_3 \times D_1 + C_2 \quad (22)$$

Then, SVD applied for both matrices ($DFFP_1$, $DFFP_2$) and replacement of the singular values of ($DFFP_1$) with singular value of ($DFFP_2$) is performed as stated in previous steps to get new matrices ($EFFP_1$, $EFFP_2$):

$$[UDFFP_1, SFFPD_1, VFFPD_1] = SVD(DFFP_1) \quad (23)$$

$$[UDFFP_2, SFFPD_2, VFFPD_2] = SVD(DFFP_2) \quad (24)$$

So that:

$$EFFP_1 = UDFFP_1 \times SDFFP_2 \times VDFFP_1^T \quad (25)$$

$$EFFP_2 = UDFFP_2 * SDFFP_1 * VDFFP_2^T \quad (26)$$

Step 6: Combine ($EFFP_1$ and $EFFP_2$) is one matrix:

$$F = [EFFP_1 EFFP_2] \quad (27)$$

Step 7: This step is left with two different choices to combine ($EFFP_1$ and $EFFP_2$). Matrix values are converted into normalized values for reducing the complexity of the above step. Scaling normalization is applied to acquire the scaling invariance for the circular region. It makes the transformation of the image into its standard form by translating the origin of the image to its centroid. Feature scaling used to bring all values into the range [0,1]. This is also called unity-based normalization. This can be generalized to restrict the range of values in the dataset between any arbitrary points a and b using:

$$Fm' = a + \frac{(F - F_{min})(b - a)}{F_{max} - F_{min}} \quad (28)$$

with:

$$a = \sqrt{\frac{\beta?}{m_{0,0}}} b = \sqrt{\frac{\beta}{?m_{0,0}}} \quad (29)$$

Where:

a = The factors of the frame to one and they are defined by $al_{VF} = bl_F$

b = The factors of the frame to one and they are defined by $al_{VF} = bl_F$

l_{VF} = The height of the frame β and $m_{0,0}$

l_F = The width of the frame β and $m_{0,0}$

The zero order moment of f(VF/a), f(VF/b) and f(VF, F) and $\gamma$is the aspect ratio of the frame and is defined as $\gamma = l_F/l_{VF}$. The text files need to be converted into a matrix to performing the embedding process for the cover image matrix. Conversion of the text files into the matrix consists of the following steps : Consider the text file contains 2 sentences:

- This is very very nice picture
- The picture quality is nice

The file is converted into the following matrix format. The header line is all the common words in the text file. The second line represents the frequency of words in each sentence. The output matrix is:

$$\begin{bmatrix} 1 & 1 & 2 & 1 & 1 & 0 & 0 \\ 0 & 1 & 0 & 1 & 1 & 1 & 1 \end{bmatrix}$$

This is very nice picture the quality. Then the watermarked text matrix and the frame matrix are combined into a single matrix.

Watermark embedding: The Noise Visibility Function (NVF) (Sajasi and Moghadam, 2013) describes the local features of the frame and offers a way to do the texture masking in spatial domain. The local variance for each segmented region is computed using NVF:

$$NVF(VF(i,j)) = \frac{h(i,j)}{h(i,j) + s_s^2 R^{NS}} \quad (30)$$

PRINCIPAL.
K. S. R. INSTITUTE FOR
ENGINEERING AND TECHNOLOGY,
K. S. R. KALVI NAGAR,
TIRUCHENGODE-637 215,
NAMAKKAL DT, TAMIL NADU.

Where:

$$h(i,j) = \rho_s\left(?\left(\rho_s\right)\right)^{\rho_s} 1/\left|r(i,j)\right|^{2-\rho_s} \quad (31)$$

$$\eta(\rho_s) = \sqrt{\frac{\Gamma\left(\frac{3}{\rho_s}\right)}{\Gamma\left(\frac{1}{\rho_s}\right)}} \quad (32)$$

$$r(i,j) = \frac{x(i,j) - \mu_s}{s_s R^{NS}} \quad (33)$$

where, ρ_s is the shape parameter ranging from 0.3-2 for most of the frames in the video and μ_s, $\sigma_s R^{NS}$ be the mean and standard deviation for the selected region frame, respectively. The watermark embedding equation with NVF is given in Eq. 34:

$$F_s = VF_s + (1 - NVF).a.w \quad (34)$$

Where:

VF_S = The original video frame data in the circular region
α = The predefined embedding strength
w = The random watermark sequence which is developed under normal distribution and is the same size as one circular region

The watermark embedding procedure comprises of the following steps:

- Use the Pseudo random Number (PN) generator to yield a watermark text data sequence which is a spread spectrum consisting of both positive and negative values
- The adaptive embedding of the watermark text data into each of the selected circular regions is done using the following equation

$$f_s'(VF,F) = f_s(VF,F) + [1 - NVF(f_s(VF,F)].a.w \quad (35)$$

Where:

$f_s(VF, F)$ = One of the circular regions of the original video frame
$f_s'(VF, F)$ = The watermarked result, α is initially set as 2
S = The size of region

If the PSNR of the watermarked image is >40 dB, the watermark embedding is successful. Otherwise, α will be decreased by 0.1 iteratively until either of the following criteria is attained:

- The embedding strength is not bigger than 1.5
- The PSNR of the watermarked image increases to 40 dB

After completion of the process of watermark embedding, attack detection is conducted on the basis of attack resistant methods such as rotation, scaling, cropping, sharpening and filtering.

Rotation: It is also a type of attack. The image is rotated to 90° and tested. Once the reference feature points are selected, assignment of the rotation and scaling invariant properties to the circular regions centered at the selected feature points is done.

Scaling: It is the ability of a system, network or process to cope up with a increasing amount of work in an efficient manner .The watermarked video frame is scaled to 0.25, 0.5, 0.6, 0.8.

Cropping: It denotes the removal of the outer parts of an image to enhance framing. Based on the application, it may be performed on a physical photograph, artwork or film footage. It is regarded as a type of noise in the network and detailed investigation is done.

Sharpening: It refers to another type of attack and the image is also tested in sharpened form. It is a type of transformation which helps in bringing out the image details. The edges are sharpened, so that the eye can pick up the image very quickly. Reduced blurring in the image is obtained. Gaussian noise is added to the watermarked image and then removed from it using the median filtering method.

Gaussian noise: It is a kind of statistical noise that has its probability density function equal to that of the normal distribution. It is also known as Gaussian distribution. In many applications, Gaussian noise is mostly utilized as additive white noise to give additive white Gaussian noise.

Median filter is a non linear filtering method and it is used in the reduction of noises for watermarked image samples to improve the quality of the image. The sliding median filter of a pre-specified image window with size W×W centered at image pixels $i = (i_1, i_2)$ progress consistently over the noisy watermarked image g and selects median of the pixels within a specified range of pixels for spatial domain Ω_i^w approximately to have g(i) and noisy image g(i) is replaced by μ. For the set of pixels

PRINCIPAL.
K. S. R. INSTITUTE FOR
ENGINEERING AND TECHNOLOGY,
K. S. R. KALVI NAGAR,
TIRUCHENGODE-637 215,
NAMAKKAL DI, TAMIL NADU.

within a square window WD×WD, centered at $i = (i_1, i_2)$ and defined specified range of pixels for spatial domain Ω_i^w approximately by equation, the median, μ of the pixels in spatial domain Ω_i^w is:

$$u(i) = \mu_i = \text{median}\left\{\frac{g(j)}{j} \in O_i^w\right\} \quad (36)$$

Thus, the output of the median filter is defined as θ which gives lesser error rate results with the entire pixels in the local neighborhood defined by the mask. The output of the median filter at spatial location i can also be specified as:

$$u(i) = \mu_i = \arg\min_{?} \sum_{r \in O^w} |g(r) - \theta|$$

Watermark detection: During watermark detection, the linear correlation described by Eq. 37 is used for detection of the existence of the watermark in the circular regions:

$$\gamma_{l_c} = \frac{1}{S_s} \sum_{VF,Fes} w.f_s'(VF,F) \quad (37)$$

Where:

γl_c = The linear correlation
s = One of the circular regions
S_s = The area of the region and w is the watermark generated by the same key which is created from SVD and it is used for the watermark embedding process

Watermark detection comprises the following steps:

- Use PN generator for the generation of the same watermark as the one used for watermark embedding
- Location of the RST invariant regions for watermarking using the Non stationary Gaussian scale model
- Calculation of the linear correlation between the watermark and the watermarked data using Eq. 37. The watermark is detected in one circular region when the result is larger than a predefined threshold

The algorithm formulated in this research paper works in the spatial domain and the watermark embedding regions are usually homogeneous because of the selection scheme for the watermarking circular region.

Therefore, the nonlinearity does not produce much improvement in the detector's performance. The following experiments depict the detector's performance. In the tests, 100 different watermarks are embedded into one circular region of the frame image from video and the linear correlation results are computed during the watermark detection. The change of the orientation of reference feature points should be in uniform coherence with the rotation applied to the image. Suppose the initial orientation of a reference feature point is θ_0, after the image is rotated for degree $\theta_0+\theta_1$.

RESULTS AND DISCUSSION

The efficiency of the algorithm can be exhibited using the following five sets of experiments. Four types of attacks are tested: rotation, scaling, cropping, sharpening and Gaussian noise. The algorithm is tested on different video frame images which consist of a variety of portraits, landscapes, people, natural scenes and should be capable of covering most of applications for the image watermarking scheme. The same watermark sequence is embedded into the selected circular regions of several video frame images. The watermark sequence is generated in a random manner under normal distribution. The input video files sample is shown in Fig. 3. The segmented video file sample is shown in Fig. 4.

The Water marked image sample is shown in Fig. 5. The results of the encrypted image matrix and the question image matrix are combined into a single image as shown in Fig. 6. The types of attacks added in the embedded video file sample are shown in Fig. 7 and 8. The extracted image sample is shown in Fig. 9.

Rotation: Under rotation, the algorithm is tested with various rotation angles ranging from 0-300 with a step of 3. The horizontal axis of each sub-figure is indicative of

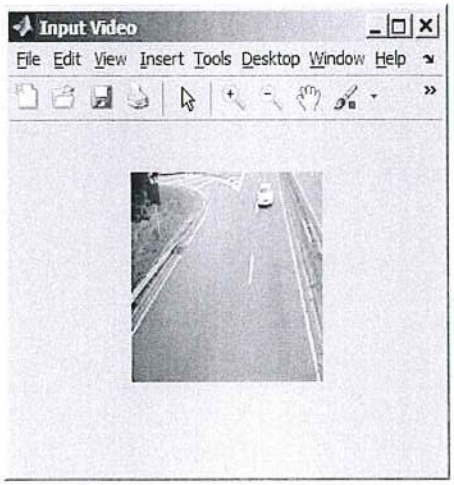

Fig. 3: Video file sample

PRINCIPAL.
K. S. R. INSTITUTE FOR
ENGINEERING AND TECHNOLOGY,
K. S. R. KALVI NAGAR,
TIRUCHENGODE-637 215,
NAMAKKAL Dt. TAMIL NADU.

the rotation angles. The vertical axis conveys the values of linear correlations. Both the false positive probabilities and the false negative probabilities are 0 which means that the watermark can be accurately detected under rotation.

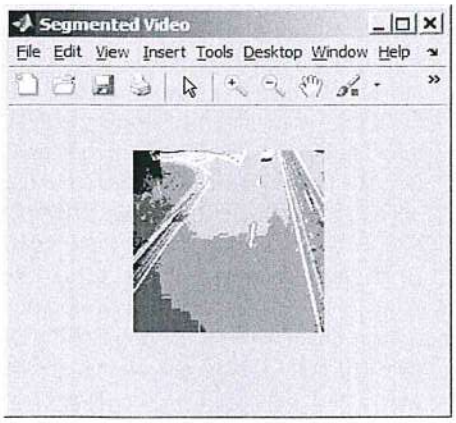

Fig. 4: Segmented video file sample

The horizontal axis of each sub-figure in Fig. 10 displays the rotation angles. The vertical axis indicates the values of linear correlations. The results of the proposed Non-stationary Gaussian distribution with SVD watermarking, Gaussian model (GM), Non Stationary Gaussian Distribution model (NGDM)-SVD and Markov Random Field(MRF)-SVD are compared. It shows that the proposed MRF has high linear correlation than the available methods, since attack resistance analysis is conducted in the proposed work MRF-SVD.

Proposed MRF-SVD algorithm is tested under scaling distortion with scale factor varying from 0.7-1 with a step of 0.1. Results corresponding to the video frames are shown in Fig. 11. The suggested MRF-SVD algorithm performs well against scaling. Also, it is proven that the

MATHEMATICS

61. If $z=(\lambda+3)+i\sqrt{5-\lambda^2}$, then the locus of z is
(a) $x^2+y^2=25$ (b) $x^2+y^2=9$
(c) $x^2+y^2-6x+4=0$ (d) $x^2+y^2-6x+25=0$

62. If $\cos\theta+i\sin\theta$ is a root of the equation $a_0x^n+a_1x^{n-1}+\ldots\ldots\ldots+a_n=0$, then the value of $a_1+a_1\cos\theta+a_2\cos2\theta+\ldots\ldots\ldots+a_n\cos n\theta$ is
(a) 0 (b) n (c) $\cos(n+1)\theta$ (d) $\sin(n+1)\theta$

63. If $\cos A+\cos B+\cos C=0=\sin A+\sin B+\sin C$, then the value of $\cos(A-B)+\cos(B-C)+\cos(C-A)$ is
(a) 1/2 (b) -3 (c) 3/2 (d) $-3/2$

64. Given that $\sin A$, $\cos A$ and $\tan A$ are in G.P., the value of $\cot^6 A-\cot^2 A$ is
(a) -1 (b) 0 (c) 1 (d) 2

65. If $\sin^{-1}\left(\frac{2a}{1+a^2}\right)-\cos^{-1}\left(\frac{1-b^2}{1+b^2}\right)=\tan^{-1}\left(\frac{2x}{1-x^2}\right)$, then 'x' is

(a) $\frac{a+b}{1+ab}$ (b) $\frac{a-b}{1+ab}$ (c) $\frac{a-b}{1-ab}$ (d) $\frac{a+b}{1-ab}$

66. The value of $\begin{vmatrix} x-y-z & 2x & 2x \\ 2y & y-z-x & 2y \\ 2z & 2z & z-x-y \end{vmatrix}$ is
(a) $xyz(x+y+z)$ (b) xyz
(c) $(x+y+z)^3$ (d) $x^2y^2z^2(x+y+z)$

67. The positive solution of the equation $\begin{vmatrix} 3-x & -6 & 3 \\ -6 & 3-x & 3 \\ 3 & 3 & -6-x \end{vmatrix}=0$ is
(a) 3 (b) 9 (c) 12 (d) 6

Rough work

Fig. 5: Water mark image

PRINCIPAL.
K. S. R. INSTITUTE FOR
ENGINEERING AND TECHNOLOGY,
K. S. R. KALVI NAGAR,
TIRUCHENGODE-637 215,
NAMAKKAL Dt, TAMIL NADU.

linear correlation values become smaller when the image shrinks or enlarges with a larger ratio. In this technique, MRF-SVD methods also perform well for scaling attack resistant results. The proposed MRF-SVD algorithm is furthermore tested under Gaussian noise pollution. The variance of the noise varies from 0.001-0.1 with a step of 0.001. The results are shown in Fig. 12. The maximum and minimum values for the linear correlation of the watermarked images are 3.1553 and 0.7878.

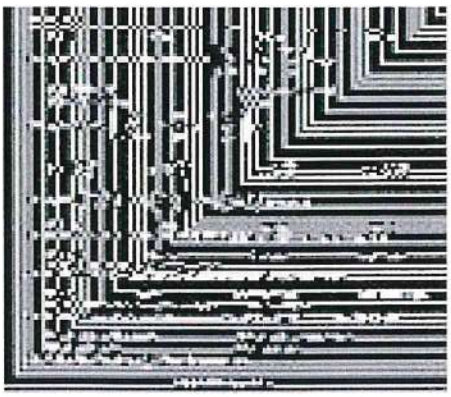

Fig. 6: Encrypted image

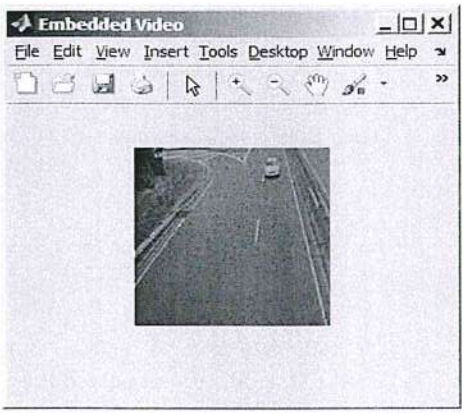

Fig. 7: Embeeded video file sample

Peak Signal to Noise Ratio (PSNR): The ratio between the maximum possible powers to the power of corrupting noise is known as Peak Signal to Noise Ratio. The fidelity of its representation is affected. It can be also described that it is the logarithmic function of peak value of image and mean square error.

$$PSNR = 10\log_{10}\log_{10}\left(MAX_i^2 / MSE\right) \tag{38}$$

Mean square error: Mean Square Error (MSE) of an estimator is the quantification of the difference between an estimator and the true value of the quantity which is being approximated.

$$MSE = \frac{1}{mn}\sum_{i=0}^{m-1}\sum_{j=0}^{n-1}\left[I(i,j) - K(i,j)\right]^2 \tag{39}$$

The perceptual quality is measured after attacks are added to the watermarked images. The Peak of Signal-to-Noise Ratio (PSNR) is calculated to estimate the quality of the watermarked video frames in comparison

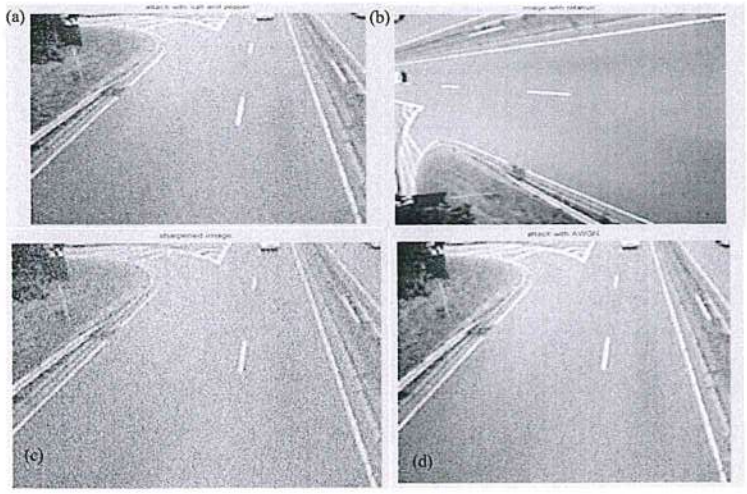

Fig. 8: Attacks added to embedded image samples: a) Salt and pepper noise; b) Rotation; c) Sharpening noise; d) AWGN

PRINCIPAL.
K. S. R. INSTITUTE FOR
ENGINEERING AND TECHNOLOGY,
K. S. R. KALVI NAGAR,
TIRUCHENGODE-637 215,
NAMAKKAL Dt, TAMIL NADU.

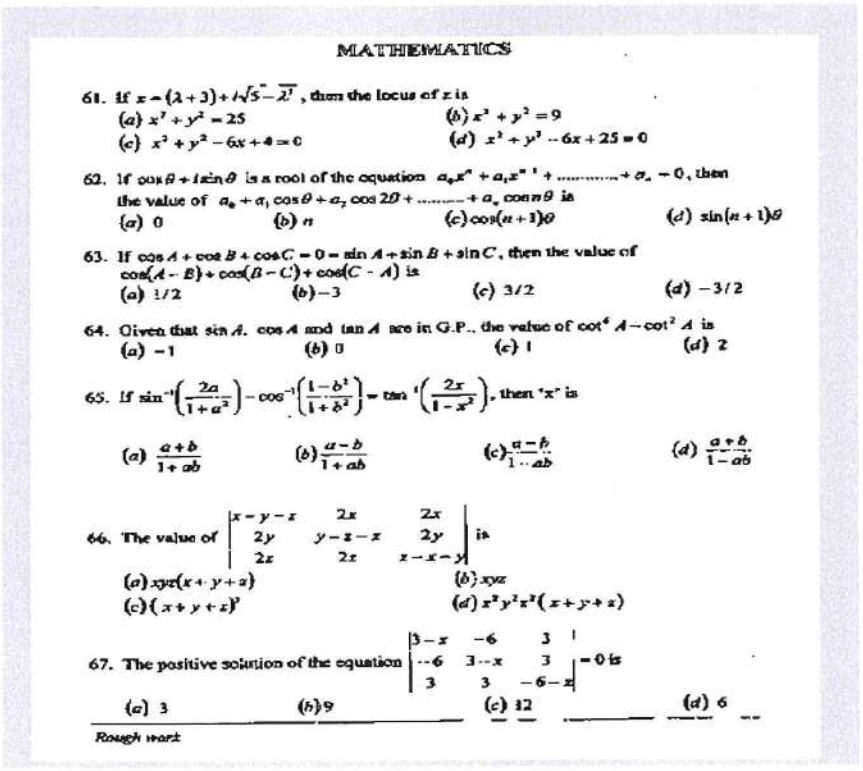

MATHEMATICS

61. If $z=(\lambda+3)+i\sqrt{5-\lambda^2}$, then the locus of z is
(a) $x^2+y^2=25$ (b) $x^2+y^2=9$
(c) $x^2+y^2-6x+4=0$ (d) $x^2+y^2-6x+25=0$

62. If $\cos\theta+i\sin\theta$ is a root of the equation $a_0x^n+a_1x^{n-1}+\ldots\ldots\ldots+a_n=0$, then the value of $a_0+a_1\cos\theta+a_2\cos 2\theta+\ldots\ldots\ldots+a_n\cos n\theta$ is
(a) 0 (b) n (c) $\cos(n+1)\theta$ (d) $\sin(n+1)\theta$

63. If $\cos A+\cos B+\cos C=0=\sin A+\sin B+\sin C$, then the value of $\cos(A-B)+\cos(B-C)+\cos(C-A)$ is
(a) 1/2 (b) -3 (c) 3/2 (d) $-3/2$

64. Given that $\sin A$, $\cos A$ and $\tan A$ are in G.P., the value of $\cot^6 A-\cot^2 A$ is
(a) -1 (b) 0 (c) 1 (d) 2

65. If $\sin^{-1}\left(\frac{2a}{1+a^2}\right)-\cos^{-1}\left(\frac{1-b^2}{1+b^2}\right)=\tan^{-1}\left(\frac{2x}{1-x^2}\right)$, then "x" is

(a) $\frac{a+b}{1+ab}$ (b) $\frac{a-b}{1+ab}$ (c) $\frac{a-b}{1-ab}$ (d) $\frac{a+b}{1-ab}$

66. The value of $\begin{vmatrix} x-y-z & 2x & 2x \\ 2y & y-z-x & 2y \\ 2z & 2z & z-x-y \end{vmatrix}$ is
(a) $xyz(x+y+z)$ (b) xyz
(c) $(x+y+z)^3$ (d) $x^2y^2z^2(x+y+z)$

67. The positive solution of the equation $\begin{vmatrix} 3-x & -6 & 3 \\ -6 & 3-x & 3 \\ 3 & 3 & -6-x \end{vmatrix}=0$ is
(a) 3 (b) 9 (c) 12 (d) 6

Rough work

Fig. 9: Extracted image samples

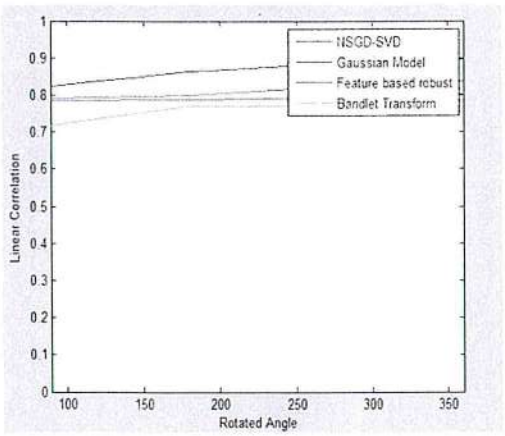

Fig. 10: Rotated angles vs. linear correlation

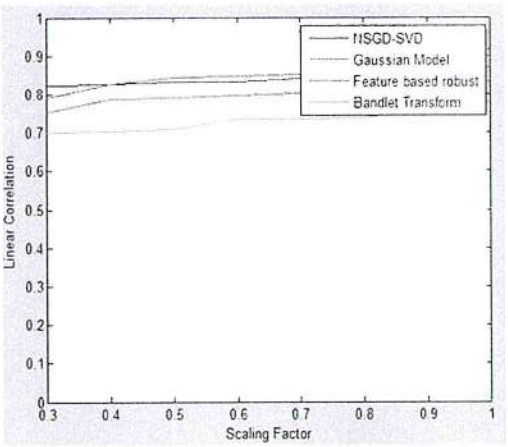

Fig. 11: Scale factor vs. linear correlation

with the original ones. The performance of the proposed MRF-SVD scheme is compared with the existing watermarking GM and NGDM-SVD. The PSNR results of the proposed MRF-SVD schema is higher after the attacks such as scaling, rotation, sharpening, Cropping and filtering when compared to existing watermarking methods is shown in Fig. 13.

The comparison of the performance of the MRF-SVD scheme is done with the already available watermarking GM and NGDM-SVD schemes for MSE comparison. In the scientific work, MRF-SVD MSE is computed between the watermarked images and watermarked with attacks

PRINCIPAL.
K. S. R. INSTITUTE FOR
ENGINEERING AND TECHNOLOGY,
K. S. R. KALVI NAGAR,
TIRUCHENGODE-637 215,
NAMAKKAL Dt, TAMIL NADU.

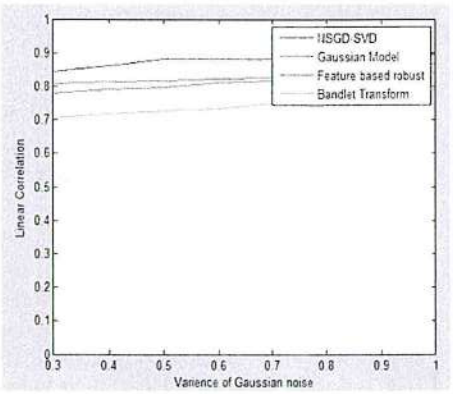

Fig. 12: Experimental results against gaussian noise pollution

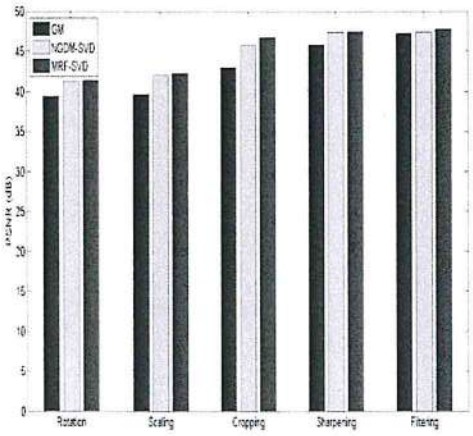

Fig. 13: Experimental results of PSNR comparison against attacks

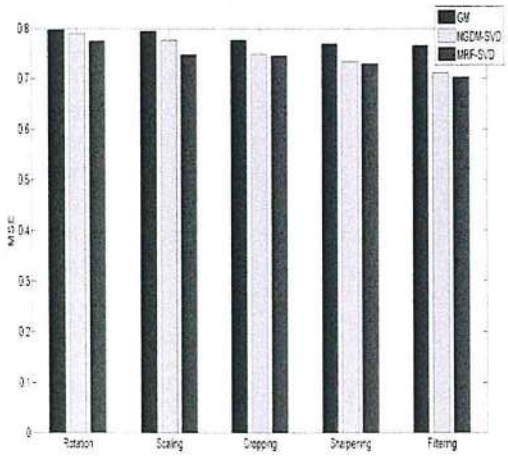

Fig. 14: Experimental results of MSE comparison against attacks

detected image which reveals that the MSE results of the proposed MRF0-SVD have reduced MSE error rate for all types of attacks as shown in Fig. 14.

CONCLUSION

In this research, a relatively new video watermarking technique to model video frames using the Markov Rrandom Field in spatial domain is proposed. The video frames are first segmented using K-Dependence Bayesian (KDB) into several homogeneous areas. Each region is then denoted utilizing Markov Random Field (MRF). The MRF model is used to locate the salient feature points which can be used as the reference points and are useful for defining the circular regions for the watermark embedding or detection procedures. After the salient features are selected it is protected using the SVD method. Frame encryption techniques scramble the feature point's pixels of the frames and reduce the correlation among the pixels, so that lower correlation among the pixels and the encrypted frame is obtained. Hence, the features within each embedding or detection region are consistent. In embedding stage the text files are embedded in the encrypted frame matrix. It gives better guidance for adaptive adjustment of the watermark embedding strength utilizing NVF. Attack resistance analysis is conducted on the watermarked video frame. In this stage, removal of Gaussian noise is performed using the median filtering techniques and sharpening is also done to find attacks in the video embedded frame. The results obtained from experiments depict that the studied MRF-SVD algorithm is a good performer against rotation, scaling, cropping, sharpening and Gaussian noise removal computed using PSNR and MSE. The capability of the watermarking algorithm can be enhanced if some other perceptual models instead of NVF can be brought into place. In addition, contrast sensitive function and texture sensitive function can be used here. The spread spectrum is useful for watermark embedding and gives good performance of robustness. Other coding techniques and modulation can also be put in place, particularly after the image is segmented into different regions which can be dealt as parallel transmission channels.

REFERENCES

Al-Taweel, S.A. and P. Suma, 2009. Robust video watermarking based on 3D-DWT domain. Proceeding of the IEEE, Conference on TENCON Region 10, January 23-26, 2009, IEEE, Singapore, ISBN: 978-1-4244-4546-2, pp: 1-6.

PRINCIPAL.
K. S. R. INSTITUTE FOR
ENGINEERING AND TECHNOLOGY,
K. S. R. KALVI NAGAR,
TIRUCHENGODE-637 215,
NAMAKKAL Dt. TAMIL NADU.

Bhatnagar, G. and B. Raman, 2012. Wavelet packet transform-based robust video watermarking technique. Sadhana, 37: 371-388.

Coria, L., P. Nasiopoulos, R. Ward and M. Pickering, 2007. An access control video watermarking method that is robust to geometric distortions. J. Inform. Assurance Secur., 2: 266-274.

Elbasi, E., 2007. Robust Video Watermarking Scheme. ProQuest, Ann Arbor, Michigan, USA., Pages: 193.

Fouda, Y.M., 2015. A robust template matching algorithm based on reducing dimensions. J. Signal Inf. Process., 6: 109-122.

Jayamalar, T. and V. Radha, 2010. Survey on digital video watermarking techniques and attacks on watermarks. Intl. J. Eng. Sci. Technol., 2: 6963-6967.

Lowe, D.G., 2004. Distinctive image features from scale-invariant keypoints. Intl. J. Comput. Vis., 60: 91-110.

Mirza, H.H., H.D. Thai, Y. Nagata and Z. Nakao, 2007. Digital video watermarking based on principal component analysis. Proceeding of the 2nd International IEEE Conference on Innovative Computing, Information and Control, September 5-7, 2007, IEEE, Kumamoto, Japan, ISBN: 0-7695-2882-1, pp: 290-290.

Mostafa, S.A.K., A.S. Tolb, F.M. Abdelkader and H.M. Elhindy, 2009. Video watermarking scheme based on principal component analysis and wavelet transform. Int. J. Comput. Sci. Network Security, 9: 45-52.

Park, H., S.H. Lee and Y.S. Moon, 2006. Adaptive Video Watermarking Utilizing Video Characteristics in 3D-DCT Domain. In: Digital Watermarking. Shi, Y.Q. and B. Jeon (Eds.). Springer Berlin Heidelberg, Berlin, Germany, ISBN: 978-3-540-48825-5, pp: 397.

Rubio, A. and J.A. Gamez, 2011. Flexible learning of k-dependence Bayesian network classifiers. Proceedings of the 13th Annual ACM Conference on Genetic and Evolutionary Computation, July 12-16, 2011, ACM, New York, USA., ISBN: 978-1-4503-0557-0, pp: 1219-1226.

Sajasi, S. and A.M.E. Moghadam, 2013. A high quality image hiding scheme based upon noise visibility function and an optimal chaotic based encryption method. Proceeding of the 5th RoboCup Iran Open International Symposium and 3rd Joint IEEE Conference on AI & Robotics and RIOS, April 8, 2013, IEEE, Tehran, Iran, pp: 1-7.

Seo, J.S. and C.D. Yoo, 2006. Image watermarking based on invariant regions of scale-space representation. IEEE Trans. Signal Process., 54: 1537-1549.

Wang, L., H. Ling, F. Zou and Z. Lu, 2011. Real-time compressed-domain video watermarking resistance to geometric distortions. IEEE. MultiMedia, 19: 70-79.

Yuan, X.C. and C.M. Pun, 2013. Feature based video watermarking resistant to geometric distortions. Proceeding of the 12th International IEEE Conference on Trust, Security and Privacy in Computing and Communications, July 16-18, 2013, IEEE, Melbourne, Victoria, Australia, pp: 763-767.

Zheng, D., S. Wang and J. Zhao, 2009. RST invariant image watermarking algorithm with mathematical modeling and analysis of the watermarking processes. Image Process. IEEE. Trans., 18: 1055-1068.

Zheng, D., Y. Liu and J. Zhao, 2007. A survey of RST invariant image watermarking algorithms. ACM Comput. Surv., Vol. 39. 10.1145/1242471.1242473.

PRINCIPAL,
K. S. R. INSTITUTE FOR
ENGINEERING AND TECHNOLOGY,
K. S. R. KALVI NAGAR,
TIRUCHENGODE-637 215,
NAMAKKAL Dt. TAMIL NADU.

Asian Journal of Information Technology 15 (17): 3398-3406, 2016
ISSN: 1682-3915
© Medwell Journals, 2016

A Misdirected Route Avoidance Using Topological Transform Adaptive Relational QOS Routing in Wireless Sensor Network

[1]P. Vijayalakshmi and [2]B.G. Geetha
[1]Department of Computer Science and Engineering,
Shri Shanmugha College of Engineering and Technology, Tamil Nadu, India
[2]Department of Computer Science and Engineering,
K.S.R. College of Technology, Tamil Nadu, India

Abstract: Wireless Sensor Network (WSN) continues to grow and consequently an effective routing scheme is required when the topological changes occur. Existing Distributed algorithm for Time-bounded Essential Localization (DTEL) over a sensor network minimizes the time taken for the broadcasting of packets. But, investigating the throughput level on the different topological route paths is not focused. Topological changes in the wireless sensor network measure the throughput level using Ternary Content Addressable Memory (TCAM)-based packet classification systems. TCAM based sensor network system improves the throughput level but the topological transformation sometimes lead to the misdirected routing in WSN. To improve the routing scheme on the different topological structure, Topological Transform Adaptive Relational Quality of Service Routing (TTA-RQoSR) scheme is proposed in this study. TTA-RQoSR scheme develops the framework with the three main objectives such as adaptively, avoiding the misdirected route and improving the throughput level. TTA-RQoSR scheme uses the abstained misdirected routing to remove the misdirected route path of packet transfer from the source to the destination. The abstained misdirected routing adjusts the flow relationship exclusively on locally observed paths using the erlang's C formula. erlang's C formula uses the Poisson arrival process with arrival rate to avoid the misdirected route. Secondly, TTA-RQoSR scheme uses the Relational QoS Routing to attain approximately 5% improved throughput level on changing mobility of sensor node and sink node in WSN. Experiment is conducted using the simulation tool on the factors such as throughput level on varying topological structure, avoidance rate of misdirected route and delay time.

Keywords: Relational QoS routing, wireless sensor network, Erlang's C formula, misdirected route path, topological change, abstained misdirected routing

INTRODUCTION

Wireless sensor networks are normally composed of many low-powered sensors nodes with a few relatively robust sink nodes to perform the powerful communication. WSN usually gathers the data by the individual nodes where it is eventually routed to the sink nodes. A rate monitoring simply makes use of the idea to forward packets with user required topological structure. The topological structures of different forms are used in sensor network field. Topological structure in WSN is illustrated in Fig. 1.

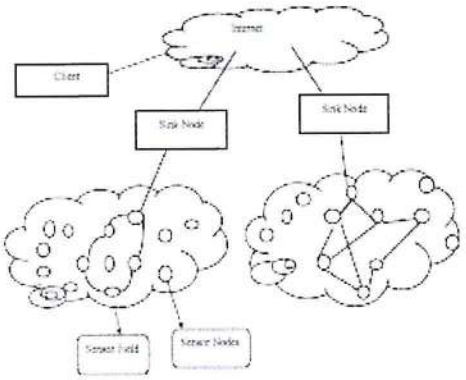

Fig. 1: Topological WSN Structure

Topological routing in WSN is very demanding due to the essential characteristics that distinguish from other wireless networks. Existing joint authentication and Topology Control (JATC) scheme in Guan *et al.* (2012) improve the throughput rate by as a discrete stochastic optimization method. Joint authentication considers spanning over the entire protocol stack for the

Corresponding Author: P. Vijayalakshmi, Department of Computer Science and Engineering,
Shri Shanmugha College of Engineering and Technology, Tamil Nadu, India

PRINCIPAL.
K. S. R. INSTITUTE FOR
ENGINEERING AND TECHNOLOGY,
K. S. R. KALVI NAGAR,
TIRUCHENGODE-637 215,
NAMAKKAL Dt. TAMIL NADU.

overall wireless network performance measurement. But, not working on the dynamic changing topology.

In internet (Obaidat and Guelzim, 2010), Wi-fi Protected Access (WPA) scheme presents an encryption and decryption process for providing authentication for dynamic changing topology. WPA suffers from a few flaws on using the existing algorithm to interfere with the deployed wireless network. WPA is not suitable for providing quality of services in wireless networks because it does not solve the delay time factor. Localized Quality of Service (QoS) routing protocol make use of an Acknowledgment (ACK) system by Djenouri and Balasingham (2011) to reduce the delay time in sensor network.

Localized QoS factor based on Exponential Weighted Moving Average (EWMA) method consume small memory to transfer the packets from source to destination. The protocol uses multi queuing with priority where higher priority is given for the lager load factor thereby reducing the delay time with minimal memory consumption. A ternary Content Addressable Memory (TCAM)-based packet classification system as demonstrated in (Meiners *et al*., 2011) measures the throughput level. TCAM space for an encoded classifier is three times lesser in space when compared with the re-encoded classifier and its transformers. TCAM based sensor network system improves the throughput level but the topological transformation sometimes leads to failure in routing.

To attain the routing on the topological transformation, Harmony Search and Learning Automata based Topology Control (HSLATC) protocol is described by Yang *et al*. (2012) that determines an appropriate transition radius of the sensor nodes while building the route for packet transmission. In HSLATC, accurate result obtained on selecting the transition radius of sensor nodes but fails to offer the full QoS connectivity on sensor network. Adaptive Location-oriented QoS content delivery as demonstrated by Zhang *et al*. (2012) performs packet movement on mobile sensor nodes. Semi-Markov process is used in the existing work for the movement of packets in sensor network but not developed with energy effective routing protocol.

Optimal selective forward routing as illustrated in (Valles *et al*., 2011) provides the most of the significance approach to save the energy and improve the throughput level. Optimal selective routing approach maximize the sensor to successfully transfer the packet from the sink node to the sensor nodes in the sensor field but eventually misdirection occurs on the large set of sensor nodes.

To correctly direct the route, Energy-Aware Clustering algorithm (EADC) is presented in (Yu *et al*., 2012) to cluster the routes. The EADC uses opposition range clusters of even sizes for routing. The cluster always holds the cluster head with minimal energy consumption but the EADC fails in balancing the load factor. To balance the traffic load in wireless network, Topology Aware Adaptive Routing (TAAR) is presented by Chen *et al*. (2013). TAAR has three routing modes which used on dynamically adjusting the topology status of the routing path, thereby flexibility on small set of wireless network system is improved.

For the large set of wireless network nodes, Position-based Opportunistic Routing (POR) protocol is used for transmission of packets. POR as demonstrated by Zhang *et al*. (2011a) has possessions of geographic routing and transmit the packet in wireless medium. When a data packet is sent out, some of the neighbor nodes eavesdrops the transmission by misdirect the route. The misdirection of route increases the communication overhead and latency time. To reduce the communication overhead, a general random network model is described by Zhang *et al*. (2011b) for enhancing the network performance. A secure communication is carried out with the minimal overhead but not worked on with the very large scale wireless sensor network.

Similarly, to reduce the latency time on geographic routing, Multi-hop Delaunay Triangulation (MDT) method is developed by Nikravan and Jameii (2012) with dynamic topological structure. MDT protocol suite has a packet forwarding protocol for nodes construction and maintains distributed MDT for routing but, MDT method leads to misdirection of routes on the rare scenarios.

First, due to the huge number of sensor nodes, it is not possible to build a scheme for the deployment of a large number of sensor nodes when the overhead of routing maintenance is high. Secondly, large number of sensor nodes also leads to the misdirection of routes in the sensor field. The misdirection leads to the lesser throughput level. Existing Distributed algorithm for Time-bounded Essential Localization (DTEL) as described by Cheng *et al*. (2013) over a sensor network minimizes the time taken for the broadcasting of packets and also integrated the regular payload transmissions. However, investigating the throughput level on the different topological route paths is not focused in DTEL method. DTEL are not broadly developed on social network applications.

In this study, Topological Transform Adaptive Relational Quality of Service Routing (TTA-RQoSR) scheme is developed for enhancing the routing structure without any misdirection. TTA-RQoSR scheme uses the abstained misdirected routing method to remove the misdirected route path of packet transfer from the source to the destination. The routing misdirection is measured using the Erlang's C Formula. Arrived Poisson

PRINCIPAL.
K. S. R. INSTITUTE FOR
ENGINEERING AND TECHNOLOGY,
K. S. R. KALVI NAGAR,
TIRUCHENGODE-637 215.
NAMAKKAL Dt, TAMIL NADU.

distribution result is explained briefly and Relational QoS Routing improves the throughput rate in TTA-RQoSR scheme. TTA-RQoSR Scheme plays a vital role in the sensor network structure to avoid the misdirection route and improve the throughput level on packet transferring.

Literature review: The routing along the shortest paths in the sensor field concentrates on reducing the energy consumption. A multi constraint routing using fuzzy logic (Chelliah *et al*., 2012) was developed to improve the performance of WMN and reduces the possibilities of congestion in the network. However, group communication is not focused in wireless mesh networks.

Routing protocols and simulation analysis in Chowdhury *et al*. (2012) uses the GloMoSim-2.03 to find the shortcomings of routing protocols. However, Routing protocols are not effective on solving the data redundancy, energy efficiency. Adaptive routing is also not effective on limiting the memory consumption rate in wireless sensor network structure. Neighbour Aware Multicast Routings Protocol (NAMP) (Pathan *et al*., 2008) is a tree based hybrid multicast routing protocol that enhances the performance of the network with minimum transmission time.

Mobility framework (Ogwu *et al*., 2007) developed for specifying a probabilistic QoS guarantee in mobile ad-hoc network. This model characterizes a mobile user particularly in a large ad hoc network. However, routing is very complex in mobile ad hoc network. Token-Based (TB) robust deadlock-free dynamic reconfiguration protocol (Kadhar, 2014) provides solution for deadlock free reconfiguration protocol and reduced the packet loss.

An adaptive push system as described by Nicopolitidis *et al*. (2010) broadcast the packets in underwater acoustic wireless networks and achieves the low latency broadcasting of packets. But, throughput rate is lesser. To achieve the higher throughput rate in Yuen *et al*. (2009), using the alternate user strategy in the partially overlapping-interests which significantly improved the multiuser diversity of information in infestation network.

MATERIALS AND METHODS

Topological transform adaptive relational QoS routing scheme: The main objective of the proposed routing scheme is to avoid the misdirection routing on varying topological structure in the WSN. The QoS routing is offered to select the effective route path for transferring the packet from the source to destination sensor nodes. The relational QoS routing assume the source routing model with varying network topology information. The information is available in all source nodes for the easy transfer of packets from source to destination. The

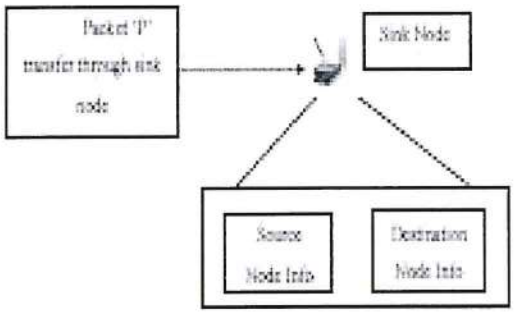

Fig. 2: Packet transferring through sink node

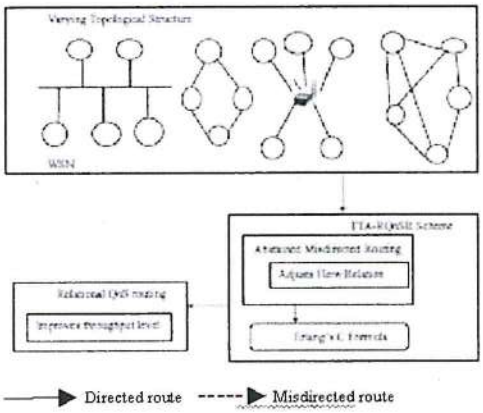

Fig. 3: Architecture diagram of TTA-RQoSR scheme

packet flow is routed along the explicit routed paths in TTA-RQoSR Scheme to improve the throughput level.

TTA-RQoSR Scheme initially identifies the relationship among the route path nodes and recognizes the mutually disjoint routes. The notion of the abstained misdirection routing is introduced to deal with the misdirected route among the different route paths. The avoidance of misdirected route is carried out in the TTA-RQoSR scheme that improves the throughput level.

The packet of varying length is transferred on the wireless sensor route path through the sink node as described in Fig. 2. The network usually transfers the packet through the sink node to the sensor field of varying range. Sink node contains the information about the source and destination route nodes with the intermediate node information. TTA-RQoSR scheme is used to avoid the misdirection route of packets transfer and architecture Diagram of TTA-RQoSR scheme is described in Fig. 3.

As illustrated in Fig. 3, sensor network with sensor nodes consists of the various topological structures. The

PRINCIPAL.
K. S. R. INSTITUTE FOR
ENGINEERING AND TECHNOLOGY,
K. S. R. KALVI NAGAR,
TIRUCHENGODE-637 215,
NAMAKKAL Dt, TAMIL NADU.

directed route path for packet transfer varies due to the mobility of sensor nodes within the sensor field. The misdirection of route path leads to the delay on the packet transfer and reduces the throughput level. The misdirected routing avoided through the Abstained Misdirected Routing in TTA-RQoSR scheme. It adjusts the flow relationship on the movable nodes using the Erlang's C formula. Erlang's C formula helps in reducing the delay time using the Poisson arrival process rate. Erlang's C formula finally helps on avoiding the misdirection route path for packet transfer and Relational QoS routing helps in improving the throughput level.

Abstained misdirected routing: Consider a scenario with '500' sensor nodes of topological structure on the sensor network as described in Fig. 2 where the source 's' and a destination 'd' are connected by disjoint paths path 1, path 2, ..., path n in TTA-RQoSR scheme. Each path 'i' has a capacity of b_i to transfer the packet from the source in average flow rate. The flow relation is accommodated with b_i flows at any 't'. The QoS state of path is achieved in TTA-RQoSR scheme using the delay time minimization. The delay time is minimized using the erlang's C formula. The packet load capacity in sensor network is computed as:

$$\text{Packet load capacity}(c) = \frac{b_i}{l_i b_i} \quad (1)$$

Equation 1 load capacity is illustrated with load l_i of '10' KB with average 'b_i' capacity of '50' KB in sensor network. The packet load capacity 'c' is:

$$c = \frac{3.041409320 \times 10^{64}}{500}$$

$$c = \frac{3.041409320 \times 10^{62}}{5}$$

$$c = 60.8281 \times 10^{60}$$

The packet load capacity is measured on the overall sensor network to compute the packet flow relationship. The average flow relation on the varying topological structure is computed as:

$$\text{Packet flow relation}(F_i) = D(l_i, b_i) = \frac{c}{\sum_{n=0}^{b_i} \frac{l_i^n}{n}} \quad (2)$$

Equation 2 clearly describes the flow relationship of packets on varying load l_i on the path 'i' in WSN. The 'D' denotes the delay reduced on the varying load l_i and path capacity b_i on transferring of packets form's' to'd' in WSN. The 'n' denotes the number of packet to be transferred from source to destination. The flow relationship is adjusted on the varying topological structure. The flow relationship adjustment is denoted as:

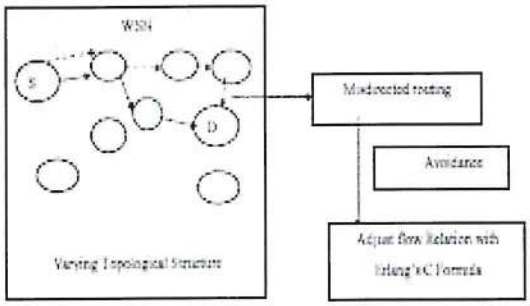

Fig. 4: Abstained misdirected routing procedure

$$\text{Flow relation Adjustment}(A_i) = \frac{l_i^{(i)}}{\sum_{j=1}^{n} l_j^{(i)}} \quad (3)$$

$$\text{Flow relation Adjustment}(A_n) = \frac{l_i^{(i)}}{\sum_{j=1}^{n} l_j^{(n)}} \quad (4)$$

Equation 3 denotes the first level of adjustment on the packet flow through the varying load capacity path 'i'. The path 'i' is adjusted to the path 'j'. Likewise to the path 'n', (i.e.,) till the misdirection is avoided in the TTA-RQoSR scheme. The misdirection avoidance with minimal delay time is computed using the Erlang's C formula where it improves the throughput level rate. The total load and the path capacity b_i in TTA-RQoSR scheme are computed to avoid the misdirected route path. The abstained misdirected routing is represented through the diagrammatic form in Fig. 4.

Figure 4 clearly describes the procedure of the avoiding the misdirected route path in WSN using the abstained misdirected routing. The objective of the TTA-RQoSR scheme is to find a set of relational routes through which the packet can be transferred. The transferred route path capacity is analyzed and then minimize the overall delay rate by shifting some load from path 'i' to path 'j'. The optimal relationship is analyzed and then the packet flow relationship is adjusted based on the path capacity in TTA-RQoSR scheme.

Erlang's C formula: In the TTA-RQoSR scheme, Erlang's C formula identifies the poisson arrival rate 'λ' and service

PRINCIPAL,
K. S. R. INSTITUTE FOR
ENGINEERING AND TECHNOLOGY,
K. S. R. KALVI NAGAR,
TIRUCHENGODE-637 215,
NAMAKKAL DT, TAMIL NADU.

rate 'μ' with exponential distribution of finite mean time to compute the delay. Erlang's C Formula imagines the stability condition to avoid the misdirection routing on the varying topological structure. The steady state in the Poisson distribution is computed as:

$$\text{Erlang's C formula } C(s,d) = \frac{\frac{l_i}{b_i(1-\rho)}}{\sum_{n=1}^{l-1}\frac{d^n}{n} + b_i(1-\rho)} \quad (5)$$

Equation 5 described the formula which avoids the misdirection using the Poisson distribution. The l_i load capacity is determined and then the Poisson distribution 'ρ' is computed. The source node 'n' and destination route path'd' factorial is computed on identifying the misdirection route path in WSN.

Relational QoS routing: Relational quality of service routing in TTA-RQoSR scheme reduces the delay time and improves the throughput level rate. The misdirection is avoided and relational routing precedes the work with sequence of variable length packets in TTA-RQoSR scheme. During each sequence, incoming packet flows are routed along paths selected in the sensor field. A path is selected with frequency determined by prescribed relations. The adjustment on the flow relation avoids the misdirection on the movable sensor nodes and improves the throughput rate.

In TTA-RQoSR scheme, packet flow relationship on the different topological structure from source to destination sensor node is determined. The flow relationship in TTA-RQoSR scheme improved the throughput rate with minimal delay time.

Algorithmic procedure of RQoS routing: Relational QoS routing is developed in proposed TTA-RQoSR scheme for avoiding the misdirection route on the changing mobility of sensor node and sink nodes. The algorithmic procedure of relational QoS routing is described as:

RQoS routing procedure:

Begin
Input: Source sensor node 's', Destination sensor node 'd', load 'i' and capacity range 'b' of sensor node in sensor field
Output: Packet transmit form's' to'd' without any misdirection with higher throughput rate
Step 1: Select the Eligible path 'i' to transfer packet of length 'N'
Step 2: Increment the flow counter from source's' to 's+1'
Step 3: Compute Packet flow relation (F_i) on each topological structure
Step 4: Assign a relationship on QoS routing to avoid misdirection
Step 5: If relationship not matched
Sep 5.1: $\text{Flow Relation Adjustment}(A_i) = \frac{l_i^{(b)}}{\sum_{i=1}^{n} l_i^{(b)}}$

Computed on 'n' adjustment values
Step 6: End If
Step 7: Computed new relation improves the throughput rate on varying topological sensor field.
End

The above algorithmic procedure improves the relationship between the packet flows in sensor field using the packet flow relationship adjustment. TTA-RQoSR scheme also works on the varying load capacity, thereby increasing the throughput rate without any misdirection of packets in sensor field. If the topological system load changes suddenly, the old flow relationship result is terminated and new sequence adjustment carried out to transmit the packet with the higher throughput level.

Experimental evaluation: Topological Transform Adaptive Relational QoS Routing (TTA-RQoSR) scheme performs the experimental evaluation on NS2 simulator. In the simulations, 85 sensor nodes are constructed in sensor network environment. The sensor nodes use the DSDV routing protocol to perform the experiment on the randomly moving objects. In the Random Way Point (RWM) Model, each sensor node moves to an irregularly chosen location. The RWM uses standard number of sensor nodes for scheduling the nodes. The chosen location with an arbitrarily selected speed contains a predefined amount and speed count.

The movement of all nodes generated over a 900×900 m sensor field. The nodes moves at the random speed of 5 m sec^{-1} and an average pause of 0.01 sec. For simulation, the proposed TTA-RQoSR scheme is compared with existing Distributed algorithm for Time-bounded Essential Localization (DTEL) (Pathan *et al*., 2008) and Ternary Content Addressable Memory (TCAM)-based packet classification systems (Meiners *et al*., 2011). The TTA-RQoSR scheme experiments the research on factors such as throughput level on varying topological structure, avoidance rate of misdirected route, energy consumption on varying sensor node mobility, delay time, communication overhead on varying sensor node density level and false positive rate.

Throughput level is the rate at which the successful packet delivered through the communication channel. The packet delivered over a physical link without any misdirection of route in the network node:

$$\text{Throughput} = \frac{\text{Packet size}}{\text{Transmission speed}}$$

Throughput level takes the packet of Kilo Byte size for the experimental research. Transmission time is about '5' m sec^{-1}. Avoidance of misdirection in the wireless

PRINCIPAL.
K. S. R. INSTITUTE FOR
ENGINEERING AND TECHNOLOGY,
K. S. R. KALVI NAGAR,
TIRUCHENGODE-637 215,
NAMAKKAL Dt, TAMIL NADU.

network structure is defined as the avoidance rate and measured in terms of percentage (%). Avoidance rate on the different Route path (R) are measured in terms of Joules (J). The amount of energy used on transmitting the packets is defined as the energy consumption rate:

$$\text{Energy consumption} = \text{Node mobilty rate} \times \text{Simulation time}$$

The node mobility rate in sensor network is measured in terms of bits per second. Simulation time gets doubled as the mobility rate increases. The higher mobility rate, then the energy consumption is also getting increased. Delay time in the wireless network structure denotes the amount of time get elapsed for transmitting the packet from one sensor node 'N' to another in the sensor field. Assume a packet transfer carried on 10 sensor nodes:

$$\text{Delay time} = (T_1 - T_2) + (T_2 - T_3) + \ldots + (T_9 - T_{10})$$

Where:

T_1 = First sensor node start time
T_2 = Second sensor node
T_{10} = Tenth sensor node

Similarly, sensor node time taken for packet transmission from one place to another is computed. The proportion of time spends on communicating with network structure rather than transmitting the packets is termed as the communication overhead. Communication overhead is measured in terms of percentage. False positive refers to the probability of falsely rejecting the null hypothesis (misdirection) for a particular packet transmission. Packet transmission misdirection is minimized, so the false positive rate is of negligible percentage.

RESULTS AND DISCUSSION

The TTA-RQoSR scheme is compared with the existing Distributed algorithm for Time-bounded Essential Localization (DTEL) (Pathan *et al*., 2008) and Ternary Content Addressable Memory (TCAM)-based packet classification systems (Meiners *et al*., 2011). The below Table 1 values are used for plotting the graph in this section.

Table 1 illustrates the throughput rate based on packet size using TTA-RQoSR scheme and comparison is made with two other existing methods, namely DTEL Method (Pathan *et al*., 2008) and TCAM System (Meiners *et al*., 2011). The increased throughput rate improves the performance of TTA-RQoSR scheme.

Table 1: Tabulation for throughput rate

	Throughput rate (Mbps)		
Packet size (kb)	DTEL method	TCAM system	TTA-RQoSR scheme
1000	190	200	210
2000	390	400	420
3000	550	575	599
4000	785	805	825
5000	935	955	985
6000	1130	1165	1200
7000	1270	1310	1350
8000	1510	1550	1585

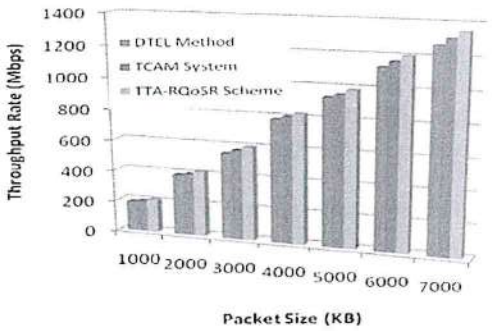

Fig. 5: Measure of throughput rate

Figure 5 shows the measures of throughput rate based on the packet size using TTA-RQoSR scheme, DTEL Method (Pathan *et al*., 2008) and TCAM System (Meiners *et al*., 2011). The packet size is measured in terms of KB. In Fig. 5, the proposed TTA-RQoSR scheme provides higher throughput rate when compared to the DTEL Method (Pathan *et al*., 2008) and TCAM System (Meiners *et al*., 2011). This is because of the application of Erlang's C formula and relational QoS Routing in proposed TTA-RQoSR scheme. Erlang's C formula avoids the misdirection route path for packet transfer and therefore, Relational QoS routing improves the throughput level. TTA-RQoSR scheme improves the throughput level rate by 5-10% when compared with DTEL Method (Pathan *et al*., 2008) thereby selecting the path with a frequency determined relations. In TTA-RQoSR scheme, packet flow relationship on the different topological structure from source to destination sensor node is determined using relational QoS routing, so throughput level improved by 2-5% when compared with the TCAM System (Meiners *et al*., 2011).

Avoidance rate is demonstrated in Fig. 6 where the misdirection is avoided and relational routing precedes the work with sequence of variable length packets. As shown in the figure, the proposed TTA-RQoSR scheme provides higher avoidance rate when compared to the DTEL Method (Pathan *et al*., 2008) and TCAM

PRINCIPAL.
K. S. R. INSTITUTE FOR
ENGINEERING AND TECHNOLOGY,
K. S. R. KALVI NAGAR,
TIRUCHENGODE-637 215,
NAMAKKAL Dt. TAMIL NADU.

Table 2: Tabulation for avoidance rate

Route path count (R)	Avoidance rate of misdirected route (Avoidance %)		
	DTEL	TCAM	TTA-RQoSR
4	49.5	46.5	43.6
8	99	95.1	92.4
12	65.2	62.7	59.1
16	20	19.5	18.4
20	24.8	23.4	22.6
25	42.6	40.5	38.9
30	34.5	33.1	31.9

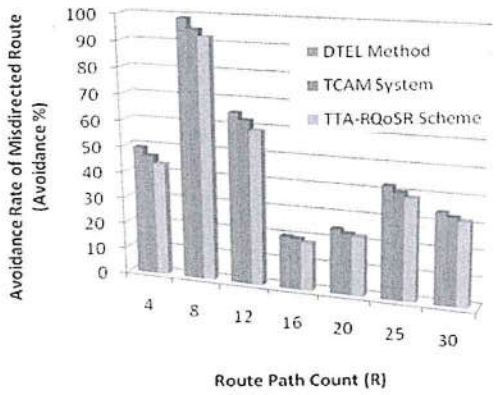

Fig. 6: Measure of avoidance rate

System (Meiners *et al*., 2011). This is because of the application of erlang's C formula in proposed TTA-RQoSR scheme. Erlang's C Formula uses the Poisson arrival process with arrival rate to avoid the misdirected route, therefore the proposed TTA-RQoSR scheme improved the avoidance rate by 6-11% when compared with the DTEL Method (Pathan *et al*., 2008). The abstained misdirected routing adjusts the flow relationship entirely on locally observed paths which improves the avoidance rate by 2-6 % when compared with the TCAM System (Meiners *et al*., 2011) (Table 2).

The results of energy consumption using TTA-RQoSR scheme with two state-of-the-art methods like DTEL Method (Pathan *et al*., 2008) and TCAM System (Meiners *et al*., 2011) is shown in Table 3.

Table 3 and Fig. 7 illustrate the energy consumption based on the sensor node mobility range. Energy consumption is reduced in TTA-RQoSR Scheme by identifying the relationship among the route path nodes and recognizes the mutually disjoint routes at the initial stage. The network usually transfers the packet through the sink node to the sensor field of varying range without any delay, so the energy consumption is reduced by 3-8% when compared with DTEL method (Pathan *et al*., 2008) and 2-5 % when compared with TCAM system (Meiners *et al*., 2011), respectively.

Table 3: Tabulation for energy consumption

Sensor node mobility (bits/sec)	Energy consumption		
	DTEL method	TCAM system	TTA-RQoSR Scheme
10	215	205	200
20	875	830	800
30	1900	1850	1800
40	3330	3270	3200
50	5160	5300	5000
60	7450	7500	7200
70	10700	10200	9800

Table 4: Tabulation for delay time

No. of Node (N)	Delay time (sec)		
	DTEL method	TCAM system	TTA-RQoSR Scheme
5	42	39	37
10	70	66	62
15	138	122	111
20	156	145	136
25	250	240	231
30	177	166	152
35	225	207	195

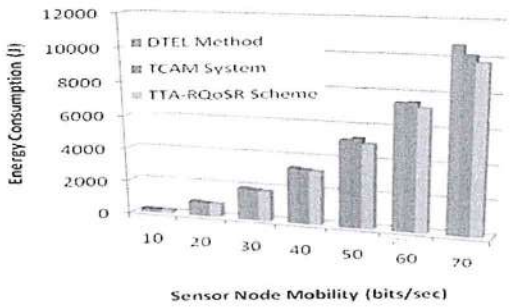

Fig. 7: Measure of Energy Consumption

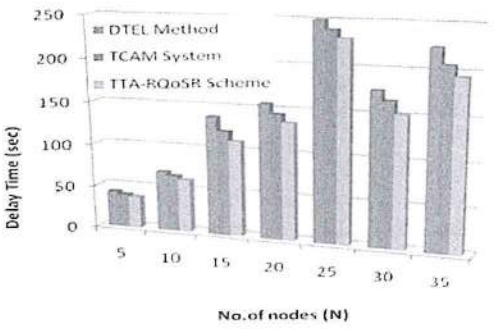

Fig. 8: Measure of delay time

Table 4 demonstrates the delay time based on number of sensor nodes using TTA-RQoSR scheme and comparison is made with two other existing methods, namely DTEL Method (Pathan *et al*., 2008) and TCAM System (Meiners *et al*., 2011).

Figure 8 measure the delay based on the node count. From Fig. 8 the proposed TTA-RQoSR scheme

PRINCIPAL.
K. S. R. INSTITUTE FOR
ENGINEERING AND TECHNOLOGY,
K. S. R. KALVI NAGAR,
TIRUCHENGODE-637 215,
NAMAKKAL Dt. TAMIL NADU.

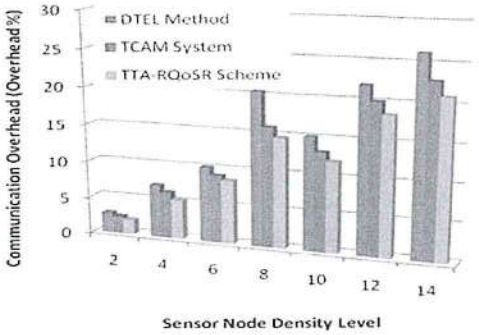

Fig. 9: Measure of communication overhead

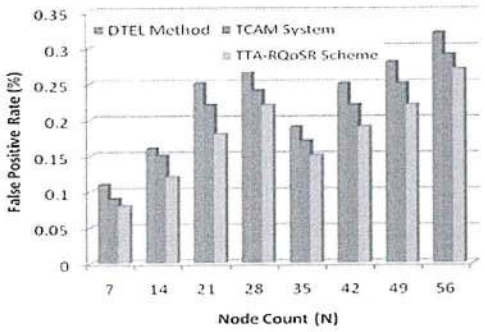

Fig. 10: Measure of false positive rate

Table 5: Tabulation for communication overhead

	Communication Overhead (%)		
Sensor node density level	DTEL method	TCAM system	TTA-RQoSR Scheme
2	2.750	2.350	2.010
4	7.130	6.270	5.320
6	10.12	9.120	8.560
8	20.49	16.00	14.74
10	15.12	13.23	12.12
12	22.01	20.05	18.45
14	26.20	22.85	21.02

Table 6: Tabulation for false positive rate

	False positive rate (%)		
Node count (N)	DTEL method	TCAM system	TTA-RQoSR Scheme
7	0.11	0.09	0.08
14	0.16	0.15	0.12
21	0.25	0.22	0.18
28	0.27	0.24	0.22
35	0.19	0.17	0.15
42	0.25	0.22	0.19
49	0.28	0.25	0.22
56	0.32	0.29	0.27

provides minimum delay time when compared to the DTEL Method (Pathan *et al*., 2008) and TCAM System (Meiners *et al*., 2011). This is because of the application of Erlang's C formula in proposed TTA-RQoSR scheme. The Erlang's C formula implementation in TTA-RQoSR Scheme reduces the delay time from 7-19% when compared with DTEL Method (Pathan *et al*., 2008). Erlang's C formula uses the stability condition to avoid the delay (i.e., elapsed time) on the varying topological structure. The transferred route path capacity is analyzed and then the overall delay rate is minimized by 3-9 % when compared to the TCAM System (Meiners *et al*., 2011).

Table 5 and Fig. 9 show the communication overhead based on sensor node density level. From the figure it is illustrative that the communication overhead is reduced using the proposed TTA-RQoSR scheme when compared to the two other existing works. Communication overhead is reduced in TTA-RQoSR Scheme by computing the load capacity. Load capacity formula demonstrated in Abstained Misdirected Routing reduces the overhead by 15-28% when compared with the DTEL Method (Pathan *et al*., 2008). The packet load capacity is measured on the overall sensor network to reduce the overhead by 6-15% when compared with the TCAM System (Meiners *et al*., 2011).

Table 6 illustrates the false positive rate based on node count using TTA-RQoSR scheme and comparison is made with two other existing methods, namely DTEL Method (Pathan *et al*., 2008) and TCAM System (Meiners *et al*., 2011). When false positive rate is reduced, proposed TTA-RQoSR scheme is said to be more efficient.

Figure 10 describes the false positive rate using TTA-RQoSR Scheme and existing method (Pathan *et al*., 2008; Meiners, 2011). From the figure we can note that the false positive rate is lower using the proposed TTA-RQoSR Scheme when compared to the existing methods DTEL Method (Pathan *et al*., 2008) and TCAM System (Meiners *et al*., 2011) respectively. The steady state in the Poisson distribution reduces the false positive rate by 15-28% when compared with the DTEL Method (Pathan *et al*., 2008) and 6-20% when compared with the TCAM System (Meiners *et al*., 2011), respectively.

Finally, Topological Transform Adaptive Relational Quality of Service Routing scheme enhances the routing structure with the higher throughput level. Abstained misdirected routing method in TTA-RQoSR scheme remove the misdirected route path for packet transfer from the source to the destination.

CONCLUSION

In this research, a novel method called Topological Transform Adaptive Relational Quality of Service Routing

PRINCIPAL.
K. S. R. INSTITUTE FOR
ENGINEERING AND TECHNOLOGY,
K. S. R. KALVI NAGAR,
TIRUCHENGODE-637 215,
NAMAKKAL Dt. TAMIL NADU.

(TTA-RQoSR) is presented. TTA-RQoSR scheme focused on the QoS metric and achieves the higher throughput rate. At the first step, the design is made on avoiding the misdirection of route over the various topological structures using the abstained misdirected routing method. The routing misdirection is computed based on the packet flow relation measure and adjusted packet flow relation measure. After the measurement in the first step of TTA-RQoSR scheme, Erlang's C formula is used to avoid the misdirected route. At the second step, TTA-RQoSR scheme uses the Relational QoS Routing to attain an improved throughput level on mobility of sensor node and sink node in WSN. Finally, TTA-RQoSR scheme achieves adaptively, avoiding the misdirected route and improving the throughput level. TTA-RQoSR scheme attains the 3.69% higher throughput level and avoidance rate. TTA-RQoSR scheme reduced the communication overhead by 9.71% and also minimizes the delay time, false positive rate and energy consumption.

REFERENCES

Chelliah, M., S. Sankaran, S. Prasad, N. Gopalan and B. Sivaselvan, 2012. Routing for wireless mesh networks with multiple constraints using fuzzy logic. Int. Arab J. Inf. Technol., 9: 1-8.

Chen, K.C., S.Y. Lin, H.S. Hung and A.Y.A. Wu, 2013. Topology-aware adaptive routing for nonstationary irregular mesh in throttled 3D NoC systems. IEEE. Trans. Parallel Distrib. Syst., 24: 2109-2120.

Cheng, W., N. Zhang, X. Cheng, M. Song and D. Chen, 2013. Time-bounded essential localization for wireless sensor networks. IEEE./ACM. Trans. Networking (TON), 21: 400-412.

Chowdhury, S.A., M.A. Uddin and S.A. Noor, 2012. A survey on routing protocols and simulation analysis of WRP, DSR and AODV in Wireless Sensor Networks. Intl. J. Mach. Learn. Comput., 2: 501-501.

Djenouri, D. and I. Balasingham, 2011. Traffic-differentiation-based modular qos localized routing for wireless sensor networks. IEEE Trans. Mobile Comput., 10: 797-809.

Guan, Q., F.R. Yu, S. Jiang and V.C. Leung, 2012. Joint topology control and authentication design in mobile ad hoc networks with cooperative communications. IEEE. Trans. Veh. Technol., 61: 2674-2685.

Kadhar, M.A., 2014. A deadlock-free dynamic reconfiguration protocol for distributed routing on interconnection networks. Int. Arab J. Inf. Technol., 11: 616-622.

Meiners, C.R., A.X. Liu and E. Torng, 2011. Topological transformation approaches to TCAM-based packet classification. IEEE./ACM. Trans. Networking (TON), 19: 237-250.

Nicopolitidis, P., G.I. Papadimitriou and A.S. Pomportsis, 2010. Adaptive data broadcasting in underwater wireless networks. IEEE. J. Oceanic Eng., 35: 623-634.

Nikravan, M. and S.M. Jameii, 2012. Combining harmony search and learning automata for topology control in wireless sensor networks. Intl. J. Wireless Mob. Networks, 4: 87-98.

Obaidat, M.S. and T. Guelzim, 2010. A Counter Disassociation Mechanism (CDM) for wireless LANs and its performance simulation analysis. IEEE. Syst. J., 4: 57-64.

Ogwu, F.J., M. Talib, G.A. Aderounmu and A. Adetoye, 2007. A framework for quality of service in mobile ad hoc networks. Int. Arab J. Inf. Technol., 4: 33-40.

Pathan, A.S.K., M.M. Monowar, M.F. Rabbi, M.M. Alam and C.S. Hong, 2008. NAMP: Neighbor aware multicast routing protocol for mobile ad hoc networks. Int. Arab J. Inf. Technol., 5: 102-107.

Valles, A.R., A.G. Marques and J.C. Sueiro, 2011. Optimal selective forwarding for energy saving in wireless sensor networks. IEEE. Trans. Wirel. Commun., 10: 164-175.

Yang, S., C.K. Yeo and B.S. Lee, 2012. Toward reliable data delivery for highly dynamic mobile ad hoc networks. IEEE Trans. Mobile Comput., 11: 111-124.

Yu, J., Y. Qi, G. Wang and X. Gu, 2012. A cluster-based routing protocol for wireless sensor networks with nonuniform node distribution. AEU-Int. J. Electron. Commun., 66: 54-61.

Yuen, W.H., S.C. Mau and R.D. Yates, 2009. Existence of data and multiuser diversities in noncooperative mobile infostation networks. IEEE. Trans. Mob. Comput., 8: 1117-1131.

Zhang, C., Y. Song, Y. Fang and Y. Zhang, 2011. On the price of security in large-scale wireless ad hoc networks. IEEE./ACM. Trans. Networking (TON), 19: 319-332.

Zhang, Y., Z. Wu and W. Trappe, 2011. Adaptive location-oriented content delivery in delay-sensitive pervasive applications. IEEE. Trans. Mob. Comput., 10: 362-376.

PRINCIPAL,
K. S. R. INSTITUTE FOR
ENGINEERING AND TECHNOLOGY,
K. S. R. KALVI NAGAR,
TIRUCHENGODE-637 215,
NAMAKKAL Dt. TAMIL NADU.

Asian Journal of Information Technology 15 (19): 3734-3741, 2016
ISSN: 1682-3915
© Medwell Journals, 2016

Resource Optimized Spectral Route Selection Protocol for WMSN Surveillance Application

[1]K. Gowsic, [2]N. Shanthi and [3]B. Preetha
[1,3]AP/CSE,Sri ShanmughaCollege of Engineering and Technology, Salem, Tamil Nadu, India
[2]Dean, Computer Science and Engineering, Nandha Engineering College, Perundurai, Tamil Nadu, India

Abstract: Most of the energy-aware routing protocols used for routing in Wireless Multimedia Sensor Networks (WMSN) employ shortest path routing for efficient transmission of data.The increasing availability of low cost wireless sensor devices enable audio, video and text data being sensed and transmitted through wireless network.However, Wireless Multimedia Sensor Networks (WMSN) requires a new routing algorithm for effective multimedia transmission. In this study we plan to develop a Resource Optimized Spectral Route Selection (RO-SRS) technique for efficient transmission of multimedia content with high and stable quality of service in WMSN surveillance applications. Spectral route selection strategy is designed by aggregating the sensed multimedia data content with similar size and same destination sink into different groups. The possible routes between the sensed multimedia content sensors to respective sink are selected from the wireless sensor communication. This point allowsmore links to be available for RO-SRS to explore more routingpaths and enables RO-SRS to be different from existing route selection technique. With possible routes, spectrum of routes is identified for efficient transmission with high throughput, minimal data loss and delay. Simulation comparison in this paper indicates that RO-SRS is highly suitable for multimedia transmission in WMSNs.

Key words: Wireless Multimedia Sensor Networks (WMSN), resource, spectral route selection, routing, employ

INTRODUCTION

Wireless multimedia sensor networks are used to enhance existing surveillance applications against crime and terrorist attacks. Largescale networks with wireless multimedia sensor networks of video sensors extend the ability of law-enforcement agencies in monitoring more sensitive areas, keeping watch on public events, private properties criminal identification and so on. Multimedia sensors record potentially relevant activities (i.e. occurrence of thefts, road traffic patrol, traffic violations) and make multimediacontent accessible for future query. Many prevalent research for sensing multimedia information using wireless technologies has received greater attention due to the increasing in surveillance applications. To achieve an improvement in (Quality of user Experience) QoE, Joint User Experience and Energy Efficiency (U-UEEE) (Singhal *et al*., 2014) method was presented using scalable video coding. However, to improve the geographic routing, a Two Phase geographic Greedy Forwarding (TPGF) (Shu *et al*., 2010) was presented owing to improvement in multimedia transmission. Another method based on Ant model was introduced in (Cobo *et al*., 2010) with the aim of providing significant QoS for multiple types of services in wireless multimedia sensor networks. Rapid advances for multimedia streaming have set the stage for layered multicasting (Shao *et al*., 2011), optimal bandwidth assignment (Xia *et al*., 2011) in WMSN. Layered multicast for multimedia streaming realized the full potential for network coding using flow optimization. On the contrary, the optimal bandwidth assignment for multiple coded video was performed aiming at achieving maximal user satisfaction. Reliable and fast content discovery was performed in (Wang and Yeo, 2011) using peer nodes to improve the rate of throughput and minimize the time delay using hybrid content discovery mechanism. Another method based on overall compression was presented by Wang *et al*. (2011) using spatial correlation model resulting in the improved data delivery through efficient identification of route path. The additional challenges created by the scalability for video multicasting must be addressed in order to deploy a model for improved video quality. Hua *et al*. (2011), an optimal

Corresponding Author: K.Gowsic, AP/CSE, Sri ShanmughaCollege of Engineering and Technology, Salem, Tamil Nadu, India

PRINCIPAL.
K. S. R. INSTITUTE FOR
ENGINEERING AND TECHNOLOGY,
K. S. R. KALVI NAGAR,
TIRUCHENGODE-637 215,
NAMAKKAL DT. TAMIL NADU.

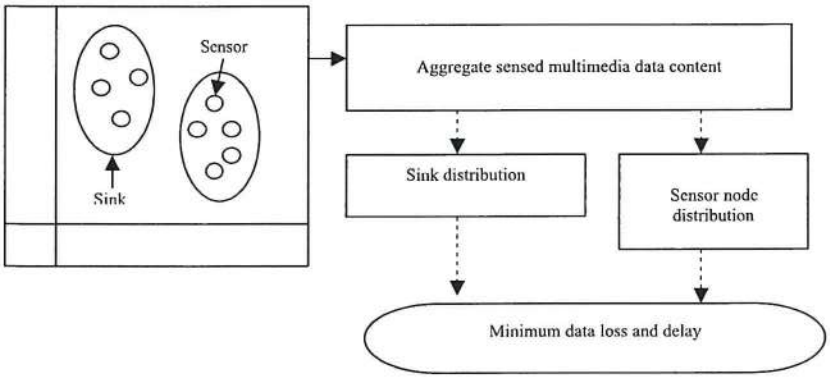

Fig. 1: Block diagram of gaussian distribution-based data aggregation

Gaussian distribution-based data aggregation: As mentioned in the previous section, the abovedescribed spectral route selection yield minimum data loss and delay with the sensed multimedia content. In this section we considerthe problem of minimum data loss and delay during route selection, i.e., finding spectral band which maximizes the rate of throughput utility. Spectrum route selection in RO-SRS technique allows the sensor nodes to switch in a dynamic manner by aggregating the sensed multimedia data content between different channels. The sensed nodes communicate with eachother with similar size and same destination sink into different groups. The Gaussian distribution-based data aggregation determine how the sensors aredistributed in the transmission area possessing similar size and specify a sink that holds a group of sensors into different groups.The Gaussian distribution-based data aggregation is used as sensors deploymentin RO-SRS techniquedue to its high capability where the number of sensor nodes is very large with differentiated channels (bands) for different groups.On the other hand, Poisson distribution model is used for sinks distribution that includes same destination sink into different groups. Figure 1 shows the block diagram of Gaussian distribution-based data aggregation.

Let us consider 'n' sensor nodes 'Sn_i = $SN_1,SN_2,...SN_n$where i = 1,2,...n' and 'm' sink nodes 'S_j = $S_1,Sn_2,...,S_m$ where I = 1,2,..., m', over a square region with sensor nodes distributed to each sink over a circularregion equal to '$\pi r^2 S_i$'.The sink nodes in WMSN are distributed using the Poisson distributionrepresented by 'γ_i' such that 'γ_i = SN_i/Area' where 'SN_i' symbolizes the sensors in each sink in WMSN and 'Area' symbolizes the area of WMSN. The probability of 'm_i' sinks distributionover group of sensors with one sink for eachgroup of sensors that includes same destination into one group is given by:

$$\text{Prob}(S_i) = \frac{\left(\frac{SN_i}{\text{Area}}\right)^{m_i}}{m_i} \quad (2)$$

On the other hand, the Gaussian density in RO-SRS technique distributes one sensor node in WMNS with similar size that has coordinates 'a_2, b_2' to monitor square area 'Area' using'(σ a_2, b_2)' is mathematically formulated as given below:

$$f(a_2,b_2) = \frac{1}{\sqrt{2\pi\sigma a_2^2 b_2^2}} e^{\frac{(a_2-b_2)^2}{2\pi\sigma a_2^2 b_2^2}} \quad (3)$$

In this way, sensed multimedia data content with similar size using Gaussian density and same destination sink using Poisson distributioninto different groups are aggregated resulting in minimum data loss and delay. The algorithmic description of multimedia data aggregation using Poisson and Gaussian distribution:

Multimedia data aggregation algorithm:

Input: Sensor nodes 'Sn_i = $SN_1,SN_2..SN_n$' sink nodes '$S_j = S_1,S_2,...S_m$'
Output: Minimized data loss
Step 1: Begin
Step 2: For each sensor nodes 'SN_i'
Step 3: For each sink nodes 'S_j'
Step 4: Send data from 'Sn_i' to 'S_j'
Step 5: Group sensor nodes 'Sn_i' based on similar size using (3)
Step 6: Group sink nodes 'S_j' based on same destinatioon using (2)
Step 7: End for
Step 8: End for
Step 9: End

As shown in the figure, the multimedia data aggregation initially groups the sensor nodes based on similar size using Gaussian distribution function aiming at reducing the delay. Next, the sink nodes are grouped based on the same destination using Poisson distribution function aiming at minimizing the data loss.

PRINCIPAL,
K. S. R. INSTITUTE FOR
ENGINEERING AND TECHNOLOGY,
K. S. R. KALVI NAGAR,
TIRUCHENGODE-637 215,
NAMAKKAL Dt, TAMIL NADU.

$$T(SN_i, SN_j, b) = MAX(b)(SN_i, SN_j) \quad (4)$$

The spectral route selection based on spectrum band routes sensed multimedia data across paths with higher spectrum availability, resulting in better utilization of the available spectrum and therefore improving the rate of throughput. The algorithmic representation of optimal throughput arrived through spectral route selection based on spectrum band.

Spectrum Route Identification algorithm:
Input: Source Node 'S' Sink Node 'S_i = $S_1, S_2, ..., S_n$', Destination Node'DN'
Output: Optimal throughput
Step 1: Begin
Step 2: For each source node 'S'
Step 3: For each destination node 'DN'
Step 4: Perform route identification based on spectrum bandwidth using (4)
Step 5: End for
Step 6: End for
Step 7: End

As shown in the figure, the spectrum route identification algorithm utilizeavailable spectrum bands by routing sensed multimedia content over pathswith higher spectrum availability. In RO-SRS technique, routes possessing highest spectrum band are then selected as candidate routes through which the sensed multimedia content is transmitted. With possible routes, spectrum of routes is identified for efficient transmission resulting in higher rate of throughput.

RESULTS AND DISCUSSION

Simulation experiments were conducted to analyze the performance of RO-SRS technique by using Network Simulation package (NS2). This environment is used to test the proposed WMSN management system and compare it with existing multimedia broadcast model. In our simulation, the WMSN is divided into multiple groups with each group consisting of many sensor nodes. Each group is responsible for aggregating the sensed multimedia data content about its environment with sensor nodes distributed in square area 'Area'. The simulation parameters are listed in Table 1. In order to evaluate the performance of our simulation, certain metrics are introduced to describe the supposed WMSN configurations. The simulation performance parameters are in the following.

Table 1: Simulation settings

Simulation parameters	Values
Simulation time	400ms
Number of runs	7
Node density	70
Node speed	0–10 m sec^{-1}
Transmission radius	105 M
Coverage area	1200×1200 m
Packet size	200 Kbps
Bandwidth	20 MHz
Initial energy	20J
Number of data packets	10, 20, 30, 40, 50, 60, 70

Throughput demonstration of RO-SRS: The main goal of our experiments is to determine the rate of throughput for providing efficient transmission of data packets to the wireless multimedia sensor network with resource optimization.We randomly generated networks between 10 and 70 data packets. We created at random networks with data packets in the range 10-70, data packet size 200 Kbps, coverage area limit 900×900 m. To achieve results in a reasonable time, we set node speed to 0-0 m sec, limiting the execution time of RO-SRS. With this network setting the rate of throughput is defined as given below.

Throughput: is one of performance metrics calculated at each sink node. Throughput measures the number of successful packets received at the sink node to the total number of the packets sent to the sink node. The rate of throughput is formulated as given below.

$$T = \frac{DP_r}{DP_s} * 100 \quad (5)$$

Where 'T' measures the throughput which is the ratio of data packets received 'DP_r' to the data packets sent 'DP_s' in WMSN.

Figure 3 shows the rate of throughput versus data packets sent. In Fig. 3, we can observe that the rate of throughput grows with the rate of data packets being sent. The experiment was conducted for data packets in the range from 10-70 but for number of data packets with 40, given network was infeasible reducing the rate of throughput. However, the rate of throughput increased with the increase in the data packets being sent. The rate of throughput is themost significant one in terms of the data packets transmission. This is implied by the fact that spectral route selection requirements improve the solution space significantly and consequentlythe rate of throughput solutions grows. With spectrum of routes identified using RO-SRS, the data packets arrived are successfully routed through available spectrum band, resulting in the improved rate of throughput. By applying RO-SRS, the rate of throughput is said to be improved by 11.80% compared to O-UEEE and 25.37% compared to TPGF.

Delay demonstration of RO-SRS: In the simulation, to clearly compare the features of both RO-SRS and existing

PRINCIPAL.
K. S. R. INSTITUTE FOR
ENGINEERING AND TECHNOLOGY,
K. S. R. KALVI NAGAR,
TIRUCHENGODE-637 215,
NAMAKKAL Dt, TAMIL NADU.

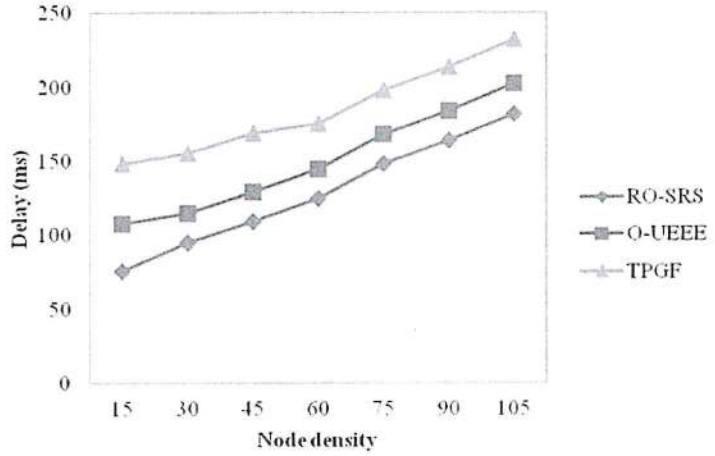

Fig. 4: Measure of routing delay

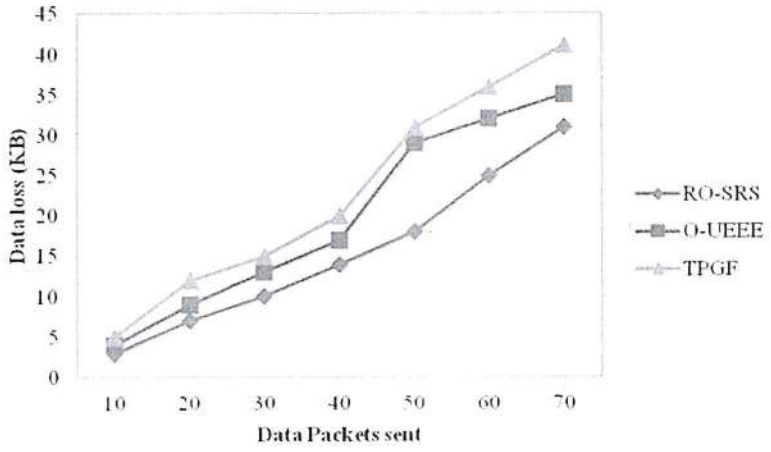

Fig. 5: Measure of data loss

for different set of node density (10–70) and node speed (0-8 m sec^{-1}). The results presented in Fig. 5 shows the data loss when sink nodes are grouped based on the same destination. We can see that the values of data loss decreased with the decrease in the data packets sent, when nodes are grouped based on the same destination using Poisson distribution. Moreover, the values of the observed parameter also increase with the increase in the number of data packets when different sink nodes exist in the network. The important observation from the figure given above is that the data loss during routing is directly proportional to the number of data packets sent. Therefore though major deviations are not being observed but comparatively the RO-SRS proved to be better. Column difference shows the percentage differenceof the particular routing scenario with respect to the data loss occurrence using three different methods. The data loss for 10-data packets and 20-data packets was reduced in RO-SRS by 33.33 and 28.57% in the case compared with O-UEEE; 66.66 and 71.42% in the case compared with TPGF.

CONCLUSION

Using multimedia sensor nodes can enhance the capabilityof WMSNs for efficient route selection by aggregating the sensed multimedia data content with similar size and same destination sink into different

PRINCIPAL,
K. S. R. INSTITUTE FOR
ENGINEERING AND TECHNOLOGY,
K. S. R. KALVI NAGAR,
TIRUCHENGODE-637 215,
NAMAKKAL Dt, TAMIL NADU.

World Applied Sciences Journal 34 (7): 871-877, 2016
ISSN 1818-4952
© IDOSI Publications, 2016
DOI: 10.5829/idosi.wasj.2016.34.7.122

A High Step-Up Hybrid DC-DC Converter with Reduced Voltage Stress for Renewable Energy Applications

[1]S. Ravivarman, [2]R. Jeyabharath and [2]P. Veena

[1]K.S. Rangasamy College of Technology, Tiruchengode, Tamilnadu, India - 637215
[2]KSR Institute for Engineering and Technology, Tiruchengode, Tamilnadu, India - 637215

Abstract: This paper proposes a high step-up dc-dc converter with voltage-lifted switched inductor cell, switched-capacitor and voltage multiplier cell. The voltage multiplier cell is used to reduce the voltage stress across the switch and to extend the voltage gain. In addition, this converter consists of simple control system, since there is only one active switch. The operating principle, key waveforms and design details are also presented. The proposed topology is simulated in PSIM to verify the performance of the proposed converter.

Key words: Boost converter · Switch voltage stress · Switched capacitor · Switched inductor · Voltage-lift

INTRODUCTION

The International Energy Agency (IEA), forecasts that the global primary energy demand on 2030 increases by 1.5% annually from now. Developing Asian countries are the main contributors to this growth, followed by the Middle East region. Growth in per capita energy consumption in the past two decades has occurred in all parts of the world primarily because of increased participation in the transport sector, followed by manufacturing. Exceptions to this trend are China and India, where growth is mainly taken in the manufacturing sector, followed by the household sector. A large and sustainable economic growth in India is to develop a great demand for energy resources. Demand and the imbalance between the supply of energy sources is a widespread phenomenon that requires serious efforts of the Government of India to increase the energy supply. More than 50% of the population is little or no energy business for life and living. Renewable energy can make a significant contribution in each of the areas mentioned above. In this context, the role of renewable energy must be seen. Alternative energy such as photovoltaic, bio-fuel and chemical energy such as fuel cell become increasingly key part of the solution to the country's energy needs. The renewable energy is an important element in the energy planning process in India for more than two decades.

Power Electronic devices continues to innovate and the importance of switching power converter is increasing, in which boost converter is widely used in renewable energy systems. In order to boost the available low voltage to high voltage of 380 V, which is required by the full-bridge inverter to connect with a 220 V grid. A huge number of dc-dc converter topologies were proposed and implemented in the range of hundred watt to multiples of kW. The dc-dc converters are generally classified in to two: isolated converters and non-isolated converters. The isolated converters use transformer for isolation which may be necessary or not in some countries. In order to reduce the cost of the system without compromising gain and efficiency, the non-isolated dc-dc converters are to be used in renewable energy applications [1, 2]. The non-isolated dc-dc converters are classified into five categories, such as cascaded dc-dc converter, coupled inductor based boost converter, switched capacitor (SC) based boost converter, switched inductor (SL) based boost converter and voltage multiplier (VM) cell based boost converter.

The conventional boost converters are cascaded is series and/or parallel to increase the voltage gain of the converter [3-5]. The cascaded converters consist of large number of components, so it is not suitable for high power applications. Coupled inductors are a different method used to increase the voltage gain, reduce the reverse recovery problem of the output diode and to

Corresponding Author: S. Ravivarman, Department of EEE, K.S. Rangasamy College of Technology, Thokkavadi Post, Tiruchengode, Namakkal District, Tamilnadu, India - 637215.

PRINCIPAL,
K. S. R. INSTITUTE FOR
ENGINEERING AND TECHNOLOGY,
K. S. R. KALVI NAGAR,
TIRUCHENGODE - 637 215,
NAMAKKAL Dt, TAMIL NADU.

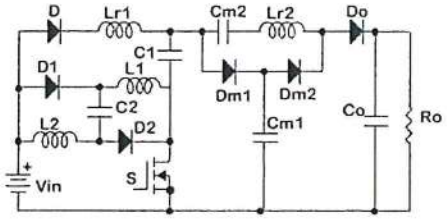

Fig. 1: Proposed Voltage-Lifted Switched-Inductor-Capacitor (VLSIC) converter

reduce the input current ripple [4-8]. The capacitors are switched to charge and discharge in a dc-dc converter to increase the voltage gain. The switched capacitor converter requires a large number of components to achieve high output voltage, which in turn increases the cost, weight and volume of the converter [9-12]. The switched inductor (SL) and voltage-lifted switched-inductor (VLSI) based converters have been explored [13-16]. The voltage multiplier cells are incorporated in the boost converter topologies to increase the voltage gain as well as to reduce the voltage stress across the switch [17-20].

The proposed voltage-lift switched-inductor-capacitor converter is different from existing high step-up dc-dc converters and it is derived from the topology proposed in [21]. The proposed converter has less voltage stress in the power switch and the voltage gain is high when compared to conventional boost converter adopted with any of the techniques like SL, SC, VM and VLSI. This paper is organized as follows. The topology and operation of the proposed converter are presented in section 2. The analysis and expressions for the voltage gain and voltage stress are given in section 3. The simulation results and the performance evaluation are given in section 4. Finally, this paper is concluded in section 5.

Proposed Converter: The topology proposed in [21] is modified by replacing the switched inductor cell with voltage-lift switched inductor (VLSI) cell and it is given in Figure 1. The VLSI cell is formed by D_1, D_2, L_1, L_2 and C_2. The capacitor C_1 forms the switched-capacitor (SC) cell. The main purpose the inductors, L_r is to reduce the current peak formed by the capacitors in SC and VM cells. The VLSI and SC cell are connected in parallel with the source when they are charging and they are connected in series when discharging. The resonant inductor forms a tank circuit and we have to ensure that the zero crossing of inductor current before the switch is turned off.

Operating Principle: The assumptions made to analyze the circuit are as follows: All the converter components are ideal; The inductors and capacitors are very large, then the voltage across capacitor and current through the inductor will be constant and continuous. The operating modes of the proposed topology are shown in Figure 2.

Mode 1 (t_0-t_1): In this mode, the power switch, S is in turned off condition. The diodes D_{M1} and D_O are forward biased and diodes D and D_{M2} are reverse biased. The capacitor C_1, the inductors L_1 and L_2 are connected in series with the input voltage source as shown in Figure 2(a). The energy stored previously in the capacitor, C_1 is discharged to C_{M1} through D_{M1}, to capacitor C_{M2} through L_{r2} and to output capacitor C_O through D_O. The current in the resonant inductor L_{r2} (i_{Lr2}) is increased up to the level of VLSI cell input current and simultaneously the current in the diode D_{M1} is reduced. This change in current occurs in linear manner. Simultaneously, the voltage across the multiplier capacitor, C_{M1} is increased and across multiplier capacitor, C_{M2} is decreased and the voltage across resonant inductor, L_{r2} is constant in this mode.

Mode 2 (t_1-t_2): At instant t_1, the diode current i_{DM1} is zero and the current i_{Lr2} and VLSI cell inductor current are equal as shown in Figure 3. The energy stored in the VLSI cell inductors are transmitted to load though the output diode D_O. The inductor current and the capacitor voltage both decreases at the instant t_2.

Mode 3 (t_2-t_3): At the time instant t_2, the switched is turned on. The diodes D_{M1} and D_O are reverse biased; D_{S1}, D_{S2}, D_{M2} and D are forward biased. The VLSI cell inductors and the capacitor C_1 forms the tank circuit. The tank circuit will cause a sinusoidal resonant current in C_1 and the VLSI cell inductor current will increase as shown in Figure 3. Once the amplitude of current oscillation reaches zero, the diode, D is reverse biased. The energy stored in the C_{M1} is transferred to C_{M2} through D_{M2} until the time instant t_3. Once the energy is fully transferred from C_{M1} to C_{M2}, the diode D_{M2} is reverse biased. The average output voltage will appear across the output capacitor C_O and it will be the sum of the voltage across the capacitor C_{M2} and the voltage at the input of multiplier cell.

Mode 4 (t_3-t_4): Once the resonance condition stops in the VLSI cell, the power switch, S continues to conduct. So the VLSI cell inductor current increases further. Since the capacitor is fully charged, there will be no current flowing through it. Similarly, at t_3, the current in

PRINCIPAL,
K. S. R. INSTITUTE
ENGINEERING AND TE
K. S. R. KALVI NA
TIRUCHENGODE - 63
NAMAKKAL Dt, TAMIL NADU

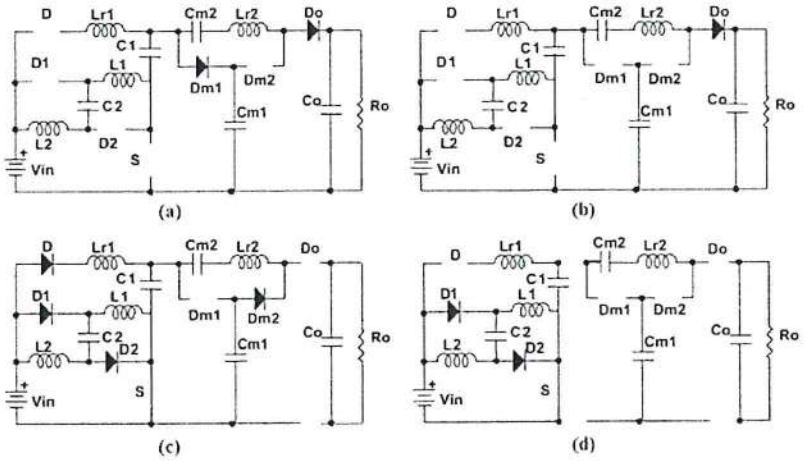

Fig. 2: Operating modes of the proposed converter. (a) Mode 1, (b) Mode 2, (c) Mode 3, (d) Mode 4

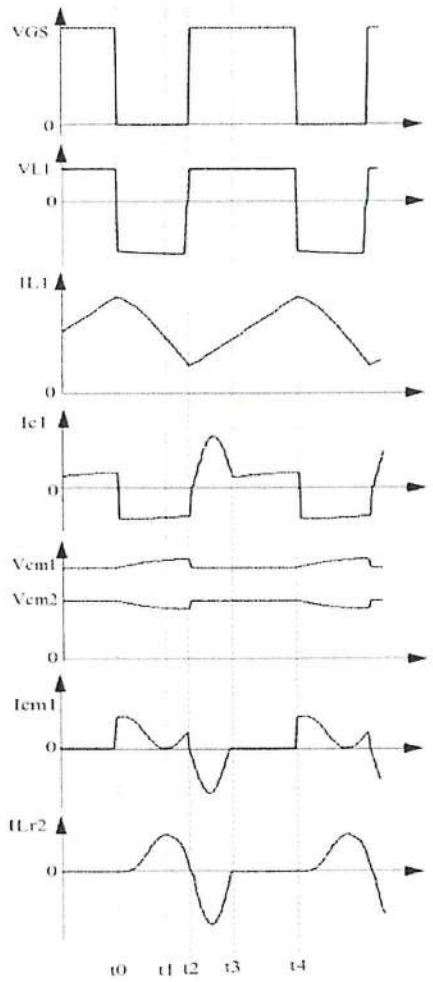

Fig. 3: Theoretical waveforms of the proposed converter

the resonant inductor L_{r2} is zero and in turn it reverse biases the VM cell diode, D_{M2}. Therefore, the output circuit is completely isolated from the source, the VLSI cell inductors will charge from the input voltage source. The VLSI cell and switched capacitor cell will remain in this state until the switch is turned off as shown in Figure 3. Once the switch is turned off, the above four modes will be repeated. Since the diodes in the VLSI and VM cells are turned off naturally, the reverse recovery problems are alleviated.

Analysis and Design Specifications: During switching-on period, the capacitors C_1 and C_2 are charged from the input voltage V_{in} as shown in Figure 2(c), since the capacitors are sufficiently large, both voltages are equal.

$$VC_1 = V_{in} \tag{1}$$

$$V_{C2} = V_{in} \tag{2}$$

$$V_{CM2} = V_{CM1}\, V_{in} \tag{3}$$

The inductor current increases during the on period and decreases during the off period of the power switch, S. The voltage appears across the inductors L_1 and L_2 during on period is V_{in}.

$$V_{L1} = V_{L2} = V_{in} \tag{4}$$

From Figure 2(a), the voltage across the inductor L_1 or L_2 during off state is given by.

$$V_{L1} = V_{L2} = \frac{V_{CM1} - V_{in} - V_{C1} - V_{C2}}{2} \tag{5}$$

PRINCIPAL,
K. S. R. INSTITUTE FOR
ENGINEERING AND TECHNOLOGY,
K. S. R. KALVI NAGAR,
TIRUCHENGODE - 637 215,
NAMAKKAL Dt, TAMIL NADU.

Table 1: Comparison of proposed converter and other converters

Converter	Conventional boost converter	Converter proposed in [22]	Converter proposed in [23]	Converter proposed in [24]	Converter proposed in [21]	Proposed converter
Voltage gain	2.5	7	6	7.5 for n=2	9	11
Output voltage	30 V	84 V	72 V	90 V	108 V	132 V
Voltage stress of active switch	7.2 V	48 V	30 V	30 V	48 V	42 V
Voltage stress of output diode	7.2 V	96 V	-	-	48 V	60 V
Voltage stress of intermediate diodes	-	12 V	30 V	30 V	12 V	
				48 V	18 V	30V
				60 V	48 V	60 V

And the output voltage is equal to the sum of multiplier capacitor voltages.

$$V_O = V_{CM1} + V_{CM2} \tag{6}$$

From (1) and (2), the inductor voltage can be rewritten as;

$$V_{L1} = V_{L2} = \frac{V_{CM1} - 3V_{in}}{2} \tag{7}$$

By applying the volt-second balance principle, the voltage across the inductor is given by;

$$DV_{in} = (1-D)\frac{V_{CM1} - 3V_{in}}{2} \tag{8}$$

Hence, the voltage across the multiplier capacitor, C_{M1} is;

$$V_{CM1} = \frac{(3-D)V_{in}}{1-D} \tag{9}$$

Substituting (9) in (3) gives the voltage across the multiplier capacitor C_{M2}

$$V_{CM2} = \frac{2}{1-D} \tag{10}$$

Substituting (9) and (10) in (6), the output voltage is;

$$V_O = \frac{5-D}{1-D}V_{in} \tag{11}$$

Therefore, the voltage gain of the proposed converter is;

$$G = \frac{5-D}{1-D} \tag{12}$$

From Figure 2(a), the voltage stress on switch, S is given by;

$$V_S = V_{CM1} - V_{C1} = \frac{2-D}{1-D}V_{in} \tag{13}$$

Also from Figure 2(a) the voltage stress across the diode D_{M2} is;

$$V_{DM2} = V_O - V_{CM1} = V_{CM2} = \frac{2}{1-D}V_{in} \tag{14}$$

From Figure 2(c) the voltage stress across the multiplier diode D_{M1} and output diode D_O is calculated.

$$V_{DM2} = V_{CM1} - V_{C1} = V_{CM2} = \frac{2}{1-D}V_{in} \tag{15}$$

$$V_{DO} = V_O - V_{CM1} = V_{CM2} = \frac{2}{1-D}V_{in} \tag{16}$$

The voltage stress on the diodes D_1 and D_2 are

$$V_{D1} = V_{L2(Mode\ 1)} + V_{C2} \tag{17}$$

$$V_{D2} = V_{L1(Mode\ 1)} + V_{C2} \tag{18}$$

$$V_{D1} = V_{D2} = \frac{V_{in}}{1-D} \tag{19}$$

From (13) to (19), it is clear that the voltage stress across all the semiconductor devices are lesser than the half of the output voltage. Table 1 gives the comparison of voltage gain and voltage stress across the semiconductor devices of the proposed converter with conventional boost converter and various converter topologies proposed in [21-25], when operating at duty cycle of 0.6 with 12 V input.

Simulation Results: In order to verify the theoretical analysis and the performance of the converter, the proposed converter is simulated in PSIM v9.0. The circuit parameters are calculated from the design equations and they are: $V_{in} = 12$ V, $L_1 = L_2 = 44$ µH, $C_1 = C_2 = 47$ µF, $C_{M1} = C_{M2} = 1$ µF, $C_O = 220$ µF, $L_{r1} = L_{r2} = 1$ µH, R = 60 Ω. The switching frequency and the duty ratio are selected as 100 kHz and 0.6. Figure 4 shows the gate drive voltage of the power switch, output voltage and current and the voltage stress across the output diode. The output voltage is 132 V and it is equal to the theoretical value calculated by using the voltage gain formula. The ripple in the output voltage is very low and it is in acceptable limit.

PRINCIPAL,
K. S. R. INSTITUTE FOR
ENGINEERING AND TECHNOLOGY,
K. S. R. KALVI NAGAR,
TIRUCHENGODE - 637 215.
NAMAKKAL Dt, TAMIL NADU.

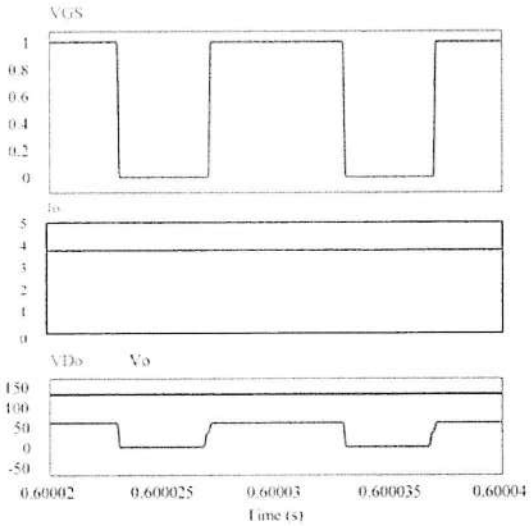

Fig. 4: Gate voltage, output current, output diode voltage stress and output voltage of the proposed converter

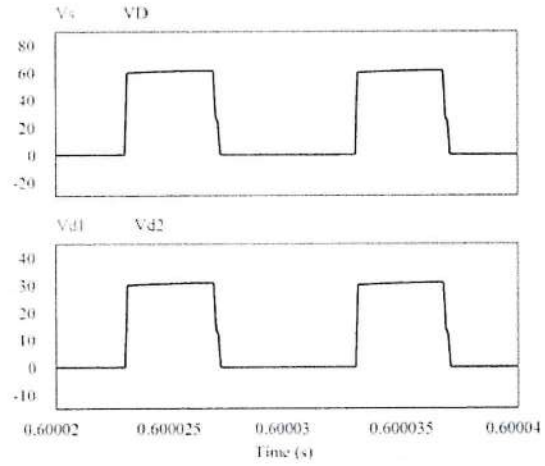

Fig. 5: Voltage stress across the semiconductor devices of the proposed converter

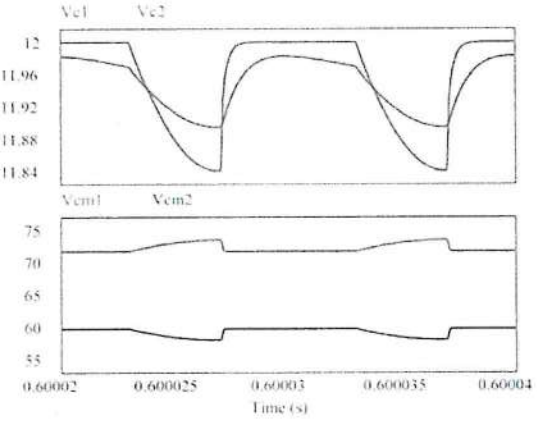

Fig. 6: Voltage across the various capacitors of the proposed converter

PRINCIPAL,
K. S. R. INSTITUTE FOR
ENGINEERING AND TECHNOLOGY,
K. S. R. KALVI NAGAR,
TIRUCHENGODE - 637 215,
NAMAKKAL DT, TAMIL NADU.

The voltage stress across the output diode is 60 V that is lower than the output voltage. Figure 5 shows the voltage stress across the switch and diodes and they are also lesser than the output voltage. Therefore, the switch and diodes with low R_{DS-on} can be used to reduce the cost and conduction losses of the converter. The voltage across the capacitors are shown in Figure 6 and its values validate the theoretical analysis. The voltage across all the elements and devices in the simulation results are same as theoretical results.

CONCLUSION

In this paper, a new high step-up converter that can be used in renewable energy applications is proposed. The proposed converter topology has the capability to obtain high voltage gain in low duty cycle. This converter has low voltage stress on the switch and diodes and hence the semiconductor devices with low turning-on resistance can be used to reduce the conduction losses. The converter consists of only one power switch which makes its control easy. The operation of the converter is presented and it is simulated in both PSIM and Multisim. The simulation results confirm the theoretical analysis and performance of the proposed converter and it is evident that the proposed converter can be used in wide areas where large dc-dc gain is required.

REFERENCES

1. Wai, R.J. and W.H. Wang, 2008. Grid-Connected Photovoltaic Generation System. IEEE Transactions on Circuits and Systems I: Regular Papers, 55(3): 953-964.
2. Wai, R.J., W.H. Wang and C.Y. Lin, 2008. High-Performance Stand-Alone Photovoltaic Generation System. IEEE Transactions on Industrial Electronics, 55(1): 240-250.
3. Huber, L. and M.M. Jovanovic, 2000. A design approach for server power supplies for networking applications. In the proceedings of Fifteenth Annual IEEE Applied Power Electronics Conference and Exposition, 2: 1163-1169.
4. Li, W., J. Xiao, J. Wu, J. Liu and X. He, 2009. Application Summarization of Coupled Inductors in DC/DC Converters. In the proceedings of Twenty-Fourth Annual IEEE Applied Power Electronics Conference and Exposition, pp: 1487-1491.
5. Ping Yang, Jianping Xu, Guohua Zhou and Shiyu Zhang, 2012. A new quadratic boost converter with high voltage step-up ratio and reduced voltage stress. In the proceedings of 7th International Power Electronics and Motion Control Conference (IPEMC), pp: 1164-1168.
6. Chen, Z., Q. Zhou and J. Xu, 2015. Coupled-inductor boost integrated flyback converter with high-voltage gain and ripple-free input current. IET Power Electronics, 8(2): 213-220.
7. Qun, Zhao and F.C. Lee, 2003. High-efficiency, high step-up DC-DC converters. IEEE Transactions on Power Electronics, 18(1): 65-73.
8. Moon-Hwan Keum, Yoon Choi, Sang-Kyoo Han and Jeong-Il Kang, 2013. High efficiency voltage-clamped coupled-inductor boost converter. In the proceedings of 39th Annual Conference of the IEEE Industrial Electronics Society, IECON, pp: 828-833.
9. Liang, T.J., S.M. Chen, L.S. Yang, J.F. Chen and A. Ioinovici, 2012. Ultra-Large Gain Step-Up Switched-Capacitor DC-DC Converter With Coupled Inductor for Alternative Sources of Energy. IEEE Transactions on Circuits and Systems I: Regular Papers, 59(4): 864-874.
10. Ren Xie, Longlong Zhang, M. Mellincovsky, A. Ioinovici and Dehong Xu, 2012. A new large DC gain converter based on a switched-capacitor-inductor circuit in conjunction with fuel cell. In the proceedings of 7th International Power Electronics and Motion Control Conference (IPEMC): 379-383.
11. Gu, D., D. Czarkowski and A. Ioinovici, 2011. A large DC-gain highly efficient hybrid switched-capacitor-boost converter for renewable energy systems. In the proceedings of 2011 IEEE Energy Conversion Congress and Exposition, pp: 2495-2500.
12. Tang, Y., T. Wang and Y. He, 2014. A Switched-Capacitor-Based Active-Network Converter With High Voltage Gain. IEEE Transactions on Power Electronics, 29(6): 2959-2968.
13. Axelrod, B., Y. Berkovich and A. Ioinovici, 2008. Switched-Capacitor/Switched-Inductor Structures for Getting Transformerless Hybrid DC–DC PWM Converters. IEEE Transactions on Circuits and Systems I: Regular Papers, 55(2): 687-696.
14. Luo, F.L., 1999. Positive output Luo converters: voltage lift technique," in the proceedings of IEE Proceedings - Electric Power Applications, 146(4): 415-432.

PRINCIPAL,
K. S. R. INSTITUTE FOR
ENGINEERING AND TECHNOLOGY,
K. S. R. KALVI NAGAR,
TIRUCHENGODE - 637 215,
NAMAKKAL Dt, TAMIL NADU.

15. Zhu, M. and F.L. Luo, 2008. Series SEPIC implementing voltage-lift technique for DC-DC power conversion. IET Power Electronics, 1(1): 109-121.
16. Zhu, M. and F.L. Luo, 2010. Enhanced Self-Lift Cûk Converter for Negative-to-Positive Voltage Conversion. IEEE Transactions on Power Electronics, 25(9): 2227-2233.
17. Gules, R., L.L. Pfitscher and L.C. Franco, 2003. An interleaved boost DC-DC converter with large conversion ratio. In the proceedings of 2003 IEEE International Symposium on Industrial Electronics, 1: 411-416.
18. Zhou, L.W., B.X. Zhu, Q.M. Luo and S. Chen, 2014. Interleaved non-isolated high step-up DC/DC converter based on the diode-capacitor multiplier. IET Power Electronics, 7(2): 390-397.
19. Prudente, M., L.L. Pfitscher, G. Emmendoerfer, E.F. Romaneli and R. Gules, 2008. Voltage Multiplier Cells Applied to Non-Isolated DC–DC Converters. IEEE Transactions on Power Electronics, 23(2): 871-887.
20. Alcazar, Y.J.A., D. De Souza Oliveira, F.L. Tofoli and R.P. Torrico-Bascopé, 2013. DC–DC Nonisolated Boost Converter Based on the Three-State Switching Cell and Voltage Multiplier Cells. IEEE Transactions on Industrial Electronics, 60(10): 4438-4449.
21. Shanmugasundaram, R., J. Rajaiah and V. Parasunath, 2016. Analysis and Design of Single Switch Hybrid Step-Up Converter. Circuits and Systems, 7(4): 211-221.
22. Tang, Y., D. Fu, T. Wang and Z. Xu, 2015. Hybrid Switched-Inductor Converters for High Step-Up Conversion. IEEE Transactions on Industrial Electronics, 62(3): 1480-1490.
23. Wu, B., S. Li, Y. Liu and K. Ma Smedley, 2016. A New Hybrid Boosting Converter for Renewable Energy Applications. IEEE Transactions on Power Electronics, 31(2): 1203-1215.
24. Das, M. and V. Agarwal, 2016. Design and Analysis of a High-Efficiency DC–DC Converter With Soft Switching Capability for Renewable Energy Applications Requiring High Voltage Gain. IEEE Transactions on Industrial Electronics, 63(5): 2936-2944.

PRINCIPAL,
K. S. R. INSTITUTE FOR
ENGINEERING AND TECHNOLOGY,
K. S. R. KALVI NAGAR,
TIRUCHENGODE - 637 215,
NAMAKKAL Dt, TAMIL NADU.

Asian Journal of Information Technology 15 (22): 4662-4668, 2016
ISSN: 1682-3915
© Medwell Journals, 2016

Fuzzy Controlled Bridgeless Cuk Converter Fed Switched Reluctance Motor

[1]Kulandaivel Velusamy, [2]Veena Parasunath and [1]Jeyabharath Rajaiah
[1]Department of EEE, K.S. Rangasamy College of Technology, Tamil Nadu, India
[2]Department of EEE, KSR Institute for Engineering and Technology, Tamil Nadu, India

Abstract: The researchin this study aims at designing and modelling of a bridgeless cuk converter for driving a switched reluctance motor. Bridgeless Cuk converters are new series of AC-DC converters, it contain very less ripple of voltage and current and have output wave with good quality, high power concentration and good transfer voltage gain and no circuit elements parasitic limits of traditional converters. Bridgeless Cuk converters have good voltage transfer gains in arithmetic development on step by step. For the switched reluctance Motor drive, the C-dump converter is used. The present design aims at improving the effectiveness of the switched reluctance motor drive system by the incorporation of the Bridgeless Cuk converter between the electrical source and the drive system. The rule base of the fuzzy logic controller is modified to improve the stability of the controller without affecting the system performance. MATLAB simulation results are presented in this paper to explain the working of the proposed drive.

Key words: Bridgeless CUK converter, SRM, fuzzy logic controller, DC-DC converter, C-dump converter

INTRODUCTION

Switched Reluctance Motors (SRM) have inherent merits such as easy structure with non-winding assembly in rotor side, better tolerance, heftiness, low cost with no permanent magnet in the construction and it can operate with high temperatures or in extreme temperature variations (Ahn *et al*., 2010). It is an electric machine which converts the reluctance torque into mechanical output. In SRM, the stator and rotor enclose a structure of salient-pole, due to salient poles it generate a high output torque. The torque is created by the arrangement inclination of poles (Ahn *et al*., 2010).

Bridgeless Cuk converters allow power transfer in both directions (Kavitha and Uma, 2008). Due to their capability to reverse the direction of flow of power and thereby the current direction of the motor is changed. Power quality issues are the major issue, for reducing the harmonics in supply current by various international power quality standard like the International Electro technical Commission (Bist and Singh, 2014) (IEC) 61000-3-2. In all AC-DC converters, the power transfer efficiency and output voltage are limited by power electronic elements. But in calculation, usual converters can produce high voltage with high efficiency. BL-Cuk converters (Luo and Ye, 2013) are new AC-DC converters that defeat the above disadvantages effects and for the increasing of voltage and the power transfer efficiency. These converters produce improved voltage from low voltage of photovoltaic operation.

However, fundamental converters like as Boost converter and Buck converter cannot be use in the high-power circumstances and at the similar time have many limitations. In modern years, conversion methods have been improved rapidly and there are stacks of topologies of DC-DC converters. Bridgeless converters are more suitable in order to improve the power factor at Source of supply. The distinctive characteristic of a bridgeless PFC converter is which eliminates the need of a diode bridge rectifier at the input. Which reduce the power losses, so we get improves overall system efficiency as a result with equal cost savings. PFC rectifiers are used to recover the rectifier power density and to decrease noise emissions via soft switching methods or coupled magnetic techniques (Yang, 2012; Agirman *et al*., 2001).

A usual PFC scheme has lower efficiency due to major losses in the diode bridge. Usually boost converters are used as front end rectifiers (Barnes and Pollock, 1998; Lee *et al*., 2007). For low level voltage applications like computer industry or telecommunication an isolation transformer or extra converter is needed to step down the voltage level. Bridgeless PFC buck converters are restricted for step down applications (Tseng *et al*., 2000). Input line current cannot trace the input voltage around zero crossings of the input line voltage.

Corresponding Author: Kulandaivel Velusamy, Department of EEE, K.S. Rangasamy College of Technology, Tamil Nadu, India

PRINCIPAL,
K. S. R. INSTITUTE FOR
ENGINEERING AND TECHNOLOGY,
K. S. R. KALVI NAGAR,
TIRUCHENGODE-637 215,
NAMAKKAL Dt. TAMIL NADU.

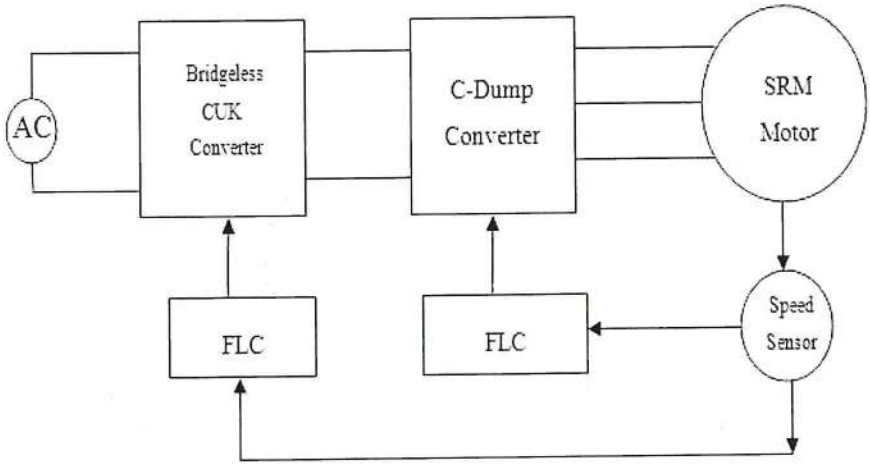

Fig. 1: CUK converter based SRM drive

SRM drive requires the power converters to control the switching sequence of the stator windings (Agirman *et al*., 2001). An asymmetric bridge SRM converter has 2 switches (plus 2 diodes) per phase. This type of converter topology gives more flexible and effective control to current waveforms of an SRM but it contains large number of switches (Barnes and Pollock, 1998). The c-dump circuit has only one switch per phase (Lee *et al*., 2007). Stator winding is transferring the stored magnetic energy after it turn-off the power switch, to the storage capacitor and it sent to the power supply through a step-down dc chopper. The technique could limit the overall cost of the SRM drive.

The self-tuning fuzzy logic controller is used to adjust the output scaling factor with their current states of the controller (Mudi and Pal, 1999). The membership functions and scaling factors are tuned for their corresponding working operation is said to be self-tuning fuzzy logic controller (Chung *et al*., 1998).

Proposed CUK converter fed switched reluctance motor drive: In the proposed circuit model given input AC supply is converted into the dc supply with the help of the BL-CUK. The CUK converter is used to improve the output quality of the supply. It means in the CUK converter output it contain the low level harmonics, small distortion and less ripple. By controlling the CUK converter output, SRM motor output performance is improved. The CUK converter operation and SRM Drive operation is controlled by using Fuzzy Logic Controller (FLC). Thus the C- Dump converter (Lee *et al*., 2013) is the more efficient converter compare to another converter.

Thus, the C- Dump converter is use to drive the SRM motor. The FLC is used to give the rotor position and also it produces the pulse signal to the C-dump converter. The features of FLC are five fuzzy sets for input and output, triangular membership function, mamdani fuzzy inference system with implication by min operator and defuzzification using centroid method. The switching of the Cuk converter switches are controlled by FLC thereby controlling the SRM drive ripples in torque and current (Fig.1).

MATERIALS AND METHODS

Operating principle of BL-Cuk converter: Cuk converter is actually combination of a boost converter and a buck converter. Cuk converter has the following merits. Such as continuous output current, continuous input current, output voltage can be either improved or fewer than the input voltage.

The bridgeless Cuk converter working in a DICM mode which gives an inherent PFC and require a easy voltage follower method for the voltage control and small size of heat sink for the switches (Luo and Ye, 2003, 2004; Silpa and Chitra, 2014).

Operation of bridgeless Cuk converters: The mode of operation of a PFC converter is a crucial problem because it affects the cost and rating of the components used in the PFC converter. Discontinuous Conduction Mode (DCM) and Continuous Conduction Mode (CCM) are broadly used in practical application. In DCM or CCM, the current of the inductor or the voltage across in-between capacitor in a PFC converter remains discontinuous or

PRINCIPAL,
K. S. R. INSTITUTE FOR
ENGINEERING AND TECHNOLOGY,
K. S. R. KALVI NAGAR,
TIRUCHENGODE-637 215,
NAMAKKAL Dt. TAMIL NADU.

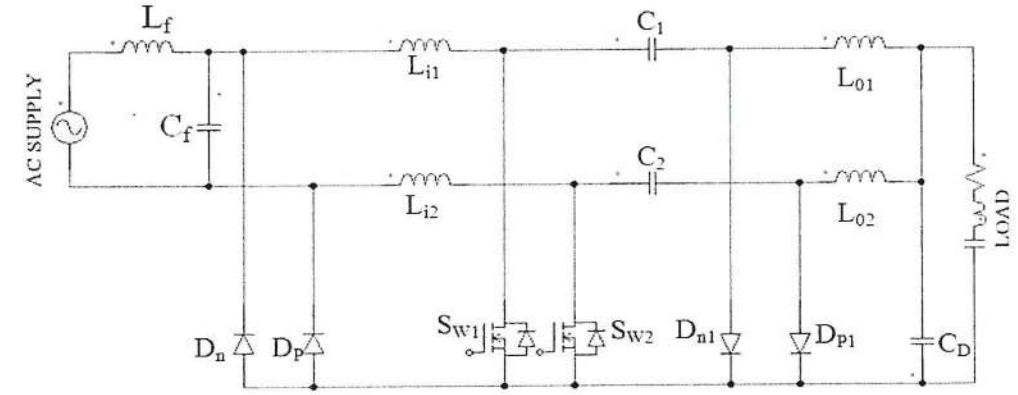

Fig. 2: Bridgeless Cuk converter

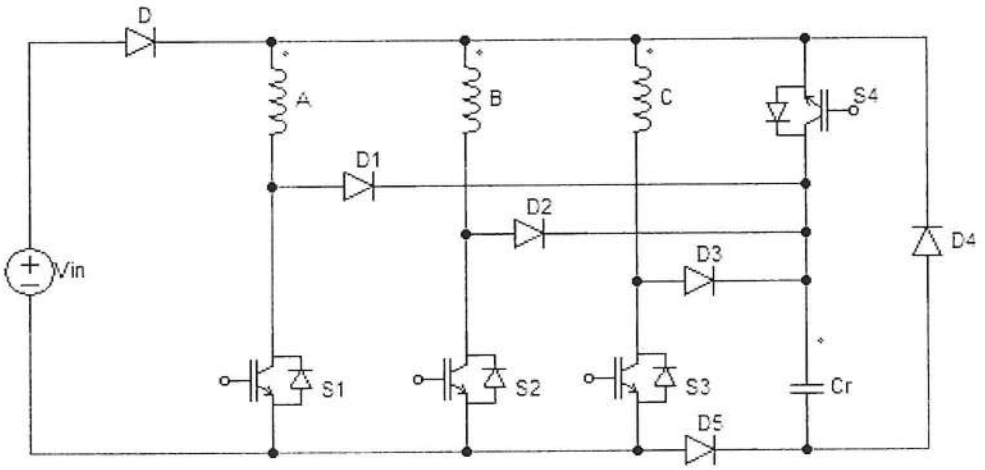

Fig. 3: C-dump converter

continuous in a switching period correspondingly. To activate a PFC converter in CCM, it requires three sensors (2 voltage, current) while a DCM process achieved by using only one voltage sensor. While the PFC converter operates in DCM mode the stresses is high, when compared to CCM mode operation. By operating the converter in DCM, many merits can be achieved such as near to unity power factor, at zero current the power switches are turned ON and output diodes are turned OFF (Fig. 2).

Operation of converter is depending upon the application. For high power applications CCM is suitable and low power application DCM is preferred. Conversely, DCM operation considerably increases the conduction losses due to the large current stress through circuit apparatus. DCM leads to one limitation, it can operate at low-power applications only (>300 W). So the DCM is chosen for low-power applications.

C- Dump converter for SRM drive: It is derived from the C-dump converter (Lee *et al*., 2007) circuit by eliminating the inductor of the Cuk converter. The energy can be stored in the capacitor and it is used for the next phase and being returned to the dc supply of conventional C-dump representation. At that time the capacitor have the voltage level of 2 V_{dc} in C-dump converter, its proper utilization significantly improves the drive performance.

By the modified C-dump converter, the energy in the dump capacitor is directly utilized to energize phase windings and to maintain the dump capacitor voltage at V_{dc} rather than $2V_{dc}$. Control of the dump capacitor voltage is streamlined and replication of the phase currents is enabled in an energy efficient C-dump converter. Figure 3 shows the energy competent C-dump converter topology, derived from the conventional C-dump converter (Tseng *et al*., 2000). The topology could

PRINCIPAL.
K. S. R. INSTITUTE FOR
ENGINEERING AND TECHNOLOGY,
K. S. R. KALVI NAGAR.
TIRUCHENGODE-637 215,
NAMAKKAL Dt. TAMIL NADU.

minimize the whole cost of the switched reluctance motor drive. The potential ratings of the c-dump capacitor and a few of the switching devices in the energy efficient C-dump converter are reduced to the supply voltage (V_{dc}) level likened to twice the supply voltage ($2V_{dc}$) in the conventional C-dump converter. In addition, the converter has modest control requirements and allows the motor phase current to freewheel during chopping mode.

The A phase starts to magnetize together S1 and S4 on. The phase is energized from the capacitor that is transfer to the main source until the capacitor voltage drops to the level of supply voltage. At that time the blocking diode becomes forward biased and the source begins to provide for energy to the phase. The current is maintained at the charge level by switch S1 on and off. The phase current freewheels throughout diode D1 and S4 when S1 is "off". The current commutates from S1 and S4 "off" and charges the dump capacitor. Diode D5 stop the demagnetizing current which flowed throughout the source. While A phase is being demagnetized, B phase can be magnetized by turn on S2. During this period, the current through B phase is maintained at the command value by dumping any extra energy into the capacitor. These can be continued for the next phase also.

RESULTS AND DISCSUSSION

Without Cuk converter fed SRM drive: Figure 4 shows the without cuk converter outputs for flux and current. In the results torque range of the motor is reduced and the speed range is also low. Figure 5 shows the without Cuk onverter outputs for torque and speed. The ripple in the motor flux is high and also the current range of the motor is low. Without Cuk converter circuit the motor takes 0.2 sec to reach the steady state condition.

UK converter fED SRM drive: Figure 6 shows the With cuk converter outputs for flux and current. In the results torque range of the motor is increased and the speed range also high. The ripple in the motor flux is low and the current range of the motor is increased. Figure 7 shows the with cuk converter outputs for torque and speed.

With CUK converter circuit the motor takes 0.12 sec to reach the steady state condition when compared to the without CUK converter operation. The acceleration in the torque is high. In the given Simulation results the output torque ripple is reduced when compared to the without CUK converter circuit.

Figure 8 shows the output waveform of the speed for switched reluctance motor using PI controller. From the waveform it shows the desired output speed is attained after 0.22 sec with the set point speed of 2000 rpm. Figure 9 Shows the switched reluctance motor using fuzzy logic controller speed output waveform. From the graphical representation it shows that desired output speed is attained before 0.09 sec with the set point speed of 2000 rpm.

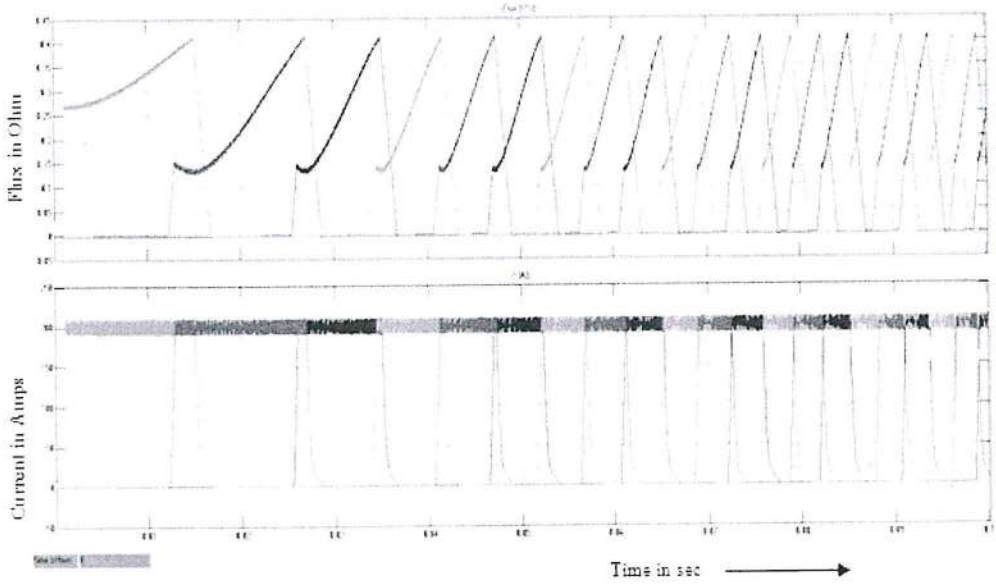

Fig. 4: Without Cuk converter outputs for flux and current

PRINCIPAL,
K. S. R. INSTITUTE FOR
ENGINEERING AND TECHNOLOGY,
K. S. R. KALVI NAGAR,
TIRUCHENGODE-637 215,
NAMAKKAL Dt, TAMIL NADU.

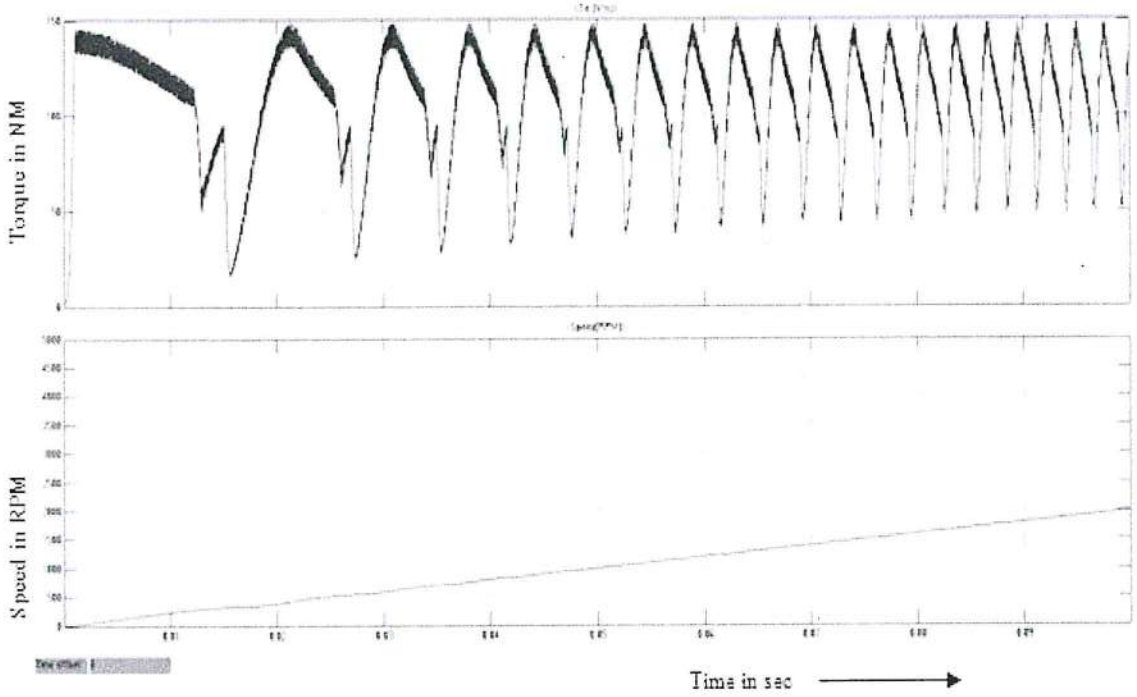

Fig. 5: Without CUK converter outputs for torque and speed

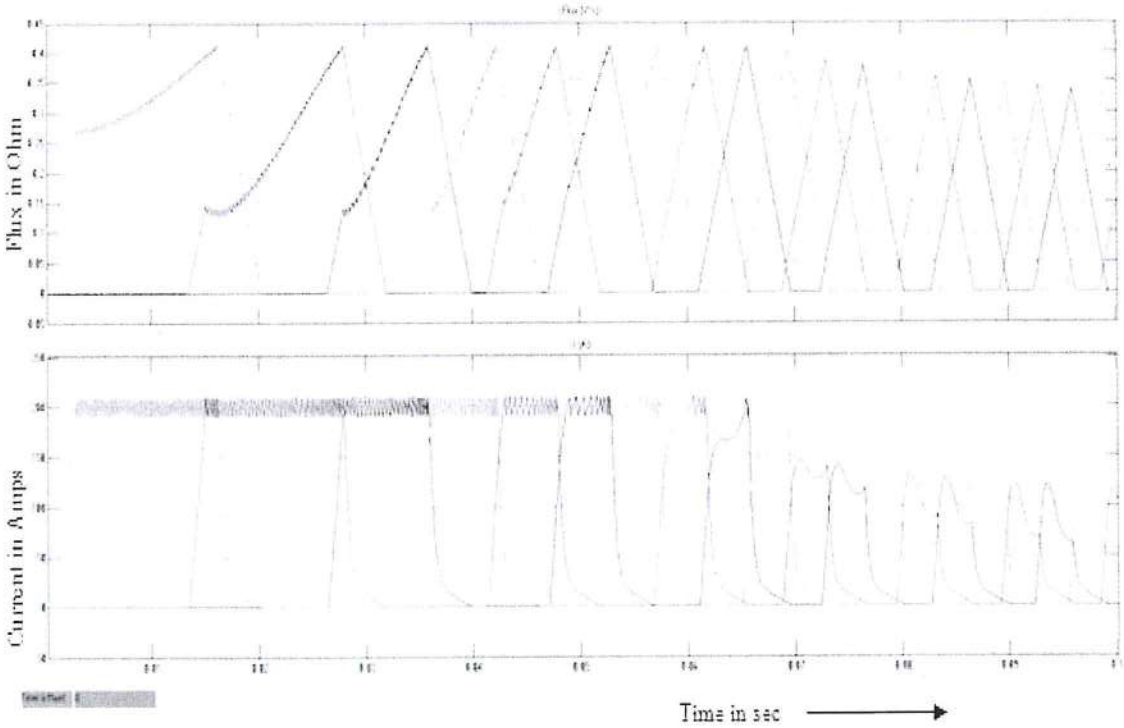

Fig. 6: With Cuk converter outputs for flux and current

PRINCIPAL,
K. S. R. INSTITUTE FOR
ENGINEERING AND TECHNOLOGY,
K. S. R. KALVI NAGAR,
TIRUCHENGODE-637 215,
NAMAKKAL Dt, TAMIL NADU.

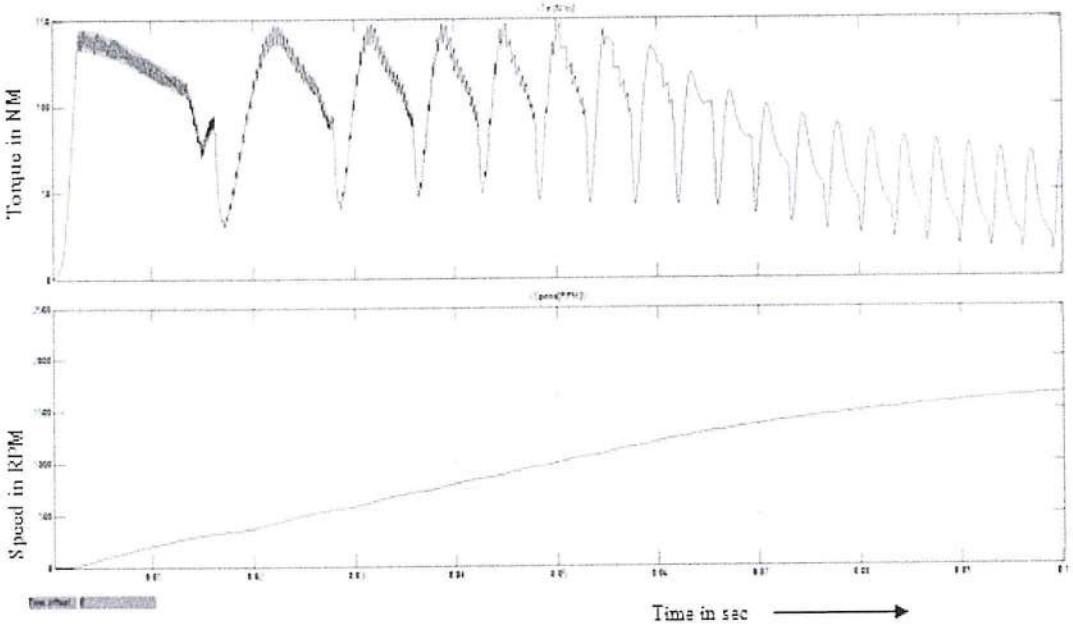

Fig. 7: With CUK converter outputs for torque and speed

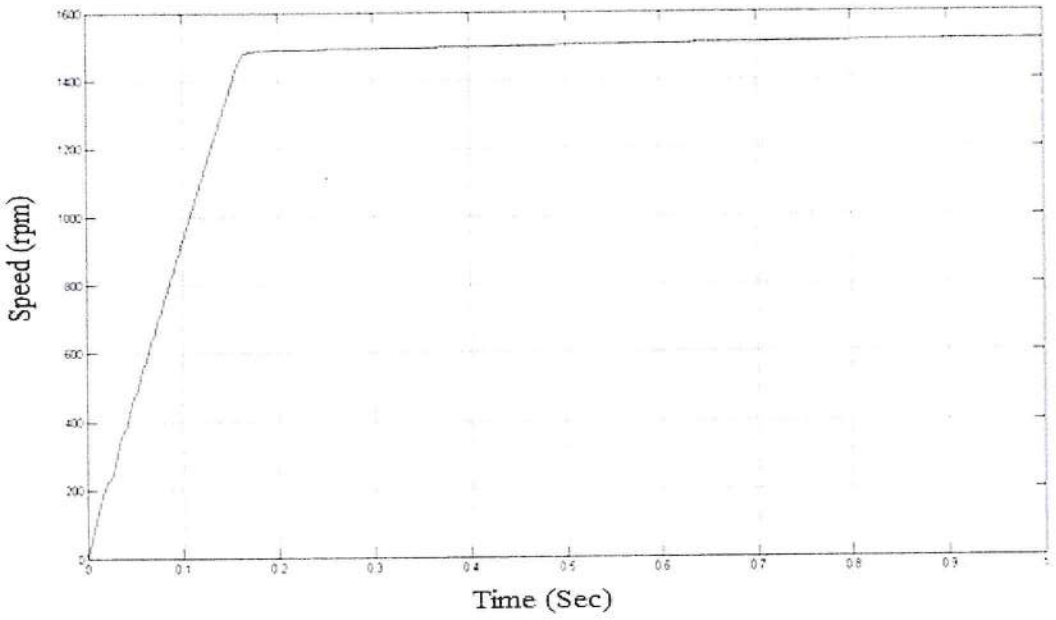

Fig. 8: SRM PI controller speed output waveform

Table 1 shows the various set speed and settling time in PI controller and fuzzy logic speed controller. From the tabulation it shows, the settling time of fuzzy logic controller as low compared to PI controller.

Table 1: Comparative study of set speed and settling time

Speed (RPM)	PI (Settling time)	Fuzzy controller (Settling time)
1500	0.16	0.05
2000	0.22	0.09
2500	0.26	0.12
3000	0.32	0.15

PRINCIPAL.
K. S. R. INSTITUTE FOR
ENGINEERING AND TECHNOLOGY,
K. S. R. KALVI NAGAR,
TIRUCHENGODE-637 215,
NAMAKKAL Dt. TAMIL NADU.

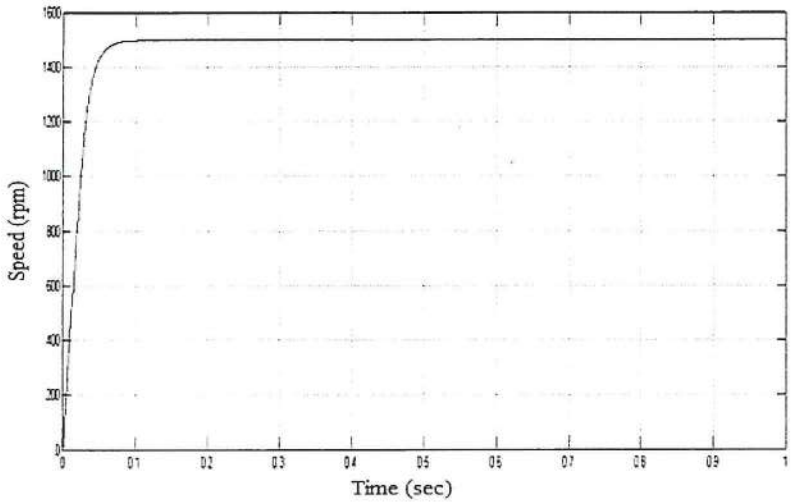

Fig. 9: SRM FLC speed output waveform

CONCLUSION

In this study, a Cuk converter fed Switched Reluctance drive has been introduced. The proposed drive provides increased drive efficiency when compared to the drive without Cuk converter. Here, for the Cuk converter normal PWM pulse generator is used. In future for the Cuk converter operation SVPWM, NEURAL or GENETIC algorithm methods will be implemented for improving the performance of Cuk converter with SRM drive and also for the switched reluctance drive the space vector modulation technique may be implemented. Due to the implementation of Cuk converter the speed of the motor is increased and the torque ripple also reduced. Bridge Cuk converter has to be replaced with Bridgeless Cuk converter so that the power factor is improved when compared to the conventional converters.

REFERENCES

Agirman, I., A.M. Stankovic, G. Tadmor and A.H. Lev, 2001. Adaptive torque-ripple minimization in switched reluctance motors. IEEE. Trans. Ind. Electron., 48: 664-672.

Ahn, J.W., J. Liang and D.H. Lee, 2010. Classification and analysis of switched reluctance converters. J. Electric. Eng. Technol., 5: 571-579.

Barnes, M. and C. Pollock, 1998. Power electronic converters for switched reluctance drives. IEEE. Trans. Power Electr., 13: 1100-1111.

Bist, V. and B. Singh, 2014. An adjustable-speed PFC bridgeless buck-boost converter-fed BLDC motor drive. IEEE. Trans. Ind. Electron., 61: 2665-2677.

Chung, H.Y., B.C. Chen and J.J. Lin, 1998. A PI-type fuzzy controller with self-tuning scaling factors. Fuzzy Sets Syst., 93: 23-28.

Kavitha, A. and G. Uma, 2008. Experimental verification of Hopf bifurcation in DC--DC luo converter. IEEE. Trans. Power Electron., 23: 2878-2883.

Lee, T.W., Y.H. Yoon, Y.C. Kim, B.K. Lee and C.Y. Won, 2007. Control of c-dump converters fed switched reluctance motor on an automotive application. Electr. Power Syst. Res., 77: 804-812.

Luo, F.L. and H. Ye, 2003. Negative output super-lift converters. IEEE. Transac. Power Electronics, 18: 1113-1121.

Luo, F.L. and H. Ye, 2004. Positive output multiple-lift push-pull switched-capacitor Luo-converters. IEEE. Trans. Ind. Electron., 51: 594-602.

Mudi, R.K. and N.R. Pal, 1999. A robust self-tuning scheme for PI-and PD-type fuzzy controllers. IEEE. Trans. Fuzzy syst., 7: 2-16.

Silpa, N. and J. Chitra, 2014. An improved LUO converter for high voltage applications. J. Emerging Technol. Adv. Eng., 4: 262-267.

Tseng, K.J., S. Cao and J. Wang, 2000. A new hybrid C-dump and buck-fronted converter for switched reluctance motors. IEEE. Trans. Ind. Electron., 47: 1228-1236.

Yang, H., 2012. A pedagogical approach for modeling and simulation of switching mode DC-DC converters for power electronics course. Indonesian J. Electr. Eng. Comput. Sci., 10: 1319-1326.

PRINCIPAL,
K. S. R. INSTITUTE FOR
ENGINEERING AND TECHNOLOGY,
K. S. R. KALVI NAGAR,
TIRUCHENGODE-637 215,
NAMAKKAL Dt. TAMIL NADU.

ADVANCES in NATURAL and APPLIED SCIENCES

ISSN: 1995-0772
EISSN: 1998-1090
2016june10(8): pages 6-14

Published BYAENSI Publication
http://www.aensiweb.com/ANAS
Open Access Journal

Evolutionary Computing Technique for Torque Ripple Minimization of 8/6 Switched Reluctance Motor

[1]T.Srihari, [2]R.Jeyabharath, [3]P.Veena

[1]Assistant Professor,Department of Electrical and Electronics Engineering,KSR Institute for Engineering and Technology,Tiruchengode, Tamilnadu, India.
[2]Professor,Department of Electrical and Electronics Engineering,KSR Institute for Engineering and Technology,Tiruchengode, Tamilnadu, India.
[3]Professor,Department of Electrical and Electronics Engineering,KSR Institute for Engineering and Technology,Tiruchengode, Tamilnadu, India.

Received 25 April 2016; Accepted 28 May 2016; Available 2 June 2016

Address For Correspondence:
T. Srihari, Assistant Professor, Department of Electrical and Electronics Engineering, KSR Institute for Engineering and Technology, Tiruchengode, Tamilnadu, India.

Copyright © 2016 by authors and American-Eurasian Network for Scientific Information (AENSI Publication). This work is licensed under the Creative Commons Attribution International License (CC BY).http://creativecommons.org/licenses/by/4.0/

Open Access

ABSTRACT

Background: Switched Reluctance Motor's (SRMs) doubly salient structure and its high torque feature make it as to play important role in electric vehicle industry. The good efficiency, high torque and variable speed ratio in addition to low cost, high reliability and fault-tolerance make the Switched Reluctance Motor (SRM) a candidate with real chances on the market of vehicle propulsion. The main drawbacks of the SRM related to the torque ripple, acoustic noise and vibration make the research object in R&Ds all over the world. **Objective:** In this paper the objective of the work is focused on the development of an efficient design of drive system for 8/6 switched reluctance motor based upon Direct Torque Control (DTC) using evolutionary computing technique. DTC is implemented through Space Vector Modulation (SVM) technique which reduces the torque ripple and provides significant control over torque than conventional technique. **Results:** Evolutionary computing involves in tuning the controller parameter through genetic algorithm. Matlab/Simulink model is constructed for the proposed scheme of switched reluctance motor drive model and validate the work with minimization of torque ripple. **Conclusion:** The simulation results show that the designed PI controller performs satisfactorily to track the reference torque with actual torque. This new technique can be implemented in real time with low cost microcontrollers and higher simplicity.

KEYWORDS: Direct Torque Control, Space Vector Modulation, Genetic Algorithm, Switched Reluctance Motor Drive

INTRODUCTION

The policies to reduce emissions from transportation are focusing on the optimization of the efficiency of the existing vehicles, and the electrification of the vehicles. The continuously increasing price of the permanent magnets and the shortage of rare earths demand the finding of alternatives in several domains as hybrid and full electric propulsion due to their best overall performances. The good efficiency, high torque and variable speed ratio in addition to low cost, high reliability and fault-tolerance make the Switched Reluctance Motor (SRM) a candidate with real chances on the market of vehicle propulsion. The converter topology and switching calculation because of the unipolar operation, keeping away from shoot through errors makes SRM worthwhile in utilizations of aviation, which require high unwavering quality. Additionally it finds wide application in car commercial ventures, direct drive machine apparatuses and so forth.

ToCite ThisArticle:T. Srihari, R. Jeyabharath, P. Veena.,Evolutionary Computing Technique for Torque Ripple Minimization of 8/6 Switched Reluctance Motor.**Advances in Natural and Applied Sciences**. 10(8); Pages: 6-14

PRINCIPAL.
K. S. R. INSTITUTE FOR
ENGINEERING AND TECHNOLOGY,
K. S. R. KALVI NAGAR,
TIRUCHENGODE-637 215,
NAMAKKAL Dt. TAMIL NADU.

6. Elbuluk, M.E., T. liu and I. Husain, 2002. 'Neural-network-based model reference adaptive systems for high-performance motor drives and motion controls', IEEE Trans. Ind. Applicat., 38: 879-886. http://dx.doi.org/10.1109/TIA.2002.1003444
7. Hassan-Halleh, Meisam-Rahmani and Bahram-Kimiaghalam, 2008. 'Direct Torque Control of Induction Motors with Fuzzy Logic Controller' International Conference on Control, Automation and Systems, 14-17: 345-350. http://dx.doi.org/10.1109/ICCAS.2008.4694669
8. Soliman,H.F.E. and M.E. Elbuluk, 2007. "Direct Torque Control of a Three Phase Induction Motor Using a Hybrid PI/Fuzzy Controller," Industry Applications Conference, 2007. 42nd IAS Annual Meeting. Conference Record of the 2007 IEEE, New Orleans, LA, pp: 1681-1685 http://dx.doi.org/10.1109/07ias.2007.258

PRINCIPAL,
K. S. R. INSTITUTE FOR
ENGINEERING AND TECHNOLOGY,
K. S. R. KALVI NAGAR,
TIRUCHENGODE-637 215,
NAMAKKAL DT. TAMIL NADU.

The main disadvantages of SRM are the highly nonlinear and discrete nature of torque production mechanism. The total torque in SRM is the sum of torques generated by each of the stator phase, which are independently controlled. When torque production mechanism is transferred from one active phase to another, pulsations are produced leading to vibrations and acoustic noise. The nonlinear magnetization characteristics make the control of motor really complex.

The control of SRM is the late pattern of explorationas there are complications implemented due to mutual coupling of the motor phase and parameter variation of inductance characteristics. Previous control schemes involve using of linear or nonlinear models. An adaptive feedback controller assuming linear magnetic circuits was proposed in [1]. In another scheme, an analytical solution was developed for production motor voltages to provide a smooth torque [2].

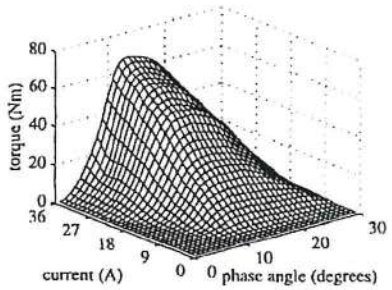

Fig. 1: Measured Nonlinear Characteristics of SRM

Though linear systems were simple, they were highly inaccurate as torque and flux are both nonlinear functions. So some schemes developed nonlinear characteristics of SR motor (Fig. 1). In [3] feedback linearization provides compensation for the magnetic nonlinearity. Also ripples were reduced to provide smooth torque in [4]. Some nonlinear adaptive schemes were also developed. The implementation of a nonlinear model in real time was complex, expensive and affected by variations in saturation. To overcome all these problems, the Direct Torque Control (DTC) was proposed which gave straightforward answer for control the motor speed and torque and reduced torque ripple [5]. Early scheme used concept of short flux pattern that links two separated poles of the SRM stator. However, this needed a new winding configuration, which is expensive and inconvenient. This scheme can only be theoretically achieved, as they required bipolar currents in opposition to unipolar currents SRM. In recent day many more intelligent controller [6] [7] [8] were developed such as fuzzy logic controller and neural network controller in order to reduce torque ripple content in SRM drive system which provides many excellent results and can be effectively implemented if their complexity reduces. This paper mainly focused on implementation of genetic controller for driving SVM based DTC on SRM drive system which provides minimum torque ripple of 0.138 Nm, which were modeled through MATLAB/SIMULINK. This scheme reduces the complexity and gives better results of previous techniques so that it can be effectively implemented in hardware.

SRM Drive System:

The physical look of a SRM resemble that of other rotating motors (AC and DC) Induction Motor and DC motor and so forth. The structure of 8/6 (8 stator and 6 rotor) SRM is uncovered in Fig. 2. It has particularly important development. Normally number of stator and rotor poles is even number. The windings development of the SRM are exceptionally less difficult than that of different sorts of motor. Just winding is for stator poles, and basically twisted on it and rotor poles are unwinded. The winding of inverse poles is associated in arrangement or in parallel making no of phases exactly half the number of stator poles. Along these lines excitation of single phase energizes two stator poles.

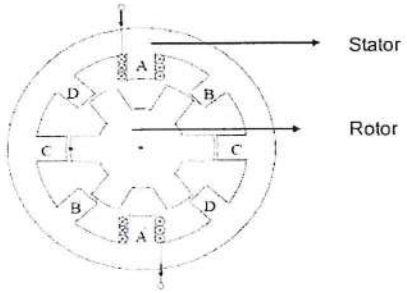

Fig. 2: Construction of 8/6 SRM

PRINCIPAL.
K. S. R. INSTITUTE FOR
ENGINEERING AND TECHNOLOGY,
K. S. R. KALVI NAGAR,
TIRUCHENGODE-637 215,
NAMAKKAL Dt. TAMIL NADU.

The rotor has simple coatedwith salient pole structure without winding. The principle operation of SRM is grounded on the tendency of an electromagnetic system to obtain a constant equilibrium position minimizing magnetic reluctance. Whenever diametrically opposite stator poles of a SRM are excited, the closest rotor poles are attracted, resulting in torque production. When these two rotor poles become aligned with the two stator poles, a second pair of stator poles is excited to bring a second pair of rotor poles into alignment. The successive movement of a 4 -phase, 8/6 SRM is shown in Fig. 3. The synchronization of the stator phase excitation is readily accomplished with rotor position feedback.

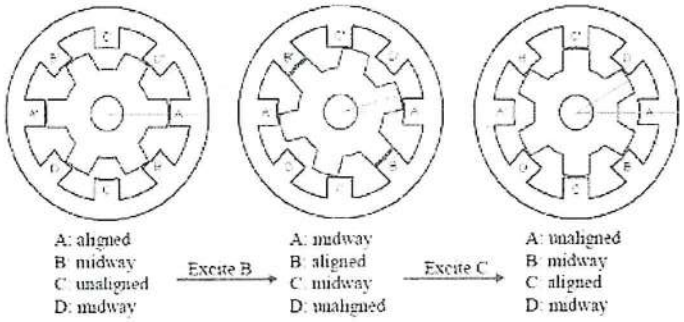

Fig. 3: Construction of 8/6 SRM

In the fully-aligned position, the phase winding inductance is maximum and the reluctance of the magnetic circuit is minimum. Similarly in the non-aligned position, the inductance is minimum and the reluctance S is maximum. The motor torque is expressed as given in equation 1.

$$T = \frac{1}{2} i^2 \frac{dL}{d\vartheta} \quad (1)$$

Rotor has six poles, therefore, when rotor completes one revolution, inductance will pass through 6 maximum and 6 minimum values. The angle between the axes of two consecutive rotor poles is 60° and that of stator poles is 45°, hence, if variation of inductance for phase2 is plotted, it will have similar variation as of phase1, but displaced by 15°. Therefore waveforms of phase 3 and 4 will similarly be shifted with respect to phase1 waveforms by 30° and 45° respectively.

Torque ripple is characterized as the contrast between the most extreme and least quick torque communicated as a rate of the normal torque amid steady state operation. Scientifically, Percentage Torque ripple is communicated as given in condition (2).

$$\text{Torque Ripple}(\%) = \frac{T_{inst(max)} - T_{inst(min)}}{T_{avg}} \times 100 \quad (2)$$

Where T_{inst} is the instantaneous torque and T_{avg} is the average torque.

Direct Torque Control:

Based on field oriented control the direct torque control system works. Field Oriented Control (Vector Control) takes after space vector hypothesis to control magnetic field introduction and direct discretion sets up an interesting recurrence of inverter working given a particular dc link voltage and a particular stator flux level. The working guideline of DTC is to first recognize stator voltage vectors as indicated by the contrasts between the reference torque and the real estimations of stator flux linkage. The standards of DTC in the ac machine can be inferred by investigating the motor equations. The stator flux linkage vector can communicated as underneath condition (3).

$$\overrightarrow{\psi_s} = \int (\vec{v} - \vec{i}R) dt \quad (3)$$

Different techniques have been proposed in the past to minimize torque ripple. The proposed technique is Space vector modulation (SVM) based DTC of 4 phase 8/6 SRM by choosinganappropriate set of 8 space voltage vectors. The DTC of SRM drive is simulated for consistent torque burden to watch the steady state and transient execution of the drive. It is watched that the torque is kept up inside the set hysteresis band. This new arrangement of space vectors demonstrates a critical change in the torque execution of DTC based SRM contrasted with the present control technique.

On the basis of the errors calculation between the reference value and estimated values of torque and also flux, it is easy to directly control on the inverter states in order to decrease the torque and flux error within the

PRINCIPAL.
K. S. R INSTITUTE FOR
ENGINEERING AND TECHNOLOGY,
K. S. R. KALVI NAGAR,
TIRUCHENGODE-637 215,
NAMAKKAL Dt. TAMIL NADU.

prefixed band limits. The DTC scheme as initially proposed is very simple; in its basic configuration. It consists of pair of hysteresis comparator, torque and flux calculator, a lookup table, and voltage source inverter. The configuration is much simpler than FOC system due to the absence of frame transformer, pulse width modulator, and position encoder. The general block diagram of DTC is shown in Fig. 4. Two of the major issues which are normally addressed in DTC drives are the variation of switching frequency of the inverter used in the DTC drives with operating condition and the high torque ripple.

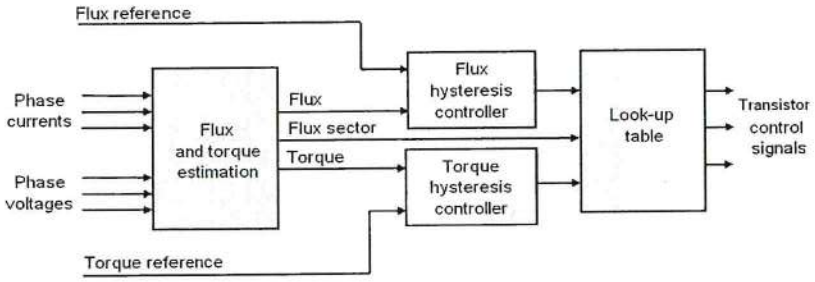

Fig. 4: Block Diagram of DTC

It is shown that the switching frequency is highly influenced by the motor speed. The motor DTC system comprises of three basic functions, namely: A motor model estimates the actual torque, stator flux and shaft speed by means of measurement of two motor phase currents, the immediate circuit DC voltage on the state of the power switched. Calculations are performed every 25 microseconds and these include corrections for temperature and saturation effects. The parameter of the motor model is estimated by an identification run, which made during commissioning. A two level hysteresis controller, where the torque and flux references are compared with the actual values calculated from the motor model. The magnitude of the stator flux is normally kept constant and the motor torque is controlled by means of the angle between the stator and rotor flux. Optimal switching logic that translates the controller output into the appropriate commands to the power switching devices. There are eight voltage vectors available in the two level voltage source inverter and the optimum switching logic determines the required selection every 25 microseconds.

Space Voltage Vector for SRM:

Like the AC drives, SRM likewise characterize the comparable space vectors. The voltage space vector for every phase is characterized on the center axis of the stator shaft in light of the fact that the flux linkage for a current and voltage connected to the motor phase will have phasor course in accordance with the center of the pole axis which does not require any physical change in winding topology. It is appeared in Fig. 5, every motor phase can have three conceivable voltage states for a unidirectional current. At the stage, when both switches in a motor phase are turned on. For this situation positive voltage is given to the motor phase. At the point when current begins streaming one device is turned off, along these lines a zero voltage circle happens and the state succession is given as 0. At long last, when both devices are turned off, there is no present or freewheeling current courses through the upper diodes. For this situation negative voltage is experienced by the motor phase and the state arrangement is characterized as negative voltage. Among the eight conceivable expresses any one is chosen at one time so as to keep the stator flux linkage and the motor torque inside hysteresis groups.

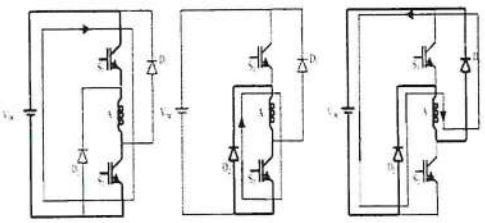

Fig. 5: SRM Phase Voltage States

As in the conventional DTC scheme, if the stator flux linkage lies in the k-th zone, the magnitude of the flux can be improved by the importance if switching vectors v(k+1) and v(k-1) and diminished by the presence of vectors v(k+2) and v(k+2). Hence whenever the stator flux linkage reaches its upper limit in the hysteresis band, it is reduced by applying voltage vectors which are directed toward the center of the flux vector space and vice-versa.

PRINCIPAL,
K. S. R. INSTITUTE FOR
ENGINEERING AND TECHNOLOGY,
K. S. R. KALVI NAGAR,
TIRUCHENGODE-637 215,
NAMAKKAL Dt. TAMIL NADU

The motoring torque is controlled by an acceleration or deceleration of the stator flux relative to the rotor movement. Hence, if an increase in torque is required, voltage vectors that advance the stator flux linkage in the direction of rotation are selected. This corresponds to selection of vector v(k+1) and v(k+2) for a stator flux linkage in the k-th zone. When the torque is to be decrease, voltage vectors are applied which decelerate the stator flux linkage vector. This corresponds to the vectors v(k-1) and v(k-2) in the zone k. Switching table for controlling the stator flux linkage and motor torque can be defined as shown in Table 1.

Table 1: Switching Table for DTC

Torque	INCREASE	INCREASE	DECREASE	DECREASE
Flux	INCREASE	DECREASE	INCREASE	DECREASE
Selection of Vector	v(k+1)	v(k-1)	v(k+2)	v(k-2)

In order to control the flux and torque within the hysteresis bands, the instantaneous torque and stator flux vector magnitude must be known. In the SR motor voltages in the motor are highly non-sinusoidal and thus more effective insight may be gained by firstly finding the individual flux linkages of each phase using the voltage.

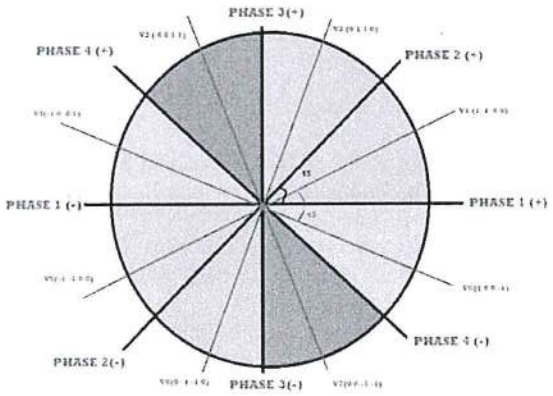

Fig. 6: Space Voltage Vector for SRM

In this case the magnitude of the individual phase flux linkages varies with time, but the direction is always along the stator pole axis. Torque look up table estimated previous and stored processor for adjustable Dwell angle. Space voltage vector representation for 8/6 switched reluctance motor is shown in Fig. 6. Pseudo codes for different voltage states were depict in Table 2.

Table 2: Pseudo Code for Voltage States

Voltage vectors	Voltage states for four phase				Voltage Vector	Voltage state for four phase			
	A	B	C	D		A	B	C	D
V1	1	1	0	0	V5	-1	-1	0	0
V2	0	1	1	0	V6	0	-1	-1	0
V3	0	0	1	1	V7	0	0	-1	-1
V4	-1	0	0	1	V8	1	0	0	-1

Control switching table is used to select the voltage command based on the present zone of the flux linkage that can be determined by the angle. For the first time, considering 4phase motor, vector number is four and so combination of vector is zero with appear on rectangular plane. In real system arbitrary phase will be excited first to detect the initial rotor position. Rotor position move to arbitrary aligned position. Therefore we solve this problem with initial value of 45 degree on 4 phase. The orthogonal flux vector are expressed as

$$\psi_\alpha = \psi_1 - \psi_2 \cos 60° - \psi_3 \cos 60° \quad (4)$$

$$\psi_\beta = \psi_2 \sin 60° - \psi_3 \sin 60° \quad (5)$$

The magnitude of $\vec{\psi}$ and angle δ of the equivalent flux vector is defined as

$$\psi_s = \sqrt{{\psi_\alpha}^2 + {\psi_\beta}^2} \quad (6)$$

$$\delta = \arctan\left(\frac{\psi_\beta}{\psi_\alpha}\right) \quad (7)$$

Proposed Evolutionary Computing Technique:

PRINCIPAL.
K. S. R. INSTITUTE FOR
ENGINEERING AND TECHNOLOGY,
K. S. R. KALVI NAGAR,
TIRUCHENGODE-637 215,
NAMAKKAL Dt. TAMIL NADU.

The GA has discovered application in the region of the programmed tuning process for traditional and intelligent controllers. Same exploration has been directed utilizing genetic algorithms to help on-line or logged off control frameworks. It has basically been used as a logged off procedure for performing a guided quest for the ideal answer for an issue. In this paper, the GA is utilized logged off controller execution to adaptively seek through a populace of controllers and decide the part most fit to be implemented over a given sampling period.

Here in Genetic PI controller tuning, each chromosome has a genes producing as possible proportional and integral gain values. The implementation of GA-PI control technique for Four-Phase 8/6 SRM to reduce the torque ripple and to obtain quick torque response. The block diagram of the proposed project is shown in Fig. 7.

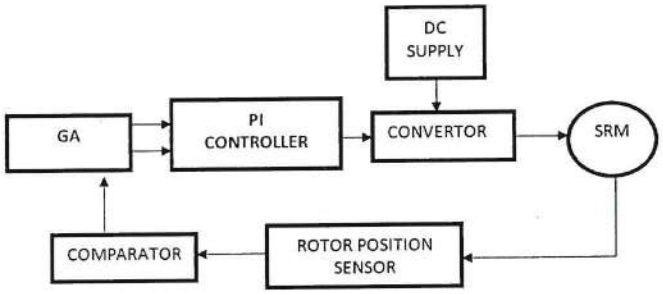

Fig. 7: Block Diagram of Proposed Scheme

In this proposed model, feedback signals are the position θ and the phase currents $i_{a,b,c,d}$ the position signal is used to calculate the torque. The PI controller with signal generator is used to control turn-on angle θ_{on}, turn-off angle θ_{off}, and pulse width modulation duty cycle.

The steps for torque control are summarized as follows:

1 The current and rotor position signal of the SRM are Sampled.

2 Current error due to change are calculated.

3 Select the number of digits to represent each controller parameter Kp and Ki, choose crossover probability (pc) and mutation probability (pm).

4 Assume an initial population of Kp and Ki gains (we make a random selection) sample time T and set time t.

5 ProduceKp and Ki gain values for the error value and it determine the proper turn on and turn off angle to the converter.

6 The motor torque ripples is reduced effectively by proper selection of Kpgain values, Ki gain values, turn on and turn off angles.

These are the several steps that involve in our proposed project to minimize the torque ripple using genetic algorithm principles.

Simulation Model:

To simulate the system a Matlab/Simulink closed loop model based upon evolutionary computing of DTC of 8/6 SRM was constructed as in Fig. 8. The motor parameter such as torque, phase flux and position are obtained from 4φ SRM. The four phase flux vector is transformed on to a stationary orthogonal $\alpha - \beta$ reference frame to calculate the net flux. The multiphase drives divide the controlled power on more inverter legs. The increased phase number reduces the current stress on each switch.

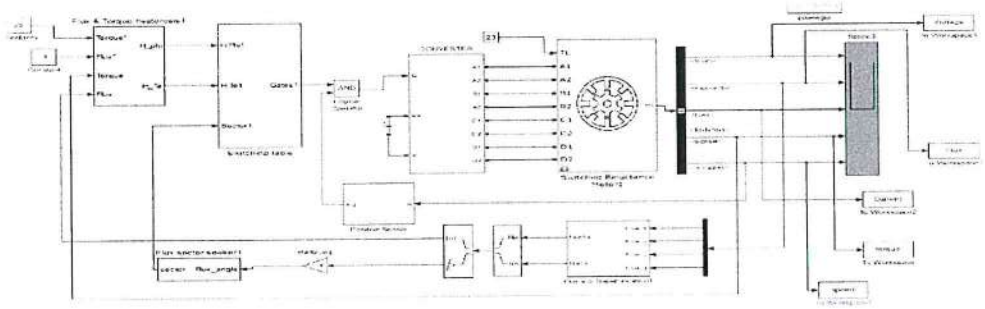

Fig. 8: Simulink Modeling of Proposed Scheme

PRINCIPAL,
K. S. R. INSTITUTE FOR
ENGINEERING AND TECHNOLOGY,
K. S. R. KALVI NAGAR,
TIRUCHENGODE-637 215,
NAMAKKAL Dt. TAMIL NADU.

The converter topologies selected for giving input to the Switched Reluctance motor is asymmetrical converter. This torque ripple is a particular characteristic of the SRM and it depends mainly on the converter s turn-on and turn-off angles. The SRM torque characteristic can be optimized by applying appropriated pre-calculated turn-on and turn-off angles in function of the motor current and speed.

RESULTS AND DISCUSSION

For the purpose of analysis, a comparative work is done between conventional technique and evolutionary computing based DTC of 8/6 SRM and percentage of torque ripple is compared. A DC supply voltage of 120 V is used for the converter configuration. The torque gets controlled when comparing with previous conventional technique. The simulation result of proposed space vector modulation based direct torque control of Switched Reluctance Motor is shown in Fig. 9. And its maximized view is shown in Fig. 10.The FFT analysis on conventional system and proposed schemes were shown in Fig. 11. & Fig.12. The results were obtained from the model developed from four phase 8/6 switched reluctance motor implementing direct torque control based upon space vector modulation technique and Genetic Algorithm were implemented for tuning of PI controller to minimize the torque error. The torque ripple is reduced much reduced than conventional technique. Hence space vector modulation implemented in DTC holds good control over torque response.

The simulation results show that the designed PI controller performs satisfactorily to track the reference torque with actual torque. It is also observed that the designed PI controller completely eliminates ripples at high speeds. The designed PI controller is tuned through genetic algorithm which is done through effective selection of global best and local best done through random selection. The simulation result made the quicker convergence of PI controller by effective genetic tuning of K_p and K_i values than conventional system. The comparison Table 3. for the proposed design of Direct Torque Control with Genetic PI Controller with other controller is made on discussing the torque ripple parameter on closed loop design.

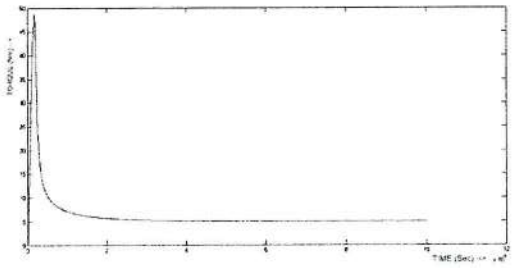

Fig. 9: Simulation Result of Proposed System for 5 Nm.

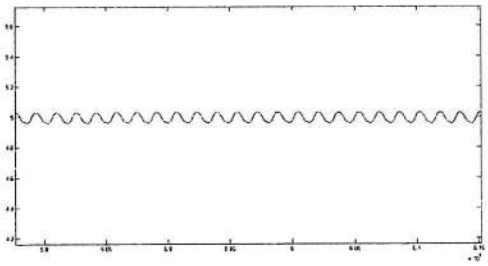

Fig. 10: Magnified view of Simulation for 5 Nm.

PRINCIPAL.
K. S. R. INSTITUTE FOR
ENGINEERING AND TECHNOLOGY,
K. S. R. KALVI NAGAR,
TIRUCHENGODE-637 215,
NAMAKKAL Dt. TAMIL NADU.

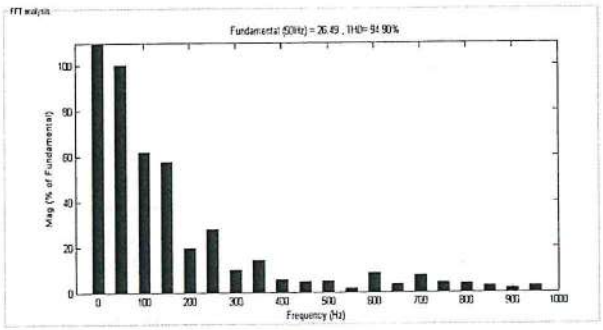

Fig. 11: FFT Analysis for Conventional System

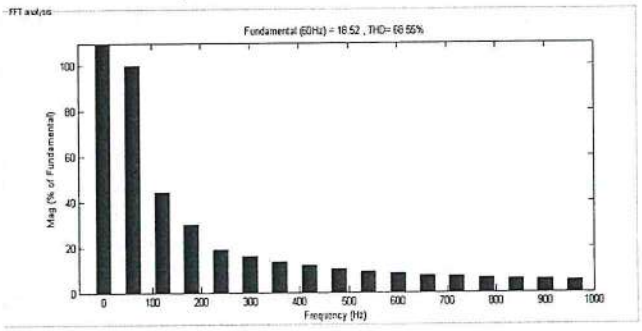

Fig. 12: FFT Analysis for Proposed Scheme

Table 3: Comparison Table of Torque Ripple for Different Controller

CONTROLLER	TORQUE RIPPLE (Nm)	TORQUE RIPPLE (%)
Conventional Controller	0.42 Nm	21 %
Genetic PI Controller	0.22 Nm	11 %
Direct Torque control with PI controller	0.172 Nm	8.8 %
Direct Torque Control With Genetic PI Controller	0.138 Nm	6.9 %

Conclusion:

Direct Torque Control (DTC) for 8/6 SRM drive based upon evolutionary computing is made through comparing the actual torque with reference torque and generating error and then error is tuned by genetic based PI-controller. DTC is implemented through space vector modulation thus by effective switching of nine voltage vector to the convertor at appropriate switching time and angle for smooth operation of motor. The quicker convergence of PI controller is made through evolutionary computing. The results obtained from the Matlab/Simulink model validate the proposed scheme by reducing the ripple than conventional controller. The GA-PI Controller technique produce the quick torque response and reduced torque ripple than the individual controllers such as PI, Neural, and Fuzzy logic controllers. By applying this technique the torque is maintained at 23.5 Nm and the ripple is reduced to 11% where as in the conventional methods the torque is about 22%. Hence by using this GA-PI controller the torque ripple is minimized effectively.

REFERENCES

1. Taylor, D.G., 1991. "Adaptive control design for a class of doubly-salient motors," In Proc. 30th IEEE Conf. Dec. Contr., 3: 2903-2908, http://dx.doi.org/10.1109/cdc.1991.261069
2. Nagel,N.J. and R.D. Lorenz, 1999. "Complex rotating vector method for smooth torque control of a saturated switched reluctance motor," in Proc. 34th Annual Meeting IEEE Ind. Application., 4: 2591-2598 http://dx.doi.org/10.1109/ias.1999.799204
3. Ilic-Spong, M., R. Marino, S.M. Peresada and D.G. Taylor, 1987. "Feedback linearizing control of switched reluctance motors," IEEE Trans. Automat. Contr., AC-32: 371-379. http://dx.doi.org/10.1109/TAC.1987.1104616
4. Stankovic, M., G. Tadmor, Z.J. Coric and I. Agirman, 1999. "On torque ripple reduction in current-fed switched eluctance motors," IEEE Trans.Ind. Electron., 46: 177-183.http://dx.doi.org/10.1109/41.744409
5. Jinupun,P. and P. Chi-KwongLuk, 1998. "Direct torque control for sensorless switched reluctance motor drives," Power Electronics and Variable Speed Drives, Seventh International Conference on (456): 329-334. http://dx.doi.org/10.1049/cp:19980546

PRINCIPAL.
K. S. R. INSTITUTE FOR
ENGINEERING AND TECHNOLOGY,
K. S. R. KALVI NAGAR,
TIRUCHENGODE-637 215,
NAMAKKAL DT. TAMIL NADU.

Middle-East Journal of Scientific Research 24 (12): 3667-3677, 2016
ISSN 1990-9233
© IDOSI Publications, 2016
DOI: 10.5829/idosi.mejsr.2016.3667.3677

Performance Analysis and Speed Regulation Estimation of SR Motor Using FT-ANN Controller with Steady State Stability and Fft Analysis

[1]Murugesan Arumugam and [2]Jeyabharath Rajaiah

[1]Research Scholar, Anna University/Assistant Professor/EEE,
KSR Institute for Engineering and Technology, Tamilnadu, India
[2]Professor, Department of EEE, KSR Institute for Engineering and Technology, Tamilnadu, India

Abstract: A closed loop speed regulation estimation of Switched Reluctance (SR) Motor with Fuzzy Tuned Artificial Neural Network (FT-ANN) Controller has been simulated and presented in this paper. The FT-ANN has been used for the closed loop controller and the speed regulation of the SR motor has been estimated with Fuzzy Logic Controller (FLC) and FT_ANN. The comparative results are presents for both static and dynamic conditions. The mathematical model of the SR motor has been developed for steady state stability analysis and simulated using MATLAB. The Harmonic Spectrum (FFT) and steady state error for various speed and load condition have been obtained to validate the role of FT-ANN controller. The FT-ANN based system is expected to give better speed regulation for various load conditions. A prototype 300-W, 50Hz model is designed and built for experimental demonstrations; the transient and steady-state performances for the SR motor are compared from the simulation studies. The result of MATLAB simulation and execution it is clear that the FT-ANN can have better controller compared with Fuzzy Logic Controller (FLC).

Key words: Switched Reluctance Motor · Artificial Neural Network · Fuzzy Logic Controller · Stability analysis · PWM Inverter

INTRODUCTION

The design and developed of SR motor have been focused for variable speed applications with high power density in the recent past. It has been found that these types of special motor have several advantages such as simplicity, less maintenance, robustness, higher torque volume ratio, high starting torque, high efficiency, low manufacturing cost and high speed. The SR motor is highly nonlinear and it operates to steady state region to maximum torque region. This type of special motor having a torque is nonlinear function of rotor position and current. The many researchers has been experimentally demonstrated and reported related to SR motor to solve above problems using different controllers.

Hany M *et al.* [1] have developed the torque ripple minimization of the SR motor with digital controller. The model of SR motor has been presented with torque equation. There is no analysis of the performance of the motor. The speed control of the switched reluctance generator with artificial neural network controller has been presented in. The performance of the generator has been analyzed with variable speed turbine connected in grid. Kioskeridis *et al.* [2] have demonstrated the single pulse controlled SR motor with high efficiency. This control technique is more complicate compare to FT-ANN controller. The dynamic and steady state performance of the motor was not presented.

Yana Zhou *et al.* [3] have developed the torque ripple minimization of the SR motor with sensor less controller using neural network. The neural network structural design was not present. The speed variation with load changes was not present. The speed controller of the SR motor has been developed and presented with adaptive neural network controller in. The dynamic behavior of the motor has been presented. The load disturbance of the motor has been presented with controller performance. Here there is no analysis of the steady state and stability of the motor. Any M *et al.* [4] have demonstrated the speed control of SR motor with adaptive neuro-fuzzy

Corresponding Author: Murugesan Arumugam, Research Scholar, Anna University/Assistant Professor/ EEE, KSR Institute for Engineering and Technology, Tamilnadu, India.

PRINCIPAL.
K. S. R. INSTITUTE FOR
ENGINEERING AND TECHNOLOGY,
K. S. R. KALVI NAGAR,
TIRUCHENGODE-637 215,
NAMAKKAL Dt. TAMIL NADU.

controller. The performance of the controller has been described. The analysis of the controller design and dynamic performance of the motor were not present. The stability analysis of the SR motor with fuzzy sliding mode controller was presented in.The speed regulation and load disturbance of the motor performance were not present. The different type of power converter fed SR motor is presented with pulse with modulation technique. The performance of the converter was found for better speed regulation.

P.Kavitha *et al.* [5] have demonstrated the R dumped converter fed SR motor with fuzzy controller. The experimental result of the SR motor was not present. The design procedure of the motor and converter was not present. The performance of the motor speed regulation was present. Gamal M. Hashem *et al.* [6] have described the fuzzy controller for SR motor. The speed regulation of the motor has been presented. The dynamic and transient performance of the motor was not present. M. A. A. Morsy *et al.* [7] have described the speed regulation of the SR motor with fuzzy sliding mode controller. The variable structural control has been developed and presented with comparison of fuzzy sliding mode controller. The static and dynamic analysis of the SR motor was not present.

It is concluded from the literatures that the speed regulation against load and supply voltage fluctuation have important role in the design of high speed drives. The FT-ANN controller is expected to have the speed regulation, high efficiency and better performance in the time of load disturbance. Considering the above facts in view, the FT-ANN controller based SR motor has been designed and the performance is analyzed for estimating various responses. The state space analysis is used for the stability analysis of the motor. The state space equation has been derived from motor model and simulated using MATLAN/Simulink. The FFT analysis of the motor has been present.

Proposed FT-ANN Controller based SR Motor with State Space Analysis: The block diagram of the FT-ANN controller based switch reluctance motor is shown in fig.1. The first stage three phase AC voltages are converting in to DC voltage V_{dc} by using rectifier circuit. The Second stage the inverter is converts in to three phase ac voltage i_a, i_b, i_c.. The motor speed measured by sensor and the signal is given to the error detector unit. A tacho generator (pulse type) is used for sensing the speed. This sensing speed is considered for feedback of the controller. Error detector is used to compare the reference speed and actual speed. The difference error speed is calculated and to generate the error signal which is given to controller block. The Fuzzy tuned Artificial Neural Network Controller gives control signal to the inverter according to the error signal. The speed of the motor is controlled by the inverter through proper excitation of their corresponding windings [8-10].

The FT-ANN controller has been used as two feedback loops. One is outer speed control loop and second one is inner current control loop. The current control loop is used to control the PWM pluses whenever the motor current reached to the maximum value. The speed control loop, the actual speed N is sensed by tacho generator and given to the error detector, the set speed N_{ref} also given to the error detector and the error signal e is obtained by comparing the set speed N_{ref} with the actual speed N. The (Δe) change in error is procured from the (e) present error and pervious error ($e_{previous}$). The (e) error and (Δe) change in error are set as inputs to the FT-ANN controller.

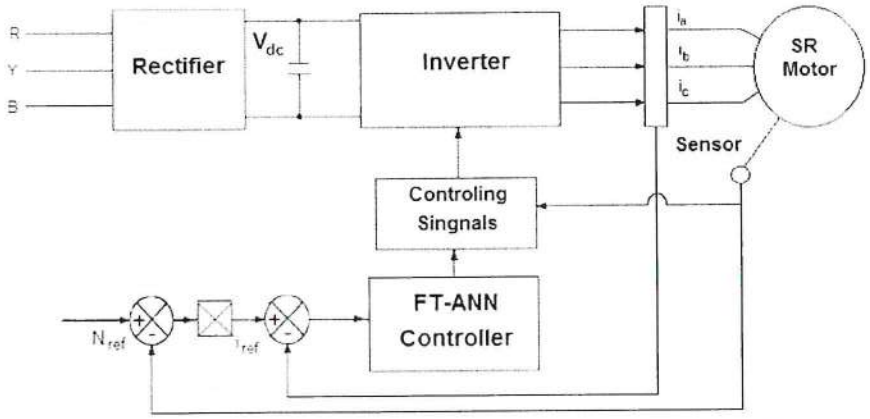

Fig. 1: Block Diagram of the FT-ANN controller based SR motor

PRINCIPAL.
K. S. R. INSTITUTE FOR
ENGINEERING AND TECHNOLOGY,
K. S. R. KALVI NAGAR,
TIRUCHENGODE-637 215,
NAMAKKAL Dt. TAMIL NADU.

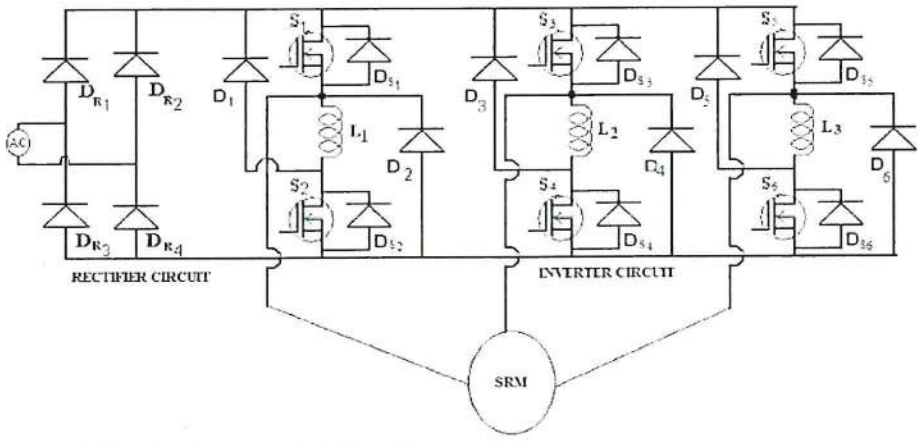

Fig. 2: Structure of Classical Inverter circuit for SR motor

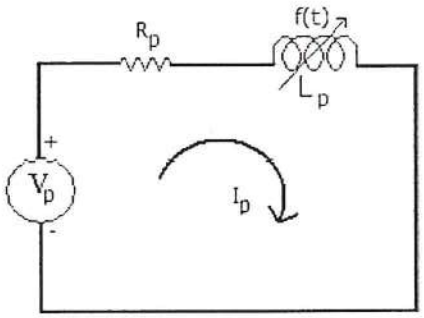

Fig. 3: Equivalent circuit of Single phase SR motor

The output of the controller is PWM Signal. The change in PWM Signal ΔP is given to the inverter and the controller is calculated from the new PWM Signal P(k) and previous PWM Signal p(k-1). The input and output gain of the controller can be estimated by simulation. To obtain the error value is zero by changing the pulse signal which is given to the inverter [11]. The schematic diagram of the proposed system is shown in fig.2.

Mathematical Modeling of the SR motor with Sate Space Analysis: The SR motor is a highly non-linear system, the non-linear system describing the behavior of the motor is developed. A mathematical model can be created based on this construction. The SR motor electromagnetic circuit is characterized by non-linear magnetization. The torque generated by the motor phase is a function of the magnetic flux; therefore, the phase torque is not constant for a constant phase current for different motor positions. This creates torque ripple and noise in the SR motor. The model is based on the electrical diagram of the motor, incorporating phase resistance and phase inductance. The diagram for one phase is shown in fig.3 [11-17].

The applied voltage to a phase is equal to the sum of the resistive voltage drop and the rate of the flux linkages and is given as:

$$V_p(t) = R_p I_p(t) - V_{Lp}(t) \tag{1}$$

$$V_{Lp}(t) = \frac{d\sigma(I_p,\theta_p)}{dt} \tag{2}$$

$$= \frac{d\sigma(I_p,\theta_p)}{dI_p}.\frac{di_p}{dt} + \frac{d\sigma(I_p,\theta_p)}{d\theta_p}.\frac{d\theta_p}{dt} \tag{3}$$

The phase voltage can be expressed as

$$V_p(t) = R_p.I_p(t) + \frac{d\sigma(I_p,\theta_p)}{dI_p}.\frac{di_p}{dt} + \frac{d\sigma(I_p,\theta_p)}{d\theta_p}.N \tag{4}$$

Where N is the speed of the motor

For 3 phase SR motors Equ.3 can be expanded as follows

$$V_R(t) = R_R.I_R(t) + \frac{d\sigma(I_R,\theta_R)}{dI_R}.\frac{di_R}{dt} + \frac{d\sigma(I_R,\theta_R)}{d\theta_R}.N \tag{5}$$

$$V_Y(t) = R_Y.I_Y(t) + \frac{d\sigma(I_Y,\theta_Y)}{dI_Y}.\frac{di_Y}{dt} + \frac{d\sigma(I_Y,\theta_Y)}{d\theta_Y}.N \tag{6}$$

$$V_B(t) = R_B.I_B(t) + \frac{d\sigma(I_B,\theta_B)}{dI_B}.\frac{di_B}{dt} + \frac{d\sigma(I_B,\theta_B)}{d\theta_B}.N \tag{7}$$

The torque generated by one phase can be expressed as

$$T_p = \int_0^I \frac{d\sigma(I_p,\theta_p)}{d\theta_p} dI_p \tag{8}$$

PRINCIPAL,
K. S. R. INSTITUTE FOR
ENGINEERING AND TECHNOLOGY,
K. S. R. KALVI NAGAR,
TIRUCHENGODE-637 215,
NAMAKKAL DT. TAMIL NADU.

The mathematical model of an SR motor is represented by a system of equations, describing the conversion of electromechanical energy. Power associated with change in stored energy is $\frac{dW'}{dt}$

$$\frac{dW'}{dt} = \frac{1}{2} L_p(2i)\frac{di}{dt} + \frac{1}{2} I^2 \frac{dL_p}{dt} \tag{9}$$

This equation can be written as

$$= L_p i \frac{di}{dt} + \frac{1}{2} I^2 \omega \frac{dL_p}{d\theta}$$

Where $\omega = \frac{d\theta}{dt}$

The motor Power can be converted into mechanical P_m the developed power equation is

$$P_m = \frac{1}{2} I^2 \omega \frac{dL_p}{d\theta} \tag{10}$$

The SR motor Torque developed equation as

$$\dot{T} = \frac{P_m}{\omega} = \frac{\frac{1}{2} I^2 \omega \frac{dL_p}{d\theta}}{\omega}$$

$$T = \frac{1}{2} I^2 \frac{dL_p}{d\theta} \text{N-m} \tag{11}$$

The SR motor system model using state space technique can be obtained assuming there is no magnetic saturation, losses and mutual inductance. By using the above basic torque and power equation the vector space equation for the motor can be developed and is given by [11].

$$\frac{di}{dt} = -L^{-1}(\theta) K_i \omega + L^{-1}(\theta) V_p \tag{12}$$

$$\frac{d\omega}{dt} = \frac{T}{J} - \frac{T_L}{J} - \frac{B}{J}\omega \tag{13}$$

$$\omega = \frac{d\theta}{dt} \tag{14}$$

The SR motor reference speed (ω^*) and actual speed (ω) taken as a state variables, the state space equation of the motor as

$$x_1 = \omega = \omega^* \tag{15}$$

$$x_2 = \dot{\omega} = -\frac{B}{J}\omega + \frac{T}{J} - \frac{T_L}{J} \tag{16}$$

By taking the inverse Laplace transform from the equation (15 and 16) we get the state space equation of the SR motor is

$$\begin{pmatrix} \dot{x}_1 \\ \dot{x}_2 \end{pmatrix} = \begin{pmatrix} 0 & 1 \\ 0 & -\frac{B}{J} \end{pmatrix} \begin{pmatrix} x_1 \\ x_2 \end{pmatrix} + \begin{pmatrix} 0 \\ \frac{1}{J} \end{pmatrix} \dot{T} \tag{17}$$

Output Equation is

$$y = \begin{pmatrix} 0 & \dot{\omega}^* \\ 0 & \frac{T_L}{J} \end{pmatrix} \begin{pmatrix} x_1 \\ x_2 \end{pmatrix} \tag{18}$$

These state equations can be used to analysis the stability of the system furthermore the equation can be used to estimate the value of parasitic elements.

RESULTS AND DISCUSSIONS

Design of Fuzzy Logic Controller: The Fuzzy Logic Controller (FLC) provides an adaptive control for improved system performance [13]. FLC is intended to give solution for controlling the non-linear processes and to handle ambiguous and uncertain situations. The performance of the Controller is developed with MATLAB/Simulink in terms of speed and load variation. The FLC have three stages namely Fuzzification, Rule-Base and Defuzzification. The fuzzy control is developed using input membership functions for error 'e' and change in error 'Δe' and the output membership function for 'Δu' the duty ratio of inverter. The output of the fuzzy control algorithm is the change in PWM Signal [δd(α)]. The PWM Signald (α), at the α^{th} sampling time, is determined by adding the previous PWM Signal [d (α -1)] to the calculated change in PWM Signal:

d (α) =d (α -1) +δd (α)

The fuzzy rule variables error 'e', change in eror 'Δe' and output 'Δu' are described by triangular membership functions. The graphical diagram of triangular membership function is shown in fig.4. Seven triangular membership functions are taken for creating the rules. Table 1 present the fuzzy rules. Fuzzy memberships NB, NM,NS, Z, PS, PM,PB are defined as negative big, negative medium, negative small, zero, positive small, positive medium and positive big.

PRINCIPAL,
K. S. R. INSTITUTE FOR
ENGINEERING AND TECHNOLOGY,
K. S. R. KALVI NAGAR,
TIRUCHENGODE-637 215,
NAMAKKAL Dt. TAMIL NADU.

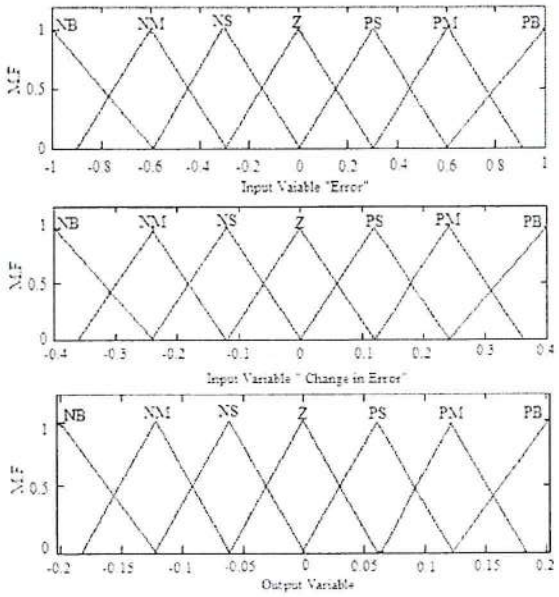

Fig. 4: Fuzzy Membership Function

Table 1: Fuzzy Rules

	NB	NM	NS	Z	PS	PM	PB
NB	NB	NB	NB	NB	NS	PS	Z
NM	NB	NM	NM	NS	NS	Z	NS
NS	NB	NM	NB	NS	Z	NS	PS
Z	NB	NS	NS	Z	PS	NM	PB
PS	NS	NS	Z	PS	PB	NM	PB
PM	NS	Z	PS	PB	PB	NM	PB
PB	Z NS	PS	PB	PB	PB	PB	

Design of Fuzzy Tuned Artificial Neural Network (FT-ANN) Controller: The FT- ANN based control of SR motor is described in reference [9, 12]. Before analyses the results are not attain the prescribed solution, it's desired to be improved further. The performance of SR motor to be improved using the Fuzzy Tuned Artificial Neural Network based controller (FT-ANN). The FLC data is used to design the Artificial Neural Network algorithm (ANN). The proposed controller is working properly due to its well trained algorithm and also it minimize the computational time. The FT-ANN is designed with a small number of neurons and single hidden layer. The feed forward neural network is developed with double neurons in the input layer, thrice in the hidden layer and single in the output layer. The two inputs are taken as error e (α) and change in error Δe(α), these inputs are developed and biased properly. From the FLC the network is designed and trained with the set of inputs and desired outputs.

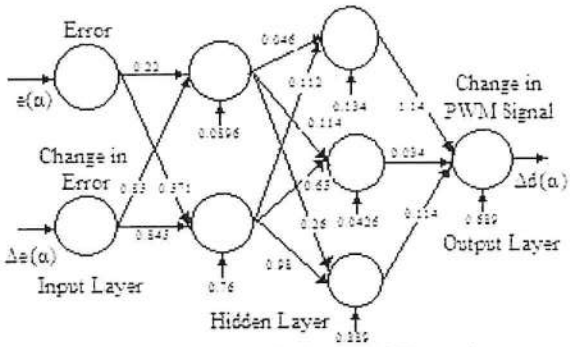

Fig. 5: Configuration of trained Neural Network

A feed forward back propagation neural network-training algorithm is used and it is trained with minimum error. The output of the network is change in PWM Signal Δd(α). The FT-ANN is designed and trained with the error goal value of 0.00596325 at 11 epochs. The complete configuration of the trained network with the weights and bias is shown in figure 5.

The proposed FT-ANN system is simulated using MATLAB software. The simulink model of SR motor is developed with FT-ANN as given in figure 6. The set reference speed and motor actual speed is taken as input. The error and change in error are calculated and then given as input to the FT-ANN. The output of the PWM pulse signal is given as input to the PWM generator of the inverter.

The 100Hz of switching frequency is produced from the PWM unit. Then the current controller receives the pulse signal from the PWM unit. The reference current is equal to the motor current then the current controller permit the PWM signal. The PWM pulse signal is given to the main inverter circuit then the change output voltage changes from variable voltage to fixed voltage. Then the speed of the motor runs with the reference speed. The FT-ANN controller model is shown in fig.7.

Simulation Results of the Proposed System: The simulation of the proposed system is carried out using MATLAB/Simulink software. The FT-ANN controller is used as a closed loop for the SR motor performance estimation. The speed control of the motor has been carried out using fuzzy logic controller and fuzzy tuned artificial neural network controller. The variation of the speed is shown in below fig.8 the expended view also presented. The output of the speed flow the reference with better accuracy, showing a better tracking performance of the controller. Its shows that the FT-ANN controller is settling time and percentage overshoot is very less compare to other controller.

PRINCIPAL,
K. S. R. INSTITUTE FOR
ENGINEERING AND TECHNOLOGY,
K. S. R. KALVI NAGAR,
TIRUCHENGODE-637 215,
NAMAKKAL Dt. TAMIL NADU.

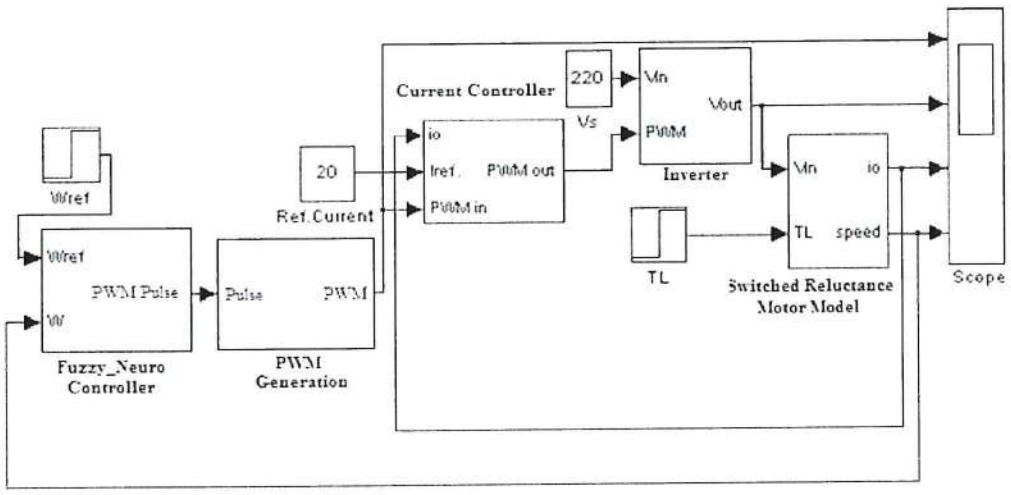

Fig. 6: MATLAB/Simulink Model of the proposed system

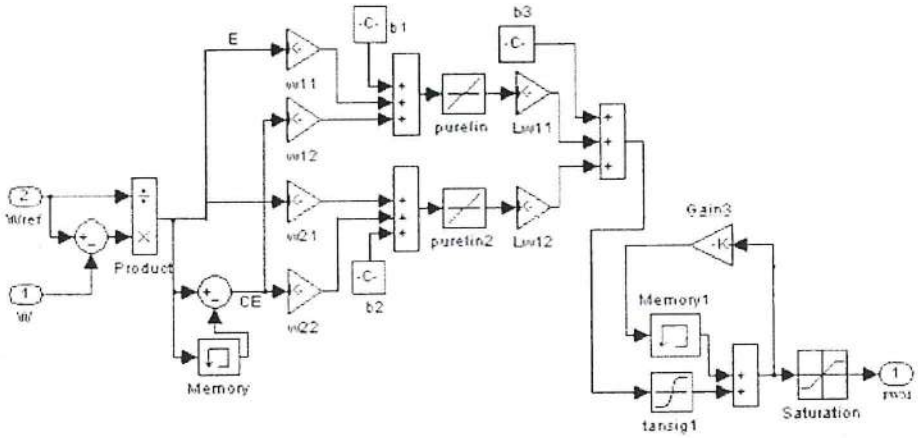

Fig. 7: Simulink Model of FT-ANN Controller

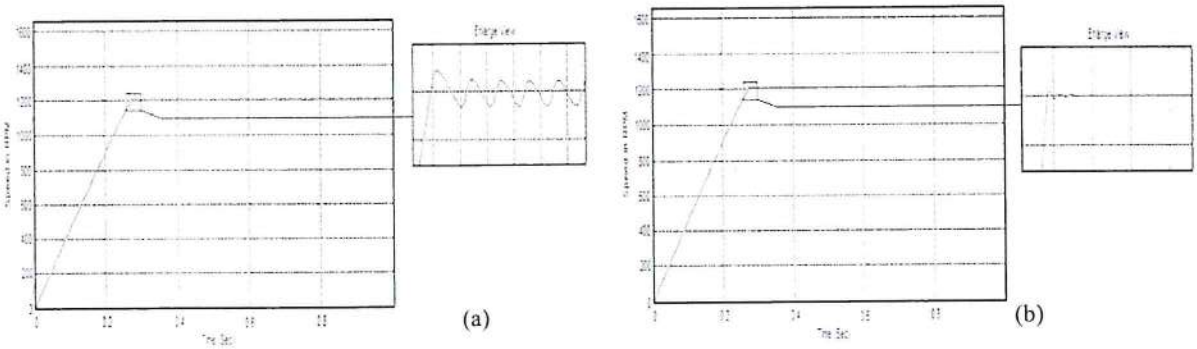

Fig. 8: SR motor Speed (a) using FLC (b) using FT-ANN controller

The maximum overshoot and percentage error is very small and it tends to zero as shown in fig.8 (b) the rise time and settling is near to 0.01 sec its very less compare to FLC. The expended view diagram shows that the steady state error is near equal to 0.001sec. It is clear that the FT-ANN controller eliminating the rise time, overshoot and suppers the harmonics.

PRINCIPAL,
K. S. R. INSTITUTE FOR
ENGINEERING AND TECHNOLOGY,
K. S. R. KALVI NAGAR,
TIRUCHENGODE-637 215,
NAMAKKAL Dt. TAMIL NADU.

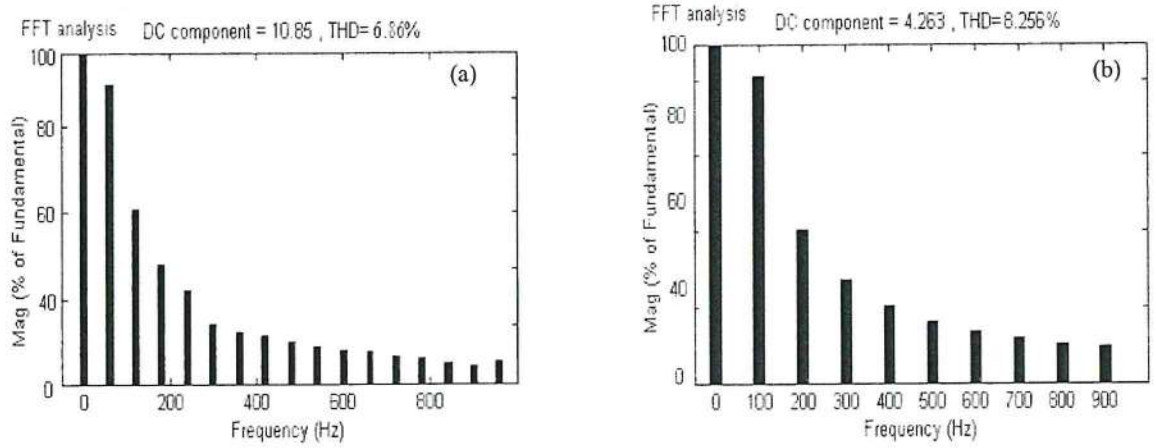

Fig. 9: FFT analysis (a) FT-ANN (b) FLC

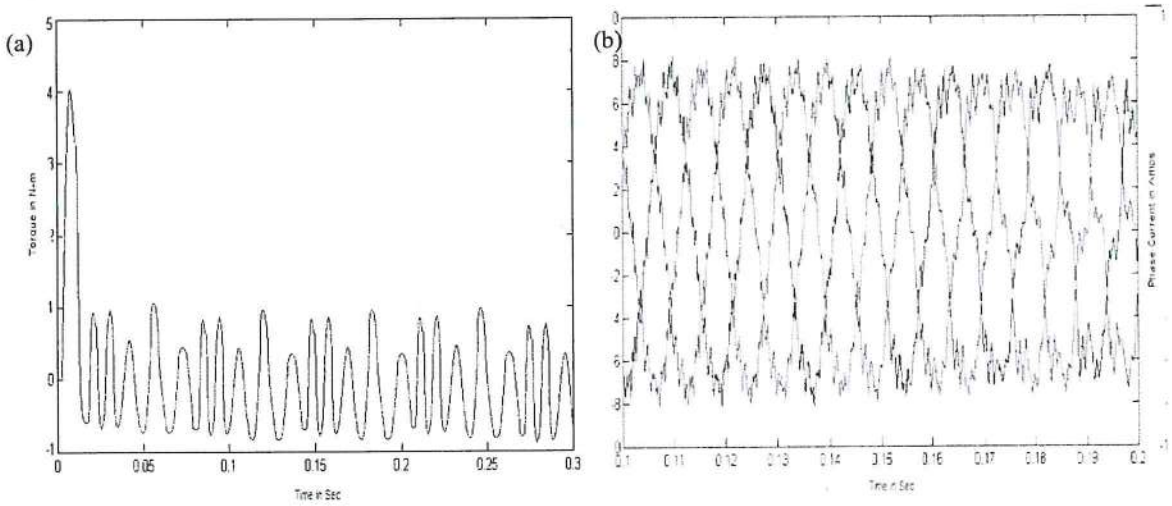

Fig. 10: (a) Torque Response (b) Phase current

Table 2: Comparative analysis of transient and steady state performance for different controllers

Controller	% Overshoot	Rise time in Sec	Steady state error	Settling Time in Sec.	THD in %
FLC	0.36	0.85	0.04	1	8.25
FT-ANN	nil	0.52	0.001	0.68	6.8

The FFT analysis of the SR motor for the output voltage as shown fig.9. The Total Harmonics distraction (THD) is calculated from the inverter side. It's found from the above FFT analysis clearly shows that the controller tracking performance is good and THD values are less compared to fuzzy controller. The developed torque performance of the SR motor as shown in fig.10 (a) and the phase current of the motor are present in fig.10(b)

The performance of the controller response for SR motor speed control has been estimated and provided in table.2. It is seen that the FLC/FT-ANN closed loop controllers give the better settling time. This ensures that the controller provide the effective feedback. It is concluded from the above table 2 the FT-ANN controller has improved the transient and dynamic performance of the SR motor. The harmonics spectrum analysis of the motor speed can be estimated and provided in table.2.

In further to analysis the performance of the SR motor controller the simulation is carried out different set speed changes it is shown in fig.11 and 12 respectively. The set speed changes from 500 rpm to 1000 rpm and 1000 rpm to 1600 rpm. The fuzzy controller shows a comparatively

PRINCIPAL.
K. S. R. INSTITUTE FOR
ENGINEERING AND TECHNOLOGY,
K. S. R. KALVI NAGAR,
TIRUCHENGODE-637 215,
NAMAKKAL Dt. TAMIL NADU.

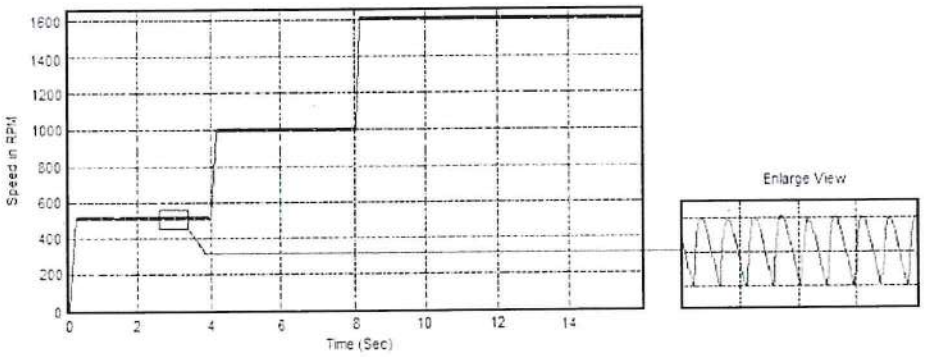

Fig. 11: Speed control from 500 RPM to 1000 RPM, 1000 RPM to 1600 RPM at 4 sec and 8sec respectively (using FLC)

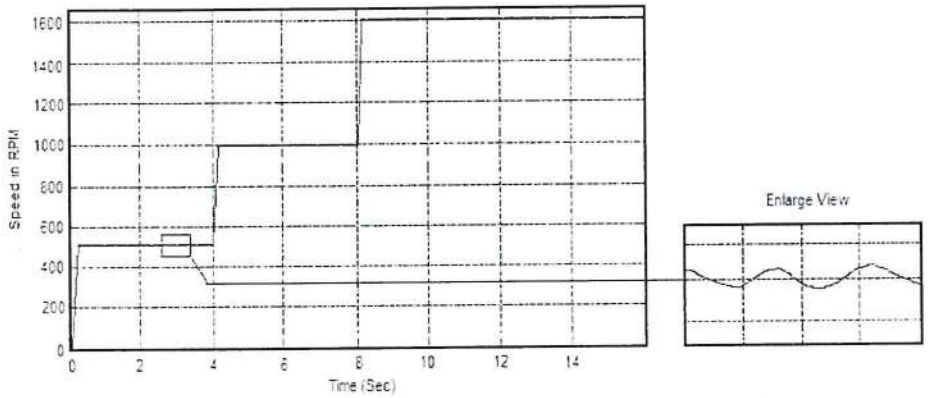

Fig. 12: Speed control from 500 RPM to 1000 RPM,1000 RPM to 1600 RPM at 4 Sec and 8sec respectively

Table 3: Transient response of the controllers in with reference speed changes

	Change in speed from 0 to 500 RPM		Change in speed from 500 to 1000 RPM		Change in speed from 1000 to 1600 RPM	
Controllers	% over Shoot	Settling time in Sec.	% over Shoot	Settling time in Sec.	% over Shoot	Settling time in Sec.
FLC	0.2	0.35	0.29	0.295	0.3	0.39
FT-ANN	0.001	0.15	0.001	0.18	0.001	0.19

maximum percentage overshoot and more time to settle, there is no steady-state error as shown in fig.11. It's clearly found that the FT-ANN controller gives the least amount of overshoot and zero steady state error and the rise time and settling time is near to 0.001 as shown in fig.12.

From the above figure we found that the transient and dynamic performance is more in fuzzy logic controller due to more oscillation and its very minimum in FT-ANN controller. While the motor is running to the rated speed the variation is very minimum at both speed changes. The transient performance of the different controllers with speed changes as provided in table.3. It is clear from the table 3 that the transient performance is under control limit in FT-ANN controller compared to FLC. It is learn that the steady state error is very less in the proposed controller.

Stability Analysis of the Proposed System: The plot has drawn for SR motor basic equation with torque equation from the state space model equations (17and 18). It is clear that the proposed system is stable for the system speed changes. It is concluded that the -0.5+j0 point is encircled in the all direction in single time. Hence overall encirclement is zero. Also the open loop system has no poles at the right half of s-plan. So the proposed system is stable.The nyquist plot as shown in figure 13.

PRINCIPAL.
K. S. R. INSTITUTE FOR
ENGINEERING AND TECHNOLOGY,
K. S. R. KALVI NAGAR,
TIRUCHENGODE-637 215,
NAMAKKAL Dt. TAMIL NADU.

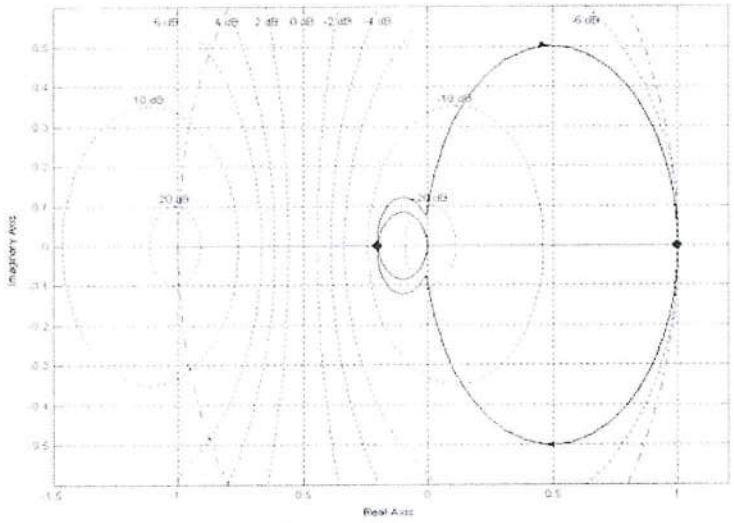

Fig. 13: Stability analysis using nyquist plot for SR motor

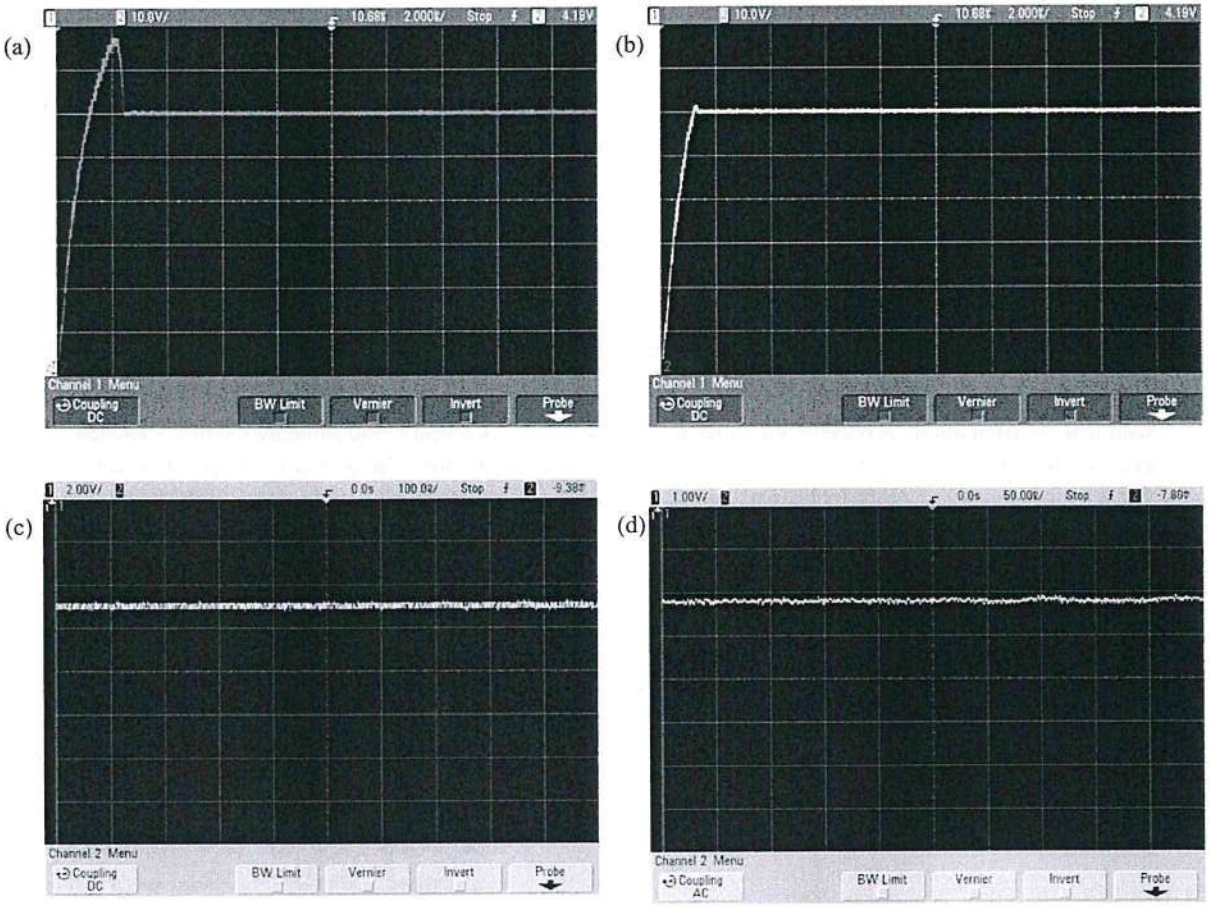

Fig. 14: Experimental waveform of SR motor speed (a) with FLC (b) with FT-ANN controller (c) Steady state error voltage for FLC (d) (c) Steady state error voltage for FT-ANN

PRINCIPAL.
K. S. R. INSTITUTE FOR
ENGINEERING AND TECHNOLOGY,
K. S. R. KALVI NAGAR,
TIRUCHENGODE-637 215,
NAMAKKAL Dt. TAMIL NADU.

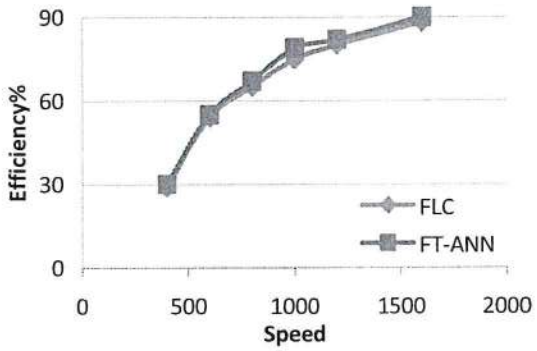

Fig. 15: Speed Vs Efficiency of the SR motor

Experimental Results: The SR motor model is fabricated and performance is tested. A prototype SR motor with FT-ANN controller is operating 300W, 50Hz is designed. The P89V51RD2BN microcontroller is used for generating the driving pulses and IRFP840 MOSFET used as switches in the inverter bridge circuit.MUR4100 diodes used in the rectifier circuit. The frequency level of the generated PWM is 10 KHz. the open collector optocoupler CYN 17-1 is generate the PWM signal from the microcontroller through isolator and IR2110 driver IC. The speed of the motor can be controlled from inverter output. The motor speed is sensed by a digital type pulse sensor GP1L53V. The PWM pulse signal is given to a LM2907 voltage converter IC and feedback signal is given to the microcontroller through an ADC IC ADC0808CCN.

Figure 14 (a) shows the speed voltage waveform with reference speed of 1500 rpm using FLC, it is clearly shows that 4 seconds of time to settle the reference speed. It seen that the oscillations is present due to delay of pulse generation of the controller. Figurer 14 (b) it is observed that there is a minimum steady state error, less percentage overshoot and the minimum settling time at 2.5 seconds. Fig 14(c and d) shows the output voltage of the motor. The steady state error is very minimum compare to FLC. Based on the fig.(14 b,d),. It's clearly seen that FT-ANN based controller having the better transient and steady state performance. The comparison chart is shown in fig.15. The motor speed with efficiency is plotted, it is observed that the proposed controller has high efficiency with step change speed. It is seen form this plot the SR motor have a better efficiency while using FT-ANN controller.

CONCLUSION

The steady state stability analysis of the SR motor has been developed and simulated for estimating the performance for various speed changes using MATLAB/simulink. It has been found from the analysis that the FT-ANN controller provides better efficiency and speed regulation. The comparison results were presented for both controllers. It's found from that FT-ANN controller performs better than fuzzy controller. The proposed controller provides a good speed tracking without overshoot. The proto type model was design and the experimental results are closely agreed with simulation results.

REFERENCE

1. Hany M. Hasanien and S.M. Muyeen, 2012. Speed control of grid-connected switched reluctance generator driven by variable speed wind turbine using adaptive neural network controller, Electric Power Systems Research, Elsevier, 84(1): 206-213.
2. Kioskeridis and C. Mademlis, 2005. Maximum Efficiency in Single-Pulse Controlled Switched Reluctance Motor Drives, IEEE Transactions on Energy Conversion, 20(4): 809-817.
3. Zhou Yana, Changliang Xia, Ziming He and Ximing Xie, 2007. Torque Ripple Minimization in a Sensorless Switched Reluctance Motor Based on Flexible Neural Networks, in Proc. IEEE International Conference of Control and Automation.
4. Hasanien Hany M., S.M. Muyeen and Junji Tamura, 2010. Switched Reluctance Machine, Praise Worthy Prize Press, Napoli, Italy and ISBN 978-88-96329-02-3.
5. Kavitha, P. and B. Umamaheswari, 2014. Speed Control of Sinusoidally Excited Switched Reluctance Motor Using Fuzzy Logic Control, Journal of Theoretical and Applied Information Technology, 68(2).
6. Hashem Gamal M. and Hany M. Hasanien, 2010. Speed Control of Switched Reluctance Motor Based on Fuzzy Logic Controller", Proceedings of the 14th International Middle East Power Systems Conference (MEPCON'10), Cairo University, Egypt, pp: 288-292.
7. Morsy, M.A.A., M. Said A. Moteleb and H.T. Dorrah, 2008. Design and Implementation of Fuzzy Sliding Mode Controller for Switched Reluctance Motor, Proceedings of the International MultiConference of Engineers and Computer Scientists 2008,IMECS 2008, 19-21 March, Hong Kong, 2.
8. Eastham Miller Timothy John., 1993.Switched Reluctance Motors and Their Control", Magna Physics, Oxford University Press.

PRINCIPAL,
K. S. R. INSTITUTE FOR
ENGINEERING AND TECHNOLOGY,
K. S. R. KALVI NAGAR,
TIRUCHENGODE-637 215.
NAMAKKAL Dt. TAMIL NADU

9. Ahmed, T., A. Hamza, A. Abdel Ghani and A. Mohamed, 2006. Fuzzy controller of switched reluctance motor, Acta Electrotehnica, 47(3): 124-131.
10. Lawrenson, P.J., J.M. Stephenson, P.T. Blenkinsop, J. Corda and N.N. Fulton, 1980. Variable speed switched reluctance motors, IEE Proceedings B-Electric Power Applications, 127(4): 253-265.
11. Hasanien Hany M., S.M. Muyeen and Junji Tamura, 2010. Torque ripple minimization of axial laminations switched reluctance motor provided with digital lead controller", Elsevier, Energy Conversion and Management, 51(12): 2402-2406.
12. Tahour Ahmed, Hamza Abid and Abdel Ghani Aissaoui, 2007.Adaptive Neuro-Fuzzy Controller of Switched Reluctance Motor, Serbian Journal of Electrical Engineering, 4(1): 23-34.
13. Hasanien Hany M., 2013. Speed Control of Switched Reluctance Motor Using an Adaptive Neuro-fuzzy Controller, Proceedings of the World Congress on Engineering 2013 Vol II, WCE 2013, London, U.K.
14. Chan, C.C., Y.J. Zhan and K.T. Chau, 1998. Stability Analysis of Fuzzy Sliding Mode Controlled Switched Reluctance Motor Drives, The 29th Annual IEEE Power Electronics Specialists Conference (PESC'98), Fukuoka, Japan, pp: 1283-1289.
15. Thangaraju, I., M. Muruganandam and C. Nagarajan, 2015. Implementation of PID Trained Artificial Neural Network Controller for Different DC Motor Drive, Middle-East Journal of Scientific Research, 23(4): 606-618.
16. Nagarajan, C. and M. Madheswaran, 2012. Experimental Study and steady state stability analysis of CLL-T Series Parallel Resonant Converter with Fuzzy controller using State Space Analysis, Iranian Journal of Electrical & Electronic Engineering, 8(3): 259-267.
17. Mahmoud Samia M., Mohsen Z. El-Sherif and Emad S. Abdel-Aliem, 2013. Studying Different Types of Power Converters Fed Switched Reluctance Motor, 2013. International Journal of Electronics and Electrical Engineering, 1(4): 281-290.

PRINCIPAL.
K. S. R. INSTITUTE FOR
ENGINEERING AND TECHNOLOGY,
K. S. R. KALVI NAGAR,
TIRUCHENGODE-637 215,
NAMAKKAL Dt. TAMIL NADU.

World Applied Sciences Journal 34 (7): 871-877, 2016
ISSN 1818-4952
© IDOSI Publications, 2016
DOI: 10.5829/idosi.wasj.2016.34.7.122

A High Step-Up Hybrid DC-DC Converter with Reduced Voltage Stress for Renewable Energy Applications

[1]S. Ravivarman, [2]R. Jeyabharath and [2]P. Veena

[1]K.S. Rangasamy College of Technology, Tiruchengode, Tamilnadu, India - 637215
[2]KSR Institute for Engineering and Technology, Tiruchengode, Tamilnadu, India - 637215

Abstract: This paper proposes a high step-up dc-dc converter with voltage-lifted switched inductor cell, switched-capacitor and voltage multiplier cell. The voltage multiplier cell is used to reduce the voltage stress across the switch and to extend the voltage gain. In addition, this converter consists of simple control system, since there is only one active switch. The operating principle, key waveforms and design details are also presented. The proposed topology is simulated in PSIM to verify the performance of the proposed converter.

Key words: Boost converter · Switch voltage stress · Switched capacitor · Switched inductor · Voltage-lift

INTRODUCTION

The International Energy Agency (IEA), forecasts that the global primary energy demand on 2030 increases by 1.5% annually from now. Developing Asian countries are the main contributors to this growth, followed by the Middle East region. Growth in per capita energy consumption in the past two decades has occurred in all parts of the world primarily because of increased participation in the transport sector, followed by manufacturing. Exceptions to this trend are China and India, where growth is mainly taken in the manufacturing sector, followed by the household sector. A large and sustainable economic growth in India is to develop a great demand for energy resources. Demand and the imbalance between the supply of energy sources is a widespread phenomenon that requires serious efforts of the Government of India to increase the energy supply. More than 50% of the population is little or no energy business for life and living. Renewable energy can make a significant contribution in each of the areas mentioned above. In this context, the role of renewable energy must be seen. Alternative energy such as photovoltaic, bio-fuel and chemical energy such as fuel cell become increasingly key part of the solution to the country's energy needs. The renewable energy is an important element in the energy planning process in India for more than two decades.

Power Electronic devices continues to innovate and the importance of switching power converter is increasing, in which boost converter is widely used in renewable energy systems. In order to boost the available low voltage to high voltage of 380 V, which is required by the full-bridge inverter to connect with a 220 V grid. A huge number of dc-dc converter topologies were proposed and implemented in the range of hundred watt to multiples of kW. The dc-dc converters are generally classified in to two: isolated converters and non-isolated converters. The isolated converters use transformer for isolation which may be necessary or not in some countries. In order to reduce the cost of the system without compromising gain and efficiency, the non-isolated dc-dc converters are to be used in renewable energy applications [1, 2]. The non-isolated dc-dc converters are classified into five categories, such as cascaded dc-dc converter, coupled inductor based boost converter, switched capacitor (SC) based boost converter, switched inductor (SL) based boost converter and voltage multiplier (VM) cell based boost converter.

The conventional boost converters are cascaded is series and/or parallel to increase the voltage gain of the converter [3-5]. The cascaded converters consist of large number of components, so it is not suitable for high power applications. Coupled inductors are a different method used to increase the voltage gain, reduce the reverse recovery problem of the output diode and to

Corresponding Author: S. Ravivarman, Department of EEE, K.S. Rangasamy College of Technology, Thokkavadi Post, Tiruchengode, Namakkal District, Tamilnadu, India - 637215.

PRINCIPAL,
K. S. R. INSTITUTE FOR
ENGINEERING AND TECHNOLOGY,
K. S. R. KALVI NAGAR,
TIRUCHENGODE - 637 215,
NAMAKKAL Dt, TAMIL NADU.

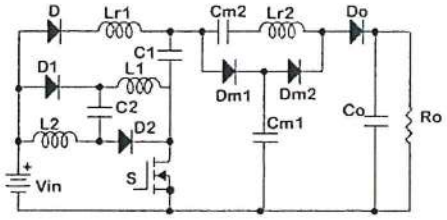

Fig. 1: Proposed Voltage-Lifted Switched-Inductor-Capacitor (VLSIC) converter

reduce the input current ripple [4-8]. The capacitors are switched to charge and discharge in a dc-dc converter to increase the voltage gain. The switched capacitor converter requires a large number of components to achieve high output voltage, which in turn increases the cost, weight and volume of the converter [9-12]. The switched inductor (SL) and voltage-lifted switched-inductor (VLSI) based converters have been explored [13-16]. The voltage multiplier cells are incorporated in the boost converter topologies to increase the voltage gain as well as to reduce the voltage stress across the switch [17-20].

The proposed voltage-lift switched-inductor-capacitor converter is different from existing high step-up dc-dc converters and it is derived from the topology proposed in [21]. The proposed converter has less voltage stress in the power switch and the voltage gain is high when compared to conventional boost converter adopted with any of the techniques like SL, SC, VM and VLSI. This paper is organized as follows. The topology and operation of the proposed converter are presented in section 2. The analysis and expressions for the voltage gain and voltage stress are given in section 3. The simulation results and the performance evaluation are given in section 4. Finally, this paper is concluded in section 5.

Proposed Converter: The topology proposed in [21] is modified by replacing the switched inductor cell with voltage-lift switched inductor (VLSI) cell and it is given in Figure 1. The VLSI cell is formed by D_1, D_2, L_1, L_2 and C_2. The capacitor C_1 forms the switched-capacitor (SC) cell. The main purpose the inductors, L_r is to reduce the current peak formed by the capacitors in SC and VM cells. The VLSI and SC cell are connected in parallel with the source when they are charging and they are connected in series when discharging. The resonant inductor forms a tank circuit and we have to ensure that the zero crossing of inductor current before the switch is turned off.

Operating Principle: The assumptions made to analyze the circuit are as follows: All the converter components are ideal; The inductors and capacitors are very large, then the voltage across capacitor and current through the inductor will be constant and continuous. The operating modes of the proposed topology are shown in Figure 2.

Mode 1 (t_0-t_1): In this mode, the power switch, S is in turned off condition. The diodes D_{M1} and D_O are forward biased and diodes D and D_{M2} are reverse biased. The capacitor C_1, the inductors L_1 and L_2 are connected in series with the input voltage source as shown in Figure 2(a). The energy stored previously in the capacitor, C_1 is discharged to C_{M1} through D_{M1}, to capacitor C_{M2} through L_{r2} and to output capacitor C_O through D_O. The current in the resonant inductor L_{r2} (i_{Lr2}) is increased up to the level of VLSI cell input current and simultaneously the current in the diode D_{M1} is reduced. This change in current occurs in linear manner. Simultaneously, the voltage across the multiplier capacitor, C_{M1} is increased and across multiplier capacitor, C_{M2} is decreased and the voltage across resonant inductor, L_{r2} is constant in this mode.

Mode 2 (t_1-t_2): At instant t_1, the diode current i_{DM1} is zero and the current i_{Lr2} and VLSI cell inductor current are equal as shown in Figure 3. The energy stored in the VLSI cell inductors are transmitted to load though the output diode D_O. The inductor current and the capacitor voltage both decreases at the instant t_2.

Mode 3 (t_2-t_3): At the time instant t_2, the switched is turned on. The diodes D_{M1} and D_O are reverse biased; D_{S1}, D_{S2}, D_{M2} and D are forward biased. The VLSI cell inductors and the capacitor C_1 forms the tank circuit. The tank circuit will cause a sinusoidal resonant current in C_1 and the VLSI cell inductor current will increase as shown in Figure 3. Once the amplitude of current oscillation reaches zero, the diode, D is reverse biased. The energy stored in the C_{M1} is transferred to C_{M2} through D_{M2} until the time instant t_3. Once the energy is fully transferred from C_{M1} to C_{M2}, the diode D_{M2} is reverse biased. The average output voltage will appear across the output capacitor C_O and it will be the sum of the voltage across the capacitor C_{M2} and the voltage at the input of multiplier cell.

Mode 4 (t_3-t_4): Once the resonance condition stops in the VLSI cell, the power switch, S continues to conduct. So the VLSI cell inductor current increases further. Since the capacitor is fully charged, there will be no current flowing through it. Similarly, at t_3, the current in

PRINCIPAL,
K. S. R. INSTITUTE
ENGINEERING AND TE
K. S. R. KALVI NA
TIRUCHENGODE - 63
NAMAKKAL Dt, TAMIL NADU

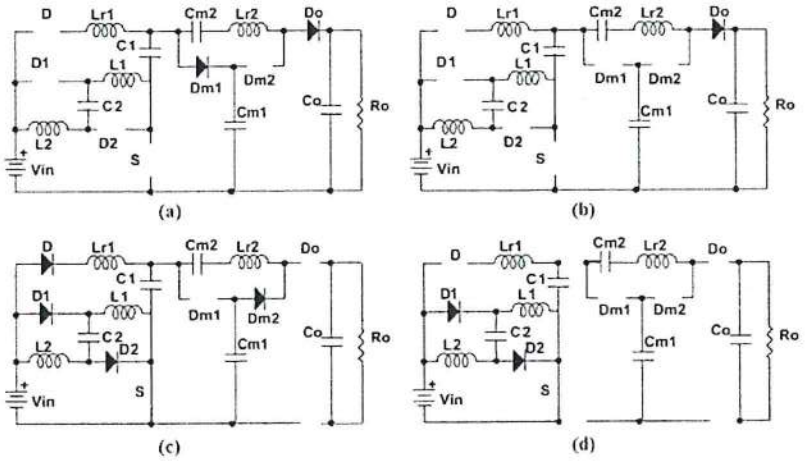

Fig. 2: Operating modes of the proposed converter. (a) Mode 1, (b) Mode 2, (c) Mode 3, (d) Mode 4

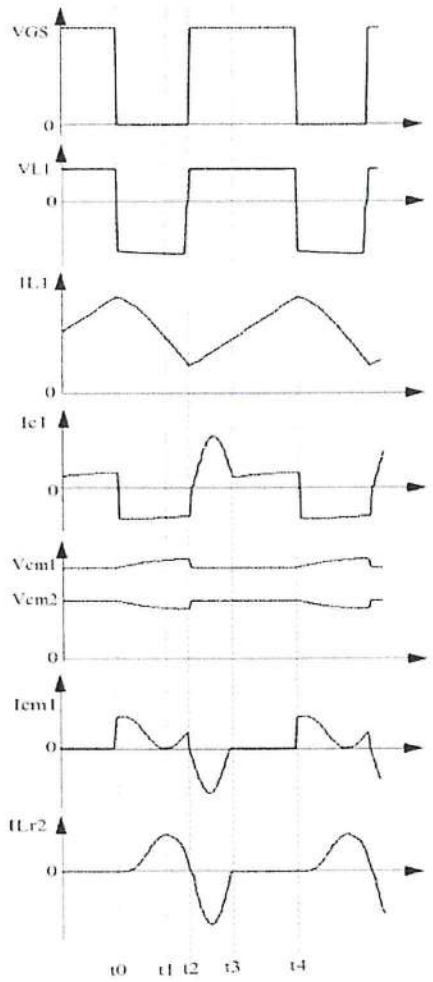

Fig. 3: Theoretical waveforms of the proposed converter

the resonant inductor L_{r2} is zero and in turn it reverse biases the VM cell diode, D_{M2}. Therefore, the output circuit is completely isolated from the source, the VLSI cell inductors will charge from the input voltage source. The VLSI cell and switched capacitor cell will remain in this state until the switch is turned off as shown in Figure 3. Once the switch is turned off, the above four modes will be repeated. Since the diodes in the VLSI and VM cells are turned off naturally, the reverse recovery problems are alleviated.

Analysis and Design Specifications: During switching-on period, the capacitors C_1 and C_2 are charged from the input voltage V_{in} as shown in Figure 2(c), since the capacitors are sufficiently large, both voltages are equal.

$$VC_1 = V_{in} \tag{1}$$

$$V_{C2} = V_{in} \tag{2}$$

$$V_{CM2} = V_{CM1}\, V_{in} \tag{3}$$

The inductor current increases during the on period and decreases during the off period of the power switch, S. The voltage appears across the inductors L_1 and L_2 during on period is V_{in}.

$$V_{L1} = V_{L2} = V_{in} \tag{4}$$

From Figure 2(a), the voltage across the inductor L_1 or L_2 during off state is given by.

$$V_{L1} = V_{L2} = \frac{V_{CM1} - V_{in} - V_{C1} - V_{C2}}{2} \tag{5}$$

PRINCIPAL,
K. S. R. INSTITUTE FOR
ENGINEERING AND TECHNOLOGY,
K. S. R. KALVI NAGAR,
TIRUCHENGODE - 637 215,
NAMAKKAL Dt, TAMIL NADU.

Table 1: Comparison of proposed converter and other converters

Converter	Conventional boost converter	Converter proposed in [22]	Converter proposed in [23]	Converter proposed in [24]	Converter proposed in [21]	Proposed converter
Voltage gain	2.5	7	6	7.5 for n=2	9	11
Output voltage	30 V	84 V	72 V	90 V	108 V	132 V
Voltage stress of active switch	7.2 V	48 V	30 V	30 V	48 V	42 V
Voltage stress of output diode	7.2 V	96 V	-	-	48 V	60 V
Voltage stress of intermediate diodes	-	12 V	30 V	30 V	12 V	
				48 V	18 V	30V
				60 V	48 V	60 V

And the output voltage is equal to the sum of multiplier capacitor voltages.

$$V_O = V_{CM1} + V_{CM2} \tag{6}$$

From (1) and (2), the inductor voltage can be rewritten as;

$$V_{L1} = V_{L2} = \frac{V_{CM1} - 3V_{in}}{2} \tag{7}$$

By applying the volt-second balance principle, the voltage across the inductor is given by;

$$DV_{in} = (1-D)\frac{V_{CM1} - 3V_{in}}{2} \tag{8}$$

Hence, the voltage across the multiplier capacitor, C_{M1} is;

$$V_{CM1} = \frac{(3-D)V_{in}}{1-D} \tag{9}$$

Substituting (9) in (3) gives the voltage across the multiplier capacitor C_{M2}

$$V_{CM2} = \frac{2}{1-D} \tag{10}$$

Substituting (9) and (10) in (6), the output voltage is;

$$V_O = \frac{5-D}{1-D}V_{in} \tag{11}$$

Therefore, the voltage gain of the proposed converter is;

$$G = \frac{5-D}{1-D} \tag{12}$$

From Figure 2(a), the voltage stress on switch, S is given by;

$$V_S = V_{CM1} - V_{C1} = \frac{2-D}{1-D}V_{in} \tag{13}$$

Also from Figure 2(a) the voltage stress across the diode D_{M2} is;

$$V_{DM2} = V_O - V_{CM1} = V_{CM2} = \frac{2}{1-D}V_{in} \tag{14}$$

From Figure 2(c) the voltage stress across the multiplier diode D_{M1} and output diode D_O is calculated.

$$V_{DM2} = V_{CM1} - V_{C1} = V_{CM2} = \frac{2}{1-D}V_{in} \tag{15}$$

$$V_{DO} = V_O - V_{CM1} = V_{CM2} = \frac{2}{1-D}V_{in} \tag{16}$$

The voltage stress on the diodes D_1 and D_2 are

$$V_{D1} = V_{L2(Mode\ 1)} + V_{C2} \tag{17}$$

$$V_{D2} = V_{L1(Mode\ 1)} + V_{C2} \tag{18}$$

$$V_{D1} = V_{D2} = \frac{V_{in}}{1-D} \tag{19}$$

From (13) to (19), it is clear that the voltage stress across all the semiconductor devices are lesser than the half of the output voltage. Table 1 gives the comparison of voltage gain and voltage stress across the semiconductor devices of the proposed converter with conventional boost converter and various converter topologies proposed in [21-25], when operating at duty cycle of 0.6 with 12 V input.

Simulation Results: In order to verify the theoretical analysis and the performance of the converter, the proposed converter is simulated in PSIM v9.0. The circuit parameters are calculated from the design equations and they are: $V_{in} = 12$ V, $L_1 = L_2 = 44$ µH, $C_1 = C_2 = 47$ µF, $C_{M1} = C_{M2} = 1$ µF, $C_O = 220$ µF, $L_{r1} = L_{r2} = 1$ µH, R = 60 Ω. The switching frequency and the duty ratio are selected as 100 kHz and 0.6. Figure 4 shows the gate drive voltage of the power switch, output voltage and current and the voltage stress across the output diode. The output voltage is 132 V and it is equal to the theoretical value calculated by using the voltage gain formula. The ripple in the output voltage is very low and it is in acceptable limit.

PRINCIPAL,
K. S. R. INSTITUTE FOR
ENGINEERING AND TECHNOLOGY,
K. S. R. KALVI NAGAR,
TIRUCHENGODE - 637 215.
NAMAKKAL Dt, TAMIL NADU.

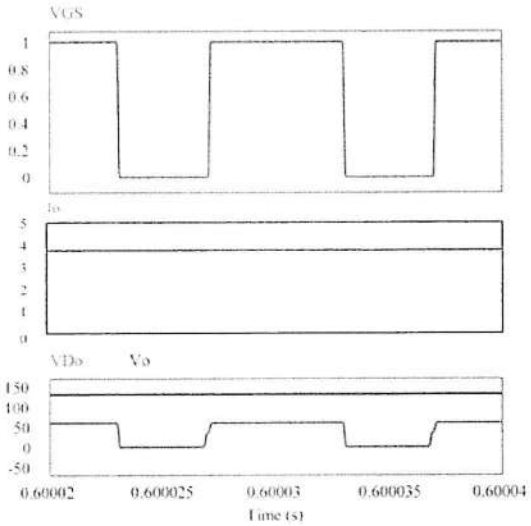

Fig. 4: Gate voltage, output current, output diode voltage stress and output voltage of the proposed converter

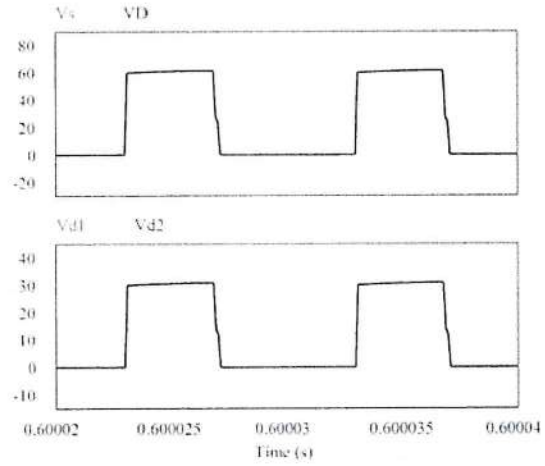

Fig. 5: Voltage stress across the semiconductor devices of the proposed converter

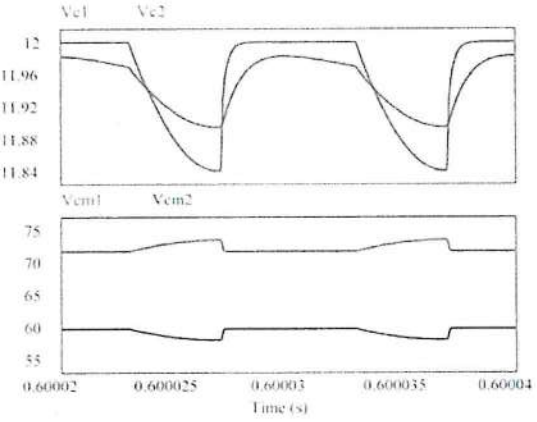

Fig. 6: Voltage across the various capacitors of the proposed converter

PRINCIPAL,
K. S. R. INSTITUTE FOR
ENGINEERING AND TECHNOLOGY,
K. S. R. KALVI NAGAR,
TIRUCHENGODE - 637 215,
NAMAKKAL DT, TAMIL NADU.

The voltage stress across the output diode is 60 V that is lower than the output voltage. Figure 5 shows the voltage stress across the switch and diodes and they are also lesser than the output voltage. Therefore, the switch and diodes with low R_{DS-on} can be used to reduce the cost and conduction losses of the converter. The voltage across the capacitors are shown in Figure 6 and its values validate the theoretical analysis. The voltage across all the elements and devices in the simulation results are same as theoretical results.

CONCLUSION

In this paper, a new high step-up converter that can be used in renewable energy applications is proposed. The proposed converter topology has the capability to obtain high voltage gain in low duty cycle. This converter has low voltage stress on the switch and diodes and hence the semiconductor devices with low turning-on resistance can be used to reduce the conduction losses. The converter consists of only one power switch which makes its control easy. The operation of the converter is presented and it is simulated in both PSIM and Multisim. The simulation results confirm the theoretical analysis and performance of the proposed converter and it is evident that the proposed converter can be used in wide areas where large dc-dc gain is required.

REFERENCES

1. Wai, R.J. and W.H. Wang, 2008. Grid-Connected Photovoltaic Generation System. IEEE Transactions on Circuits and Systems I: Regular Papers, 55(3): 953-964.
2. Wai, R.J., W.H. Wang and C.Y. Lin, 2008. High-Performance Stand-Alone Photovoltaic Generation System. IEEE Transactions on Industrial Electronics, 55(1): 240-250.
3. Huber, L. and M.M. Jovanovic, 2000. A design approach for server power supplies for networking applications. In the proceedings of Fifteenth Annual IEEE Applied Power Electronics Conference and Exposition, 2: 1163-1169.
4. Li, W., J. Xiao, J. Wu, J. Liu and X. He, 2009. Application Summarization of Coupled Inductors in DC/DC Converters. In the proceedings of Twenty-Fourth Annual IEEE Applied Power Electronics Conference and Exposition, pp: 1487-1491.
5. Ping Yang, Jianping Xu, Guohua Zhou and Shiyu Zhang, 2012. A new quadratic boost converter with high voltage step-up ratio and reduced voltage stress. In the proceedings of 7th International Power Electronics and Motion Control Conference (IPEMC), pp: 1164-1168.
6. Chen, Z., Q. Zhou and J. Xu, 2015. Coupled-inductor boost integrated flyback converter with high-voltage gain and ripple-free input current. IET Power Electronics, 8(2): 213-220.
7. Qun, Zhao and F.C. Lee, 2003. High-efficiency, high step-up DC-DC converters. IEEE Transactions on Power Electronics, 18(1): 65-73.
8. Moon-Hwan Keum, Yoon Choi, Sang-Kyoo Han and Jeong-Il Kang, 2013. High efficiency voltage-clamped coupled-inductor boost converter. In the proceedings of 39th Annual Conference of the IEEE Industrial Electronics Society, IECON, pp: 828-833.
9. Liang, T.J., S.M. Chen, L.S. Yang, J.F. Chen and A. Ioinovici, 2012. Ultra-Large Gain Step-Up Switched-Capacitor DC-DC Converter With Coupled Inductor for Alternative Sources of Energy. IEEE Transactions on Circuits and Systems I: Regular Papers, 59(4): 864-874.
10. Ren Xie, Longlong Zhang, M. Mellincovsky, A. Ioinovici and Dehong Xu, 2012. A new large DC gain converter based on a switched-capacitor-inductor circuit in conjunction with fuel cell. In the proceedings of 7th International Power Electronics and Motion Control Conference (IPEMC): 379-383.
11. Gu, D., D. Czarkowski and A. Ioinovici, 2011. A large DC-gain highly efficient hybrid switched-capacitor-boost converter for renewable energy systems. In the proceedings of 2011 IEEE Energy Conversion Congress and Exposition, pp: 2495-2500.
12. Tang, Y., T. Wang and Y. He, 2014. A Switched-Capacitor-Based Active-Network Converter With High Voltage Gain. IEEE Transactions on Power Electronics, 29(6): 2959-2968.
13. Axelrod, B., Y. Berkovich and A. Ioinovici, 2008. Switched-Capacitor/Switched-Inductor Structures for Getting Transformerless Hybrid DC–DC PWM Converters. IEEE Transactions on Circuits and Systems I: Regular Papers, 55(2): 687-696.
14. Luo, F.L., 1999. Positive output Luo converters: voltage lift technique," in the proceedings of IEE Proceedings - Electric Power Applications, 146(4): 415-432.

PRINCIPAL,
K. S. R. INSTITUTE FOR
ENGINEERING AND TECHNOLOGY,
K. S. R. KALVI NAGAR,
TIRUCHENGODE - 637 215,
NAMAKKAL Dt, TAMIL NADU.

15. Zhu, M. and F.L. Luo, 2008. Series SEPIC implementing voltage-lift technique for DC-DC power conversion. IET Power Electronics, 1(1): 109-121.
16. Zhu, M. and F.L. Luo, 2010. Enhanced Self-Lift Cûk Converter for Negative-to-Positive Voltage Conversion. IEEE Transactions on Power Electronics, 25(9): 2227-2233.
17. Gules, R., L.L. Pfitscher and L.C. Franco, 2003. An interleaved boost DC-DC converter with large conversion ratio. In the proceedings of 2003 IEEE International Symposium on Industrial Electronics, 1: 411-416.
18. Zhou, L.W., B.X. Zhu, Q.M. Luo and S. Chen, 2014. Interleaved non-isolated high step-up DC/DC converter based on the diode-capacitor multiplier. IET Power Electronics, 7(2): 390-397.
19. Prudente, M., L.L. Pfitscher, G. Emmendoerfer, E.F. Romaneli and R. Gules, 2008. Voltage Multiplier Cells Applied to Non-Isolated DC–DC Converters. IEEE Transactions on Power Electronics, 23(2): 871-887.
20. Alcazar, Y.J.A., D. De Souza Oliveira, F.L. Tofoli and R.P. Torrico-Bascopé, 2013. DC–DC Nonisolated Boost Converter Based on the Three-State Switching Cell and Voltage Multiplier Cells. IEEE Transactions on Industrial Electronics, 60(10): 4438-4449.
21. Shanmugasundaram, R., J. Rajaiah and V. Parasunath, 2016. Analysis and Design of Single Switch Hybrid Step-Up Converter. Circuits and Systems, 7(4): 211-221.
22. Tang, Y., D. Fu, T. Wang and Z. Xu, 2015. Hybrid Switched-Inductor Converters for High Step-Up Conversion. IEEE Transactions on Industrial Electronics, 62(3): 1480-1490.
23. Wu, B., S. Li, Y. Liu and K. Ma Smedley, 2016. A New Hybrid Boosting Converter for Renewable Energy Applications. IEEE Transactions on Power Electronics, 31(2): 1203-1215.
24. Das, M. and V. Agarwal, 2016. Design and Analysis of a High-Efficiency DC–DC Converter With Soft Switching Capability for Renewable Energy Applications Requiring High Voltage Gain. IEEE Transactions on Industrial Electronics, 63(5): 2936-2944.

PRINCIPAL,
K. S. R. INSTITUTE FOR
ENGINEERING AND TECHNOLOGY,
K. S. R. KALVI NAGAR,
TIRUCHENGODE - 637 215,
NAMAKKAL Dt, TAMIL NADU.

Asian Journal of Information Technology 15 (22): 4662-4668, 2016
ISSN: 1682-3915
© Medwell Journals, 2016

Fuzzy Controlled Bridgeless Cuk Converter Fed Switched Reluctance Motor

[1]Kulandaivel Velusamy, [2]Veena Parasunath and [1]Jeyabharath Rajaiah
[1]Department of EEE, K.S. Rangasamy College of Technology, Tamil Nadu, India
[2]Department of EEE, KSR Institute for Engineering and Technology, Tamil Nadu, India

Abstract: The researchin this study aims at designing and modelling of a bridgeless cuk converter for driving a switched reluctance motor. Bridgeless Cuk converters are new series of AC-DC converters, it contain very less ripple of voltage and current and have output wave with good quality, high power concentration and good transfer voltage gain and no circuit elements parasitic limits of traditional converters. Bridgeless Cuk converters have good voltage transfer gains in arithmetic development on step by step. For the switched reluctance Motor drive, the C-dump converter is used. The present design aims at improving the effectiveness of the switched reluctance motor drive system by the incorporation of the Bridgeless Cuk converter between the electrical source and the drive system. The rule base of the fuzzy logic controller is modified to improve the stability of the controller without affecting the system performance. MATLAB simulation results are presented in this paper to explain the working of the proposed drive.

Key words: Bridgeless CUK converter, SRM, fuzzy logic controller, DC-DC converter, C-dump converter

INTRODUCTION

Switched Reluctance Motors (SRM) have inherent merits such as easy structure with non-winding assembly in rotor side, better tolerance, heftiness, low cost with no permanent magnet in the construction and it can operate with high temperatures or in extreme temperature variations (Ahn *et al*., 2010). It is an electric machine which converts the reluctance torque into mechanical output. In SRM, the stator and rotor enclose a structure of salient-pole, due to salient poles it generate a high output torque. The torque is created by the arrangement inclination of poles (Ahn *et al*., 2010).

Bridgeless Cuk converters allow power transfer in both directions (Kavitha and Uma, 2008). Due to their capability to reverse the direction of flow of power and thereby the current direction of the motor is changed. Power quality issues are the major issue, for reducing the harmonics in supply current by various international power quality standard like the International Electro technical Commission (Bist and Singh, 2014) (IEC) 61000-3-2. In all AC-DC converters, the power transfer efficiency and output voltage are limited by power electronic elements. But in calculation, usual converters can produce high voltage with high efficiency. BL-Cuk converters (Luo and Ye, 2013) are new AC-DC converters that defeat the above disadvantages effects and for the increasing of voltage and the power transfer efficiency. These converters produce improved voltage from low voltage of photovoltaic operation.

However, fundamental converters like as Boost converter and Buck converter cannot be use in the high-power circumstances and at the similar time have many limitations. In modern years, conversion methods have been improved rapidly and there are stacks of topologies of DC-DC converters. Bridgeless converters are more suitable in order to improve the power factor at Source of supply. The distinctive characteristic of a bridgeless PFC converter is which eliminates the need of a diode bridge rectifier at the input. Which reduce the power losses, so we get improves overall system efficiency as a result with equal cost savings. PFC rectifiers are used to recover the rectifier power density and to decrease noise emissions via soft switching methods or coupled magnetic techniques (Yang, 2012; Agirman *et al*., 2001).

A usual PFC scheme has lower efficiency due to major losses in the diode bridge. Usually boost converters are used as front end rectifiers (Barnes and Pollock, 1998; Lee *et al*., 2007). For low level voltage applications like computer industry or telecommunication an isolation transformer or extra converter is needed to step down the voltage level. Bridgeless PFC buck converters are restricted for step down applications (Tseng *et al*., 2000). Input line current cannot trace the input voltage around zero crossings of the input line voltage.

Corresponding Author: Kulandaivel Velusamy, Department of EEE, K.S. Rangasamy College of Technology, Tamil Nadu, India

PRINCIPAL,
K. S. R. INSTITUTE FOR
ENGINEERING AND TECHNOLOGY,
K. S. R. KALVI NAGAR,
TIRUCHENGODE-637 215,
NAMAKKAL Dt. TAMIL NADU.

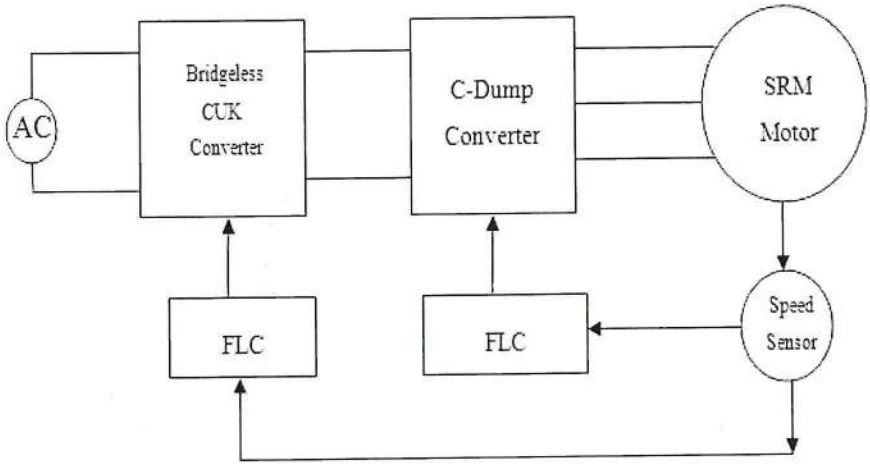

Fig. 1: CUK converter based SRM drive

SRM drive requires the power converters to control the switching sequence of the stator windings (Agirman *et al*., 2001). An asymmetric bridge SRM converter has 2 switches (plus 2 diodes) per phase. This type of converter topology gives more flexible and effective control to current waveforms of an SRM but it contains large number of switches (Barnes and Pollock, 1998). The c-dump circuit has only one switch per phase (Lee *et al*., 2007). Stator winding is transferring the stored magnetic energy after it turn-off the power switch, to the storage capacitor and it sent to the power supply through a step-down dc chopper. The technique could limit the overall cost of the SRM drive.

The self-tuning fuzzy logic controller is used to adjust the output scaling factor with their current states of the controller (Mudi and Pal, 1999). The membership functions and scaling factors are tuned for their corresponding working operation is said to be self-tuning fuzzy logic controller (Chung *et al*., 1998).

Proposed CUK converter fed switched reluctance motor drive: In the proposed circuit model given input AC supply is converted into the dc supply with the help of the BL-CUK. The CUK converter is used to improve the output quality of the supply. It means in the CUK converter output it contain the low level harmonics, small distortion and less ripple. By controlling the CUK converter output, SRM motor output performance is improved. The CUK converter operation and SRM Drive operation is controlled by using Fuzzy Logic Controller (FLC). Thus the C- Dump converter (Lee *et al*., 2013) is the more efficient converter compare to another converter.

Thus, the C- Dump converter is use to drive the SRM motor. The FLC is used to give the rotor position and also it produces the pulse signal to the C-dump converter. The features of FLC are five fuzzy sets for input and output, triangular membership function, mamdani fuzzy inference system with implication by min operator and defuzzification using centroid method. The switching of the Cuk converter switches are controlled by FLC thereby controlling the SRM drive ripples in torque and current (Fig.1).

MATERIALS AND METHODS

Operating principle of BL-Cuk converter: Cuk converter is actually combination of a boost converter and a buck converter. Cuk converter has the following merits. Such as continuous output current, continuous input current, output voltage can be either improved or fewer than the input voltage.

The bridgeless Cuk converter working in a DICM mode which gives an inherent PFC and require a easy voltage follower method for the voltage control and small size of heat sink for the switches (Luo and Ye, 2003, 2004; Silpa and Chitra, 2014).

Operation of bridgeless Cuk converters: The mode of operation of a PFC converter is a crucial problem because it affects the cost and rating of the components used in the PFC converter. Discontinuous Conduction Mode (DCM) and Continuous Conduction Mode (CCM) are broadly used in practical application. In DCM or CCM, the current of the inductor or the voltage across in-between capacitor in a PFC converter remains discontinuous or

PRINCIPAL,
K. S. R. INSTITUTE FOR
ENGINEERING AND TECHNOLOGY,
K. S. R. KALVI NAGAR,
TIRUCHENGODE-637 215,
NAMAKKAL Dt. TAMIL NADU.

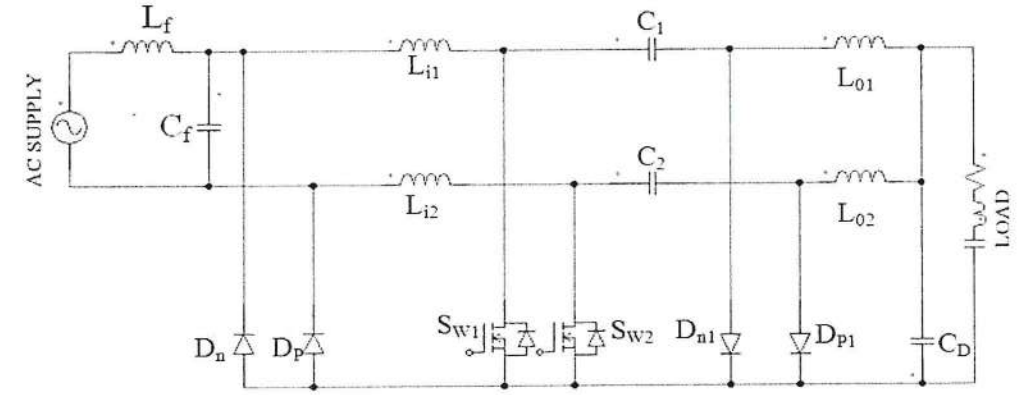

Fig. 2: Bridgeless Cuk converter

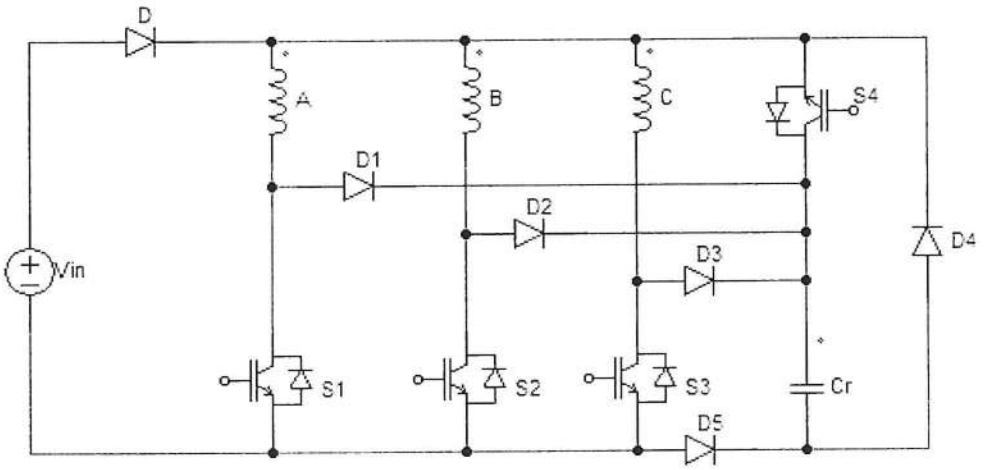

Fig. 3: C-dump converter

continuous in a switching period correspondingly. To activate a PFC converter in CCM, it requires three sensors (2 voltage, current) while a DCM process achieved by using only one voltage sensor. While the PFC converter operates in DCM mode the stresses is high, when compared to CCM mode operation. By operating the converter in DCM, many merits can be achieved such as near to unity power factor, at zero current the power switches are turned ON and output diodes are turned OFF (Fig. 2).

Operation of converter is depending upon the application. For high power applications CCM is suitable and low power application DCM is preferred. Conversely, DCM operation considerably increases the conduction losses due to the large current stress through circuit apparatus. DCM leads to one limitation, it can operate at low-power applications only (>300 W). So the DCM is chosen for low-power applications.

C- Dump converter for SRM drive: It is derived from the C-dump converter (Lee *et al*., 2007) circuit by eliminating the inductor of the Cuk converter. The energy can be stored in the capacitor and it is used for the next phase and being returned to the dc supply of conventional C-dump representation. At that time the capacitor have the voltage level of 2 V_{dc} in C-dump converter, its proper utilization significantly improves the drive performance.

By the modified C-dump converter, the energy in the dump capacitor is directly utilized to energize phase windings and to maintain the dump capacitor voltage at V_{dc} rather than $2V_{dc}$. Control of the dump capacitor voltage is streamlined and replication of the phase currents is enabled in an energy efficient C-dump converter. Figure 3 shows the energy competent C-dump converter topology, derived from the conventional C-dump converter (Tseng *et al*., 2000). The topology could

PRINCIPAL.
K. S. R. INSTITUTE FOR
ENGINEERING AND TECHNOLOGY,
K. S. R. KALVI NAGAR.
TIRUCHENGODE-637 215,
NAMAKKAL Dt. TAMIL NADU.

minimize the whole cost of the switched reluctance motor drive. The potential ratings of the c-dump capacitor and a few of the switching devices in the energy efficient C-dump converter are reduced to the supply voltage (V_{dc}) level likened to twice the supply voltage ($2V_{dc}$) in the conventional C-dump converter. In addition, the converter has modest control requirements and allows the motor phase current to freewheel during chopping mode.

The A phase starts to magnetize together S1 and S4 on. The phase is energized from the capacitor that is transfer to the main source until the capacitor voltage drops to the level of supply voltage. At that time the blocking diode becomes forward biased and the source begins to provide for energy to the phase. The current is maintained at the charge level by switch S1 on and off. The phase current freewheels throughout diode D1 and S4 when S1 is "off". The current commutates from S1 and S4 "off" and charges the dump capacitor. Diode D5 stop the demagnetizing current which flowed throughout the source. While A phase is being demagnetized, B phase can be magnetized by turn on S2. During this period, the current through B phase is maintained at the command value by dumping any extra energy into the capacitor. These can be continued for the next phase also.

RESULTS AND DISCSUSSION

Without Cuk converter fed SRM drive: Figure 4 shows the without cuk converter outputs for flux and current. In the results torque range of the motor is reduced and the speed range is also low. Figure 5 shows the without Cuk onverter outputs for torque and speed. The ripple in the motor flux is high and also the current range of the motor is low. Without Cuk converter circuit the motor takes 0.2 sec to reach the steady state condition.

UK converter fED SRM drive: Figure 6 shows the With cuk converter outputs for flux and current. In the results torque range of the motor is increased and the speed range also high. The ripple in the motor flux is low and the current range of the motor is increased. Figure 7 shows the with cuk converter outputs for torque and speed.

With CUK converter circuit the motor takes 0.12 sec to reach the steady state condition when compared to the without CUK converter operation. The acceleration in the torque is high. In the given Simulation results the output torque ripple is reduced when compared to the without CUK converter circuit.

Figure 8 shows the output waveform of the speed for switched reluctance motor using PI controller. From the waveform it shows the desired output speed is attained after 0.22 sec with the set point speed of 2000 rpm. Figure 9 Shows the switched reluctance motor using fuzzy logic controller speed output waveform. From the graphical representation it shows that desired output speed is attained before 0.09 sec with the set point speed of 2000 rpm.

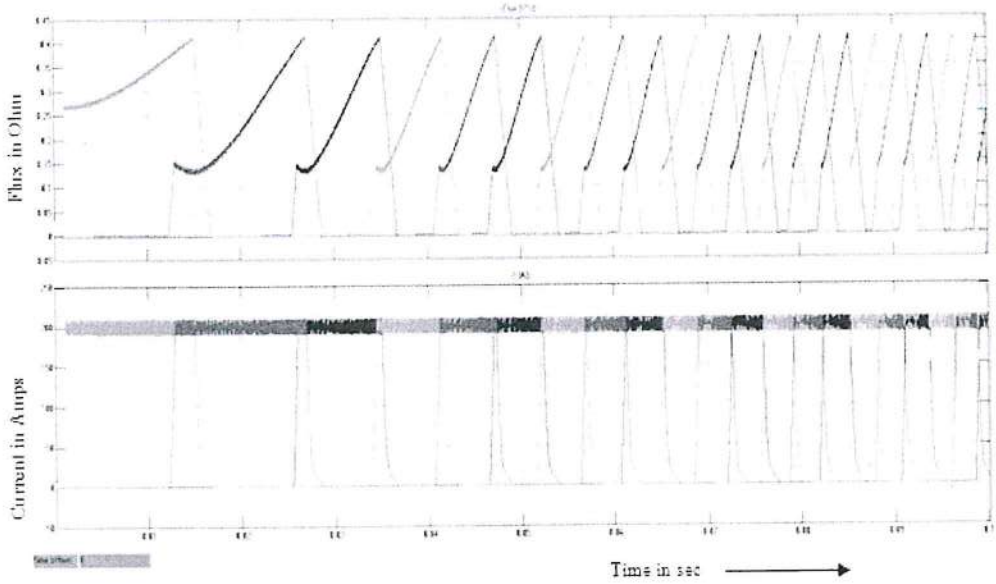

Fig. 4: Without Cuk converter outputs for flux and current

PRINCIPAL,
K. S. R. INSTITUTE FOR
ENGINEERING AND TECHNOLOGY,
K. S. R. KALVI NAGAR,
TIRUCHENGODE-637 215,
NAMAKKAL Dt, TAMIL NADU.

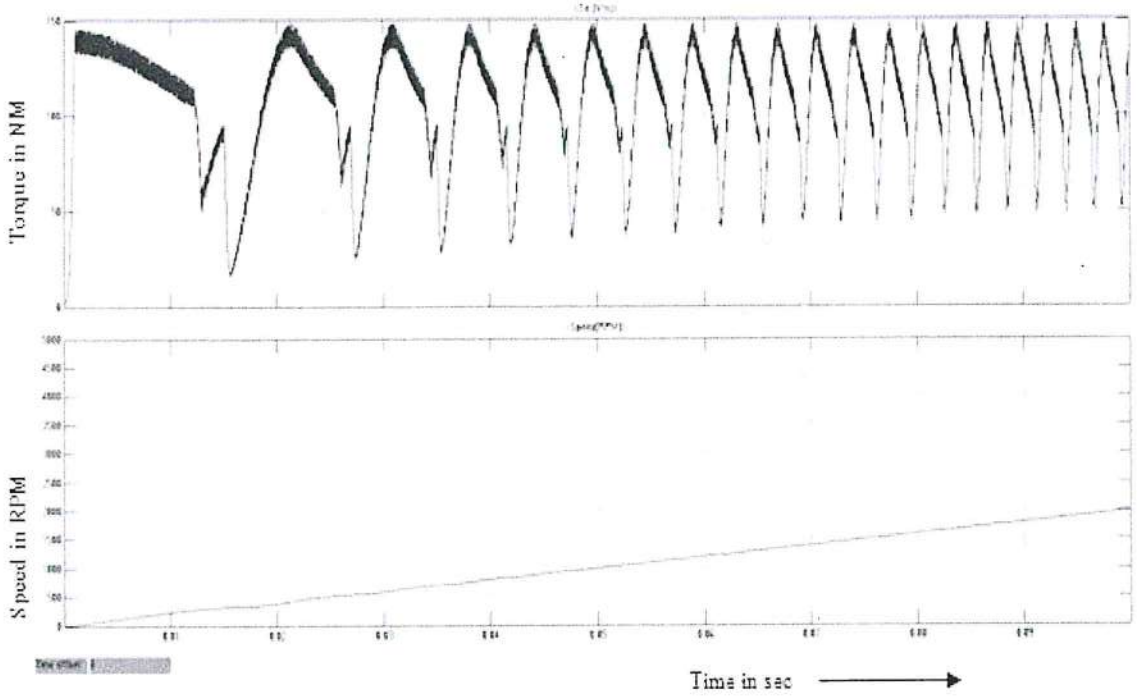

Fig. 5: Without CUK converter outputs for torque and speed

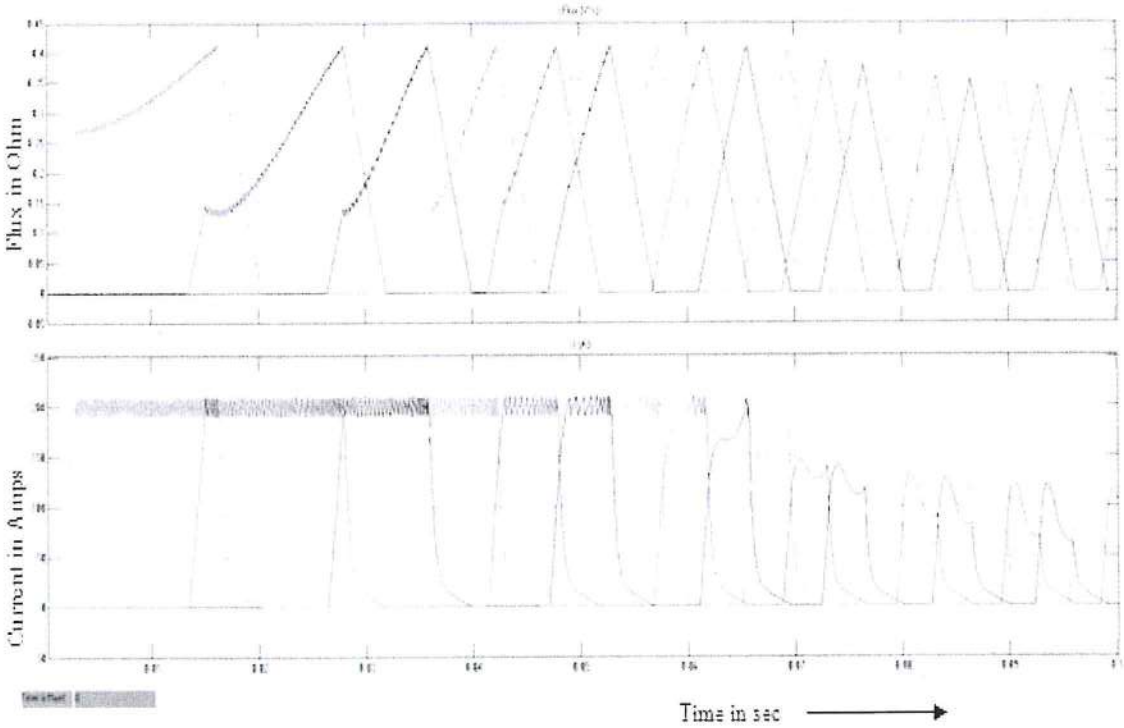

Fig. 6: With Cuk converter outputs for flux and current

PRINCIPAL,
K. S. R. INSTITUTE FOR
ENGINEERING AND TECHNOLOGY,
K. S. R. KALVI NAGAR,
TIRUCHENGODE-637 215,
NAMAKKAL Dt, TAMIL NADU.

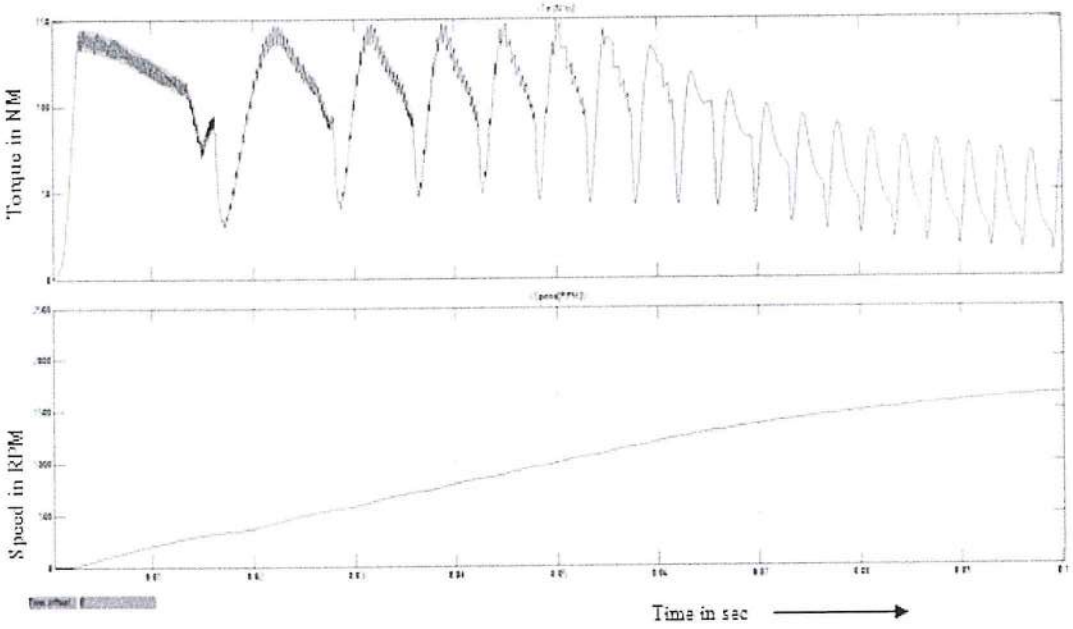

Fig. 7: With CUK converter outputs for torque and speed

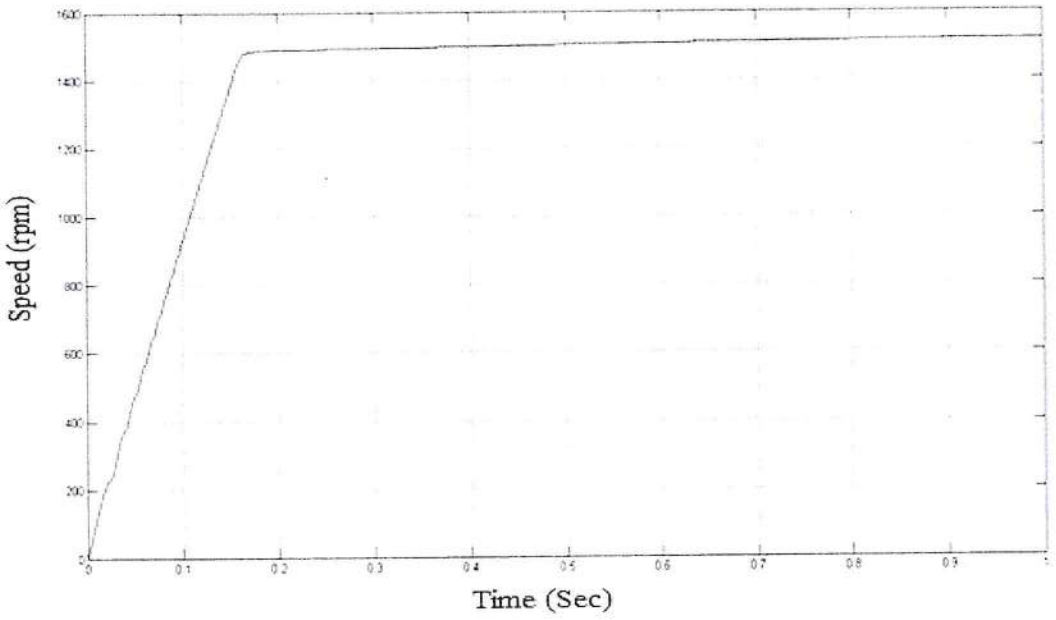

Fig. 8: SRM PI controller speed output waveform

Table 1 shows the various set speed and settling time in PI controller and fuzzy logic speed controller. From the tabulation it shows, the settling time of fuzzy logic controller as low compared to PI controller.

Table 1: Comparative study of set speed and settling time

Speed (RPM)	PI (Settling time)	Fuzzy controller (Settling time)
1500	0.16	0.05
2000	0.22	0.09
2500	0.26	0.12
3000	0.32	0.15

PRINCIPAL.
K. S. R. INSTITUTE FOR
ENGINEERING AND TECHNOLOGY,
K. S. R. KALVI NAGAR,
TIRUCHENGODE-637 215,
NAMAKKAL Dt. TAMIL NADU.

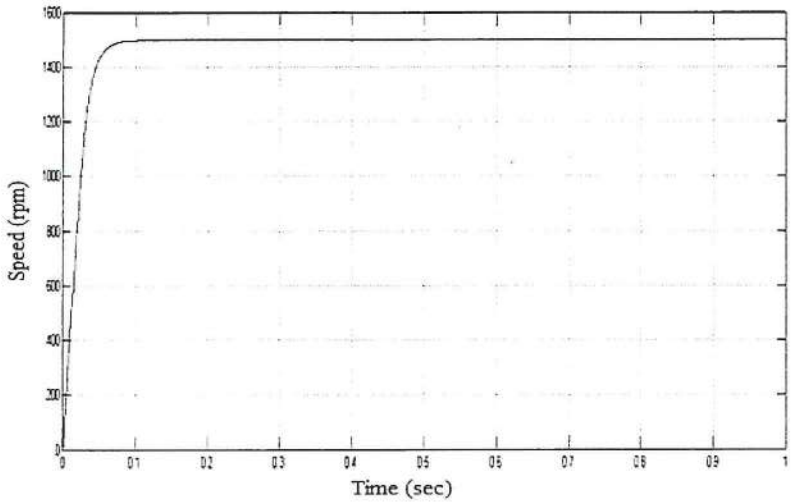

Fig. 9: SRM FLC speed output waveform

CONCLUSION

In this study, a Cuk converter fed Switched Reluctance drive has been introduced. The proposed drive provides increased drive efficiency when compared to the drive without Cuk converter. Here, for the Cuk converter normal PWM pulse generator is used. In future for the Cuk converter operation SVPWM, NEURAL or GENETIC algorithm methods will be implemented for improving the performance of Cuk converter with SRM drive and also for the switched reluctance drive the space vector modulation technique may be implemented. Due to the implementation of Cuk converter the speed of the motor is increased and the torque ripple also reduced. Bridge Cuk converter has to be replaced with Bridgeless Cuk converter so that the power factor is improved when compared to the conventional converters.

REFERENCES

Agirman, I., A.M. Stankovic, G. Tadmor and A.H. Lev, 2001. Adaptive torque-ripple minimization in switched reluctance motors. IEEE. Trans. Ind. Electron., 48: 664-672.

Ahn, J.W., J. Liang and D.H. Lee, 2010. Classification and analysis of switched reluctance converters. J. Electric. Eng. Technol., 5: 571-579.

Barnes, M. and C. Pollock, 1998. Power electronic converters for switched reluctance drives. IEEE. Trans. Power Electr., 13: 1100-1111.

Bist, V. and B. Singh, 2014. An adjustable-speed PFC bridgeless buck-boost converter-fed BLDC motor drive. IEEE. Trans. Ind. Electron., 61: 2665-2677.

Chung, H.Y., B.C. Chen and J.J. Lin, 1998. A PI-type fuzzy controller with self-tuning scaling factors. Fuzzy Sets Syst., 93: 23-28.

Kavitha, A. and G. Uma, 2008. Experimental verification of Hopf bifurcation in DC--DC luo converter. IEEE. Trans. Power Electron., 23: 2878-2883.

Lee, T.W., Y.H. Yoon, Y.C. Kim, B.K. Lee and C.Y. Won, 2007. Control of c-dump converters fed switched reluctance motor on an automotive application. Electr. Power Syst. Res., 77: 804-812.

Luo, F.L. and H. Ye, 2003. Negative output super-lift converters. IEEE. Transac. Power Electronics, 18: 1113-1121.

Luo, F.L. and H. Ye, 2004. Positive output multiple-lift push-pull switched-capacitor Luo-converters. IEEE. Trans. Ind. Electron., 51: 594-602.

Mudi, R.K. and N.R. Pal, 1999. A robust self-tuning scheme for PI-and PD-type fuzzy controllers. IEEE. Trans. Fuzzy syst., 7: 2-16.

Silpa, N. and J. Chitra, 2014. An improved LUO converter for high voltage applications. J. Emerging Technol. Adv. Eng., 4: 262-267.

Tseng, K.J., S. Cao and J. Wang, 2000. A new hybrid C-dump and buck-fronted converter for switched reluctance motors. IEEE. Trans. Ind. Electron., 47: 1228-1236.

Yang, H., 2012. A pedagogical approach for modeling and simulation of switching mode DC-DC converters for power electronics course. Indonesian J. Electr. Eng. Comput. Sci., 10: 1319-1326.

PRINCIPAL,
K. S. R. INSTITUTE FOR
ENGINEERING AND TECHNOLOGY,
K. S. R. KALVI NAGAR,
TIRUCHENGODE-637 215,
NAMAKKAL Dt. TAMIL NADU.

ADVANCES in NATURAL and APPLIED SCIENCES

ISSN: 1995-0772
EISSN: 1998-1090
2016june10(8): pages 6-14

Published BYAENSI Publication
http://www.aensiweb.com/ANAS
Open Access Journal

Evolutionary Computing Technique for Torque Ripple Minimization of 8/6 Switched Reluctance Motor

[1]T.Srihari, [2]R.Jeyabharath, [3]P.Veena

[1]Assistant Professor,Department of Electrical and Electronics Engineering,KSR Institute for Engineering and Technology,Tiruchengode, Tamilnadu, India.
[2]Professor,Department of Electrical and Electronics Engineering,KSR Institute for Engineering and Technology,Tiruchengode, Tamilnadu, India.
[3]Professor,Department of Electrical and Electronics Engineering,KSR Institute for Engineering and Technology,Tiruchengode, Tamilnadu, India.

Received 25 April 2016; Accepted 28 May 2016; Available 2 June 2016

Address For Correspondence:
T. Srihari, Assistant Professor, Department of Electrical and Electronics Engineering, KSR Institute for Engineering and Technology, Tiruchengode, Tamilnadu, India.

Copyright © 2016 by authors and American-Eurasian Network for Scientific Information (AENSI Publication). This work is licensed under the Creative Commons Attribution International License (CC BY).http://creativecommons.org/licenses/by/4.0/

Open Access

ABSTRACT

Background: Switched Reluctance Motor's (SRMs) doubly salient structure and its high torque feature make it as to play important role in electric vehicle industry. The good efficiency, high torque and variable speed ratio in addition to low cost, high reliability and fault-tolerance make the Switched Reluctance Motor (SRM) a candidate with real chances on the market of vehicle propulsion. The main drawbacks of the SRM related to the torque ripple, acoustic noise and vibration make the research object in R&Ds all over the world. **Objective:** In this paper the objective of the work is focused on the development of an efficient design of drive system for 8/6 switched reluctance motor based upon Direct Torque Control (DTC) using evolutionary computing technique. DTC is implemented through Space Vector Modulation (SVM) technique which reduces the torque ripple and provides significant control over torque than conventional technique. **Results:** Evolutionary computing involves in tuning the controller parameter through genetic algorithm. Matlab/Simulink model is constructed for the proposed scheme of switched reluctance motor drive model and validate the work with minimization of torque ripple. **Conclusion:** The simulation results show that the designed PI controller performs satisfactorily to track the reference torque with actual torque. This new technique can be implemented in real time with low cost microcontrollers and higher simplicity.

KEYWORDS: Direct Torque Control, Space Vector Modulation, Genetic Algorithm, Switched Reluctance Motor Drive

INTRODUCTION

The policies to reduce emissions from transportation are focusing on the optimization of the efficiency of the existing vehicles, and the electrification of the vehicles. The continuously increasing price of the permanent magnets and the shortage of rare earths demand the finding of alternatives in several domains as hybrid and full electric propulsion due to their best overall performances. The good efficiency, high torque and variable speed ratio in addition to low cost, high reliability and fault-tolerance make the Switched Reluctance Motor (SRM) a candidate with real chances on the market of vehicle propulsion. The converter topology and switching calculation because of the unipolar operation, keeping away from shoot through errors makes SRM worthwhile in utilizations of aviation, which require high unwavering quality. Additionally it finds wide application in car commercial ventures, direct drive machine apparatuses and so forth.

ToCite ThisArticle:T. Srihari, R. Jeyabharath, P. Veena.,Evolutionary Computing Technique for Torque Ripple Minimization of 8/6 Switched Reluctance Motor.**Advances in Natural and Applied Sciences**. 10(8); Pages: 6-14

PRINCIPAL.
K. S. R. INSTITUTE FOR
ENGINEERING AND TECHNOLOGY,
K. S. R. KALVI NAGAR,
TIRUCHENGODE-637 215,
NAMAKKAL Dt. TAMIL NADU.

6. Elbuluk, M.E., T. liu and I. Husain, 2002. 'Neural-network-based model reference adaptive systems for high-performance motor drives and motion controls', IEEE Trans. Ind. Applicat., 38: 879-886. http://dx.doi.org/10.1109/TIA.2002.1003444
7. Hassan-Halleh, Meisam-Rahmani and Bahram-Kimiaghalam, 2008. 'Direct Torque Control of Induction Motors with Fuzzy Logic Controller' International Conference on Control, Automation and Systems, 14-17: 345-350. http://dx.doi.org/10.1109/ICCAS.2008.4694669
8. Soliman,H.F.E. and M.E. Elbuluk, 2007. "Direct Torque Control of a Three Phase Induction Motor Using a Hybrid PI/Fuzzy Controller," Industry Applications Conference, 2007. 42nd IAS Annual Meeting. Conference Record of the 2007 IEEE, New Orleans, LA, pp: 1681-1685 http://dx.doi.org/10.1109/07ias.2007.258

PRINCIPAL,
K. S. R. INSTITUTE FOR
ENGINEERING AND TECHNOLOGY,
K. S. R. KALVI NAGAR,
TIRUCHENGODE-637 215,
NAMAKKAL DT. TAMIL NADU.

The main disadvantages of SRM are the highly nonlinear and discrete nature of torque production mechanism. The total torque in SRM is the sum of torques generated by each of the stator phase, which are independently controlled. When torque production mechanism is transferred from one active phase to another, pulsations are produced leading to vibrations and acoustic noise. The nonlinear magnetization characteristics make the control of motor really complex.

The control of SRM is the late pattern of explorationas there are complications implemented due to mutual coupling of the motor phase and parameter variation of inductance characteristics. Previous control schemes involve using of linear or nonlinear models. An adaptive feedback controller assuming linear magnetic circuits was proposed in [1]. In another scheme, an analytical solution was developed for production motor voltages to provide a smooth torque [2].

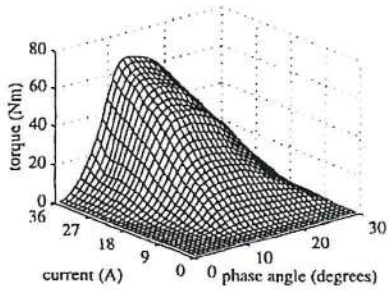

Fig. 1: Measured Nonlinear Characteristics of SRM

Though linear systems were simple, they were highly inaccurate as torque and flux are both nonlinear functions. So some schemes developed nonlinear characteristics of SR motor (Fig. 1). In [3] feedback linearization provides compensation for the magnetic nonlinearity. Also ripples were reduced to provide smooth torque in [4]. Some nonlinear adaptive schemes were also developed. The implementation of a nonlinear model in real time was complex, expensive and affected by variations in saturation. To overcome all these problems, the Direct Torque Control (DTC) was proposed which gave straightforward answer for control the motor speed and torque and reduced torque ripple [5]. Early scheme used concept of short flux pattern that links two separated poles of the SRM stator. However, this needed a new winding configuration, which is expensive and inconvenient. This scheme can only be theoretically achieved, as they required bipolar currents in opposition to unipolar currents SRM. In recent day many more intelligent controller [6] [7] [8] were developed such as fuzzy logic controller and neural network controller in order to reduce torque ripple content in SRM drive system which provides many excellent results and can be effectively implemented if their complexity reduces. This paper mainly focused on implementation of genetic controller for driving SVM based DTC on SRM drive system which provides minimum torque ripple of 0.138 Nm, which were modeled through MATLAB/SIMULINK. This scheme reduces the complexity and gives better results of previous techniques so that it can be effectively implemented in hardware.

SRM Drive System:

The physical look of a SRM resemble that of other rotating motors (AC and DC) Induction Motor and DC motor and so forth. The structure of 8/6 (8 stator and 6 rotor) SRM is uncovered in Fig. 2. It has particularly important development. Normally number of stator and rotor poles is even number. The windings development of the SRM are exceptionally less difficult than that of different sorts of motor. Just winding is for stator poles, and basically twisted on it and rotor poles are unwinded. The winding of inverse poles is associated in arrangement or in parallel making no of phases exactly half the number of stator poles. Along these lines excitation of single phase energizes two stator poles.

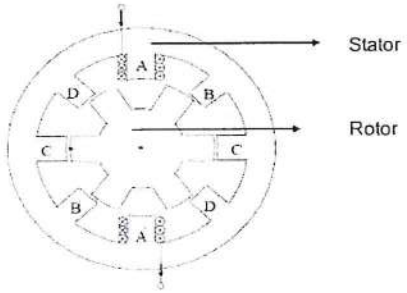

Fig. 2: Construction of 8/6 SRM

PRINCIPAL.
K. S. R. INSTITUTE FOR
ENGINEERING AND TECHNOLOGY,
K. S. R. KALVI NAGAR,
TIRUCHENGODE-637 215,
NAMAKKAL Dt. TAMIL NADU.

The rotor has simple coatedwith salient pole structure without winding. The principle operation of SRM is grounded on the tendency of an electromagnetic system to obtain a constant equilibrium position minimizing magnetic reluctance. Whenever diametrically opposite stator poles of a SRM are excited, the closest rotor poles are attracted, resulting in torque production. When these two rotor poles become aligned with the two stator poles, a second pair of stator poles is excited to bring a second pair of rotor poles into alignment. The successive movement of a 4 -phase, 8/6 SRM is shown in Fig. 3. The synchronization of the stator phase excitation is readily accomplished with rotor position feedback.

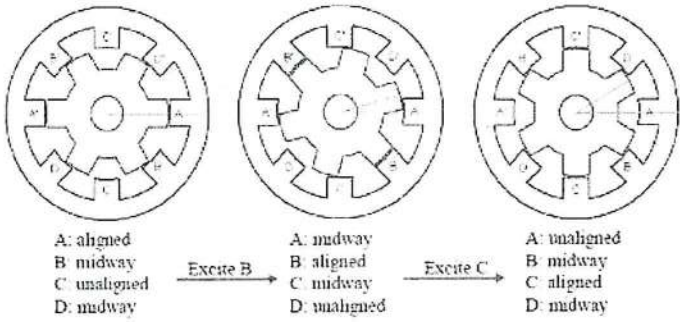

Fig. 3: Construction of 8/6 SRM

In the fully-aligned position, the phase winding inductance is maximum and the reluctance of the magnetic circuit is minimum. Similarly in the non-aligned position, the inductance is minimum and the reluctance S is maximum. The motor torque is expressed as given in equation 1.

$$T = \frac{1}{2} i^2 \frac{dL}{d\vartheta} \quad (1)$$

Rotor has six poles, therefore, when rotor completes one revolution, inductance will pass through 6 maximum and 6 minimum values. The angle between the axes of two consecutive rotor poles is 60° and that of stator poles is 45°, hence, if variation of inductance for phase2 is plotted, it will have similar variation as of phase1, but displaced by 15°. Therefore waveforms of phase 3 and 4 will similarly be shifted with respect to phase1 waveforms by 30° and 45° respectively.

Torque ripple is characterized as the contrast between the most extreme and least quick torque communicated as a rate of the normal torque amid steady state operation. Scientifically, Percentage Torque ripple is communicated as given in condition (2).

$$\text{Torque Ripple}(\%) = \frac{T_{inst(max)} - T_{inst(min)}}{T_{avg}} \times 100 \quad (2)$$

Where T_{inst} is the instantaneous torque and T_{avg} is the average torque.

Direct Torque Control:

Based on field oriented control the direct torque control system works. Field Oriented Control (Vector Control) takes after space vector hypothesis to control magnetic field introduction and direct discretion sets up an interesting recurrence of inverter working given a particular dc link voltage and a particular stator flux level. The working guideline of DTC is to first recognize stator voltage vectors as indicated by the contrasts between the reference torque and the real estimations of stator flux linkage. The standards of DTC in the ac machine can be inferred by investigating the motor equations. The stator flux linkage vector can communicated as underneath condition (3).

$$\overrightarrow{\psi_s} = \int (\vec{v} - \vec{i}R) dt \quad (3)$$

Different techniques have been proposed in the past to minimize torque ripple. The proposed technique is Space vector modulation (SVM) based DTC of 4 phase 8/6 SRM by choosinganappropriate set of 8 space voltage vectors. The DTC of SRM drive is simulated for consistent torque burden to watch the steady state and transient execution of the drive. It is watched that the torque is kept up inside the set hysteresis band. This new arrangement of space vectors demonstrates a critical change in the torque execution of DTC based SRM contrasted with the present control technique.

On the basis of the errors calculation between the reference value and estimated values of torque and also flux, it is easy to directly control on the inverter states in order to decrease the torque and flux error within the

PRINCIPAL.
K. S. R INSTITUTE FOR
ENGINEERING AND TECHNOLOGY,
K. S. R. KALVI NAGAR,
TIRUCHENGODE-637 215,
NAMAKKAL Dt. TAMIL NADU.

prefixed band limits. The DTC scheme as initially proposed is very simple; in its basic configuration. It consists of pair of hysteresis comparator, torque and flux calculator, a lookup table, and voltage source inverter. The configuration is much simpler than FOC system due to the absence of frame transformer, pulse width modulator, and position encoder. The general block diagram of DTC is shown in Fig. 4. Two of the major issues which are normally addressed in DTC drives are the variation of switching frequency of the inverter used in the DTC drives with operating condition and the high torque ripple.

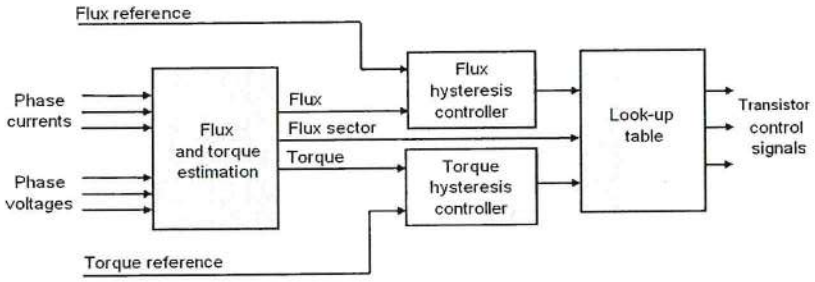

Fig. 4: Block Diagram of DTC

It is shown that the switching frequency is highly influenced by the motor speed. The motor DTC system comprises of three basic functions, namely: A motor model estimates the actual torque, stator flux and shaft speed by means of measurement of two motor phase currents, the immediate circuit DC voltage on the state of the power switched. Calculations are performed every 25 microseconds and these include corrections for temperature and saturation effects. The parameter of the motor model is estimated by an identification run, which made during commissioning. A two level hysteresis controller, where the torque and flux references are compared with the actual values calculated from the motor model. The magnitude of the stator flux is normally kept constant and the motor torque is controlled by means of the angle between the stator and rotor flux. Optimal switching logic that translates the controller output into the appropriate commands to the power switching devices. There are eight voltage vectors available in the two level voltage source inverter and the optimum switching logic determines the required selection every 25 microseconds.

Space Voltage Vector for SRM:

Like the AC drives, SRM likewise characterize the comparable space vectors. The voltage space vector for every phase is characterized on the center axis of the stator shaft in light of the fact that the flux linkage for a current and voltage connected to the motor phase will have phasor course in accordance with the center of the pole axis which does not require any physical change in winding topology. It is appeared in Fig. 5, every motor phase can have three conceivable voltage states for a unidirectional current. At the stage, when both switches in a motor phase are turned on. For this situation positive voltage is given to the motor phase. At the point when current begins streaming one device is turned off, along these lines a zero voltage circle happens and the state succession is given as 0. At long last, when both devices are turned off, there is no present or freewheeling current courses through the upper diodes. For this situation negative voltage is experienced by the motor phase and the state arrangement is characterized as negative voltage. Among the eight conceivable expresses any one is chosen at one time so as to keep the stator flux linkage and the motor torque inside hysteresis groups.

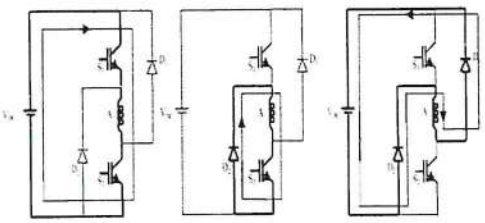

Fig. 5: SRM Phase Voltage States

As in the conventional DTC scheme, if the stator flux linkage lies in the k-th zone, the magnitude of the flux can be improved by the importance if switching vectors v(k+1) and v(k-1) and diminished by the presence of vectors v(k+2) and v(k+2). Hence whenever the stator flux linkage reaches its upper limit in the hysteresis band, it is reduced by applying voltage vectors which are directed toward the center of the flux vector space and vice-versa.

PRINCIPAL,
K. S. R. INSTITUTE FOR
ENGINEERING AND TECHNOLOGY,
K. S. R. KALVI NAGAR,
TIRUCHENGODE-637 215,
NAMAKKAL Dt. TAMIL NADU

The motoring torque is controlled by an acceleration or deceleration of the stator flux relative to the rotor movement. Hence, if an increase in torque is required, voltage vectors that advance the stator flux linkage in the direction of rotation are selected. This corresponds to selection of vector v(k+1) and v(k+2) for a stator flux linkage in the k-th zone. When the torque is to be decrease, voltage vectors are applied which decelerate the stator flux linkage vector. This corresponds to the vectors v(k-1) and v(k-2) in the zone k. Switching table for controlling the stator flux linkage and motor torque can be defined as shown in Table 1.

Table 1: Switching Table for DTC

Torque	INCREASE	INCREASE	DECREASE	DECREASE
Flux	INCREASE	DECREASE	INCREASE	DECREASE
Selection of Vector	v(k+1)	v(k-1)	v(k+2)	v(k-2)

In order to control the flux and torque within the hysteresis bands, the instantaneous torque and stator flux vector magnitude must be known. In the SR motor voltages in the motor are highly non-sinusoidal and thus more effective insight may be gained by firstly finding the individual flux linkages of each phase using the voltage.

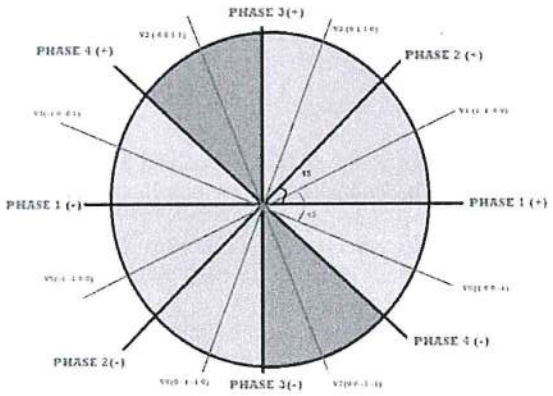

Fig. 6: Space Voltage Vector for SRM

In this case the magnitude of the individual phase flux linkages varies with time, but the direction is always along the stator pole axis. Torque look up table estimated previous and stored processor for adjustable Dwell angle. Space voltage vector representation for 8/6 switched reluctance motor is shown in Fig. 6. Pseudo codes for different voltage states were depict in Table 2.

Table 2: Pseudo Code for Voltage States

Voltage vectors	Voltage states for four phase				Voltage Vector	Voltage state for four phase			
	A	B	C	D		A	B	C	D
V1	1	1	0	0	V5	-1	-1	0	0
V2	0	1	1	0	V6	0	-1	-1	0
V3	0	0	1	1	V7	0	0	-1	-1
V4	-1	0	0	1	V8	1	0	0	-1

Control switching table is used to select the voltage command based on the present zone of the flux linkage that can be determined by the angle. For the first time, considering 4phase motor, vector number is four and so combination of vector is zero with appear on rectangular plane. In real system arbitrary phase will be excited first to detect the initial rotor position. Rotor position move to arbitrary aligned position. Therefore we solve this problem with initial value of 45 degree on 4 phase. The orthogonal flux vector are expressed as

$$\psi_\alpha = \psi_1 - \psi_2 \cos 60° - \psi_3 \cos 60° \quad (4)$$

$$\psi_\beta = \psi_2 \sin 60° - \psi_3 \sin 60° \quad (5)$$

The magnitude of $\vec{\psi}$ and angle δ of the equivalent flux vector is defined as

$$\psi_s = \sqrt{{\psi_\alpha}^2 + {\psi_\beta}^2} \quad (6)$$

$$\delta = \arctan\left(\frac{\psi_\beta}{\psi_\alpha}\right) \quad (7)$$

Proposed Evolutionary Computing Technique:

PRINCIPAL.
K. S. R. INSTITUTE FOR
ENGINEERING AND TECHNOLOGY,
K. S. R. KALVI NAGAR,
TIRUCHENGODE-637 215,
NAMAKKAL Dt. TAMIL NADU.

The GA has discovered application in the region of the programmed tuning process for traditional and intelligent controllers. Same exploration has been directed utilizing genetic algorithms to help on-line or logged off control frameworks. It has basically been used as a logged off procedure for performing a guided quest for the ideal answer for an issue. In this paper, the GA is utilized logged off controller execution to adaptively seek through a populace of controllers and decide the part most fit to be implemented over a given sampling period.

Here in Genetic PI controller tuning, each chromosome has a genes producing as possible proportional and integral gain values. The implementation of GA-PI control technique for Four-Phase 8/6 SRM to reduce the torque ripple and to obtain quick torque response. The block diagram of the proposed project is shown in Fig. 7.

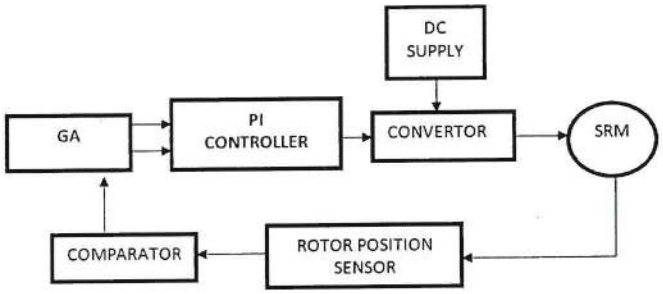

Fig. 7: Block Diagram of Proposed Scheme

In this proposed model, feedback signals are the position θ and the phase currents $i_{a,b,c,d}$ the position signal is used to calculate the torque. The PI controller with signal generator is used to control turn-on angle θ_{on}, turn-off angle θ_{off}, and pulse width modulation duty cycle.

The steps for torque control are summarized as follows:

1 The current and rotor position signal of the SRM are Sampled.

2 Current error due to change are calculated.

3 Select the number of digits to represent each controller parameter Kp and Ki, choose crossover probability (pc) and mutation probability (pm).

4 Assume an initial population of Kp and Ki gains (we make a random selection) sample time T and set time t.

5 ProduceKp and Ki gain values for the error value and it determine the proper turn on and turn off angle to the converter.

6 The motor torque ripples is reduced effectively by proper selection of Kpgain values, Ki gain values, turn on and turn off angles.

These are the several steps that involve in our proposed project to minimize the torque ripple using genetic algorithm principles.

Simulation Model:

To simulate the system a Matlab/Simulink closed loop model based upon evolutionary computing of DTC of 8/6 SRM was constructed as in Fig. 8. The motor parameter such as torque, phase flux and position are obtained from 4φ SRM. The four phase flux vector is transformed on to a stationary orthogonal $\alpha - \beta$ reference frame to calculate the net flux. The multiphase drives divide the controlled power on more inverter legs. The increased phase number reduces the current stress on each switch.

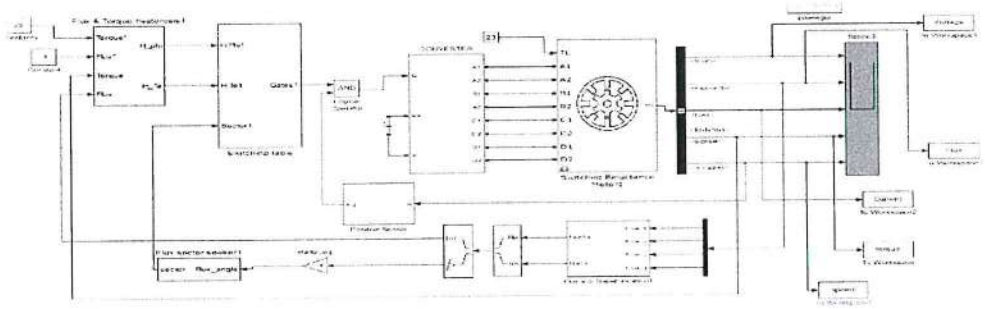

Fig. 8: Simulink Modeling of Proposed Scheme

PRINCIPAL,
K. S. R. INSTITUTE FOR
ENGINEERING AND TECHNOLOGY,
K. S. R. KALVI NAGAR,
TIRUCHENGODE-637 215,
NAMAKKAL Dt. TAMIL NADU.

The converter topologies selected for giving input to the Switched Reluctance motor is asymmetrical converter. This torque ripple is a particular characteristic of the SRM and it depends mainly on the converter s turn-on and turn-off angles. The SRM torque characteristic can be optimized by applying appropriated pre-calculated turn-on and turn-off angles in function of the motor current and speed.

RESULTS AND DISCUSSION

For the purpose of analysis, a comparative work is done between conventional technique and evolutionary computing based DTC of 8/6 SRM and percentage of torque ripple is compared. A DC supply voltage of 120 V is used for the converter configuration. The torque gets controlled when comparing with previous conventional technique. The simulation result of proposed space vector modulation based direct torque control of Switched Reluctance Motor is shown in Fig. 9. And its maximized view is shown in Fig. 10.The FFT analysis on conventional system and proposed schemes were shown in Fig. 11. & Fig.12. The results were obtained from the model developed from four phase 8/6 switched reluctance motor implementing direct torque control based upon space vector modulation technique and Genetic Algorithm were implemented for tuning of PI controller to minimize the torque error. The torque ripple is reduced much reduced than conventional technique. Hence space vector modulation implemented in DTC holds good control over torque response.

The simulation results show that the designed PI controller performs satisfactorily to track the reference torque with actual torque. It is also observed that the designed PI controller completely eliminates ripples at high speeds. The designed PI controller is tuned through genetic algorithm which is done through effective selection of global best and local best done through random selection. The simulation result made the quicker convergence of PI controller by effective genetic tuning of K_p and K_i values than conventional system. The comparison Table 3. for the proposed design of Direct Torque Control with Genetic PI Controller with other controller is made on discussing the torque ripple parameter on closed loop design.

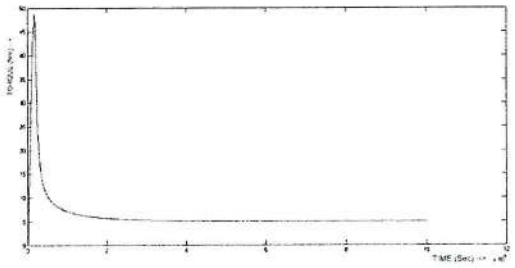

Fig. 9: Simulation Result of Proposed System for 5 Nm.

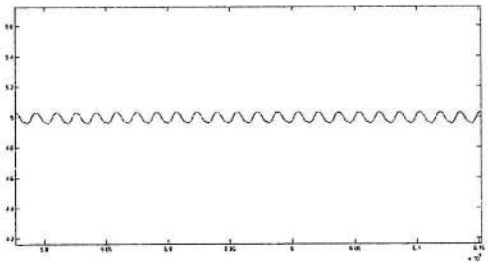

Fig. 10: Magnified view of Simulation for 5 Nm.

PRINCIPAL.
K. S. R. INSTITUTE FOR
ENGINEERING AND TECHNOLOGY,
K. S. R. KALVI NAGAR,
TIRUCHENGODE-637 215,
NAMAKKAL Dt. TAMIL NADU.

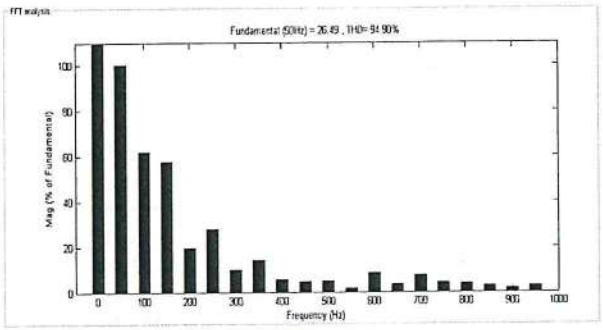

Fig. 11: FFT Analysis for Conventional System

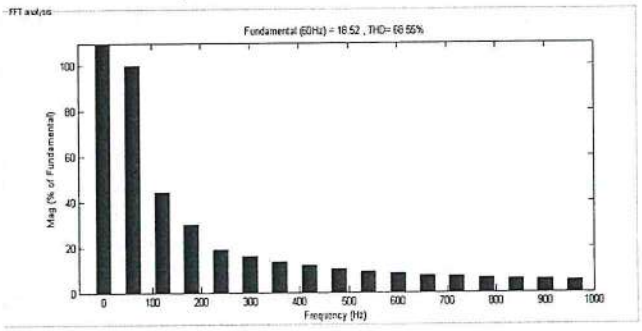

Fig. 12: FFT Analysis for Proposed Scheme

Table 3: Comparison Table of Torque Ripple for Different Controller

CONTROLLER	TORQUE RIPPLE (Nm)	TORQUE RIPPLE (%)
Conventional Controller	0.42 Nm	21 %
Genetic PI Controller	0.22 Nm	11 %
Direct Torque control with PI controller	0.172 Nm	8.8 %
Direct Torque Control With Genetic PI Controller	0.138 Nm	6.9 %

Conclusion:

Direct Torque Control (DTC) for 8/6 SRM drive based upon evolutionary computing is made through comparing the actual torque with reference torque and generating error and then error is tuned by genetic based PI-controller. DTC is implemented through space vector modulation thus by effective switching of nine voltage vector to the convertor at appropriate switching time and angle for smooth operation of motor. The quicker convergence of PI controller is made through evolutionary computing. The results obtained from the Matlab/Simulink model validate the proposed scheme by reducing the ripple than conventional controller. The GA-PI Controller technique produce the quick torque response and reduced torque ripple than the individual controllers such as PI, Neural, and Fuzzy logic controllers. By applying this technique the torque is maintained at 23.5 Nm and the ripple is reduced to 11% where as in the conventional methods the torque is about 22%. Hence by using this GA-PI controller the torque ripple is minimized effectively.

REFERENCES

1. Taylor, D.G., 1991. "Adaptive control design for a class of doubly-salient motors," In Proc. 30th IEEE Conf. Dec. Contr., 3: 2903-2908, http://dx.doi.org/10.1109/cdc.1991.261069
2. Nagel,N.J. and R.D. Lorenz, 1999. "Complex rotating vector method for smooth torque control of a saturated switched reluctance motor," in Proc. 34th Annual Meeting IEEE Ind. Application., 4: 2591-2598 http://dx.doi.org/10.1109/ias.1999.799204
3. Ilic-Spong, M., R. Marino, S.M. Peresada and D.G. Taylor, 1987. "Feedback linearizing control of switched reluctance motors," IEEE Trans. Automat. Contr., AC-32: 371-379. http://dx.doi.org/10.1109/TAC.1987.1104616
4. Stankovic, M., G. Tadmor, Z.J. Coric and I. Agirman, 1999. "On torque ripple reduction in current-fed switched eluctance motors," IEEE Trans.Ind. Electron., 46: 177-183.http://dx.doi.org/10.1109/41.744409
5. Jinupun,P. and P. Chi-KwongLuk, 1998. "Direct torque control for sensorless switched reluctance motor drives," Power Electronics and Variable Speed Drives, Seventh International Conference on (456): 329-334. http://dx.doi.org/10.1049/cp:19980546

PRINCIPAL.
K. S. R. INSTITUTE FOR
ENGINEERING AND TECHNOLOGY,
K. S. R. KALVI NAGAR,
TIRUCHENGODE-637 215,
NAMAKKAL DT. TAMIL NADU.

ADVANCES in NATURAL and APPLIED SCIENCES

ISSN: 1995-0772
EISSN: 1998-1090
2016june10(8): pages 6-14

Published BYAENSI Publication
http://www.aensiweb.com/ANAS
Open Access Journal

Evolutionary Computing Technique for Torque Ripple Minimization of 8/6 Switched Reluctance Motor

[1]T.Srihari, [2]R.Jeyabharath, [3]P.Veena

[1]Assistant Professor,Department of Electrical and Electronics Engineering,KSR Institute for Engineering and Technology,Tiruchengode, Tamilnadu, India.
[2]Professor,Department of Electrical and Electronics Engineering,KSR Institute for Engineering and Technology,Tiruchengode, Tamilnadu, India.
[3]Professor,Department of Electrical and Electronics Engineering,KSR Institute for Engineering and Technology,Tiruchengode, Tamilnadu, India.

Received 25 April 2016; Accepted 28 May 2016; Available 2 June 2016

Address For Correspondence:
T. Srihari, Assistant Professor, Department of Electrical and Electronics Engineering, KSR Institute for Engineering and Technology, Tiruchengode, Tamilnadu, India.

Copyright © 2016 by authors and American-Eurasian Network for Scientific Information (AENSI Publication). This work is licensed under the Creative Commons Attribution International License (CC BY).http://creativecommons.org/licenses/by/4.0/

Open Access

ABSTRACT

Background: Switched Reluctance Motor's (SRMs) doubly salient structure and its high torque feature make it as to play important role in electric vehicle industry. The good efficiency, high torque and variable speed ratio in addition to low cost, high reliability and fault-tolerance make the Switched Reluctance Motor (SRM) a candidate with real chances on the market of vehicle propulsion. The main drawbacks of the SRM related to the torque ripple, acoustic noise and vibration make the research object in R&Ds all over the world. **Objective:** In this paper the objective of the work is focused on the development of an efficient design of drive system for 8/6 switched reluctance motor based upon Direct Torque Control (DTC) using evolutionary computing technique. DTC is implemented through Space Vector Modulation (SVM) technique which reduces the torque ripple and provides significant control over torque than conventional technique. **Results:** Evolutionary computing involves in tuning the controller parameter through genetic algorithm. Matlab/Simulink model is constructed for the proposed scheme of switched reluctance motor drive model and validate the work with minimization of torque ripple. **Conclusion:** The simulation results show that the designed PI controller performs satisfactorily to track the reference torque with actual torque. This new technique can be implemented in real time with low cost microcontrollers and higher simplicity.

KEYWORDS: Direct Torque Control, Space Vector Modulation, Genetic Algorithm, Switched Reluctance Motor Drive

INTRODUCTION

The policies to reduce emissions from transportation are focusing on the optimization of the efficiency of the existing vehicles, and the electrification of the vehicles. The continuously increasing price of the permanent magnets and the shortage of rare earths demand the finding of alternatives in several domains as hybrid and full electric propulsion due to their best overall performances. The good efficiency, high torque and variable speed ratio in addition to low cost, high reliability and fault-tolerance make the Switched Reluctance Motor (SRM) a candidate with real chances on the market of vehicle propulsion. The converter topology and switching calculation because of the unipolar operation, keeping away from shoot through errors makes SRM worthwhile in utilizations of aviation, which require high unwavering quality. Additionally it finds wide application in car commercial ventures, direct drive machine apparatuses and so forth.

ToCite ThisArticle:T. Srihari, R. Jeyabharath, P. Veena.,Evolutionary Computing Technique for Torque Ripple Minimization of 8/6 Switched Reluctance Motor.**Advances in Natural and Applied Sciences**. 10(8); Pages: 6-14

PRINCIPAL.
K. S. R. INSTITUTE FOR
ENGINEERING AND TECHNOLOGY,
K. S. R. KALVI NAGAR,
TIRUCHENGODE-637 215,
NAMAKKAL Dt. TAMIL NADU.

6. Elbuluk, M.E., T. liu and I. Husain, 2002. 'Neural-network-based model reference adaptive systems for high-performance motor drives and motion controls', IEEE Trans. Ind. Applicat., 38: 879-886. http://dx.doi.org/10.1109/TIA.2002.1003444
7. Hassan-Halleh, Meisam-Rahmani and Bahram-Kimiaghalam, 2008. 'Direct Torque Control of Induction Motors with Fuzzy Logic Controller' International Conference on Control, Automation and Systems, 14-17: 345-350. http://dx.doi.org/10.1109/ICCAS.2008.4694669
8. Soliman,H.F.E. and M.E. Elbuluk, 2007. "Direct Torque Control of a Three Phase Induction Motor Using a Hybrid PI/Fuzzy Controller," Industry Applications Conference, 2007. 42nd IAS Annual Meeting. Conference Record of the 2007 IEEE, New Orleans, LA, pp: 1681-1685 http://dx.doi.org/10.1109/07ias.2007.258

PRINCIPAL,
K. S. R. INSTITUTE FOR
ENGINEERING AND TECHNOLOGY,
K. S. R. KALVI NAGAR,
TIRUCHENGODE-637 215,
NAMAKKAL DT. TAMIL NADU.

The main disadvantages of SRM are the highly nonlinear and discrete nature of torque production mechanism. The total torque in SRM is the sum of torques generated by each of the stator phase, which are independently controlled. When torque production mechanism is transferred from one active phase to another, pulsations are produced leading to vibrations and acoustic noise. The nonlinear magnetization characteristics make the control of motor really complex.

The control of SRM is the late pattern of explorationas there are complications implemented due to mutual coupling of the motor phase and parameter variation of inductance characteristics. Previous control schemes involve using of linear or nonlinear models. An adaptive feedback controller assuming linear magnetic circuits was proposed in [1]. In another scheme, an analytical solution was developed for production motor voltages to provide a smooth torque [2].

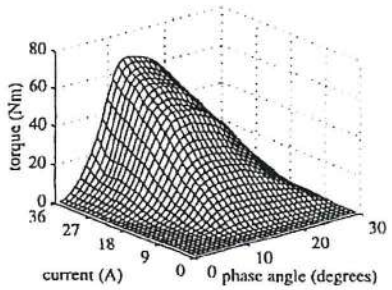

Fig. 1: Measured Nonlinear Characteristics of SRM

Though linear systems were simple, they were highly inaccurate as torque and flux are both nonlinear functions. So some schemes developed nonlinear characteristics of SR motor (Fig. 1). In [3] feedback linearization provides compensation for the magnetic nonlinearity. Also ripples were reduced to provide smooth torque in [4]. Some nonlinear adaptive schemes were also developed. The implementation of a nonlinear model in real time was complex, expensive and affected by variations in saturation. To overcome all these problems, the Direct Torque Control (DTC) was proposed which gave straightforward answer for control the motor speed and torque and reduced torque ripple [5]. Early scheme used concept of short flux pattern that links two separated poles of the SRM stator. However, this needed a new winding configuration, which is expensive and inconvenient. This scheme can only be theoretically achieved, as they required bipolar currents in opposition to unipolar currents SRM. In recent day many more intelligent controller [6] [7] [8] were developed such as fuzzy logic controller and neural network controller in order to reduce torque ripple content in SRM drive system which provides many excellent results and can be effectively implemented if their complexity reduces. This paper mainly focused on implementation of genetic controller for driving SVM based DTC on SRM drive system which provides minimum torque ripple of 0.138 Nm, which were modeled through MATLAB/SIMULINK. This scheme reduces the complexity and gives better results of previous techniques so that it can be effectively implemented in hardware.

SRM Drive System:

The physical look of a SRM resemble that of other rotating motors (AC and DC) Induction Motor and DC motor and so forth. The structure of 8/6 (8 stator and 6 rotor) SRM is uncovered in Fig. 2. It has particularly important development. Normally number of stator and rotor poles is even number. The windings development of the SRM are exceptionally less difficult than that of different sorts of motor. Just winding is for stator poles, and basically twisted on it and rotor poles are unwinded. The winding of inverse poles is associated in arrangement or in parallel making no of phases exactly half the number of stator poles. Along these lines excitation of single phase energizes two stator poles.

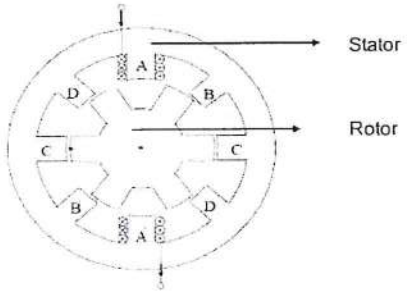

Fig. 2: Construction of 8/6 SRM

PRINCIPAL.
K. S. R. INSTITUTE FOR
ENGINEERING AND TECHNOLOGY,
K. S. R. KALVI NAGAR,
TIRUCHENGODE-637 215,
NAMAKKAL Dt. TAMIL NADU.

The rotor has simple coatedwith salient pole structure without winding. The principle operation of SRM is grounded on the tendency of an electromagnetic system to obtain a constant equilibrium position minimizing magnetic reluctance. Whenever diametrically opposite stator poles of a SRM are excited, the closest rotor poles are attracted, resulting in torque production. When these two rotor poles become aligned with the two stator poles, a second pair of stator poles is excited to bring a second pair of rotor poles into alignment. The successive movement of a 4 -phase, 8/6 SRM is shown in Fig. 3. The synchronization of the stator phase excitation is readily accomplished with rotor position feedback.

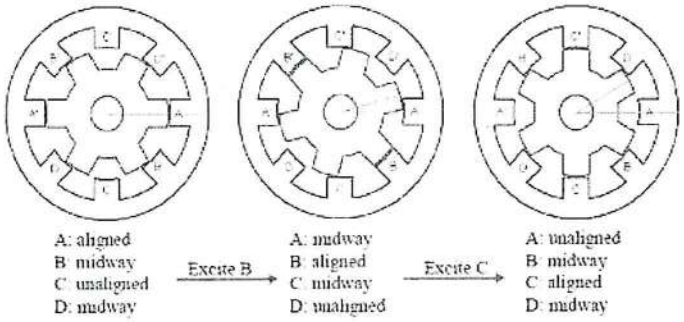

Fig. 3: Construction of 8/6 SRM

In the fully-aligned position, the phase winding inductance is maximum and the reluctance of the magnetic circuit is minimum. Similarly in the non-aligned position, the inductance is minimum and the reluctance S is maximum. The motor torque is expressed as given in equation 1.

$$T = \frac{1}{2} i^2 \frac{dL}{d\vartheta} \quad (1)$$

Rotor has six poles, therefore, when rotor completes one revolution, inductance will pass through 6 maximum and 6 minimum values. The angle between the axes of two consecutive rotor poles is 60° and that of stator poles is 45°, hence, if variation of inductance for phase2 is plotted, it will have similar variation as of phase1, but displaced by 15°. Therefore waveforms of phase 3 and 4 will similarly be shifted with respect to phase1 waveforms by 30° and 45° respectively.

Torque ripple is characterized as the contrast between the most extreme and least quick torque communicated as a rate of the normal torque amid steady state operation. Scientifically, Percentage Torque ripple is communicated as given in condition (2).

$$\text{Torque Ripple}(\%) = \frac{T_{inst(max)} - T_{inst(min)}}{T_{avg}} \times 100 \quad (2)$$

Where T_{inst} is the instantaneous torque and T_{avg} is the average torque.

Direct Torque Control:

Based on field oriented control the direct torque control system works. Field Oriented Control (Vector Control) takes after space vector hypothesis to control magnetic field introduction and direct discretion sets up an interesting recurrence of inverter working given a particular dc link voltage and a particular stator flux level. The working guideline of DTC is to first recognize stator voltage vectors as indicated by the contrasts between the reference torque and the real estimations of stator flux linkage. The standards of DTC in the ac machine can be inferred by investigating the motor equations. The stator flux linkage vector can communicated as underneath condition (3).

$$\overrightarrow{\psi_s} = \int (\vec{v} - \vec{i}R) dt \quad (3)$$

Different techniques have been proposed in the past to minimize torque ripple. The proposed technique is Space vector modulation (SVM) based DTC of 4 phase 8/6 SRM by choosinganappropriate set of 8 space voltage vectors. The DTC of SRM drive is simulated for consistent torque burden to watch the steady state and transient execution of the drive. It is watched that the torque is kept up inside the set hysteresis band. This new arrangement of space vectors demonstrates a critical change in the torque execution of DTC based SRM contrasted with the present control technique.

On the basis of the errors calculation between the reference value and estimated values of torque and also flux, it is easy to directly control on the inverter states in order to decrease the torque and flux error within the

PRINCIPAL.
K. S. R INSTITUTE FOR
ENGINEERING AND TECHNOLOGY,
K. S. R. KALVI NAGAR,
TIRUCHENGODE-637 215,
NAMAKKAL Dt. TAMIL NADU.

prefixed band limits. The DTC scheme as initially proposed is very simple; in its basic configuration. It consists of pair of hysteresis comparator, torque and flux calculator, a lookup table, and voltage source inverter. The configuration is much simpler than FOC system due to the absence of frame transformer, pulse width modulator, and position encoder. The general block diagram of DTC is shown in Fig. 4. Two of the major issues which are normally addressed in DTC drives are the variation of switching frequency of the inverter used in the DTC drives with operating condition and the high torque ripple.

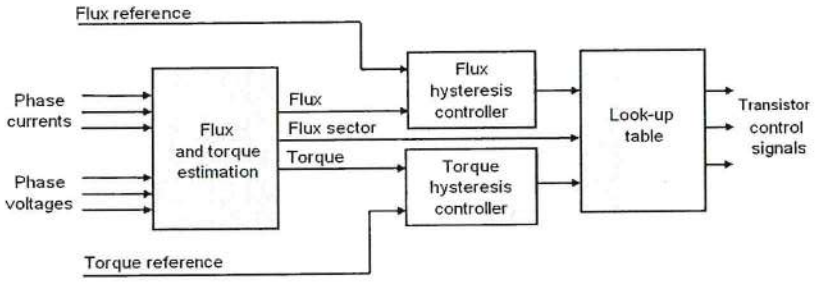

Fig. 4: Block Diagram of DTC

It is shown that the switching frequency is highly influenced by the motor speed. The motor DTC system comprises of three basic functions, namely: A motor model estimates the actual torque, stator flux and shaft speed by means of measurement of two motor phase currents, the immediate circuit DC voltage on the state of the power switched. Calculations are performed every 25 microseconds and these include corrections for temperature and saturation effects. The parameter of the motor model is estimated by an identification run, which made during commissioning. A two level hysteresis controller, where the torque and flux references are compared with the actual values calculated from the motor model. The magnitude of the stator flux is normally kept constant and the motor torque is controlled by means of the angle between the stator and rotor flux. Optimal switching logic that translates the controller output into the appropriate commands to the power switching devices. There are eight voltage vectors available in the two level voltage source inverter and the optimum switching logic determines the required selection every 25 microseconds.

Space Voltage Vector for SRM:

Like the AC drives, SRM likewise characterize the comparable space vectors. The voltage space vector for every phase is characterized on the center axis of the stator shaft in light of the fact that the flux linkage for a current and voltage connected to the motor phase will have phasor course in accordance with the center of the pole axis which does not require any physical change in winding topology. It is appeared in Fig. 5, every motor phase can have three conceivable voltage states for a unidirectional current. At the stage, when both switches in a motor phase are turned on. For this situation positive voltage is given to the motor phase. At the point when current begins streaming one device is turned off, along these lines a zero voltage circle happens and the state succession is given as 0. At long last, when both devices are turned off, there is no present or freewheeling current courses through the upper diodes. For this situation negative voltage is experienced by the motor phase and the state arrangement is characterized as negative voltage. Among the eight conceivable expresses any one is chosen at one time so as to keep the stator flux linkage and the motor torque inside hysteresis groups.

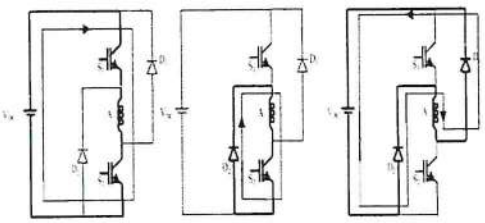

Fig. 5: SRM Phase Voltage States

As in the conventional DTC scheme, if the stator flux linkage lies in the k-th zone, the magnitude of the flux can be improved by the importance if switching vectors v(k+1) and v(k-1) and diminished by the presence of vectors v(k+2) and v(k+2). Hence whenever the stator flux linkage reaches its upper limit in the hysteresis band, it is reduced by applying voltage vectors which are directed toward the center of the flux vector space and vice-versa.

PRINCIPAL,
K. S. R. INSTITUTE FOR
ENGINEERING AND TECHNOLOGY,
K. S. R. KALVI NAGAR,
TIRUCHENGODE-637 215,
NAMAKKAL Dt. TAMIL NADU

The motoring torque is controlled by an acceleration or deceleration of the stator flux relative to the rotor movement. Hence, if an increase in torque is required, voltage vectors that advance the stator flux linkage in the direction of rotation are selected. This corresponds to selection of vector v(k+1) and v(k+2) for a stator flux linkage in the k-th zone. When the torque is to be decrease, voltage vectors are applied which decelerate the stator flux linkage vector. This corresponds to the vectors v(k-1) and v(k-2) in the zone k. Switching table for controlling the stator flux linkage and motor torque can be defined as shown in Table 1.

Table 1: Switching Table for DTC

Torque	INCREASE	INCREASE	DECREASE	DECREASE
Flux	INCREASE	DECREASE	INCREASE	DECREASE
Selection of Vector	v(k+1)	v(k-1)	v(k+2)	v(k-2)

In order to control the flux and torque within the hysteresis bands, the instantaneous torque and stator flux vector magnitude must be known. In the SR motor voltages in the motor are highly non-sinusoidal and thus more effective insight may be gained by firstly finding the individual flux linkages of each phase using the voltage.

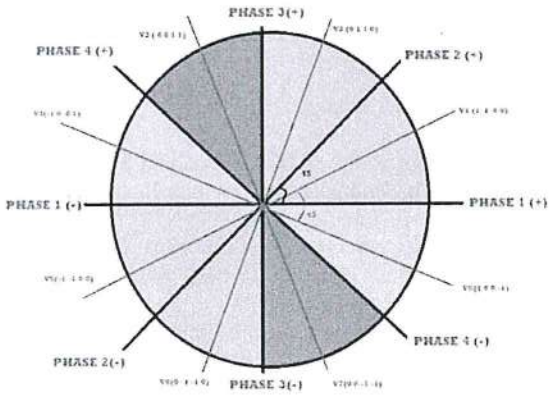

Fig. 6: Space Voltage Vector for SRM

In this case the magnitude of the individual phase flux linkages varies with time, but the direction is always along the stator pole axis. Torque look up table estimated previous and stored processor for adjustable Dwell angle. Space voltage vector representation for 8/6 switched reluctance motor is shown in Fig. 6. Pseudo codes for different voltage states were depict in Table 2.

Table 2: Pseudo Code for Voltage States

Voltage vectors	Voltage states for four phase				Voltage Vector	Voltage state for four phase			
	A	B	C	D		A	B	C	D
V1	1	1	0	0	V5	-1	-1	0	0
V2	0	1	1	0	V6	0	-1	-1	0
V3	0	0	1	1	V7	0	0	-1	-1
V4	-1	0	0	1	V8	1	0	0	-1

Control switching table is used to select the voltage command based on the present zone of the flux linkage that can be determined by the angle. For the first time, considering 4phase motor, vector number is four and so combination of vector is zero with appear on rectangular plane. In real system arbitrary phase will be excited first to detect the initial rotor position. Rotor position move to arbitrary aligned position. Therefore we solve this problem with initial value of 45 degree on 4 phase. The orthogonal flux vector are expressed as

$$\psi_\alpha = \psi_1 - \psi_2 \cos 60° - \psi_3 \cos 60° \quad (4)$$

$$\psi_\beta = \psi_2 \sin 60° - \psi_3 \sin 60° \quad (5)$$

The magnitude of $\vec{\psi}$ and angle δ of the equivalent flux vector is defined as

$$\psi_s = \sqrt{{\psi_\alpha}^2 + {\psi_\beta}^2} \quad (6)$$

$$\delta = \arctan\left(\frac{\psi_\beta}{\psi_\alpha}\right) \quad (7)$$

Proposed Evolutionary Computing Technique:

PRINCIPAL.
K. S. R. INSTITUTE FOR
ENGINEERING AND TECHNOLOGY,
K. S. R. KALVI NAGAR,
TIRUCHENGODE-637 215,
NAMAKKAL Dt. TAMIL NADU.

The GA has discovered application in the region of the programmed tuning process for traditional and intelligent controllers. Same exploration has been directed utilizing genetic algorithms to help on-line or logged off control frameworks. It has basically been used as a logged off procedure for performing a guided quest for the ideal answer for an issue. In this paper, the GA is utilized logged off controller execution to adaptively seek through a populace of controllers and decide the part most fit to be implemented over a given sampling period.

Here in Genetic PI controller tuning, each chromosome has a genes producing as possible proportional and integral gain values. The implementation of GA-PI control technique for Four-Phase 8/6 SRM to reduce the torque ripple and to obtain quick torque response. The block diagram of the proposed project is shown in Fig. 7.

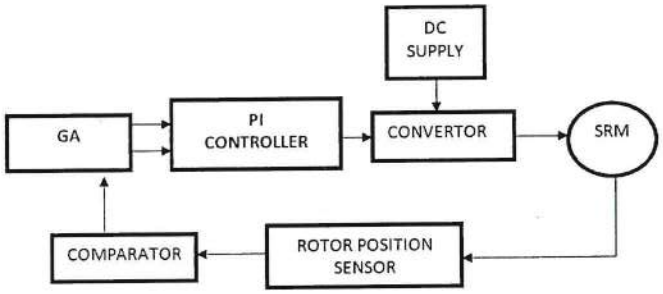

Fig. 7: Block Diagram of Proposed Scheme

In this proposed model, feedback signals are the position θ and the phase currents $i_{a,b,c,d}$ the position signal is used to calculate the torque. The PI controller with signal generator is used to control turn-on angle θ_{on}, turn-off angle θ_{off}, and pulse width modulation duty cycle.

The steps for torque control are summarized as follows:

1 The current and rotor position signal of the SRM are Sampled.

2 Current error due to change are calculated.

3 Select the number of digits to represent each controller parameter Kp and Ki, choose crossover probability (pc) and mutation probability (pm).

4 Assume an initial population of Kp and Ki gains (we make a random selection) sample time T and set time t.

5 ProduceKp and Ki gain values for the error value and it determine the proper turn on and turn off angle to the converter.

6 The motor torque ripples is reduced effectively by proper selection of Kpgain values, Ki gain values, turn on and turn off angles.

These are the several steps that involve in our proposed project to minimize the torque ripple using genetic algorithm principles.

Simulation Model:

To simulate the system a Matlab/Simulink closed loop model based upon evolutionary computing of DTC of 8/6 SRM was constructed as in Fig. 8. The motor parameter such as torque, phase flux and position are obtained from 4φ SRM. The four phase flux vector is transformed on to a stationary orthogonal $\alpha - \beta$ reference frame to calculate the net flux. The multiphase drives divide the controlled power on more inverter legs. The increased phase number reduces the current stress on each switch.

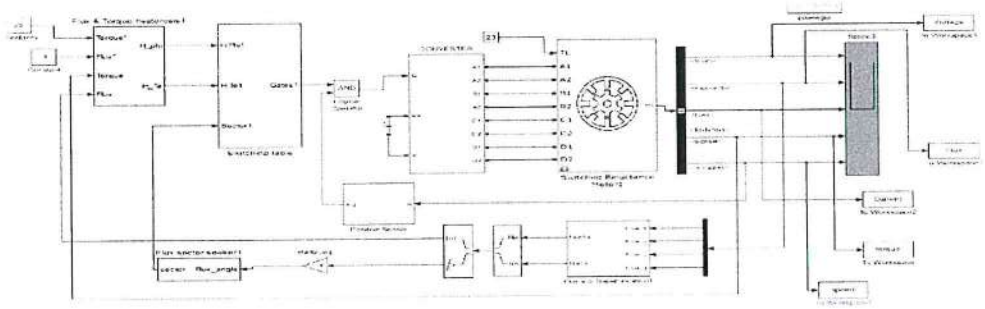

Fig. 8: Simulink Modeling of Proposed Scheme

PRINCIPAL,
K. S. R. INSTITUTE FOR
ENGINEERING AND TECHNOLOGY,
K. S. R. KALVI NAGAR,
TIRUCHENGODE-637 215,
NAMAKKAL Dt. TAMIL NADU.

The converter topologies selected for giving input to the Switched Reluctance motor is asymmetrical converter. This torque ripple is a particular characteristic of the SRM and it depends mainly on the converter s turn-on and turn-off angles. The SRM torque characteristic can be optimized by applying appropriated pre-calculated turn-on and turn-off angles in function of the motor current and speed.

RESULTS AND DISCUSSION

For the purpose of analysis, a comparative work is done between conventional technique and evolutionary computing based DTC of 8/6 SRM and percentage of torque ripple is compared. A DC supply voltage of 120 V is used for the converter configuration. The torque gets controlled when comparing with previous conventional technique. The simulation result of proposed space vector modulation based direct torque control of Switched Reluctance Motor is shown in Fig. 9. And its maximized view is shown in Fig. 10.The FFT analysis on conventional system and proposed schemes were shown in Fig. 11. & Fig.12. The results were obtained from the model developed from four phase 8/6 switched reluctance motor implementing direct torque control based upon space vector modulation technique and Genetic Algorithm were implemented for tuning of PI controller to minimize the torque error. The torque ripple is reduced much reduced than conventional technique. Hence space vector modulation implemented in DTC holds good control over torque response.

The simulation results show that the designed PI controller performs satisfactorily to track the reference torque with actual torque. It is also observed that the designed PI controller completely eliminates ripples at high speeds. The designed PI controller is tuned through genetic algorithm which is done through effective selection of global best and local best done through random selection. The simulation result made the quicker convergence of PI controller by effective genetic tuning of K_p and K_i values than conventional system. The comparison Table 3. for the proposed design of Direct Torque Control with Genetic PI Controller with other controller is made on discussing the torque ripple parameter on closed loop design.

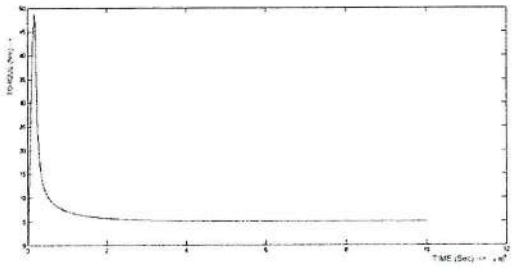

Fig. 9: Simulation Result of Proposed System for 5 Nm.

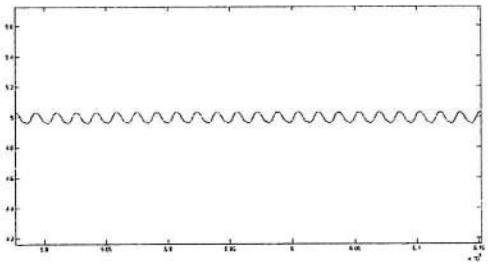

Fig. 10: Magnified view of Simulation for 5 Nm.

PRINCIPAL.
K. S. R. INSTITUTE FOR
ENGINEERING AND TECHNOLOGY,
K. S. R. KALVI NAGAR,
TIRUCHENGODE-637 215,
NAMAKKAL Dt. TAMIL NADU.

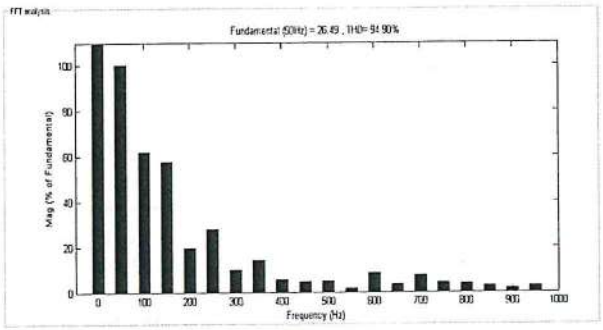

Fig. 11: FFT Analysis for Conventional System

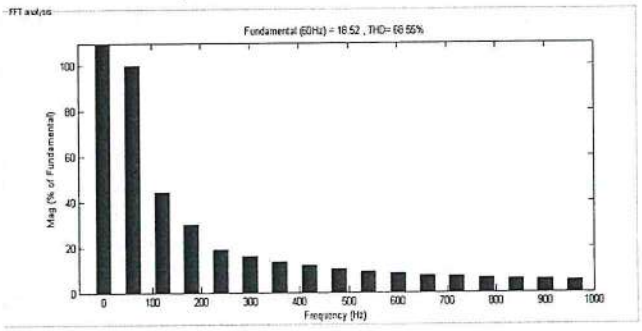

Fig. 12: FFT Analysis for Proposed Scheme

Table 3: Comparison Table of Torque Ripple for Different Controller

CONTROLLER	TORQUE RIPPLE (Nm)	TORQUE RIPPLE (%)
Conventional Controller	0.42 Nm	21 %
Genetic PI Controller	0.22 Nm	11 %
Direct Torque control with PI controller	0.172 Nm	8.8 %
Direct Torque Control With Genetic PI Controller	0.138 Nm	6.9 %

Conclusion:

Direct Torque Control (DTC) for 8/6 SRM drive based upon evolutionary computing is made through comparing the actual torque with reference torque and generating error and then error is tuned by genetic based PI-controller. DTC is implemented through space vector modulation thus by effective switching of nine voltage vector to the convertor at appropriate switching time and angle for smooth operation of motor. The quicker convergence of PI controller is made through evolutionary computing. The results obtained from the Matlab/Simulink model validate the proposed scheme by reducing the ripple than conventional controller. The GA-PI Controller technique produce the quick torque response and reduced torque ripple than the individual controllers such as PI, Neural, and Fuzzy logic controllers. By applying this technique the torque is maintained at 23.5 Nm and the ripple is reduced to 11% where as in the conventional methods the torque is about 22%. Hence by using this GA-PI controller the torque ripple is minimized effectively.

REFERENCES

1. Taylor, D.G., 1991. "Adaptive control design for a class of doubly-salient motors," In Proc. 30th IEEE Conf. Dec. Contr., 3: 2903-2908, http://dx.doi.org/10.1109/cdc.1991.261069
2. Nagel,N.J. and R.D. Lorenz, 1999. "Complex rotating vector method for smooth torque control of a saturated switched reluctance motor," in Proc. 34th Annual Meeting IEEE Ind. Application., 4: 2591-2598 http://dx.doi.org/10.1109/ias.1999.799204
3. Ilic-Spong, M., R. Marino, S.M. Peresada and D.G. Taylor, 1987. "Feedback linearizing control of switched reluctance motors," IEEE Trans. Automat. Contr., AC-32: 371-379. http://dx.doi.org/10.1109/TAC.1987.1104616
4. Stankovic, M., G. Tadmor, Z.J. Coric and I. Agirman, 1999. "On torque ripple reduction in current-fed switched eluctance motors," IEEE Trans.Ind. Electron., 46: 177-183.http://dx.doi.org/10.1109/41.744409
5. Jinupun,P. and P. Chi-KwongLuk, 1998. "Direct torque control for sensorless switched reluctance motor drives," Power Electronics and Variable Speed Drives, Seventh International Conference on (456): 329-334. http://dx.doi.org/10.1049/cp:19980546

PRINCIPAL.
K. S. R. INSTITUTE FOR
ENGINEERING AND TECHNOLOGY,
K. S. R. KALVI NAGAR,
TIRUCHENGODE-637 215,
NAMAKKAL DT. TAMIL NADU.

Middle-East Journal of Scientific Research 24 (12): 3667-3677, 2016
ISSN 1990-9233
© IDOSI Publications, 2016
DOI: 10.5829/idosi.mejsr.2016.3667.3677

Performance Analysis and Speed Regulation Estimation of SR Motor Using FT-ANN Controller with Steady State Stability and Fft Analysis

[1]Murugesan Arumugam and [2]Jeyabharath Rajaiah

[1]Research Scholar, Anna University/Assistant Professor/EEE,
KSR Institute for Engineering and Technology, Tamilnadu, India
[2]Professor, Department of EEE, KSR Institute for Engineering and Technology, Tamilnadu, India

Abstract: A closed loop speed regulation estimation of Switched Reluctance (SR) Motor with Fuzzy Tuned Artificial Neural Network (FT-ANN) Controller has been simulated and presented in this paper. The FT-ANN has been used for the closed loop controller and the speed regulation of the SR motor has been estimated with Fuzzy Logic Controller (FLC) and FT_ANN. The comparative results are presents for both static and dynamic conditions. The mathematical model of the SR motor has been developed for steady state stability analysis and simulated using MATLAB. The Harmonic Spectrum (FFT) and steady state error for various speed and load condition have been obtained to validate the role of FT-ANN controller. The FT-ANN based system is expected to give better speed regulation for various load conditions. A prototype 300-W, 50Hz model is designed and built for experimental demonstrations; the transient and steady-state performances for the SR motor are compared from the simulation studies. The result of MATLAB simulation and execution it is clear that the FT-ANN can have better controller compared with Fuzzy Logic Controller (FLC).

Key words: Switched Reluctance Motor · Artificial Neural Network · Fuzzy Logic Controller · Stability analysis · PWM Inverter

INTRODUCTION

The design and developed of SR motor have been focused for variable speed applications with high power density in the recent past. It has been found that these types of special motor have several advantages such as simplicity, less maintenance, robustness, higher torque volume ratio, high starting torque, high efficiency, low manufacturing cost and high speed. The SR motor is highly nonlinear and it operates to steady state region to maximum torque region. This type of special motor having a torque is nonlinear function of rotor position and current. The many researchers has been experimentally demonstrated and reported related to SR motor to solve above problems using different controllers.

Hany M *et al.* [1] have developed the torque ripple minimization of the SR motor with digital controller. The model of SR motor has been presented with torque equation. There is no analysis of the performance of the motor. The speed control of the switched reluctance generator with artificial neural network controller has been presented in. The performance of the generator has been analyzed with variable speed turbine connected in grid. Kioskeridis *et al.* [2] have demonstrated the single pulse controlled SR motor with high efficiency. This control technique is more complicate compare to FT-ANN controller. The dynamic and steady state performance of the motor was not presented.

Yana Zhou *et al.* [3] have developed the torque ripple minimization of the SR motor with sensor less controller using neural network. The neural network structural design was not present. The speed variation with load changes was not present. The speed controller of the SR motor has been developed and presented with adaptive neural network controller in. The dynamic behavior of the motor has been presented. The load disturbance of the motor has been presented with controller performance. Here there is no analysis of the steady state and stability of the motor. Any M *et al.* [4] have demonstrated the speed control of SR motor with adaptive neuro-fuzzy

Corresponding Author: Murugesan Arumugam, Research Scholar, Anna University/Assistant Professor/ EEE, KSR Institute for Engineering and Technology, Tamilnadu, India.

PRINCIPAL.
K. S. R. INSTITUTE FOR
ENGINEERING AND TECHNOLOGY,
K. S. R. KALVI NAGAR,
TIRUCHENGODE-637 215,
NAMAKKAL Dt. TAMIL NADU.

controller. The performance of the controller has been described. The analysis of the controller design and dynamic performance of the motor were not present. The stability analysis of the SR motor with fuzzy sliding mode controller was presented in.The speed regulation and load disturbance of the motor performance were not present. The different type of power converter fed SR motor is presented with pulse with modulation technique. The performance of the converter was found for better speed regulation.

P.Kavitha *et al.* [5] have demonstrated the R dumped converter fed SR motor with fuzzy controller. The experimental result of the SR motor was not present. The design procedure of the motor and converter was not present. The performance of the motor speed regulation was present. Gamal M. Hashem *et al.* [6] have described the fuzzy controller for SR motor. The speed regulation of the motor has been presented. The dynamic and transient performance of the motor was not present. M. A. A. Morsy *et al.* [7] have described the speed regulation of the SR motor with fuzzy sliding mode controller. The variable structural control has been developed and presented with comparison of fuzzy sliding mode controller. The static and dynamic analysis of the SR motor was not present.

It is concluded from the literatures that the speed regulation against load and supply voltage fluctuation have important role in the design of high speed drives. The FT-ANN controller is expected to have the speed regulation, high efficiency and better performance in the time of load disturbance. Considering the above facts in view, the FT-ANN controller based SR motor has been designed and the performance is analyzed for estimating various responses. The state space analysis is used for the stability analysis of the motor. The state space equation has been derived from motor model and simulated using MATLAN/Simulink. The FFT analysis of the motor has been present.

Proposed FT-ANN Controller based SR Motor with State Space Analysis: The block diagram of the FT-ANN controller based switch reluctance motor is shown in fig.1. The first stage three phase AC voltages are converting in to DC voltage V_{dc} by using rectifier circuit. The Second stage the inverter is converts in to three phase ac voltage i_a, i_b, i_c.. The motor speed measured by sensor and the signal is given to the error detector unit. A tacho generator (pulse type) is used for sensing the speed. This sensing speed is considered for feedback of the controller. Error detector is used to compare the reference speed and actual speed. The difference error speed is calculated and to generate the error signal which is given to controller block. The Fuzzy tuned Artificial Neural Network Controller gives control signal to the inverter according to the error signal. The speed of the motor is controlled by the inverter through proper excitation of their corresponding windings [8-10].

The FT-ANN controller has been used as two feedback loops. One is outer speed control loop and second one is inner current control loop. The current control loop is used to control the PWM pluses whenever the motor current reached to the maximum value. The speed control loop, the actual speed N is sensed by tacho generator and given to the error detector, the set speed N_{ref} also given to the error detector and the error signal e is obtained by comparing the set speed N_{ref} with the actual speed N. The (Δe) change in error is procured from the (e) present error and pervious error ($e_{previous}$). The (e) error and (Δe) change in error are set as inputs to the FT-ANN controller.

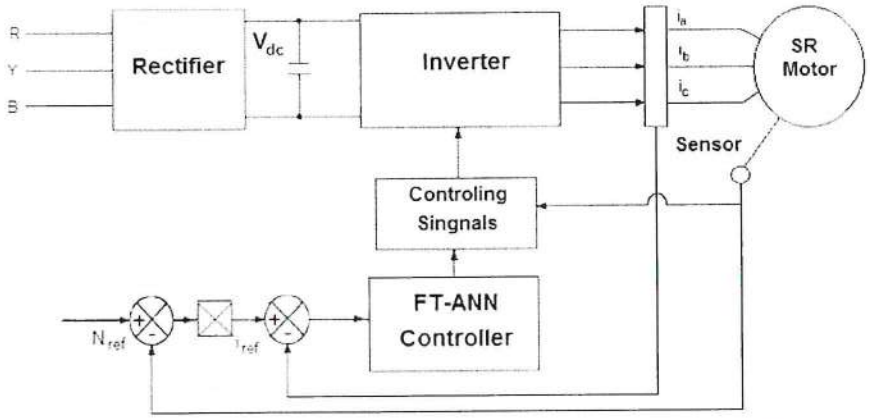

Fig. 1: Block Diagram of the FT-ANN controller based SR motor

PRINCIPAL.
K. S. R. INSTITUTE FOR
ENGINEERING AND TECHNOLOGY,
K. S. R. KALVI NAGAR,
TIRUCHENGODE-637 215,
NAMAKKAL Dt. TAMIL NADU.

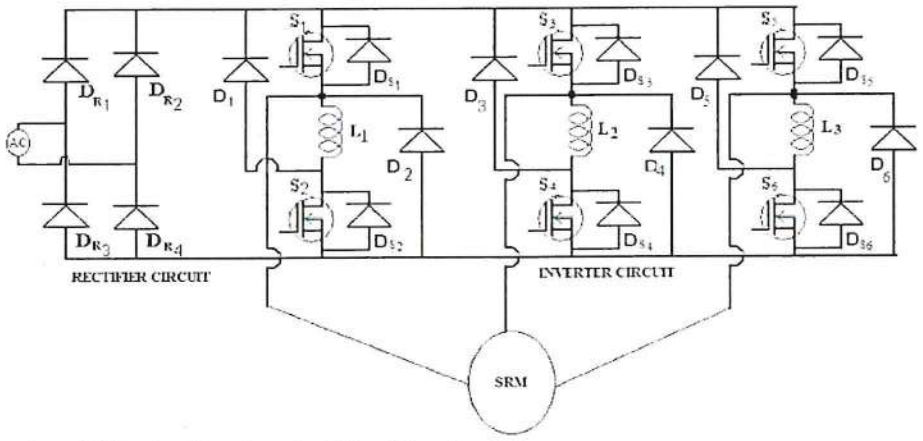

Fig. 2: Structure of Classical Inverter circuit for SR motor

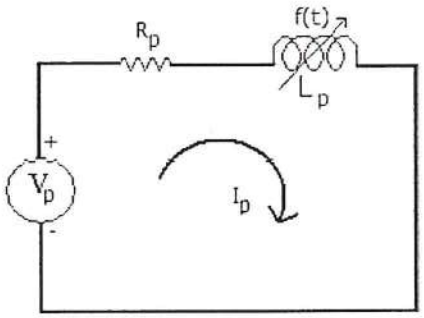

Fig. 3: Equivalent circuit of Single phase SR motor

The output of the controller is PWM Signal. The change in PWM Signal ΔP is given to the inverter and the controller is calculated from the new PWM Signal P(k) and previous PWM Signal p(k-1). The input and output gain of the controller can be estimated by simulation. To obtain the error value is zero by changing the pulse signal which is given to the inverter [11]. The schematic diagram of the proposed system is shown in fig.2.

Mathematical Modeling of the SR motor with Sate Space Analysis: The SR motor is a highly non-linear system, the non-linear system describing the behavior of the motor is developed. A mathematical model can be created based on this construction. The SR motor electromagnetic circuit is characterized by non-linear magnetization. The torque generated by the motor phase is a function of the magnetic flux; therefore, the phase torque is not constant for a constant phase current for different motor positions. This creates torque ripple and noise in the SR motor. The model is based on the electrical diagram of the motor, incorporating phase resistance and phase inductance. The diagram for one phase is shown in fig.3 [11-17].

The applied voltage to a phase is equal to the sum of the resistive voltage drop and the rate of the flux linkages and is given as:

$$V_p(t) = R_p I_p(t) - V_{Lp}(t) \tag{1}$$

$$V_{Lp}(t) = \frac{d\sigma(I_p,\theta_p)}{dt} \tag{2}$$

$$= \frac{d\sigma(I_p,\theta_p)}{dI_p}.\frac{di_p}{dt} + \frac{d\sigma(I_p,\theta_p)}{d\theta_p}.\frac{d\theta_p}{dt} \tag{3}$$

The phase voltage can be expressed as

$$V_p(t) = R_p.I_p(t) + \frac{d\sigma(I_p,\theta_p)}{dI_p}.\frac{di_p}{dt} + \frac{d\sigma(I_p,\theta_p)}{d\theta_p}.N \tag{4}$$

Where N is the speed of the motor

For 3 phase SR motors Equ.3 can be expanded as follows

$$V_R(t) = R_R.I_R(t) + \frac{d\sigma(I_R,\theta_R)}{dI_R}.\frac{di_R}{dt} + \frac{d\sigma(I_R,\theta_R)}{d\theta_R}.N \tag{5}$$

$$V_Y(t) = R_Y.I_Y(t) + \frac{d\sigma(I_Y,\theta_Y)}{dI_Y}.\frac{di_Y}{dt} + \frac{d\sigma(I_Y,\theta_Y)}{d\theta_Y}.N \tag{6}$$

$$V_B(t) = R_B.I_B(t) + \frac{d\sigma(I_B,\theta_B)}{dI_B}.\frac{di_B}{dt} + \frac{d\sigma(I_B,\theta_B)}{d\theta_B}.N \tag{7}$$

The torque generated by one phase can be expressed as

$$T_p = \int_0^I \frac{d\sigma(I_p,\theta_p)}{d\theta_p} dI_p \tag{8}$$

PRINCIPAL,
K. S. R. INSTITUTE FOR
ENGINEERING AND TECHNOLOGY,
K. S. R. KALVI NAGAR,
TIRUCHENGODE-637 215,
NAMAKKAL DT. TAMIL NADU.

The mathematical model of an SR motor is represented by a system of equations, describing the conversion of electromechanical energy. Power associated with change in stored energy is $\frac{dW'}{dt}$

$$\frac{dW'}{dt} = \frac{1}{2} L_p(2i)\frac{di}{dt} + \frac{1}{2} I^2 \frac{dL_p}{dt} \tag{9}$$

This equation can be written as

$$= L_p i \frac{di}{dt} + \frac{1}{2} I^2 \omega \frac{dL_p}{d\theta}$$

Where $\omega = \frac{d\theta}{dt}$

The motor Power can be converted into mechanical P_m the developed power equation is

$$P_m = \frac{1}{2} I^2 \omega \frac{dL_p}{d\theta} \tag{10}$$

The SR motor Torque developed equation as

$$\dot{T} = \frac{P_m}{\omega} = \frac{\frac{1}{2} I^2 \omega \frac{dL_p}{d\theta}}{\omega}$$

$$T = \frac{1}{2} I^2 \frac{dL_p}{d\theta} \text{N-m} \tag{11}$$

The SR motor system model using state space technique can be obtained assuming there is no magnetic saturation, losses and mutual inductance. By using the above basic torque and power equation the vector space equation for the motor can be developed and is given by [11].

$$\frac{di}{dt} = -L^{-1}(\theta) K_i \omega + L^{-1}(\theta) V_p \tag{12}$$

$$\frac{d\omega}{dt} = \frac{T}{J} - \frac{T_L}{J} - \frac{B}{J}\omega \tag{13}$$

$$\omega = \frac{d\theta}{dt} \tag{14}$$

The SR motor reference speed (ω^*) and actual speed (ω) taken as a state variables, the state space equation of the motor as

$$x_1 = \omega = \omega^* \tag{15}$$

$$x_2 = \dot{\omega} = -\frac{B}{J}\omega + \frac{T}{J} - \frac{T_L}{J} \tag{16}$$

By taking the inverse Laplace transform from the equation (15 and 16) we get the state space equation of the SR motor is

$$\begin{pmatrix} \dot{x}_1 \\ \dot{x}_2 \end{pmatrix} = \begin{pmatrix} 0 & 1 \\ 0 & -\frac{B}{J} \end{pmatrix} \begin{pmatrix} x_1 \\ x_2 \end{pmatrix} + \begin{pmatrix} 0 \\ \frac{1}{J} \end{pmatrix} \dot{T} \tag{17}$$

Output Equation is

$$y = \begin{pmatrix} 0 & \dot{\omega}^* \\ 0 & \frac{T_L}{J} \end{pmatrix} \begin{pmatrix} x_1 \\ x_2 \end{pmatrix} \tag{18}$$

These state equations can be used to analysis the stability of the system furthermore the equation can be used to estimate the value of parasitic elements.

RESULTS AND DISCUSSIONS

Design of Fuzzy Logic Controller: The Fuzzy Logic Controller (FLC) provides an adaptive control for improved system performance [13]. FLC is intended to give solution for controlling the non-linear processes and to handle ambiguous and uncertain situations. The performance of the Controller is developed with MATLAB/Simulink in terms of speed and load variation. The FLC have three stages namely Fuzzification, Rule-Base and Defuzzification. The fuzzy control is developed using input membership functions for error 'e' and change in error 'Δe' and the output membership function for 'Δu' the duty ratio of inverter. The output of the fuzzy control algorithm is the change in PWM Signal [δd(α)]. The PWM Signald (α), at the α^{th} sampling time, is determined by adding the previous PWM Signal [d (α -1)] to the calculated change in PWM Signal:

d (α) =d (α -1) +δd (α)

The fuzzy rule variables error 'e', change in eror 'Δe' and output 'Δu' are described by triangular membership functions. The graphical diagram of triangular membership function is shown in fig.4. Seven triangular membership functions are taken for creating the rules. Table 1 present the fuzzy rules. Fuzzy memberships NB, NM,NS, Z, PS, PM,PB are defined as negative big, negative medium, negative small, zero, positive small, positive medium and positive big.

PRINCIPAL,
K. S. R. INSTITUTE FOR
ENGINEERING AND TECHNOLOGY,
K. S. R. KALVI NAGAR,
TIRUCHENGODE-637 215,
NAMAKKAL Dt. TAMIL NADU.

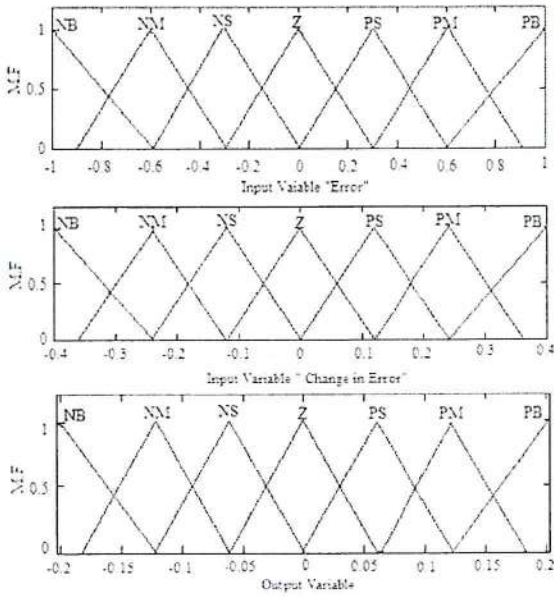

Fig. 4: Fuzzy Membership Function

Table 1: Fuzzy Rules

	NB	NM	NS	Z	PS	PM	PB
NB	NB	NB	NB	NB	NS	PS	Z
NM	NB	NM	NM	NS	NS	Z	NS
NS	NB	NM	NB	NS	Z	NS	PS
Z	NB	NS	NS	Z	PS	NM	PB
PS	NS	NS	Z	PS	PB	NM	PB
PM	NS	Z	PS	PB	PB	NM	PB
PB	Z NS	PS	PB	PB	PB	PB	

Design of Fuzzy Tuned Artificial Neural Network (FT-ANN) Controller: The FT- ANN based control of SR motor is described in reference [9, 12]. Before analyses the results are not attain the prescribed solution, it's desired to be improved further. The performance of SR motor to be improved using the Fuzzy Tuned Artificial Neural Network based controller (FT-ANN). The FLC data is used to design the Artificial Neural Network algorithm (ANN). The proposed controller is working properly due to its well trained algorithm and also it minimize the computational time. The FT-ANN is designed with a small number of neurons and single hidden layer. The feed forward neural network is developed with double neurons in the input layer, thrice in the hidden layer and single in the output layer. The two inputs are taken as error e (α) and change in error Δe(α), these inputs are developed and biased properly. From the FLC the network is designed and trained with the set of inputs and desired outputs.

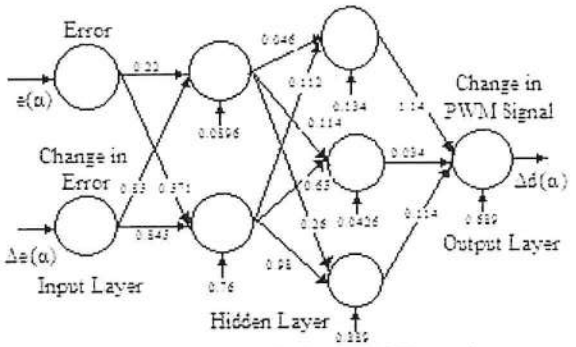

Fig. 5: Configuration of trained Neural Network

A feed forward back propagation neural network-training algorithm is used and it is trained with minimum error. The output of the network is change in PWM Signal Δd(α). The FT-ANN is designed and trained with the error goal value of 0.00596325 at 11 epochs. The complete configuration of the trained network with the weights and bias is shown in figure 5.

The proposed FT-ANN system is simulated using MATLAB software. The simulink model of SR motor is developed with FT-ANN as given in figure 6. The set reference speed and motor actual speed is taken as input. The error and change in error are calculated and then given as input to the FT-ANN. The output of the PWM pulse signal is given as input to the PWM generator of the inverter.

The 100Hz of switching frequency is produced from the PWM unit. Then the current controller receives the pulse signal from the PWM unit. The reference current is equal to the motor current then the current controller permit the PWM signal. The PWM pulse signal is given to the main inverter circuit then the change output voltage changes from variable voltage to fixed voltage. Then the speed of the motor runs with the reference speed. The FT-ANN controller model is shown in fig.7.

Simulation Results of the Proposed System: The simulation of the proposed system is carried out using MATLAB/Simulink software. The FT-ANN controller is used as a closed loop for the SR motor performance estimation. The speed control of the motor has been carried out using fuzzy logic controller and fuzzy tuned artificial neural network controller. The variation of the speed is shown in below fig.8 the expended view also presented. The output of the speed flow the reference with better accuracy, showing a better tracking performance of the controller. Its shows that the FT-ANN controller is settling time and percentage overshoot is very less compare to other controller.

PRINCIPAL,
K. S. R. INSTITUTE FOR
ENGINEERING AND TECHNOLOGY,
K. S. R. KALVI NAGAR,
TIRUCHENGODE-637 215,
NAMAKKAL Dt. TAMIL NADU.

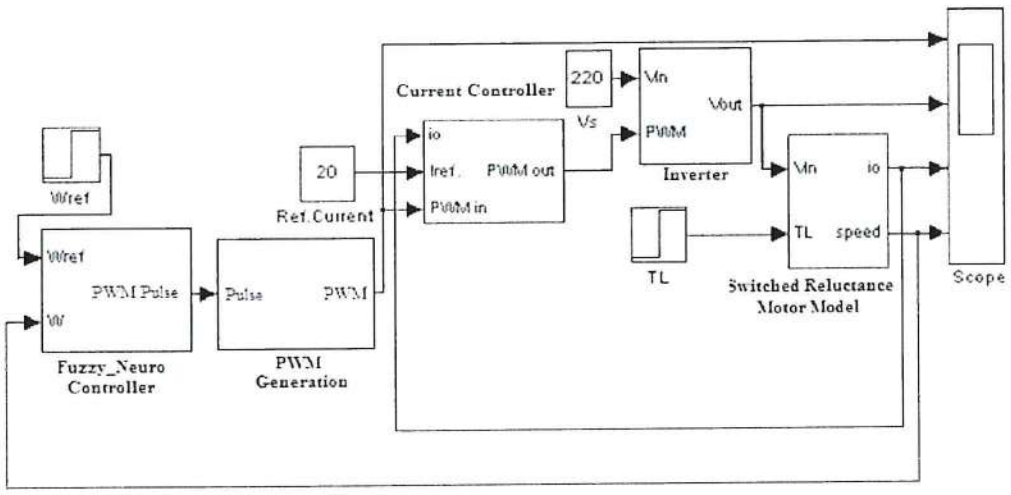

Fig. 6: MATLAB/Simulink Model of the proposed system

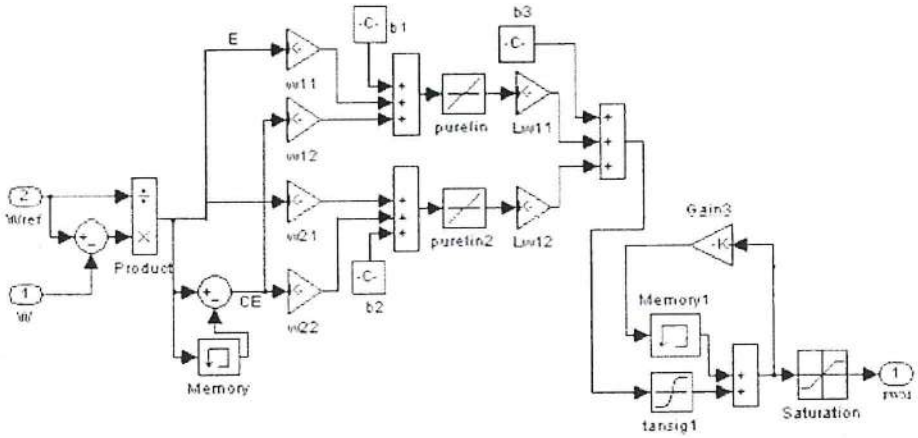

Fig. 7: Simulink Model of FT-ANN Controller

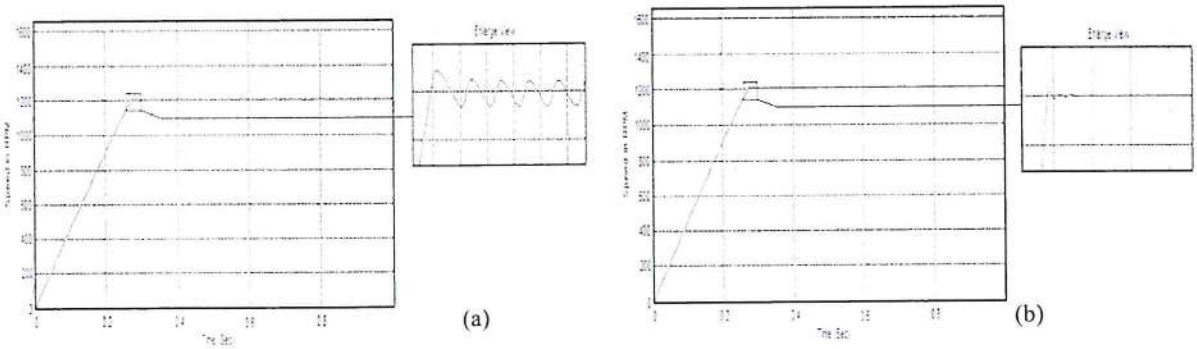

Fig. 8: SR motor Speed (a) using FLC (b) using FT-ANN controller

The maximum overshoot and percentage error is very small and it tends to zero as shown in fig.8 (b) the rise time and settling is near to 0.01 sec its very less compare to FLC. The expended view diagram shows that the steady state error is near equal to 0.001sec. It is clear that the FT-ANN controller eliminating the rise time, overshoot and suppers the harmonics.

PRINCIPAL,
K. S. R. INSTITUTE FOR
ENGINEERING AND TECHNOLOGY,
K. S. R. KALVI NAGAR,
TIRUCHENGODE-637 215,
NAMAKKAL Dt. TAMIL NADU.

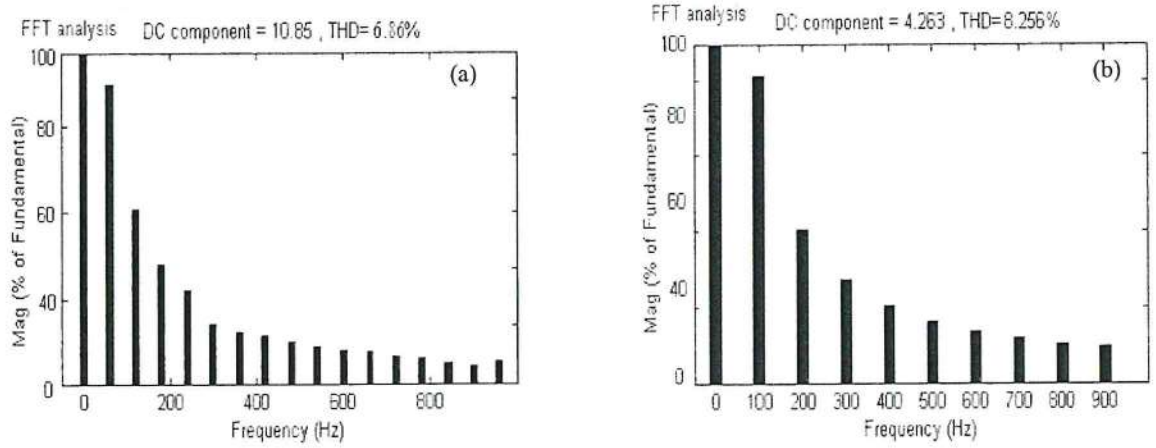

Fig. 9: FFT analysis (a) FT-ANN (b) FLC

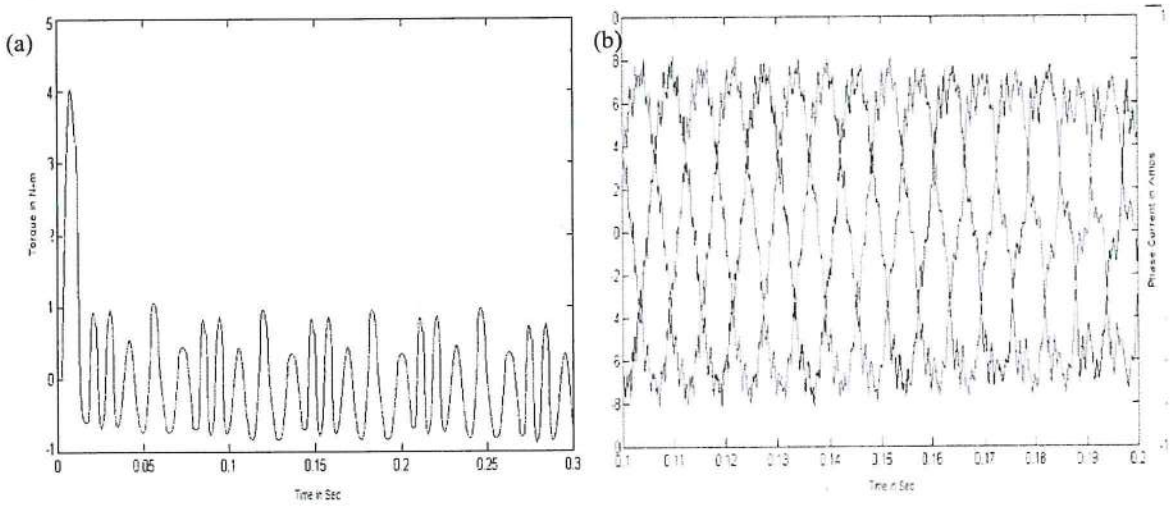

Fig. 10: (a) Torque Response (b) Phase current

Table 2: Comparative analysis of transient and steady state performance for different controllers

Controller	% Overshoot	Rise time in Sec	Steady state error	Settling Time in Sec.	THD in %
FLC	0.36	0.85	0.04	1	8.25
FT-ANN	nil	0.52	0.001	0.68	6.8

The FFT analysis of the SR motor for the output voltage as shown fig.9. The Total Harmonics distraction (THD) is calculated from the inverter side. It's found from the above FFT analysis clearly shows that the controller tracking performance is good and THD values are less compared to fuzzy controller. The developed torque performance of the SR motor as shown in fig.10 (a) and the phase current of the motor are present in fig.10(b)

The performance of the controller response for SR motor speed control has been estimated and provided in table.2. It is seen that the FLC/FT-ANN closed loop controllers give the better settling time. This ensures that the controller provide the effective feedback. It is concluded from the above table 2 the FT-ANN controller has improved the transient and dynamic performance of the SR motor. The harmonics spectrum analysis of the motor speed can be estimated and provided in table.2.

In further to analysis the performance of the SR motor controller the simulation is carried out different set speed changes it is shown in fig.11 and 12 respectively. The set speed changes from 500 rpm to 1000 rpm and 1000 rpm to 1600 rpm. The fuzzy controller shows a comparatively

PRINCIPAL.
K. S. R. INSTITUTE FOR
ENGINEERING AND TECHNOLOGY,
K. S. R. KALVI NAGAR,
TIRUCHENGODE-637 215,
NAMAKKAL Dt. TAMIL NADU.

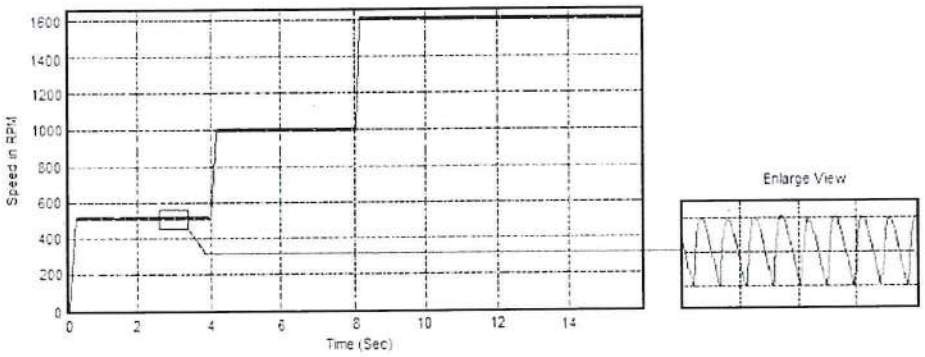

Fig. 11: Speed control from 500 RPM to 1000 RPM, 1000 RPM to 1600 RPM at 4 sec and 8sec respectively (using FLC)

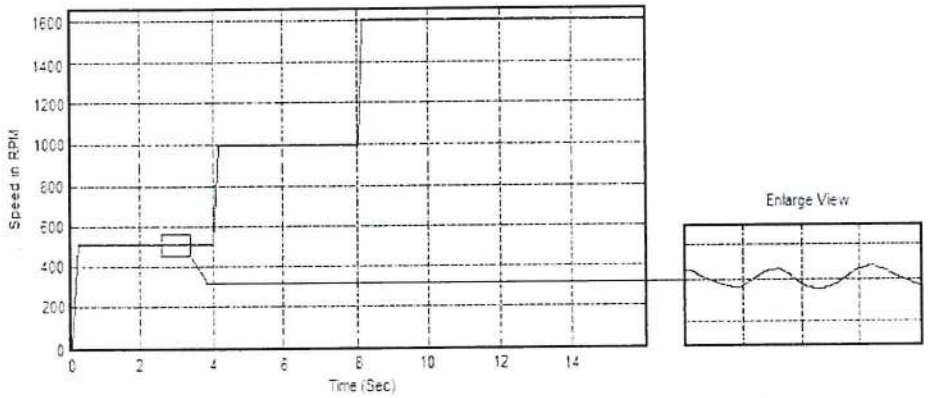

Fig. 12: Speed control from 500 RPM to 1000 RPM,1000 RPM to 1600 RPM at 4 Sec and 8sec respectively

Table 3: Transient response of the controllers in with reference speed changes

	Change in speed from 0 to 500 RPM		Change in speed from 500 to 1000 RPM		Change in speed from 1000 to 1600 RPM	
Controllers	% over Shoot	Settling time in Sec.	% over Shoot	Settling time in Sec.	% over Shoot	Settling time in Sec.
FLC	0.2	0.35	0.29	0.295	0.3	0.39
FT-ANN	0.001	0.15	0.001	0.18	0.001	0.19

maximum percentage overshoot and more time to settle, there is no steady-state error as shown in fig.11. It's clearly found that the FT-ANN controller gives the least amount of overshoot and zero steady state error and the rise time and settling time is near to 0.001 as shown in fig.12.

From the above figure we found that the transient and dynamic performance is more in fuzzy logic controller due to more oscillation and its very minimum in FT-ANN controller. While the motor is running to the rated speed the variation is very minimum at both speed changes. The transient performance of the different controllers with speed changes as provided in table.3. It is clear from the table 3 that the transient performance is under control limit in FT-ANN controller compared to FLC. It is learn that the steady state error is very less in the proposed controller.

Stability Analysis of the Proposed System: The plot has drawn for SR motor basic equation with torque equation from the state space model equations (17and 18). It is clear that the proposed system is stable for the system speed changes. It is concluded that the -0.5+j0 point is encircled in the all direction in single time. Hence overall encirclement is zero. Also the open loop system has no poles at the right half of s-plan. So the proposed system is stable.The nyquist plot as shown in figure 13.

PRINCIPAL.
K. S. R. INSTITUTE FOR
ENGINEERING AND TECHNOLOGY,
K. S. R. KALVI NAGAR,
TIRUCHENGODE-637 215,
NAMAKKAL Dt. TAMIL NADU.

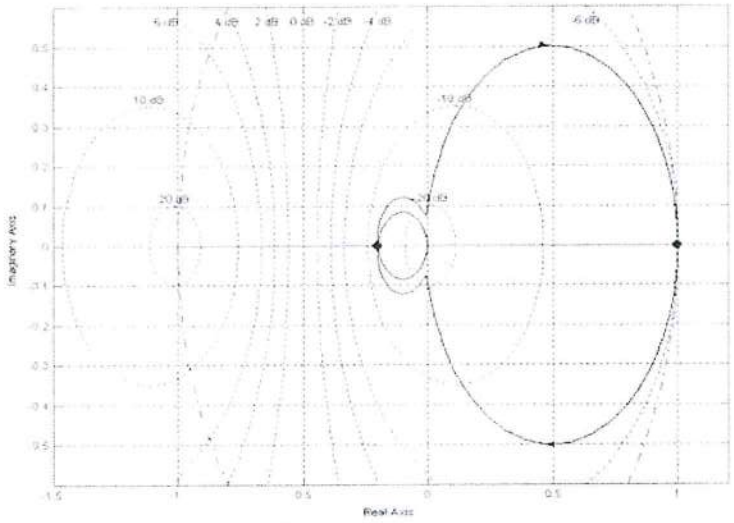

Fig. 13: Stability analysis using nyquist plot for SR motor

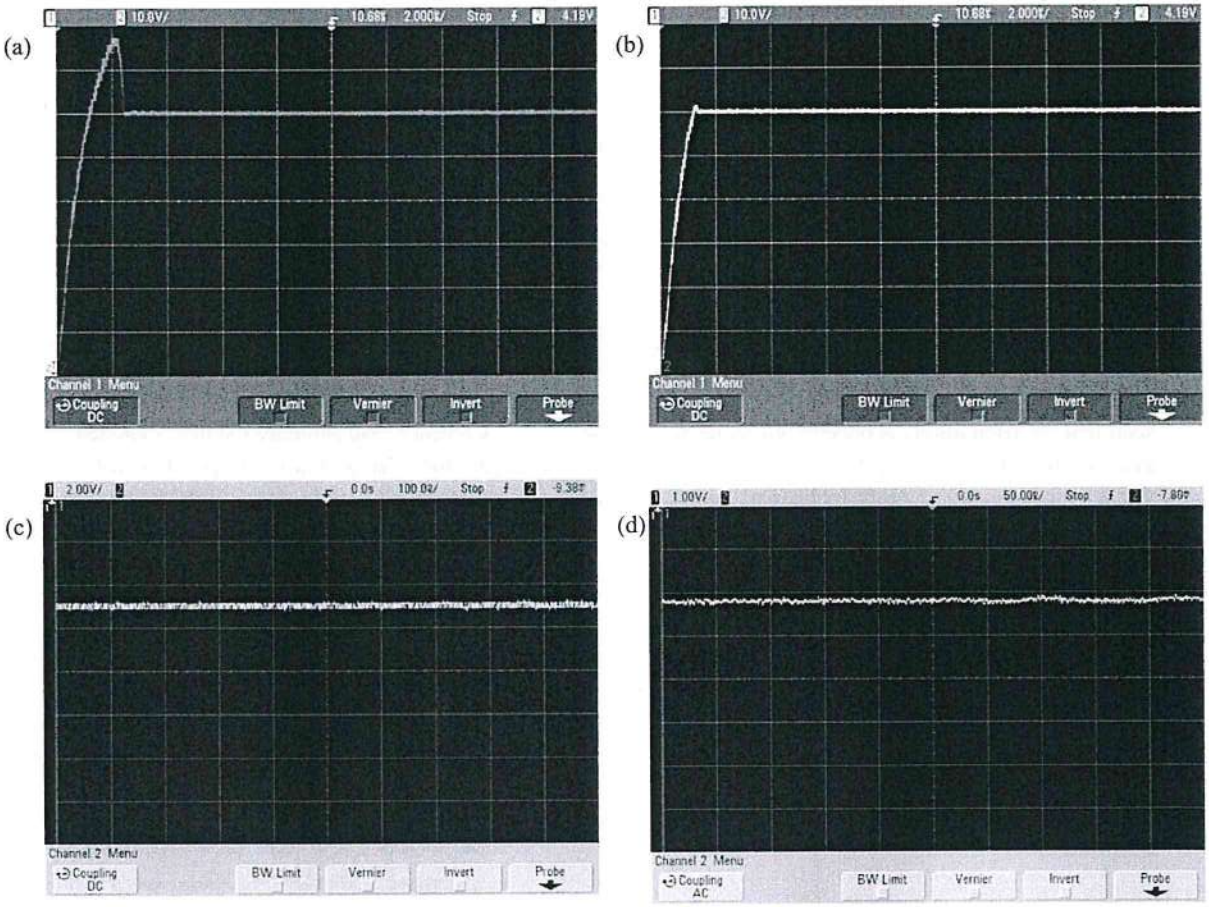

Fig. 14: Experimental waveform of SR motor speed (a) with FLC (b) with FT-ANN controller (c) Steady state error voltage for FLC (d) (c) Steady state error voltage for FT-ANN

PRINCIPAL.
K. S. R. INSTITUTE FOR
ENGINEERING AND TECHNOLOGY,
K. S. R. KALVI NAGAR,
TIRUCHENGODE-637 215,
NAMAKKAL Dt. TAMIL NADU.

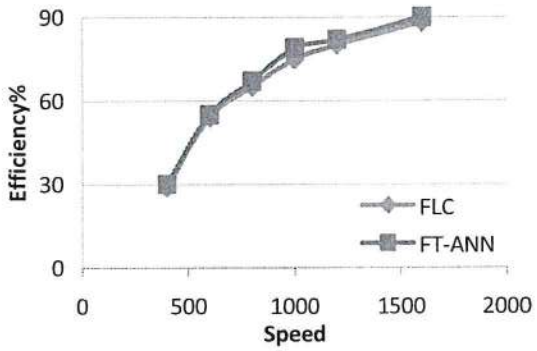

Fig. 15: Speed Vs Efficiency of the SR motor

Experimental Results: The SR motor model is fabricated and performance is tested. A prototype SR motor with FT-ANN controller is operating 300W, 50Hz is designed. The P89V51RD2BN microcontroller is used for generating the driving pulses and IRFP840 MOSFET used as switches in the inverter bridge circuit.MUR4100 diodes used in the rectifier circuit. The frequency level of the generated PWM is 10 KHz. the open collector optocoupler CYN 17-1 is generate the PWM signal from the microcontroller through isolator and IR2110 driver IC. The speed of the motor can be controlled from inverter output. The motor speed is sensed by a digital type pulse sensor GP1L53V. The PWM pulse signal is given to a LM2907 voltage converter IC and feedback signal is given to the microcontroller through an ADC IC ADC0808CCN.

Figure 14 (a) shows the speed voltage waveform with reference speed of 1500 rpm using FLC, it is clearly shows that 4 seconds of time to settle the reference speed. It seen that the oscillations is present due to delay of pulse generation of the controller. Figurer 14 (b) it is observed that there is a minimum steady state error, less percentage overshoot and the minimum settling time at 2.5 seconds. Fig 14(c and d) shows the output voltage of the motor. The steady state error is very minimum compare to FLC. Based on the fig.(14 b,d),. It's clearly seen that FT-ANN based controller having the better transient and steady state performance. The comparison chart is shown in fig.15. The motor speed with efficiency is plotted, it is observed that the proposed controller has high efficiency with step change speed. It is seen form this plot the SR motor have a better efficiency while using FT-ANN controller.

CONCLUSION

The steady state stability analysis of the SR motor has been developed and simulated for estimating the performance for various speed changes using MATLAB/simulink. It has been found from the analysis that the FT-ANN controller provides better efficiency and speed regulation. The comparison results were presented for both controllers. It's found from that FT-ANN controller performs better than fuzzy controller. The proposed controller provides a good speed tracking without overshoot. The proto type model was design and the experimental results are closely agreed with simulation results.

REFERENCE

1. Hany M. Hasanien and S.M. Muyeen, 2012. Speed control of grid-connected switched reluctance generator driven by variable speed wind turbine using adaptive neural network controller, Electric Power Systems Research, Elsevier, 84(1): 206-213.
2. Kioskeridis and C. Mademlis, 2005. Maximum Efficiency in Single-Pulse Controlled Switched Reluctance Motor Drives, IEEE Transactions on Energy Conversion, 20(4): 809-817.
3. Zhou Yana, Changliang Xia, Ziming He and Ximing Xie, 2007. Torque Ripple Minimization in a Sensorless Switched Reluctance Motor Based on Flexible Neural Networks, in Proc. IEEE International Conference of Control and Automation.
4. Hasanien Hany M., S.M. Muyeen and Junji Tamura, 2010. Switched Reluctance Machine, Praise Worthy Prize Press, Napoli, Italy and ISBN 978-88-96329-02-3.
5. Kavitha, P. and B. Umamaheswari, 2014. Speed Control of Sinusoidally Excited Switched Reluctance Motor Using Fuzzy Logic Control, Journal of Theoretical and Applied Information Technology, 68(2).
6. Hashem Gamal M. and Hany M. Hasanien, 2010. Speed Control of Switched Reluctance Motor Based on Fuzzy Logic Controller", Proceedings of the 14th International Middle East Power Systems Conference (MEPCON'10), Cairo University, Egypt, pp: 288-292.
7. Morsy, M.A.A., M. Said A. Moteleb and H.T. Dorrah, 2008. Design and Implementation of Fuzzy Sliding Mode Controller for Switched Reluctance Motor, Proceedings of the International MultiConference of Engineers and Computer Scientists 2008,IMECS 2008, 19-21 March, Hong Kong, 2.
8. Eastham Miller Timothy John., 1993.Switched Reluctance Motors and Their Control", Magna Physics, Oxford University Press.

PRINCIPAL,
K. S. R. INSTITUTE FOR
ENGINEERING AND TECHNOLOGY,
K. S. R. KALVI NAGAR,
TIRUCHENGODE-637 215.
NAMAKKAL Dt. TAMIL NADU

9. Ahmed, T., A. Hamza, A. Abdel Ghani and A. Mohamed, 2006. Fuzzy controller of switched reluctance motor, Acta Electrotehnica, 47(3): 124-131.
10. Lawrenson, P.J., J.M. Stephenson, P.T. Blenkinsop, J. Corda and N.N. Fulton, 1980. Variable speed switched reluctance motors, IEE Proceedings B-Electric Power Applications, 127(4): 253-265.
11. Hasanien Hany M., S.M. Muyeen and Junji Tamura, 2010. Torque ripple minimization of axial laminations switched reluctance motor provided with digital lead controller", Elsevier, Energy Conversion and Management, 51(12): 2402-2406.
12. Tahour Ahmed, Hamza Abid and Abdel Ghani Aissaoui, 2007.Adaptive Neuro-Fuzzy Controller of Switched Reluctance Motor, Serbian Journal of Electrical Engineering, 4(1): 23-34.
13. Hasanien Hany M., 2013. Speed Control of Switched Reluctance Motor Using an Adaptive Neuro-fuzzy Controller, Proceedings of the World Congress on Engineering 2013 Vol II, WCE 2013, London, U.K.
14. Chan, C.C., Y.J. Zhan and K.T. Chau, 1998. Stability Analysis of Fuzzy Sliding Mode Controlled Switched Reluctance Motor Drives, The 29th Annual IEEE Power Electronics Specialists Conference (PESC'98), Fukuoka, Japan, pp: 1283-1289.
15. Thangaraju, I., M. Muruganandam and C. Nagarajan, 2015. Implementation of PID Trained Artificial Neural Network Controller for Different DC Motor Drive, Middle-East Journal of Scientific Research, 23(4): 606-618.
16. Nagarajan, C. and M. Madheswaran, 2012. Experimental Study and steady state stability analysis of CLL-T Series Parallel Resonant Converter with Fuzzy controller using State Space Analysis, Iranian Journal of Electrical & Electronic Engineering, 8(3): 259-267.
17. Mahmoud Samia M., Mohsen Z. El-Sherif and Emad S. Abdel-Aliem, 2013. Studying Different Types of Power Converters Fed Switched Reluctance Motor, 2013. International Journal of Electronics and Electrical Engineering, 1(4): 281-290.

PRINCIPAL.
K. S. R. INSTITUTE FOR
ENGINEERING AND TECHNOLOGY,
K. S. R. KALVI NAGAR,
TIRUCHENGODE-637 215,
NAMAKKAL Dt. TAMIL NADU.

ISSN: 0976-9102 (ONLINE)
DOI: 10.21917/ijivp.2016.0195

ANALYSIS OF ABNORMALITIES IN COMMON CAROTID ARTERY IMAGES USING MULTIWAVELETS

R. Nandakumar[1] and K.B. Jayanthi[2]

[1]*Department of Electronics and Communication Engineering, K.S.R. Institute for Engineering and Technology, India*
E-mail: [1]nandhu.r79@gmail.com

[2]*Department of Electronics and Communication Engineering, K.S. Rangasamy College of Technology, India*
E-mail: [2]jayanthikb@gmail.com

Abstract

According to the report given by World Health Organization, by 2030 almost 23.6 million people will die from cardiovascular diseases (CVD), mostly from heart disease and stroke. The main objective of this work is to develop a classifier for the diagnosis of abnormal Common Carotid Arteries (CCA). This paper proposes a new approach for the analysis of abnormalities in longitudinal B-mode ultrasound CCA images using multiwavelets. Analysis is done using HM and GHM multiwavelets at various levels of decomposition. Energy values of the coefficients of approximation, horizontal, vertical and diagonal details are calculated and plotted for different levels. Plots of energy values show high correlation with the abnormalities of CCA and offer the possibility of improved diagnosis of CVD. It is clear that the energy values can be used as an index of individual atherosclerosis and to develop a cost effective system for cardiovascular risk assessment at an early stage.

Keywords:

Ultrasound, Common Carotid Artery, Multiwavelets, Energy Measurement, Classification

1. INTRODUCTION

For screening the cardiovascular diseases of the carotid artery, ultrasound imaging is a common procedure as the vessel is easily accessible with ultrasound probes [1]. Because of CVDs more people die annually than from any other cause. It has been reported by World Health Organization in a recent study that in the year 2008 nearly 17.3 million people died from CVDs. This represents 30% of all global deaths. In this 7.3 million people died due to coronary heart disease and 6.2 million were due to stroke [2].

Arteries are blood vessels that carry blood between the heart, different tissues and organs of the body. They have ability to expand or contract to allow more blood or control the flow. Hollow centre through which blood flows is called lumen. CCA supplies oxygenated blood to skull, brain, eyeballs, ears and external nose [3]. When the blood supply to parts of the brain is suddenly interrupted, stroke occurs. Aortic stiffness has been proven to be a strong independent predictor of all-cause and CVD. Estimation of regional stiffness of the carotid artery is of great clinical interest [4]. The changes in stiffness with age are accelerated in hypertension and highly amplified by the association with other CVDs and concomitant risk factors [5].

Atherosclerosis is the thickening and narrowing of the arteries due to formation of plaque on the walls of the artery. It causes enlargement of the arteries and thickening of the artery walls [6, 7]. The diameter of CCA decreases due to increase in the thickness. This causes a reduction of the lumen with possible vascular problems and alters the arterial properties elasticity and stiffness. Precise segmentation of carotid artery allows the computation of various biomechanical and anatomical properties of the artery wall that may be useful to clinicians to follow the evolution of the atherosclerosis diseases [8].

Ultrasound imaging has the advantage that it is noninvasive and does not involve the use of ionizing radiation. It is therefore ideally suited to serial investigations. It is also relatively inexpensive and images are acquired in real time [9, 10]. Longitudinal B-mode ultrasound images are used in this work. The resolution of diagnostic ultrasound image is significantly limited by speckle noise. It is believed that speckle is a high frequency component of the image [11]. As the texture of speckle often carries useful information, it is not truly a noise in the typical engineering sense. Ultrasound experts with insufficient experience may not often draw useful conclusions from the images due to the presence of speckle.

Though different methods are investigated for the analysis of carotid artery, the need still exists for the development, implementation and evaluation of an integrated system enabling the automated diagnosis. In the previous work boundary of CCA was extracted using watershed and wavelet transforms. The diameter was measured from the extracted boundary and used for the analysis of plaque deposit in the vessel [12][13]. In this work an effort is made to analyse the CCA using multiwavelets and correlate the findings with the atherosclerosis.

Multi scale representation has proven to be useful in many image processing applications. Recently, multiwavelets have been introduced as a more powerful multi-scale analysis tool. A scalar wavelet system is based on a single scaling function and mother wavelet. But multiwavelet system is based on several scaling functions and mother wavelets. It has several useful properties such as symmetry, orthogonality, short support and a higher number of vanishing moments simultaneously [14].

Multiwavelets can simultaneously provide perfect reconstruction, while preserving length (orthogonality), good performance at the boundary (via linear phase symmetry) and a higher order of approximation (vanishing moments). These features of multiwavelets are responsible for the better performance of multiwavelets over scalar wavelets in image processing applications [15,16]. Geronimo, Hardin and Massopust constructed one of the most well-known multiwavelets called GHM. GHM basis provides a combination of orthogonality, symmetry and compact support that is unachievable by any other scalar wavelet basis [17]. HM and GHM multiwavelets are used in this work to analyse the normal and abnormal CCA images.

PRINCIPAL,
K. S. R. INSTITUTE FOR
ENGINEERING AND TECHNOLOGY,
K. S. R. KALVI NAGAR,
TIRUCHENGODE-637 215,
NAMAKKAL Dt. TAMIL NADU.

L_1L_1	L_1L_2	L_1H_1	L_1H_2
L_2L_1	L_2L_2	L_2H_1	L_2H_2
H_1L_1	H_1L_2	H_1H_1	H_1H_2
H_2L_1	H_2L_2	H_2H_1	H_1H_2

(a)

<table>
<tr><td>L_1L_1</td><td>L_1L_2</td><td>L_1H_1</td><td>L_1H_2</td><td colspan="2" rowspan="2">$L_1H_1^1$</td><td rowspan="2">$L_1H_2^1$</td></tr>
<tr><td>L_2L_1</td><td>L_2L_2</td><td>L_2H_1</td><td>L_2H_2</td></tr>
<tr><td>H_1L_1</td><td>H_1L_2</td><td>H_1H_1</td><td>H_1H_2</td><td colspan="2" rowspan="2">$L_2H_1^1$</td><td rowspan="2">$L_2H_2^1$</td></tr>
<tr><td>H_2L_1</td><td>H_2L_2</td><td>H_2H_1</td><td>H_1H_2</td></tr>
<tr><td colspan="4">$H_1L_1^1$</td><td colspan="2">$H_1L_2^1$</td><td>$H_1H_2^1$</td></tr>
<tr><td colspan="4">$H_2L_1^1$</td><td colspan="2">H_2L_2</td><td>$H_2H_2^1$</td></tr>
</table>

(b)

Fig.4.(a) Subbands of first level decomposition (b) Subbands of second level decomposition

Four main subbands with their own four subbands are obtained as the output of the combination of filters in each decomposition level. The four subbands L_1L_1, L_1L_2, L_2L_1 and L_2L_2 are considered as approximate coefficients and remaining 12 subbands are detail coefficients. In that L_1H_1, L_1H_2, L_2H_1 and L_2H_2 are horizontal, H_1L_1, H_1L_2, H_2L_1 and H_2L_2 are vertical and H_1H_1, H_1H_2, H_2H_1 and H_2H_2 are diagonal coefficients. In each level of decomposition, only the four subbands of approximate coefficients are decomposed into 16 subbands to produce the next level decomposition [23].

GHM multiwavelet is used in this work due its versatility and accuracy. In GHM, there are two low pass and high pass filters for decomposition. GHM multiwavelet has two important features i.e., orthonormality of integer translates of scaling functions and an approximation order of two [24]. GHM scaling functions have short support, orthogonality and are symmetric about their centres. Hardin-Marasovich (HM) is also used in this analysis for comparison.

After applying HM and GHM multiwavelet decomposition on the input CCA image. Energy is calculated for each subband. In an $N \times N$ subimage, energy is computed according to the following equation

$$\text{Energy} = \sum_i \sum_j x_{ij}^2 / N^2 \quad (5)$$

where, x_{ij} is the ij^{th} pixel value of the sub images. Energy is mainly concentrated in the low frequency sections after GHM multiwavelet transformation [25]. These subband energies are analysed to find if there is any correlation between CCA abnormalities and energy coefficients.

3. RESULTS AND DISCUSSION

Video of CCA with a length of 5 second is taken and converted into images at the rate of 25 frames per second. The proposed decomposition algorithm is applied on normal and abnormal CCA images using HM and GHM multiwavelets.

The Fig.5 shows the first level GHM decomposed normal and abnormal CCA images of size 512×512. The Fig.6, Fig.7 and Fig.8 show only the subbands of approximation coefficients of second, third and fourth level GHM decomposition respectively. The size of second, third and fourth level images are 256×256, 128×128 and 64×64 respectively. Decomposition is done for four levels as the information is lost beyond that. Subband energy values are calculated for all the four levels and tabulated for analysis. The energy values obtained for normal and abnormal CCA images using GHM multiwavelet are given in Table.1.

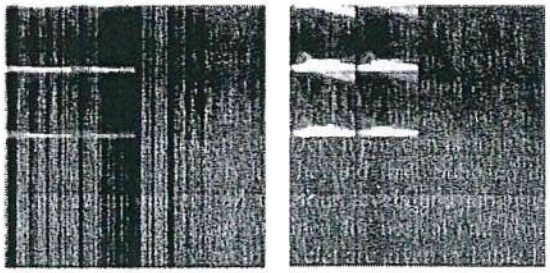

Fig.5. First level GHM decomposition of normal and abnormal images

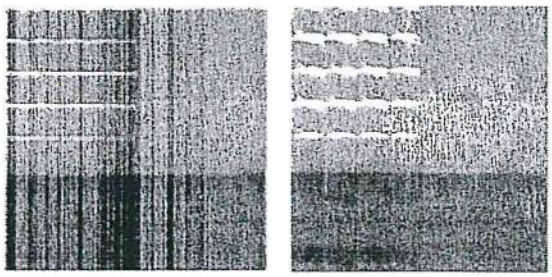

Fig.6. Second level GHM decomposition of normal and abnormal images

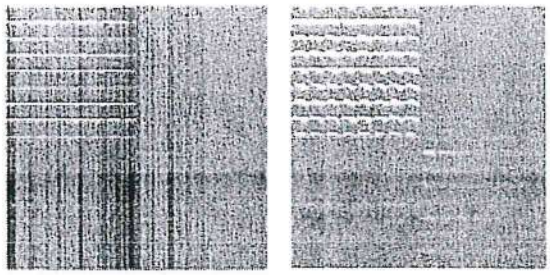

Fig.7. Third level GHM decomposition of normal and abnormal images

PRINCIPAL.
K. S. R. INSTITUTE FOR
ENGINEERING AND TECHNOLOGY,
K. S. R. KALVI NAGAR,
TIRUCHENGODE-637 215,
NAMAKKAL Dt. TAMIL NADU.

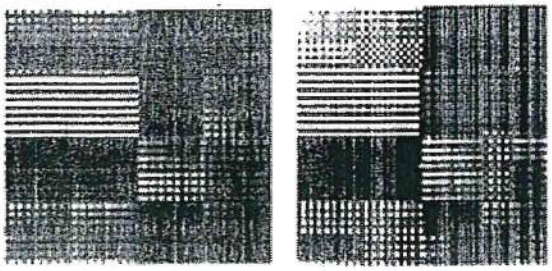

Fig.8. Fourth level GHM decomposition of normal and abnormal images

Table.1. Subband Energy coefficients of normal and abnormal CCA images using GHM multiwavelet decomposition

Sub band	Normal image				Abnormal image			
	Level 1 ($x10^{-1}$)	Level 2 ($x10^{-1}$)	Level 3 ($x10^{-1}$)	Level 4 ($x10^{-1}$)	Level 1 ($x10^{-1}$)	Level 2 ($x10^{-1}$)	Level 3 ($x10^{-1}$)	Level 4 ($x10^{-1}$)
Ea1	0.52453	1.9183	3.4689	0.516	4.1008	15.22	54.755	12.94
Ea2	0.22663	0.8388	1.6236	0.554	1.7721	6.619	24.455	10.41
Ea3	0.23089	0.9545	7.0328	18.441	1.7892	6.898	25.437	209.43
Ea4	0.09976	0.4175	2.8890	12.228	0.7732	3.009	11.043	94.64
Eh1	0.02156	0.0821	0.1799	0.078	0.1675	0.636	2.435	2.23
Eh2	0.00007	0.0011	0.0234	0.037	0.0005	0.011	0.153	0.53
Eh3	0.00949	0.0411	0.3436	1.703	0.0731	0.289	1.193	11.75
Eh4	0.00003	0.0005	0.0247	0.233	0.0002	0.006	0.127	3.61
Ev1	0.02530	0.1273	0.5811	17.141	0.1816	0.811	4.141	74.99
Ev2	0.01094	0.0557	0.2509	9.611	0.0785	0.353	1.898	30.94
Ev3	0.00080	0.0113	0.6384	0.672	0.0038	0.063	1.908	4.77
Ev4	0.00034	0.0050	0.3474	0.687	0.0016	0.028	1.025	10.21
Ed1	0.00001	0.0056	0.0081	0.0835	0.0001	0.034	0.174	3.12
Ed2	0.00001	0.0001	0.0069	0.0177	0.0001	0.001	0.069	1.21
Ed3	0.00003	0.0005	0.0305	0.0099	0.0002	0.003	0.168	0.73
Ed4	0.00001	0.0001	0.0091	0.0055	0.0001	0.001	0.099	0.65

Ea1, Ea2, Ea3 and Ea4 are energy values of four subbands of the approximation coefficients. Eh1, Eh2, Eh3 and Eh4 are the four subband energies of Horizontal coefficients. Subband energy of vertical and diagonal coefficients are given as Ev1, Ev2, Ev3, Ev4 and Ed1, Ed2, Ed3, Ed4 respectively. From Table.1, it is observed that the energy is mainly concentrated in the low frequency bands i.e. approximation coefficients. Energy level of each subband obtained from normal and abnormal images using HM and GHM multiwavelet is plotted and analysed for all the four levels of decomposition. The Fig.9 and Fig.10 show the energy plots of first and second level HM and GHM subbands energy coefficients of normal and abnormal images respectively. Subbands of normal image are shown in white bars and the subbands of abnormal images are shown in black bars in the energy level diagram.

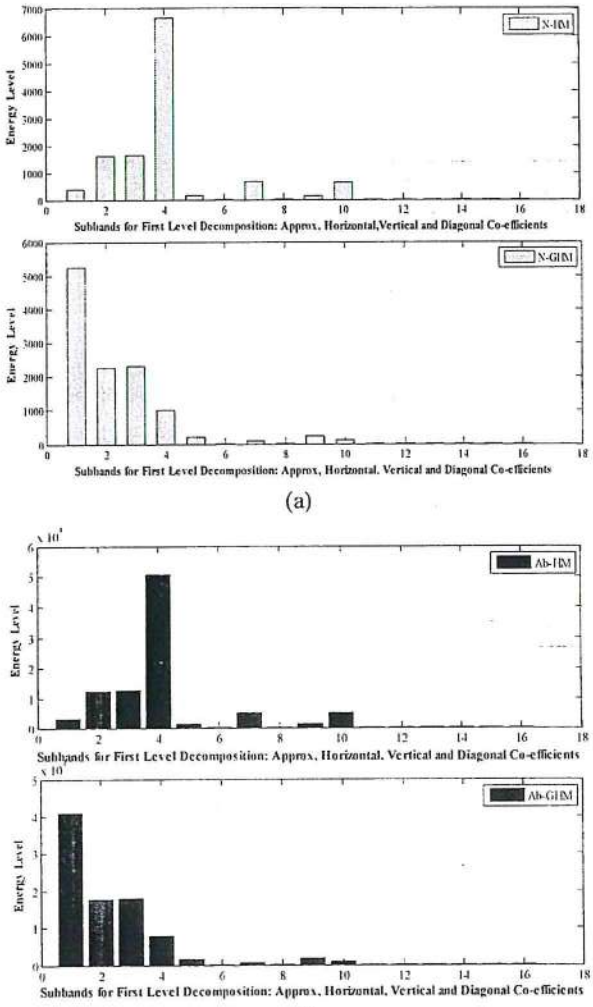

(a)

(b)

Fig.9. Subband energy comparison of normal and abnormal CCA images for HM and GHM multiwavelet first level decomposition

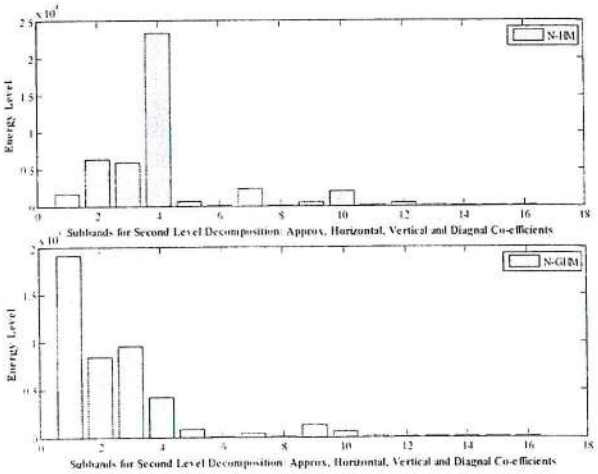

(a)

PRINCIPAL.
K. S. R. INSTITUTE FOR
ENGINEERING AND TECHNOLOGY,
K. S. R. KALVI NAGAR,
TIRUCHENGODE-637 215,
NAMAKKAL Dt, TAMIL NADU.

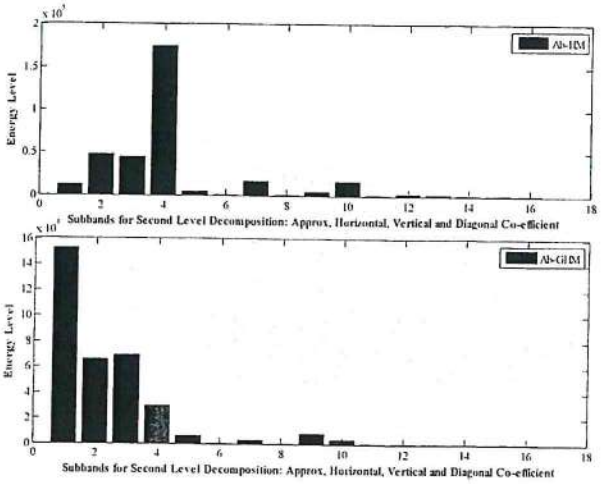

(b)

Fig.10. Subband energy comparison of normal and abnormal CCA images for HM and GHM multiwavelet second level decomposition

By analysing the variations in the energy values of subbands of normal and abnormal decomposed CCA image, it is found that the diagonal energy coefficients have very little amount of energy in all the levels of decomposition. The horizontal and vertical energy coefficients have small amount of energy. But most of the energy is preserved in the approximate coefficients and it increases for every level of decomposition. Plots clearly show that the energy values vary for normal and abnormal image in all the levels. The energy values of subbands given in the Table.1 are for a normal and abnormal subject. Multiwavelets preserve high frequency information in the image i.e edges and give very good performance at the boundaries. As the formation of plaque is in the inner walls of the artery and alters the boundary, the difference between the normal and abnormal CCA is expected to reflect in the subband energy values of diagonal coefficients. While comparing the energy values of normal and abnormal CCA image given in Table.1, the same is observed. The energy values of diagonal coefficients of normal and abnormal images differ largely. Hence these values are further used for classification. They can be used to develop classifiers to classify the normal and abnormal CCA.

4. CONCLUSION

A method is proposed to analyze the abnormalities in longitudinal B-mode ultrasound common carotid artery images using HM and GHM multiwavelets. Normal and abnormal CCA image are taken and decomposed up to four levels. The energy value of each subband is calculated, plotted and analyzed for all the four levels of decomposition. It is found that most of the energy is concentrated in approximate coefficients and a small amount of energy is present in horizontal and vertical coefficients. The energy values obtained from normal images are compared with the energy values obtained from abnormal images. It is observed that the energy values have large difference for normal and abnormal images. Hence, it is concluded that the subband energy can be used as a feature for the diagnosis of abnormalities in CCA. Atherosclerosis and CVDs are highly correlated to the risk factors such as cholesterol, blood pressure, smoking and diabetics. Future work will focus on considering all these risk factors to validate the good features to detect abnormalities in the common carotid artery. Further testing of the proposed method has to be done in a larger image dataset to classify the healthy and unhealthy subjects.

ACKNOWLEDGMENT

The authors are grateful to All India Council for Technical Education (AICTE), India for funding this project under Research Promotion Scheme (RPS). The authors would like to thank Dr. Suresh from Mediscan systems, Chennai, India and Dr. Kandasamy from Sudha Hospital, Erode, India for having kindly provided the inputs for this work.

REFERENCES

[1] Abigail Swillens, Gianluca De Santis, Joris Degroote, Lasse Lovstakken, Jan Vierendeels and Patrick Segers, "Accuracy of Carotid Strain Estimates From Ultrasonic Wall Tracking: A Study Based on Multiphysics Simulations and In Vivo Data", *IEEE Transactions on Medical Imaging*, Vol. 31, No. 1, pp. 131-139, 2012.

[2] Efthyvoulos C. Kyriacou et al.,"A Review of Noninvasive Ultrasound Image Processing Methods in the Analysis of Carotid Plaque Morphology for the Assessment of Stroke Risk", *IEEE Transactions on Information Technology in Biomedicine*, Vol. 14, No. 4, pp. 1027-1038, 2010.

[3] David C. Wang, Roberta Klatzky, Bing Wu, Gregory Weller, Allan R. Sampson and George D. Stetten, "Fully Automated Common Carotid Artery and Internal Jugular Vein Identification and Tracking Using B-Mode Ultrasound", *IEEE Transactions on Biomedical Engineering*, Vol. 56, No. 6, pp. 1691-1699, 2009.

[4] Jianwen Luo, Ronny X. Li and Elisa E. Konofagou, "Pluse Wave Imaging of the Human Carotid Artery: An In Vivo Feasibility Study", *IEEE Transactions on Ultrasonics, Ferroelectrics, and Frequency Control*, Vol. 59, No. 1, pp. 174-181, 2012.

[5] Toufik Zakaria, Zhao Qin and Roch Listz Maurice, "Optical-Flow-based B-Model Elastography: Application in the Hypertensive Rat Carotid", *IEEE Transactions on Medical Imaging*, Vol. 29, No. 2, pp. 570-578, 2010.

[6] Filippo et al., "Hypothesis Validation of Far- Wall Brightness in Carotid-Artery Ultrasound for Feature-based IMT Measurement using a Combination of Level-Set Segmentation and Registration", *IEEE Transactions on Instrumentation and Measurement*, Vol. 61, No. 4, pp. 1054-1063, 2012.

[7] C.P. Loizou, V. Murray, M.S. Pattichis, M. Pantziaris and C.S. Pattichis, "Multiscale Amplitude-Modulation Frequency-Modulation (Am-Fm) Texture Analysis of Ultrasound Images of the Intima and Media Layers of the Carotid Artery", *IEEE Transactions on Information Technology in Biomedicine*, Vol. 15, No. 2, pp. 178-188, 2011.

[8] Francois Destrempes, Jean Meunier, Marie-France Giroux, Gilles Soulez and Guy Cloutier, "Segmentation of Plaques

PRINCIPAL,
K. S. R. INSTITUTE FOR
ENGINEERING AND TECHNOLOGY,
K. S. R. KALVI NAGAR,
TIRUCHENGODE-637 215,
NAMAKKAL Dt, TAMIL NADU.

in Sequences of Ultrasonic B-Mode Images of Carotid Arteries Based on Motion Estimation and a Bayesian Model", *IEEE Transactions on Biomedical Engineering*, Vol. 58, No. 8, pp. 2202-2211, 2011.

[9] D.C. Barratt, B.B. Ariff, K.N. Humphries, S.A. Mc.G. Thom and A.D. Hughes, "Reconstruction and Quantification of the Carotid Artery Bifurcation from 3-D Ultrasound Images", *IEEE Transactions on Medical Imaging*, Vol. 23, No. 5, pp. 567-583, 2004.

[10] M. Larsson, F. Kremer, P. Claus, T. Kuznetsova, L.A. Brodin and J. Dhooge, "Ultrasound-Based Radial and Longitudinal Strain Estimation of the Carotid Artery: A Feasibility Study", *IEEE Transactions on Ultrasonics, Ferroelectrics and Frequency Control*, Vol. 58, No. 10, pp. 2244-2251, 2011.

[11] Nikolaos N. Tsiaparas, Spyretta Golemati, Ioannis Andreadis, John S. Stoitsis, Ioannis Valavanis and Konstantina S. Nikita, "Comparison of Multiresolution Features for Texture Classification of Carotid Atherosclerosis From B-Mode Ultrasound", *IEEE Transactions on Information Technology in Biomedicine*, Vol. 15, No. 1, pp. 130-137, , 2011.

[12] Jayanthi K. Balasundaram and R.S.D. Wahida Banu, "Carotid Artery Boundary Extraction for the Analysis of Cardiovascular Diseases", *International Journal of Medical Engineering and Informatics*, Vol. 1, No. 3, pp. 290-297, 2009.

[13] Jayanthi K. Balasundaram and R.S.D. Wahida Banu, "A Non-Invasive Study of Alterations of the Carotid Artery with Age using Ultrasound Images", *Medical and Biological Engineering and Computing*, Vol. 44, No. 9, pp. 767-772, 2006.

[14] Hamid Soltanian-Zadeh, Farshid Rafiee-Rad and D. Siamak Pourabdollah-Nejad, "Comparison of Multiwavelet, Wavelet, Haralick, and Shape Features for Microcalcification Classification in Mammograms", *Pattern Recognition*, Vol. 37, No. 10, pp. 1973-1986, 2004.

[15] S. Ramakrishnan and S. Selvan, "Multiwavelets Domain Singular Value Features for Image Texture Classification", *Journal of Zhejiang University-Science A*, Vol. 8, No. 4, pp. 538-549, 2007.

[16] Manju Mathew, A.B. Premkumar and A.S. Madhukumar, "Spectrum-Efficient Cognitive Radio Transceiver using Multiwavelet Filters", *International Scholarly Research Network*, Vol. 2012, pp. 1-13, 2012.

[17] Padmanabhareddy Vundela and Varadarajan Sourirajan, "A Robust Multiwavelet-based Watermarking Scheme for Copyright Protection of Digital Images using Human Visual System", *International Arab Journal of Information Technology*, Vol. 10, No. 6, pp. 4128-4228, 2011.

[18] Jing-Wein Wang, "Evolutionary Optimization Approach for Fingerprint Classification", *Proceedings of the World Congress on Engineering*, Vol. 2, pp. 1-5, 2011.

[19] Chin-Pan Huang and Ching-Chung Li, "Secret Image Sharing using Multiwavelet Transform", *Journal of Information Science and Engineering*, Vol. 27, No. 2, pp. 733-748, 2011.

[20] Ali Zifa, Mohammed Hassan Moradi and Shahriar Gharibzadeh, "Microarray Image Enhancement by Denoising using Decimated and Undecimated Multiwavelet Transforms", *Signal, Image and Video Processing*, Vol. 4, No. 2, pp. 177-185, 2010.

[21] Ivan W. Selesnick, "Multiwavelet bases with Extra Approximation Properties", *IEEE Transactions on Signal Processing*, Vol. 46, No. 11, pp. 2898-2908, 1998.

[22] N. Leelavathy, V. Prasade, S. Srinivas Kumar et al., "Oblivious Image Watermarking in Discrete Multiwavelet Domain using QIMM", *Journal of Multimedia*, Vol. 6, No. 4, pp. 359-368, 2011.

[23] U.S. Ragupathy, D. Baskar and A. Tamilarasi, "A Novel Method of Image Compression using Multiwavelets and Set Partitioning Algorithm", *Proceedings of 3rd International Conference on Industrial and Information System*, pp. 1-6, 2009.

[24] Chihang Zhao, Yongsheng Gao, Jie He and Jie Lianl, "Recognition of Driving Postures by Multiwavelet Transform and Multilayer Perceptron Classifier", *Engineering Applications of Artificial Intelligence*, Vol. 25, No. 8, pp. 1677-1686, 2012.

[25] Yuanning Liu, Fei He, Yonghua Zhao and Ning Wang, "An Iris Recognition based on GHM Multi-Wavelet Transformation", *Proceedings of 4th International Conference on Innovative Computing, Information and Control*, pp. 793-796, 2009.

PRINCIPAL,
K. S. R. INSTITUTE FOR
ENGINEERING AND TECHNOLOGY,
K. S. R. KALVI NAGAR,
TIRUCHENGODE-637 215,
NAMAKKAL DT, TAMIL NADU.

ANALYZED ON DOMINATION AND DIAMETER IN GRAPHS

Dr. K.Prabakaran and Dr. N. Lalithamani
Department of Mathematics
K.S. Rangasamy College of Technology
Tiruchengode, India
prabakaran@ksrct.ac.in,lali75bass@yahoo.co.in

Abstract—Let $\gamma(G), \gamma_t(G), \gamma_c(G)$, **and diam (G) denote respectively the domination number, total domination number and connected domination number and the diameter of a connected graph G of order p. In this paper, we prove that connect domination + diam(G) ≤ 2p-3 and characterize the extremal graphs. Similar results for domination number and total domination number are also obtained.**

Keywords— Domination number; total domination number; connected domination number; diameter.

I. INTRODUCTION

Let G = (V, E) be an undirected, connected simple graph of order p. The degree of a vertex u is the number of edges incident with u and is denoted by d(u).The maximum degree is denoted by Δ.The distance between two vertices u and v is the length of the shortest u-v path. The diameter of G is the maximum distance between any two vertices in the graph and is denoted by diam (G).The paths and cycles on n vertices are respectively denoted by $\mathbf{P_n}$ and $\mathbf{C_n}$. A subset S of V is called a *dominating set* in G if every vertex in V-S is adjacent to at least one vertex in S. The minimum cardinality taken over all minimum dominating sets in G is called the domination number of G and is denoted by $\gamma(G)$.A dominating set S is called *total* if the induced sub graph < S > has no isolated vertices and connected if < S > is connected. The minimum cardinality taken overall minimal total (connected) dominating sets in G is called the *total (connected) domination number* of G and is denoted by $\gamma_t(G)$ $(\gamma_c(G))$. A lot of research work has been done in this area [1, 3, 4, 5, 6, 7, 8, 9, 10, 11, 12, 14 &15].In [16], Joseph and Arumugam proved that $\gamma_c + \kappa \leq p$, where κ is the connectivity of G and characterized the extremal graphs. In [17], they proved $\gamma_c + \chi \leq p+1$, where χ is the chromatic number of G and characterized the extremal graphs. In this paper we prove that $\gamma_c(G)$+ diam(G) ≤ 2p-3 and characterize the extremal graphs. Similar results for $\gamma(G)$ and $\gamma_t(G)$ are also obtained.In recent years, many authors focused on domination in graphs. The domination and diameter graphs applied to several fields, electrical power networks, monitoring communication, land surveying, number of facilities (hospital, fire house) and location problem. Terms not defined in this paper, are used in the sense of Balakrishnan and Ranganathan. We use the following results and notations in the sequal.

II. PRELIMINARIES AND NOTATIONS

Theorem 1.1 [13] Let G be a connected graph of order p and maximum degree Δ. Then $\gamma_c(G) \leq$ p-Δ.

Theorem 1.2 If G is connected and Δ<p-1, then,

(i) $\gamma_t \leq$ p-Δ. (ii) $\gamma \leq \gamma_t \leq \gamma_c$.

Observation 1.3 For any graph G of order p, diam (G) ≤ p-1, and equality holds if and only if G = P_p.

Notation 1.4 The graphs obtained by introducing a new vertex v and joining it to exactly one vertex of degree ≥2 in a graph G is denoted by G (v). If v is joined to the unique centre of G, it is denoted by G(C v).A graph in the family $P_7(v)$ and $P_7(Cv)$ are given in figure 1.1.

$P_7(v)$:

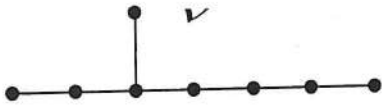

$P_7(Cv)$:

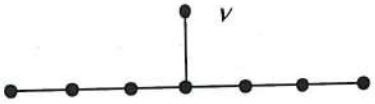

Fig 1.1

Notation 1.5 The identification of a single vertex v of a graph H to exactly one pendent vertex of G is denoted by G (H). The graphs $P_6(C_3)$ and $P_5(C_4)$ are given in figure 1.2.

$P_6(C_3)$:

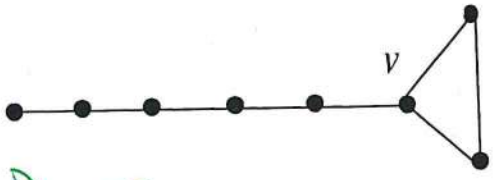

PRINCIPAL,
K. S. R. INSTITUTE FOR
ENGINEERING AND TECHNOLOGY,
K. S. R. KALVI NAGAR,
TIRUCHENGODE - 637 215,
NAMAKKAL DT, TAMIL NADU.

$P_5(C_4)$:

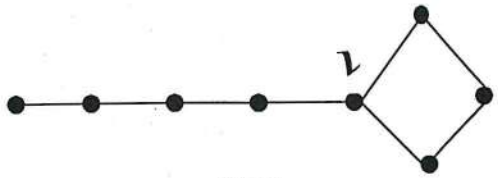

Fig 1.2

Notation 1.6 The graph obtained by introducing a new vertex v to a graph G and joining it to two adjacent vertices of degree ≥ 2 in G is denoted by G(v^3). The graphs $P_6(v^2)$ are given in figure 1.3.

$P_6(v^2)$:

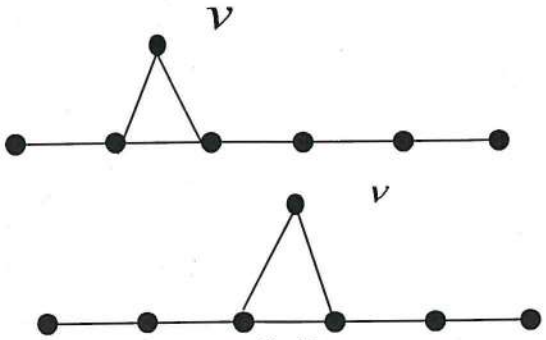

Fig 1.3

Notation 1.7 The graph obtained by introducing a new vertex v to a graph G and joining it to two non-adjacent vertices of degree ≥ 2 in G is denoted by G(nv^2).The graph $P_6(nv^2)$ is given in figure 1.4.

$P_6(nv^2)$:

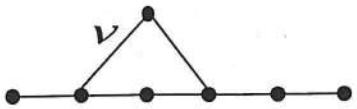

Fig 1.4

Notation 1.8 Let (u v w) be a path in G. Then the family of graph obtained by introducing a new vertex v and joining it to u, v and w is denoted by G(v^3).The graphs $P_6(v^3)$ are given

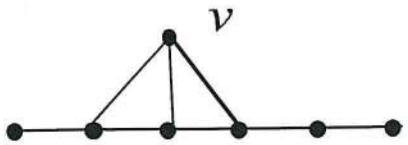

$P_6(v^3)$

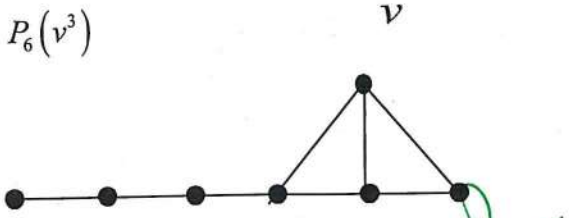

Fig 1.5

PRINCIPAL,
K. S. R. INSTITUTE FOR
ENGINEERING AND TECHNOLOGY,
K. S. R. KALVI NAGAR,
TIRUCHENGODE - 637 215,
NAMAKKAL Dt, TAMIL NADU.

III. MAIN RESULTS

Theorem 2.1 For any connected graph G of order p ≥ 3, $\gamma_c(G)$ + diam(G) $\leq$ 2p-3 and equality holds if and only if G $= P_p$.

Proof: By theorem 1.1, $\gamma_c(G) \leq$ p-Δ.

By observation 1.3, diam(G)$\leq$p-1.

Hence $\gamma_c(G)$ +diam(G)$\leq$ 2p-Δ-1

$\leq$ 2p-2-1 since $\Delta \geq 2$

= 2p-3.

Now let $\gamma_c(G)$ + diam(G)=2p-3.Then $\gamma_c(G)$ = p-2 and diam(G)=p-1. Since P_p is the only graph satisfying these qualities, G = P_p.

Converse is obvious.

Theorem 2.2 For any connected graph G with $\Delta \neq$p-1, $\gamma_t(G)$ + diam(G)$\leq$ 2p-3 and equalities holds if and only if G $= P_4, P_5$ or P_6.

Proof: By theorem 1.2, $\gamma_t(G) \leq$p-Δ. Further, diam(G)$\leq$p-1.

Hence $\gamma_t(G)$ + diam(G) $\leq$ 2p-3.Now let $\gamma_t(G)$ + diam(G) = 2p-3.Then $\gamma_t(G)$ = p-2 and diam(G) = p-1.Now diam(G) = p-1 implies that the graph must be a path. But for p$\geq$7, $\gamma_t(P_p) <$ p-2. Hence G = P_4, P_5 or P_6.

Converse can be easily verified.

Theorem 2.3 For any connected graph G of order p$\geq$3, $\gamma(G)$ +diam(G)$\leq$ 2p-3 and equality holds if and only if G = P_3 or P_4.

Proof: since $\gamma(G) \leq \gamma_c(G) \leq$ p- Δ and diam (G) $\leq$ p-1,we get $\gamma(G)$ +diam(G)$\leq$ 2p-3. Now let $\gamma(G)$ + diam(G) = 2p-3.Then $\gamma(G)$ = p-2 and diam(G) = p-1.Now diam(G)=p-1 implies that the graph must be a path. But for p $\geq$ 5, $\gamma(P_p) <$ p-2. Hence G= P_3 or P_4.

Converse can be easily verified.

Theorem 2.4 For any connected graph G of order p $\geq$ 3, $\gamma_c(G)$ +diam(G) = 2p-4 if and only if G = C_3 or C_4.

Proof: If follows from theorem 2.1 that $\gamma_c(G)$ + diam(G) = 2p-4 implies

(i) $\gamma_c(G)$ = p-3 and diam(G) = p-1 (or)

(ii) $\gamma_c(G)$ = p-2 and diam(G)= p-2

Case (i) $\gamma_c(G)$ = p-3 and diam(G) = p-1.

Now diam(G) = p-1 implies that the graph must be a path. But there is no path with $\gamma_c(G)$ = p-3 . Hence we have no graphs in this case.

Case (ii) $\gamma_c(G)$ = p-2 and diam(G) = p-2.

Now $\gamma_c(G)$ = p-2 implies that the graph must be paths or cycles. But for paths, diam(G) ≠ p-2.Hence we consider only cycles. But for $C_n(n \geq 5)$ diam$(C_n) < p-2$ .Henc G= C_3 or C_4.

Converse can be easily verified.

Theorem 2.5 For any connected graph G with Δ≠ p-1, $\gamma_t(G)$ + diam(G)=2p-4 if and only if G = C_4, P_5 or P_7.

Proof: If follows from Theorem 2.2 that $\gamma_t(G)$ + diam(G) = 2p-4 implies

(i) $\gamma_t(G)$ = p-3 and diam(G) = p-1 (or)

(ii) $\gamma_t(G)$ = p-2 and diam(G) = p-2.

Case (i) $\gamma_t(G)$ = p-3 and diam(G) = p-1.

Now diam (G) = p-1 implies that the graph must be a path. But for p≥8, $\gamma_t(P_p)$ < p-3.

Hence G = P_5 or P_7.

Case (ii) $\gamma_t(G)$ = p-2 and diam(G) = p-2.

Now $\gamma_t(G)$ = p-2 implies that the graph must be paths or cycles. But for paths, diam (G) ≠ p-2.Hence we consider only cycles. But for $C_n(n \geq 5)$, diam(G)< p-2.Hence G = C_4.

Converse can be easily verified.

Theorem 2.6 For any connected graph G of order p ≥ 3, $\gamma(G)$ + diam(G) = 2p-4 if and only if G = C_3 or C_4 and P_5.

Proof: It follows from theorem 2.3 that $\gamma(G)$ +diam(G) = 2p-4 implies

(i) $\gamma(G)$ = p-3 and diam(G) = p-1 (or)

(ii) $\gamma(G)$ = p-2 and diam(G) = p-2.

Case (i) $\gamma(G)$ = p-3 and diam(G)= p-1.

Now diam(G) = p-1 implies that the graph must be a path. But for p ≥ 6 and p = 4, $\gamma(P_P) < p-3$. Hence G=P_5.

Case (ii) $\gamma(G)$ = p-2 and diam(G)= p-2.

Now $\gamma(G)$ = p-2 implies that the graph must be paths or cycles. But for paths, diam(G) ≠ p-2.

Hence we consider only cycles. For $C_n(n \geq 5)$, diam(G)<p-2. Hence G=C_3 or C_4.

Converse can be easily verified.

Theorem 2.7 For any connected graph G of order p≥5, $\gamma_c(G)$ + diam(G)= 2p-5 iff G= C_6, $P_{p-1}(v)$, $P_{p-2}(C_3)$, $P_{p-1}(v^2)$, $P_{p-3}(C_4)$, $P_{p-1}(nv^2)$ or $P_{p-1}(v^3)$.

Proof: For G = C_6, $\gamma_c(G) = 4$ = p-2 and diam (G) =3= p-3 and hence $\gamma_c(G)$ +diam (G) = 2p-5. For all other graphs stated in the theorem, $\gamma_c(G)$ = p-3 and diam (G) = p-2 so that $\gamma_c(G)$ +diam (G) = 2p-5. Now let $\gamma_c(G)$ + diam (G) = 2p-5. If follows from Theorem 2.4 that

(A) $\gamma_c(G)$ = p-4 and diam(G) = p-1 (or)

(B) $\gamma_c(G)$ = p-1 and diam(G) = p-4 (or)

(C) $\gamma_c(G)$ = p-2 and diam(G) = p-3 (or)

(D) $\gamma_c(G)$ = p-3 and diam(G) = p-2.

There does not exit any graph for (A) and (B).

For (C), $\gamma_c(G)$ = p-2 implies that G must be paths or cycles.

But diam (G) = p-3 implies that G = C_6.

Now we consider graphs with $\gamma_c(G)$ = p-3 and diam (G) = p-2.

Case (i) G is tree.

We claim that G has exactly one vertex of degree three. Suppose not. Let u and v be two vertices of degree three. Let T_u be a sub tree of G containing u but not containing v and T_v be a sub tree of G containing v but not containing u. (see figure)

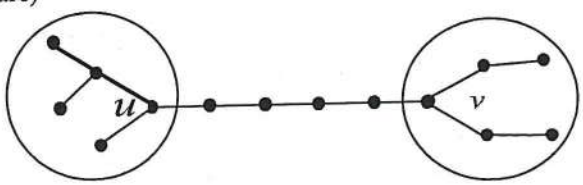

Then T_u contains at least two pendent vertices other than u and T_v contains at least two pendent other than v. Thus G contains at least four pendent vertices and hence

$\gamma_c(G)$ ≤ p- (number of pendent vertices)

≤ p-4.

This is a contradiction and hence G has exactly one vertex of degree three.

Thus G= $P_{p-1}(v)$.

Case (ii) G is not a tree.

Since diam(G) = p-2, G cannot contain C_n (n≥5).

Sub case (a) G contains C_3 only.

If G has exactly one vertex of degree three, then G= $P_{p-2}(C_3)$ .If G has exactly two vertices of degree three, then they must be adjacent. Further they must be adjacent to a common vertex to form C_3 .Hence G= $P_{p-1}(v^2)$. If G has three or more vertices of degree three, then diam(G)<p-2 and hence no graph exists in such cases.

Sub case (b) G contains C_4 only.

If G has exactly one vertex of degree three, then it must be in C_4. Hence G= $P_{p-3}(C_4)$ .If G has two vertices of degree

PRINCIPAL,
K. S. R. INSTITUTE FOR
ENGINEERING AND TECHNOLOGY,
K. S. R. KALVI NAGAR,
TIRUCHENGODE - 637 215,
NAMAKKAL DT, TAMIL NADU.

three, then they must be non adjacent, for otherwise diam (G) < p-2.

Hence G = $P_{p-1}(nv^2)$.

Sub case (c) G contains both C_3 and C_4.

Since diam (G) = p-2, G cannot have two or more disjoint C_3 and C_4 . Further there must be vertices at a distance p-2 resulting in a path P on p-1 vertices. Then the remaining vertex must be adjacent to three consecutive vertices of P. Hence G = $P_{p-1}(v^3)$.

Theorem 2.8 For any connected graph G of order p with $\Delta \neq p-1$, $\gamma_t(G)$ +diam(G)=2p-5 if and only if G= $C_5, C_6, P_8, P_9, P_{10}, P_4(v), P_5(v), P_6(v), P_7(Cv)$, $P_3(C_3), P_4(C_3), P_5(C_3), P_4(v^2), P_5(v^2), P_6(v^2)$, $P_2(C_4), P_3(C_4), P_4(C_4), P_5(nv^2), P_6(nv^2)$, $P_4(v^3), P_5(v^3)$ or $P_6(v^3)$.

Proof: For G= C_6, $\gamma_t(G)$ =3= p-2 and diam(G) = 2= p-3 and hence $\gamma_t(G)$ + diam(G) = 2p-5. For all other graphs stated in the theorem, $\gamma_t(G)$ = p-3 and diam(G) = p-2 so that $\gamma_t(G)$ +diam(G) = 2p-5.

Now let $\gamma_t(G)$ + diam (G) = 2p-5. It follows from Theorem 2.5 that

(A) $\gamma_t(G)$ = p-1 and diam(G) =p-4 (or)

(B) $\gamma_t(G)$ = p-4 and diam(G)= p-1 (or)

(C) $\gamma_t(G)$ = p-2 and diam (G) = p-3 (or)

(D) $\gamma_t(G)$ = p-3 and diam(G) = p-2

Since $\gamma_t(G) \leq$ p-2, there does not exist any graph for (A).

For (B), diam (G) = p-1 implies that the graph must be a path. But for $11 \leq p \leq 7$, $\gamma_t(P_p) \neq$ p-4. Hence G= P_8, P_9 or P_{10}.

For (C) $\gamma_t(G)$ = p-2 implies that G must be paths or cycles. But for paths, diam(G) ≠ p-3. Hence we consider only cycles. For $C_n(n \geq 7)$, diam(C_n)<p-3.

Hence G= C_5 or C_6. Now we consider graphs with $\gamma_t(G)$ = p-3 and diam (G) = p-2.

Case (i) G is tree.

As in theorem 2.7, G has exactly one vertex of degree three. Hence G must be of the form $P_n(v)$. But for n ≥ 8, $\gamma_t[P_n(v)]$< p-3.

Hence G= $P_4(v), P_5(v), P_6(v)$ or $P_7(Cv)$.

Case (ii) G is not a tree.

Since diam (G) = p-2, G cannot contain $C_n(n \geq 5)$.

Sub case (a) G contains C_3 only.

As in Theorem 2.7, if G has exactly one vertex of degree three, then G must be of the form $P_n(C_3)$. But for n≥6, $\gamma_t[P_n(C_3)]$<p-3. Hence G= $P_5(C_3), P_4(C_3)$ or $P_3(C_3)$.If G has exactly two vertices of degree three, then must be of the form $p_n(v^2)$. But for n ≥ 7, $\gamma_t(P_n(v^2))$ < p-3. Hence G = $P_4(v^2), P_5(v^2), P_6(v^2)$.If G has three or more vertices of degree three, then diam (G) < p-2 and hence no graph exists in such cases.

Sub case (b) G contains C_4 only.

As in theorem 2.7,if G has exactly one vertex of degree three, then G must be of the form $P_n(C_4)$. But for n≥5, $\gamma_t[P_n(C_4)]$<p-3. Hence G = $P_2(C_4), P_3(C_4)$ or $P_4(C_4)$. If G has two vertices of degree three, then G must be of the form $P_n(nv^2)$. But for n≥7, $\gamma_t[P_n(nv^2)]$< p-3. Hence G= $P_5(nv^2)$ or $P_6(nv^2)$.

Sub case (c) G contains both C_3 and C_4 .As in theorem 2.7, G must be of the form $P_n(v^3)$. But for n ≥ 7, $\gamma_t[P_n(v^3)]$< p-3.Hence G = $P_4(v^3), P_5(v^3), P_6(v^3)$.

Theorem 2.9 For any connected graph G of order p≥3, $\gamma(G)$+ diam(G)=2p-5 if and only if G = P_6, P_7, $P_3(v), P_4(v), P_5(Cv), P_2(C_3), P_3(C_3), P_4(v^2), P_2(C_4)$, $P_3(v^3)$ or $P_4(v^3)$.

Proof: For G = P_6 and P_7, $\gamma(G)$= p-4 and diam(G) = p-1. For all other graphs stated in the Theorem, $\gamma(G)$=p-3 and diam(G)=p-2, so that $\gamma(G)$ +diam(G) = 2p-5.

Now let $\gamma(G)$ +diam(G) = 2p-5. It follows that Theorem 2.6 that

(A) $\gamma(G)$ = p-1 and diam (G)= p-4 (or)

(B) $\gamma(G)$ = p-2 and diam(G)= p-3 (or)

(C) $\gamma(G)$ = p-4 and diam(G) = p-1(or)

(D) $\gamma(G)$ = p-3 and diam (G)= p-2 .

Since $\gamma(G) \leq$p-2, there does not exist any graph for (A). Further $\gamma(G)$ =p-2 implies that the graph must be a P_3, P_4, C_3, C_4. But diam(G) ≠ p-3 for these graphs. Thus there is no graph for (B). For (C), diam (G) = p-1 implies that the graph must be a path. But for $8 \leq p \leq 5$, $\gamma[P_p] \neq$ p-4.

Hence G = P_6 or P_7.

PRINCIPAL,
K. S. R. INSTITUTE FOR
ENGINEERING AND TECHNOLOGY,
K. S. R. KALVI NAGAR,
TIRUCHENGODE - 637 215,
NAMAKKAL DT, TAMIL NADU.

Now we consider graphs with $\gamma(G)$ = p-3 and diam (G) = p-2.

Case (i) G is a tree

As in Theorem 2.8, if G has exactly one vertex of degree three, then G must be of the form $P_n(v)$. But for n≥6, $\gamma\ [P_n(v)]$ < p-3. Hence G= $P_3(v), P_4(v)$ or $P_5(Cv)$.

Case (ii) G is not a tree.

Since diam (G) = p-2, G can not contain $C_n(n \geq 5)$.

Sub case (a) G contains C_3 only.

As in Theorem 2.8, if G has exactly one vertex of degree three, then G must be of the form $P_n(c_3)$. But for n ≥ 4, $\gamma\ [P_n(C_3)\ ]$ < p-3.Hence G = P_3 (C_3) or $P_2(C_3)$.If G has exactly two vertices of degree three, then G must be of the form $P_n(v^2)$.But for n≥5, $\gamma\ [P_n(v^2)]$<p-3. Hence G = $P_4(V^2)$. If G has three or more vertices of degree three, then diam (G) < p-2 and hence no graph exists in such cases.

Sub case (b) G contains C_4 only.

As in Theorem 2.8,if G has exactly one vertex of degree three, then G must be of the form $P_n(C_4)$.But for n ≠ 2, $\gamma[P_n(C_4)]$< p-3.Hence G= $P_2(C_4)$.If G has two vertices of degree three, $\gamma(G)$ < p-3 then and hence no graph exists.

Sub case (c) G contains both C_3 and C_4.

As in Theorem 2.8, G must be of the form $P_n(v^3)$.But for n≥5, $\gamma\ [P_n(v^3)]$ < p-3. Hence G= $P_3(v_3^3)$ or $P_4(v_3^3)$.

Open Problem 2.10 Characterize the class of graphs for which

(i) $\gamma_c(G)$ + diam(G)=2p-6

(ii) $\gamma_t(G)$ + diam(G)=2p-6

(iii) $\gamma(G)$ + diam(G)=2p-6

IV. Conculusion

In this paper analyzed the domination and diameter in different cases of graphs. These results establish key relationships between domination number, total domination number, connected domination number and other the chromatic number. Further, these results establish optimal upper bounds on the domination number in terms of the order itself, the order and the maximum degree, and the order and the minimum degree. Structural results on domination number and connect domination number and total domination number, perfect graphs were presented. The complexity questions associated with the domination number, total domination and connected domination were also discussed. We recall here several interesting open problems and conjectures on the domination number. Finally, in this paper, we proved that $\gamma_c(G)$ + diam(G) ≤ 2p-3 and characterize the extremal graphs. Similar results for $\gamma(G)$ and $\gamma_t(G)$ are also obtained.

PRINCIPAL,
K. S. R. INSTITUTE FOR
ENGINEERING AND TECHNOLOGY,
K. S. R. KALVI NAGAR,
TIRUCHENGODE - 637 215,
NAMAKKAL Dt, TAMIL NADU.

Acknowledgment

The author would like to express his thanks to Prof. J. Paulraj Joseph, Manonmaniam Sundarnar University, Tirunelveli, India for his illuminating advice and valuable discussion. Also, the author is very grateful to the reviewers for their valuable suggestions to improve the quality of the paper.

References

[1] R. Balakrishnan and K. Rangathan, Text Book of graph Theory, Springerverlag, New York, INC. 2000.

[2] W. E. Clark and B. Shekhtman , " Domination Numbers of q-analogues of Kenser graphs", Bull . Inst. combin. Appl., Vol. 19, pp. 83- 92, 1997.

[3] E. J. Cockayne , R .M .Dawes and S. T Hedetniemi , "Total Domination in graphs Networks", Vol. 10, pp.211-219, 1980.

[4] E. J. Cockayne and C .M. Mynhardt , "Domination sequences of graphs Ars,combinatorics", Vol. 33, pp. 257-275, 1992.

[5] E. J. Cockayne and C. M. Mynhardt, " Domination and Irredundance in cubic graphs", Discrete Mathematics, Vol. 167/168, pp. 205-214, 1997.

[6] F. F . Dragan, "Domination in Helly graphs without quadrangles cyber net systems" Analysis , Vol. 6, pp.47-57, 1993.

[7] S. Gravier and A. Khelladi, " On the domination numberof cross product of graphs", Discrete.Mathematics, Vol. 145, pp. 273-277, 1995.

[8] J. W. Grossman, "Dominating sets whose closed stars form spanning Trees", Discrete mathematics, Vol. 169, pp. 83-94, 1997.

[9] F. Harary and T. W. Haynes, Nordhaus-Gaddum, "Inequalities for domination in graphs", Discrete mathematics, Vol.155, pp. 99-105, 1996.

[10] T. W. Haynes, "Domination in graph, a brief overview", Combinatories Maths Combinatories Computer., Vol. 24, pp. 225-237, 1997.

[11] T. W .Haynes. ,S. T. Hedetniemi and P .J .Slater, Editors Dominations in graphs - Advanced' Topics, Marcel Dekker, Newyork, INC ,1997.

[12] T. W. Haynes, S. T. Hedetniemi and P. J. Slater, Fundamentals of domination in graphs, Marcel Dekker, New York, INC, 1998.

[13] S. T. Hedetniemi and R. Laskar, Connected domination in graphs, Graph theory and combinatorics, B.Bollabas ed., Academic press Londan., pp. 209-217, 1984 .

[14] M. A. Henning, "Domination in regular graphs" Ars combin., Vol. 43, pp.263 - 271, 1996.

[15] M. A. Henning, Dominations in graphs a survey. In G.Chartrand ,M. Jacobson, editors, Surveys in graph Theory, Vol. 116, pp.139-172, 1999.

[16] J. Paulraj Joseph and S. Arumugam , "Domination and connectivity in graphs", International Journal of Management and systems, Vol. 8, No. 3, pp. 233- 236, 1992.

[17] J.Paulraj Joseph and S.Arumugam, "Domination and colouring in graphs", International Journal of Management and systems, Vol. 15, No. 1, pp. 37- 44, 1999.

International Journal of Pure and Applied Mathematics
Volume 107 No. 3 2016, 673-682
ISSN: 1311-8080 (printed version); ISSN: 1314-3395 (on-line version)
url: http://www.ijpam.eu
doi: 10.12732/ijpam.v107i3.15

EDGE REGULAR PROPERTY OF COMPLEMENT AND μ-COMPLEMENT OF A FUZZY GRAPH AND EDGE ADJACENCY SEQUENCE IN FUZZY GRAPH

K. Radha[1], N. Kumaravel[2] §

[1]P.G. Department of Mathematics
Periyar E.V.R. College
Tiruchirappalli, 620 023, Tamil Nadu, INDIA

[2]Department of Mathematics
K.S.R. Institute for Engineering and Technology
Namakkal, 637 215, Tamil Nadu, INDIA

Abstract: In this paper, some theorems of edge regular fuzzy graphs are discussed with their complements and μ-complements. A necessary and sufficient condition under which they are equivalent is provided. Finally, adjacency sequence of edges in a fuzzy graph is defined. Using the sequences, characterization for a fuzzy graph with at most four vertices to be edge regular is obtained.

AMS Subject Classification: 03E72, 05C72
Key Words: strong fuzzy graph, complete fuzzy graph, edge regular fuzzy graph, totally edge regular fuzzy graph, complement of a fuzzy graph and μ-complement of a fuzzy graph

1. Introduction

Fuzzy graph theory was introduced by Azriel Rosenfeld in 1975 [8]. Though it is very young, it has been growing fast and has numerous applications in various fields. During the same time Yeh and Bang have also introduced various connectedness concepts in fuzzy graphs [10]. Mordeson (1994) introduced the

Received: January 17, 2016
Published: April 21, 2016

§Correspondence author

© 2016 Academic Publications, Ltd.
url: www.acadpubl.eu

concept of complement of fuzzy graphs [2]. M. S. Sunitha and A. Vijayakumar (2002) gave a modified definition of complement of fuzzy graph [9]. A. Nagoorgani and V. T. Chandrasekaran (2006), defined μ-complement of a fuzzy graph [3], which is slightly different from the definition of complement of a fuzzy graph discussed by M. S. Sunitha and A. Vijayakumar. A. Nagoorgani and K. Radha defined the concept of incidence sequence of vertices in a fuzzy graph (2008) [6]. K. Radha and N. Kumaravel (2014) introduced the concept of edge regular fuzzy graphs [7]. In this paper, we provide some theorems on edge regular property of complements and μ-complements of fuzzy graphs through various examples. We introduce edge adjacency sequence in a fuzzy graph and we use this sequence to study about the edge regular property of fuzzy graphs. First we go through some basic definitions in the next section.

2. Basic Concepts

Let V be a non-empty finite set and $E \subseteq V \times V$. A fuzzy graph $G : (\sigma, \mu)$ is a pair of functions $\sigma : V \to [0, 1]$ and $\mu : E \to [0, 1]$ such that $\mu(xy) \leq \sigma(x) \wedge \sigma(y)$ for all x, y $\in$ V. Let $G : (\sigma, \mu)$ be a fuzzy graph on $G^* : (V, E)$. The degree of a vertex x is $d_G(x) = \sum_{x \neq y} \mu(xy)$. The minimum degree of G is $\delta(G) = \wedge \{d_G(x), \forall x \in V\}$ and the maximum degree of G is $\Delta(G) = \vee \{d_G(x), \forall x \in V\}$. Let $G : (\sigma, \mu)$ be a fuzzy graph on $G^* : (V, E)$. The total degree of a vertex x is defined by $td_G(x) = \sum_{x \neq y} \mu(xy) + \sigma(x)$.

Let $G : (\sigma, \mu)$ be a fuzzy graph on $G^* : (V, E)$. If each vertex in G has same degree k, then G is said to be a regular fuzzy graph or k-regular fuzzy graph. If each vertex in G has same total degree k, then G is said to be a totally regular fuzzy graph or k -totally regular fuzzy graph.

Let $G : (\sigma, \mu)$ be a fuzzy graph on $G^* : (V, E)$. The degree of an edge $xy \in E$ is

$$d_G(xy) = \sum_{x \neq z} \mu(xz) + \sum_{z \neq y} \mu(zy) - 2\mu(xy).$$

The total degree of an edge $xy \in E$ is

$$d_G(xy) = \sum_{x \neq z} \mu(xz) + \sum_{z \neq y} \mu(zy) - \mu(xy).$$

Let $G : (\sigma, \mu)$ be a fuzzy graph on $G^* : (V, E)$. If each edge in G has same degree k, then G is said to be an edge regular fuzzy graph or k-edge regular fuzzy graph. If each edge in G has same total degree k, then G is said to be a totally edge regular fuzzy graph or k-totally edge regular fuzzy graph.

The order and size of a fuzzy graph G are defined by $O(G) = \sum_{x \in V} \sigma(x)$ and $S(G) = \sum_{xy \in E} \mu(xy)$.

A fuzzy graph G is strong, if $\mu(xy) = \sigma(x) \wedge \sigma(y)$ for all $xy \in E$. A fuzzy graph G is complete, if $\mu(xy) = \sigma(x) \wedge \sigma(y)$ for all $x, y \in V$.

Let G be a fuzzy graph. The complement of G is defined as $\overline{G} : (\sigma, \overline{\mu})$, where

$$\overline{\mu}(xy) = \sigma(x) \wedge \sigma(y) - \mu(xy),$$

for all $x, y \in V$. The μ-complement of G is defined as $G^{\mu} : (\sigma, \mu^{\mu})$, where

$$\mu^{\mu}(xy) = \begin{cases} \sigma(x) \wedge \sigma(y) - \mu(xy), & \forall xy \in E, \\ 0, & \forall xy \notin E. \end{cases}$$

The incidence sequence of a vertex v in a fuzzy graph G is defined as a sequence of membership values of edges incident to v arranged in increasing order. It is denoted by $is(v)$.

3. Edge Regular and Totally Edge Regular Property of Complements

Remark 1. If $G : (\sigma, \mu)$ is an edge regular fuzzy graph, then $\overline{G} : (\sigma, \overline{\mu})$ need not be edge regular fuzzy graph. For example, consider $G^* : (V, E)$ where $V = \{a, b, c, d\}$ and $E = \{ab, bc, bd, cd, da\}$. Define $G : (\sigma, \mu)$ by $\sigma(a) = 0.9, \sigma(b) = 1, \sigma(c) = 0.8, \sigma(d) = 0.9$ and $\mu(ab) = 0.4, \mu(bc) = 0.5, \mu(bd) = 0.9, \mu(cd) = 0.5, \mu(da) = 0.4$. Then $\overline{G} : (\sigma, \overline{\mu})$ is defined by $\overline{\mu}(ab) = 0.5, \overline{\mu}(bc) = 0.3, \overline{\mu}(ac) = 0.7, \overline{\mu}(cd) = 0.3, \overline{\mu}(da) = 0.5$. Here $d_G(ab) = 1.8$, for all $ab \in E$, but in $\overline{G} : (\sigma, \overline{\mu})$, $d_{\overline{G}}(ab) = d_{\overline{G}}(bc) = d_{\overline{G}}(cd) = d_{\overline{G}}(da) = 1.5, d_{\overline{G}}(ac) = 1.6$ and $td_{\overline{G}}(ab) = 2, td_{\overline{G}}(bc) = 1.8, td_{\overline{G}}(cd) = 1.8, td_{\overline{G}}(da) = 2, td_{\overline{G}}(ac) = 2.3$. Therefore $G : (\sigma, \mu)$ is 1. 8 - edge regular fuzzy graph, but $\overline{G} : (\sigma, \overline{\mu})$ is neither edge regular fuzzy graph nor totally edge regular fuzzy graph.

Remark 2. If $G : (\sigma, \mu)$ is totally edge regular fuzzy graph, then $\overline{G} : (\sigma, \overline{\mu})$ need not be edge regular fuzzy graph. For example, consider $G^* : (V, E)$ where $V = \{a, b, c, d\}$ and $E = \{ab, ac, ad\}$. Define $G : (\sigma, \mu)$ by $\sigma(a) = 0.9, \sigma(b) = 0.5, \sigma(c) = 0.7, \sigma(d) = 0.8$ and $\mu(ab) = 0.5, \mu(ac) = 0.4, \mu(ad) = 0.7$. Then $\overline{G} : (\sigma, \overline{\mu})$ is defined by $\overline{\mu}(ac) = 0.3, \overline{\mu}(ad) = 0.1, \overline{\mu}(bc) = 0.5, \overline{\mu}(bd) = 0.5, \overline{\mu}(cd) = 0.7$. Here $td_G(ab) = 1.6$, for all $ab \in E$, but in $\overline{G} : (\sigma, \overline{\mu})$, $d_{\overline{G}}(ac) = 1.3 = d_{\overline{G}}(bd), d_{\overline{G}}(ad) = 1.5 = d_{\overline{G}}(bc), d_{\overline{G}}(cd) = 1.4$ and $td_{\overline{G}}(ac) = 1.6 = td_{\overline{G}}(ad), td_{\overline{G}}(bc) = 2, td_{\overline{G}}(bd) = 1.8, td_{\overline{G}}(cd) = 2.1$. Therefore $G : (\sigma, \mu)$ is 1. 6 - totally edge regular fuzzy graph, but $\overline{G} : (\sigma, \overline{\mu})$ is neither edge regular fuzzy graph nor totally edge regular fuzzy graph.

Theorem 3. *Let $\mu(x,y) = [\sigma(x) \wedge \sigma(y)]/2$, for all $x, y \in V$. Then $G : (\sigma, \mu)$ is a k - edge regular fuzzy graph if and only if complement of $G : (\sigma, \mu)$ is also k - edge regular.*

Proof. Let

$$\mu(x,y) = [\sigma(x) \wedge \sigma(y)]/2, \text{ for all } x, y \in V. \tag{1}$$

By the definition of complement, $\overline{\mu}(x,y) = \sigma(x) \wedge \sigma(y) - \mu(xu)$, for all $x, y \in V$. Therefore

$$\overline{\mu}(x,y) = [\sigma(x) \wedge \sigma(y)]/2,$$

for all $x, y \in V$[by(1)]. Hence

$$\overline{\mu}(x,y) = \mu(x,y). \tag{2}$$

Therefore

$$d_{\overline{G}}(xy) = \sum_{x \neq z} \overline{\mu}(xz) + \sum_{z \neq y} \overline{\mu}(zy) - 2\overline{\mu}(xy).$$

By (2), $d_G(xy) = \sum_{x \neq z} \mu(xz) + \sum_{z \neq y} \mu(zy) - 2\mu(xy)$. Therefore $d_{\overline{G}(xy)} = d_{G(xy)}$, for all $xy \in E$. Hence $G : (\sigma, \mu)$ is k - edge regular fuzzy graph if and only if complement of $G : (\sigma, \mu)$ is also k - edge regular. □

Remark 4. The converse of theorem 3 need not be true.
For example, consider $G^* : (V, E)$, where

$$V = \{a, b, c, d\}$$

and

$$E = \{ab, ac, ad, bc, bd, cd\}\ .$$

Define $G : (\sigma, \mu)$ by $\sigma(a) = 0.9, \sigma(b) = 0.7, \sigma(c) = 0.7, \sigma(d) = 0.7$ and $\mu(ab) = 0.4, \mu(ac) = 0.35, \mu(ad) = 0.3, \mu(bc) = 0.4, \mu(bd) = 0.35, \mu(cd) = 0.3$. Then $\overline{G} : (\sigma, \overline{\mu})$ is defined by $\overline{\mu}(ab) = 0.3, \overline{\mu}(ac) = 0.35, \overline{\mu}(ad) = 0.4, \overline{\mu}(bc) = 0.3, \overline{\mu}(bd) = 0.35, \overline{\mu}(cd) = 0.4$. Here $d_G(ab) = 1.4$, for all $ab \in E$ and $d_{\overline{G}}(ab) = 1.4$, for all $ab \in \overline{E}$. Therefore $G : (\sigma, \mu)$ and $\overline{G} : (\sigma, \overline{\mu})$ are edge regular fuzzy graphs, but $\mu(x,y) \neq [\sigma(x) \wedge \sigma(y)]/2$,for $x, y \in V$.

Theorem 5. *Let $\mu(x,y) = [\sigma(x) \wedge \sigma(y)]/2$, for all $x, y \in V$. Then $G : (\sigma, \mu)$ is a k - totally edge regular fuzzy graph if and only if complement of $G : (\sigma, \mu)$ is also k - totally edge regular.*

Proof. Proof is similar to proof of theorem 3. □

Theorem 6. *Let $G : (\sigma, \mu)$ be a fuzzy graph on a regular graph $G^* : (V, E)$ such that μ is a constant function. Then $G : (\sigma, \mu)$ and $\overline{G} : (\sigma, \overline{\mu})$ are edge regular fuzzy graphs.*

Proof. Let $\mu(e) = c$, for all $e \in E$, where c is a constant. Let G^* be k - regular. Then $d_{G^*}(x) = k$, for all $x \in V$, where k is a constant. First let us prove that $G : (\sigma, \mu)$ is an edge regular fuzzy graph. By the definition of edge degree, $d_G(xy) = \sum_{x \neq z} \mu(xz) + \sum_{z \neq y} \mu(zy) - 2\mu(xy)$. Therefore

$$d_G(xy) = \sum_{x \neq z} c + \sum_{z \neq y} c - 2c = cd_{G^*}(x) + cd_{G^*}(y) - 2c$$

or $d_G(xy) = ck + ck - 2c = 2c(k-1)$. Hence $G : (\sigma, \mu)$ is an edge regular fuzzy graph. Next we prove that $\overline{G} : (\sigma, \overline{\mu})$ is an edge regular fuzzy graph. Let $|V| = n$. Then $\overline{G}^*$ is $(n-1-k)$ - regular. By the definition of complement, $\overline{\mu}(xy) = \sigma(x) \wedge \sigma(y) - \mu(xy)$, for all $x, y \in V$,

$$\overline{\mu}(xy) = \begin{cases} c \wedge c - c, & \forall xy \in E, \\ c \wedge c, & \text{otherwise.} \end{cases}$$

Therefore $\overline{\mu}(xy) = c$, for all $xy \in \overline{E}$. By the definition of edge degree, $d_{\overline{G}}(xy) = \sum_{x \neq z} \overline{\mu}(xz) + \sum_{z \neq y} \overline{\mu}(zy) - 2\overline{\mu}(xy)$, for all $xy \in \overline{E}$. Therefore

$$d_{\overline{G}}(xy) = \sum_{x \neq z} c + \sum_{z \neq y} c - 2c = cd_{\overline{G}^*}(x) + cd_{\overline{G}^*}(y) - 2c.$$

Hence $d_{\overline{G}}(xy) = 2c(n-k-2)$, for all $xy \in \overline{E}$. Hence $\overline{G} : (\sigma, \overline{\mu})$ is an edge regular fuzzy graph. □

Corollary 7. *Let $G : (\sigma, \mu)$ be a strong fuzzy graph such that σ is a constant function and let G^* be a regular graph. Then $G : (\sigma, \mu)$ and $\overline{G} : (\sigma, \overline{\mu})$ are edge regular fuzzy graphs.*

Proof. Given $G : (\sigma, \mu)$ is a strong fuzzy graph such that σ is a constant function. Then μ is a constant function. Therefore the result follows from theorem 6. □

Remark 8. The converse part of theorem 6 and corollary 7 need not be true. It can be seen from the following example. Consider $G^* : (V, E)$ where $V = \{a, b, c, d\}$ and $E = \{ab, ac, bc, cd\}$. Define $G : (\sigma, \mu)$ by $\sigma(a) = 0.4, \sigma(b) = 0.6, \sigma(c) = 0.4, \sigma(d) = 0.4$ and $\mu(ab) = 0.2, \mu(ac) = 0.4, \mu(bc) = 0.4, \mu(cd) =$

0.2. Then $\overline{G} : (\sigma, \overline{\mu})$ is defined by $\overline{\mu}(ab) = 0.2, \overline{\mu}(ad) = 0.4, \overline{\mu}(bd) = 0.4, \overline{\mu}(cd) = 0.2$. Here $d_G(ab) = 0.8$, for all $ab \in E$ and $d_{\overline{G}}(ab) = 0.8$, for all $ab \in \overline{E}$. Therefore $G : (\sigma, \mu)$ and $\overline{G} : (\sigma, \overline{\mu})$ are edge regular fuzzy graphs, but σ and μ are not constant functions, $G : (\sigma, \mu)$ is not a strong fuzzy graph and $G^* : (V, E)$ is not a regular graph.

4. Edge Regular and Totally Edge Regular Property of μ-Complements

Result 9. When G^* is complete, the complement of a fuzzy graph G is same as the μ - complement of G.

Proof. By the definition

$$\mu^{\mu}(xy) = \begin{cases} \sigma(x) \wedge \sigma(y) - \mu(xy), & \text{if } \mu(xy) > 0, \\ 0, & \text{if } \mu(xy) = 0. \end{cases}$$

Therefore $\mu^{\mu}(xy) = \sigma(x) + \sigma(y) - \mu(xy)$, for all $x, y \in V$. Hence $\mu^{\mu}(xy) = \overline{\mu}(xy)$,forall $x, y \in V$ and $xy \in E$. Also $\overline{\sigma}(x) = \sigma(x) = \sigma^{\mu}(x)$, for all $x \in V$. Hence the result. □

Remark 10. If $G : (\sigma, \mu)$ is an edge regular fuzzy graph, then $G^{\mu} : (\sigma, \mu^{\mu})$ need not be edge regular fuzzy graph. For example, consider $G^* : (V, E)$ where $V = \{a, b, c, d\}$ and $E = \{ab, ad, bc, bd, cd\}$. Define $G : (\sigma, \mu)$ by $\sigma(a) = 0.9, \sigma(b) = 1, \sigma(c) = 0.8, \sigma(d) = 1$ and $\mu(ab) = 0.4, \mu(ad) = 0.4, \mu(bc) = 0.5, \mu(bd) = 0.9, \mu(cd) = 0.5$. Then $G^{\mu} : (\sigma, \mu^{\mu})$ is defined by $\mu^{\mu}(ab) = 0.5, \mu^{\mu}(ad) = 0.5, \mu^{\mu}(bc) = 0.3, \mu^{\mu}(bd) = 0.1, \mu^{\mu}(cd) = 0.3$. Here $d_G(ab) = 1.8$, for all $ab \in E$, $d_{G^{\mu}}(ab) = d_{G^{\mu}}(ad) = d_{G^{\mu}}(bc) = d_{G^{\mu}}(cd) = 0.9, d_{G^{\mu}}(bd) = 1.6$ and $td_{G^{\mu}}(ab) = 1.4 = td_{G^{\mu}}(ad), td_{G^{\mu}}(bc) = 1.2 = td_{G^{\mu}}(cd), td_{G^{\mu}}(bd) = 1.7$. Therefore $G : (\sigma, \mu)$ is 1. 8 - edge regular fuzzy graph, but $G^{\mu} : (\sigma, \mu^{\mu})$ is neither edge regular fuzzy graph nor totally edge regular fuzzy graph.

Remark 11. If $G : (\sigma, \mu)$ is totally edge regular fuzzy graph, then $G^{\mu} : (\sigma, \mu^{\mu})$ need not be edge regular fuzzy graph. For example, consider $G^* : (V, E)$ where $V = \{a, b, c, d, e, f\}$ and $E = \{ab, bc, cd, de, ef, fa\}$. Define $G : (\sigma, \mu)$ by $\sigma(a) = 0.9, \sigma(b) = 0.6, \sigma(c) = 0.5, \sigma(d) = 0.7, \sigma(e) = 0.6, \sigma(f) = 0.7$ and $\mu(ab) = 0.6, \mu(bc) = 0.4, \mu(cd) = 0.3, \mu(de) = 0.6, \mu(ef) = 0.4, \mu(fa) = 0.3$. Then $G^{\mu} : (\sigma, \mu^{\mu})$ is defined by $\mu^{\mu}(bc) = 0.1, \mu^{\mu}(cd) = 0.2, \mu^{\mu}(ef) = 0.2, \mu^{\mu}(fa) = 0.4$. Here $td_G(ab) = 1.3$, for all $ab \in E$, $d_{G^{\mu}}(bc) = 0.2, d_{G^{\mu}}(cd) = 0.1, d_{G^{\mu}}(ef) = 0.4, d_{G^{\mu}}(fa) = 0.2$ and $td_{G^{\mu}}(bc) = 0.3 = td_{G^{\mu}}(cd), td_{G^{\mu}}(ef) =$

$0.6 = td_{G^\mu}(fa)$. Therefore $G : (\sigma, \mu)$ is 1. 3 - totally edge regular fuzzy graph, but $G^\mu : (\sigma, \mu^\mu)$ is neither edge regular fuzzy graph nor totally edge regular fuzzy graph.

Theorem 12. *Let $\mu(xy) = [\sigma(x) \wedge \sigma(y)]/2$, for all $xy \in E$. Then $G : (\sigma, \mu)$ is a k - edge regular fuzzy graph if and only if $G^\mu : (\sigma, \mu^\mu)$ is also k - edge regular.*

Proof. Given

$$\mu(xy) = [\sigma(x) \wedge \sigma(y)]/2, \text{ for all } xy \in E. \tag{3}$$

By the definition of μ - complement

$$\mu^\mu(xy) = \begin{cases} \sigma(x) \wedge \sigma(y) - \mu(xy), & \text{if } \mu(xy) > 0, \\ 0, & \text{if } \mu(xy) = 0. \end{cases}$$

Therefore $\mu^\mu(xy) = \sigma(x) \wedge \sigma(y) - [\sigma(x) \wedge \sigma(y)]/2$, for all $xy \in E$ (see (3)), or

$$\mu^\mu(xy) = [\sigma(x) \wedge \sigma(y)]/2,$$

for all $xy \in E$. Hence

$$d_{G^\mu}(xy) = \sum_{x \neq z} \mu^\mu(xz) + \sum_{z \neq y} \mu^\mu(zy) - 2\mu^\mu(xy)$$
$$= \sum_{x \neq z} \mu(xz) + \sum_{z \neq y} \mu(zy) - 2\mu(xy) = d_G(xy),$$

for all $xy \in E$. Hence $G : (\sigma, \mu)$ is a k - edge regular fuzzy graph if and only if $G^\mu : (\sigma, \mu^\mu)$ is also k - edge regular. □

Remark 13. The converse part of theorem 12 need not be true. In the following example, $G : (\sigma, \mu)$ and $G^\mu : (\sigma, \mu^\mu)$ are edge regular, but $\mu(xy) \neq [\sigma(x) \wedge \sigma(y)]/2$, for all $xy \in E$. Consider $G^* : (V, E)$ where $V = \{a, b, c, d\}$ and $E = \{ab, bc, cd, da\}$. Define $G : (\sigma, \mu)$ by $\sigma(a) = 0.9, \sigma(b) = 0.7, \sigma(c) = 0.8, \sigma(d) = 0.7$ and $\mu(ab) = 0.4, \mu(bc) = 0.4, \mu(cd) = 0.3, \mu(da) = 0.3$. Then $G^\mu : (\sigma, \mu^\mu)$ is defined by $\mu^\mu(ab) = 0.3, \mu^\mu(bc) = 0.3, \mu^\mu(cd) = 0.4, \mu^\mu(da) = 0.4$. Here $d_G(ab) = 0.7 = d_{G^\mu}(ab)$, for all $ab \in E$.

Theorem 14. *Let $\mu(xy) = [\sigma(x) \wedge \sigma(y)]/2$, for all $xy \in E$. Then $G : (\sigma, \mu)$ is a k - totally edge regular fuzzy graph if and only if $G^\mu : (\sigma, \mu^\mu)$ is also k - totally edge regular.*

Proof. Proof is similar to proof of theorem 12. □

5. Edge Adjacency Sequences

Definition 15. The adjacency sequence of an edge e in a fuzzy graph G is defined as a sequence of membership values of edges adjacent to e arranged in increasing order. It is denoted by $as(e)$.

Remark 16. 1. The number of elements in $as(e)$ is the degree of e in G^*.
2. The sum of all elements in $as(e)$ is the degree of e in G.

Example 17. *Consider the fuzzy graph in the following example.*
Consider $G^* : (V, E)$, *where* $V = \{a, b, c, d\}$ *and* $E = \{ab, ad, bd, cd\}$. *Define* $G : (\sigma, \mu)$ *by* $\sigma(a) = 0.6, \sigma(b) = 0.7, \sigma(c) = 0.8, \sigma(d) = 0.5$ *and* $\mu(ab) = 0.4, \mu(ad) = 0.5, \mu(bd) = 0.6, \mu(cd) = 0.5$. *The adjacency sequences of the edges are* $as(ab) = (0.5, 0.6), as(ad) = (0.4, 0.5, 0.6), as(bd) = (0.4, 0.5, 0.5), as(cd) = (0.5, 0.6)$.

Remark 18. When G is edge regular, the underlying graph G^* need not be edge regular. For example, consider $G^* : (V, E)$ where $V = \{a, b, c, d\}$ and $E = \{ab, ad, bd, cd\}$. Define $G : (\sigma, \mu)$ by $\sigma(a) = 0.4, \sigma(b) = 0.7, \sigma(c) = 0.6, \sigma(d) = 0.5$ and $\mu(ab) = 0.2, \mu(ad) = 0.4, \mu(bd) = 0.4, \mu(cd) = 0.2$. This is an edge regular fuzzy graph of degree 0. 8 whose underlying graph is not edge regular. Also $as(ab) \neq as(bd)$. Hence in an edge regular fuzzy graph, all the edges need not have the same adjacency sequence.

Remark 19. Even if both G and G^* are edge regular, then all the edges need not have the same adjacency sequence. For example, consider $G^* : (V, E)$ where $V = \{a, b, c, d\}$ and $E = \{ab, ac, ad, bc, bd, cd\}$. Define $G : (\sigma, \mu)$ by $\sigma(a) = 0.4, \sigma(b) = 0.7, \sigma(c) = 0.6, \sigma(d) = 0.5$ and $\mu(ab) = 0.3, \mu(ac) = 0.2, \mu(ad) = 0.2, \mu(bc) = 0.2, \mu(bd) = 0.2, \mu(cd) = 0.1$. Here both G and G^* are edge regular. But $as(ad) \neq as(cd)$.

Theorem 20. *If* G^* *is a triangle, the degree of an edge in* G *is the degree of the vertex opposite to it in* G.

Proof. Consider the fuzzy graph G on a triangle G^*. Let the vertices of G be a, b and c. In G, opposite edge of the vertex a is bc, opposite edge of the vertex b is ca and opposite edge of the vertex c is ab. Then $d_G(a) = \mu(ab) + \mu(ac) = d_G(bc)$, $d_G(b) = \mu(bc) + \mu(ba) = d_G(ca)$ and $d_G(c) = \mu(ca) + \mu(cb) = d_G(ab)$. Hence the degree of an edge in G is the degree of the vertex opposite to it in G. □

Theorem 21. *Let* G^* *be a triangle. Then* G *is an edge regular fuzzy graph if and only if* μ *is a constant and all the edges have the same adjacency*

sequence.

Proof. Let G^* be a triangle. Then G^* is 2 - regular and 2 - edge regular. Assume that μ is a constant and all the edges have the same adjacency sequence. Then G is an edge regular fuzzy graph.

Conversely, assume that G is k - edge regular fuzzy graph. Let the vertices of G be v_1, v_2 and v_3. Let the membership values of the three edges v_1v_2, v_2v_3 and v_3v_1 be k_1, k_2, k_3 respectively, where $0 \leq k_i \leq 1, i = 1, 2, 3$.

Since $d(v_iv_j) = k, i, j = 1, 2, 3$ and $i \neq j$, we have

$$k_1 + k_2 = k, \tag{4}$$

$$k_1 + k_3 = k, \tag{5}$$

$$k_2 + k_3 = k. \tag{6}$$

Equations (4)-(5) imply $k_2 - k_3 = 0 \Rightarrow k_2 = k_3$.

Equations (5)-(6) imply $k_1 - k_2 = 0 \Rightarrow k_1 = k_2$.

Hence $k_1 = k_2 = k_3$. Substituting $k_1 = k_2$ in (4), we get $k_1 = k/2$.

Therefore $k_1 = k_2 = k_3 = k/2$. Hence each edge has the same adjacency sequence $(k/2, k/2)$ and μ is a constant. □

Theorem 22. *Let G^* be a complete graph on four vertices. Then G is k - edge regular if and only if sum of the membership values of edges in each 1 - factor is $k/2$.*

Proof. Let G^* be a complete graph on four vertices. Then G^* is 4 - edge regular and every edge in G^* is adjacent to two 1 - factors. Assume that sum of the membership values of edges in each 1 - factor is $k/2$. Then G is k - edge regular. Conversely, assume that G is k - edge regular fuzzy graph. To prove that sum of the membership values of edges in each 1 - factor is $k/2$. Let the vertices of G be v_1, v_2, v_3 and v_4. Let the membership values of the six edges $v_1v_2, v_2v_3, v_3v_4, v_4v_1, v_1v_3$ and v_2v_4 be $k_1, k_2, k_3, k_4, k_5, k_6$ respectively, where $0 \leq k_i \leq 1, i = 1, 2, 3, 4, 5, 6$. Since G is k - edge regular fuzzy graph, $d(v_iv_j) = k, i, j = 1, 2, 3, 4$ and $i \neq j$. Hence, we have

$$k_4 + k_5 + k_6 + k_2 = k, \tag{7}$$

$$k_1 + k_5 + k_6 + k_3 = k, \tag{8}$$

$$k_4 + k_5 + k_6 + k_2 = k, \tag{9}$$

$$k_1 + k_5 + k_6 + k_3 = k, \tag{10}$$

$$k_1 + k_4 + k_2 + k_3 = k, \tag{11}$$

$$k_1 + k_2 + k_3 + k_4 = k. \tag{12}$$

Equations (7)-(8) imply $k_2 + k_4 - k_1 - k_3 = 0 \Rightarrow k_2 + k_4 = k_1 + k_3$. Using this fact in (11), we receive $k_2 + k_4 = k/2 = k_1 + k_3$.

Equations (9)-(11) imply $k_5 + k_6 - k_1 - k_3 = 0 \Rightarrow k_5 + k_6 = k_1 + k_3 \Rightarrow k_5 + k_6 = k/2$.

Therefore $k_1 + k_3 = k_2 + k_4 = k_5 + k_6 = k/2$. Hence sum of the membership values of edges in each 1 - factor is $k/2$. □

References

[1] Frank Harary, *Graph Thoery*, Narosa /Addison Wesley, Indian Student Edition, India (1988).

[2] J. N. Mordeson, C. S. Peng, *Operations on Fuzzy Graphs*, Information Sciences, Volume 79 (1994), 159 - 170.

[3] A. Nagoorgani, V. T. Chandrasekaran, *Free Nodes and Busy Nodes of a Fuzzy Graph*, East Asian mathematical journal, Volume 22, Number 2 (2006), 163 - 170.

[4] A. Nagoorgani, J. Malarvizhi, *Properties of μ-Complement of a Fuzzy Graph*, International Journal of Algorithms, Computing and Mathematics, Volume 2, Number 3 (2009), 73 - 83.

[5] A. Nagoorgani, K. Radha, *On Regular Fuzzy Graphs*, Journal of Physical Sciences, Volume 12 (2008), 33 - 40.

[6] A. Nagoorgani, K. Radha, *Some Sequences in Fuzzy Graphs*, Far and East Journal of Applied Mathematics, Volume 31, Number 3 (2008), 321 - 335.

[7] K. Radha, N. Kumaravel, *On Edge Regular Fuzzy Graphs*, International Journal of Mathematical Archive, Volume 5, Issue 9 (2014), 100 - 112.

[8] A. Rosenfeld, *Fuzzy graphs*, in: L. A. Zadeh, K. S. Fu, K. Tanaka and M. Shimura, (editors), Fuzzy sets and their applications to cognitive and decision process, Academic press, New York (1975), 77 - 95.

[9] M. S. Sunitha, A. Vijayakumar, *Complement of a Fuzzy Graph*, Indian Journal of Pure and Applied Mathematics, volume 33, Issue 9 (2002), 1451 - 1464.

[10] R. T. Yeh and S. Y. Bang, *Fuzzy relations, fuzzy graphs, and their applications to clustering analysis*, in: L. A. Zadeh, K. S. Fu, K. Tanaka and M. Shimura, (editors), Fuzzy sets and their applications to cognitive and decision process, Academic press, New York (1975), 125 - 149.